MODELING OF CYCLIC BEHAVIOR OF RETROFITTED BEAM COLUMN JOINT

BY

ABDULSAMEE HALAHLA

A Dissertation Presented to the

DEANSHIP OF GRADUATE STUDIES

KING FAHD UNIVERSITY OF PETROLEUM & MINERALS

DHAHRAN, SAUDI ARABIA

In Partial Fulfillment of the
Requirements for the Degree of

DOCTOR OF PHILOSOPHY

In

CIVIL ENGINEERING

May 2014

KING FAHD UNIVERSITY OF PETROLEUM & MINERALS

DHAHRAN- 31261, SAUDI ARABIA

DEANSHIP OF GRADUATE STUDIES

This thesis, written by **ABDULSAMEE MOHAMMAD HALAHLA** under the direction of his thesis advisor and approved by his thesis committee, has been presented and accepted by the Dean of Graduate Studies, in partial fulfillment of the requirements for the degree of **DOCTOR OF PHILOSOPHY IN CIVIL ENGINEERING.**
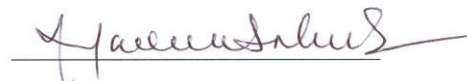
Dr. Nedal T. Ratrout
Department Chairman

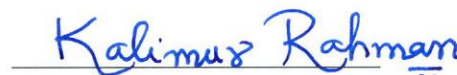Dr. Salam A. Zummo
Dean of Graduate Studies
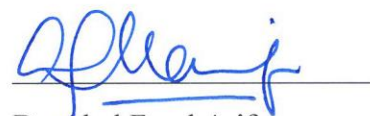
26/6/14

Date

Dr. Ali H. Al-Gadhib
(Advisor)

Dr. Mohammed H. Baluch
(Co-Advisor)

Dr. Muhammad K. Rahman
(Member)

Dr. Al-Farabi M. Sharif
(Member)

Dr. Abul Fazal Arif
(Member)

II

DEDICATED TO

MY BELOVED PARENTS,

MY WIFE AND SON,

AND

MY BROTHERS & SISTERS

ACKNOWLEDGMENTS

Thanks are due to my colleagues at the University for their friendship and support during my graduate studies.

Finally, I would like to express my deepest gratitude to my mother (late), father, my wife, my son, brothers, sisters, and all other relatives, for their emotional and moral support throughout my academic career and also for their love, patience, encouragement and prayers.

TABLE OF CONTENTS

LIST OF TABLES

LIST OF FIGURES

xiii

ABSTRACT

Full Name   : [Abdulsamee Mohammad Halahla]

Thesis Title   : [Modeling of Cyclic Behavior of Retrofitted Beam-Column Joint]

Major Field   : [Civil Engineering]

Date of Degree : [May, 2014]

Reinforced Concrete (RC) moment resisting frame structures are commonly used for lateral load resisting systems. However, such structures have often suffered damages caused by earthquakes, including permanent damage and/or failure where Beam-Column Joints (BCJs) have been identified as the weakest link in such systems. If BCJs could regain their original shape and strength with a minimum repair after an earthquake then the problems associated with permanent damage could be mitigated. Also, in a seismically active area of Saudi Arabia, prior to 1990's, most of the BCJs were constructed with seismic detailing with no shear reinforcement in the joint. This could result in the failure of these joints in the case of a seismic event.

The objectives of this research, entitled "Modeling of Cyclic Behavior of Retrofitted Beam-Column Joint" were to investigate the behavior of BCJs under cyclic loadings for two scenarios: (1) Non-retrofitted normal reinforced concrete beam column joints, (2) CFRP wrapped externally around the existing RC BCJs for the purpose of retrofitting. Three types of Beam-Column Joints specimens were tested with different detailing reinforcement and retrofitted with CFRP sheet wrapped around the joint.

A numerical modeling of joints with and without CFRP were also conducted by using finite element analysis software (ABAQUS) which helped to interpret the monitored behavior of BCJs through comparison with the numerical simulation and mechanistic models. The ABAQUS finite element software has the ability to model the nonlinear response of reinforced concrete member using Elasto-plastic-damage theory which simulates the cyclic and monotonic loading behavior of BCJs. These Beam-Column Joints are representative of existing detailed building in seismically active areas of Saudi Arabia.

ملخص الرسالة

الاسم الكامل: عبد السميع محمد عبد الهادي حلاحله

عنوان الرسالة: نمذجة التصرف الزلزالي لعناصر التقاء الاعمدة مع الجسور بعد اعادة تاهيلها

التخصص: الهندسة المدنية

تاريخ الدرجة العلمية: ايار, 2014

يعتبر المفصل الرابط بين الجسر والعمود هو عنصر هام من الإطارات الخرسانة المسلحة من اجل استيعاب القوى الافقية(الزلزالية), ويجب أن تصمم هذه المفاصل بشكل صحيح من اجل التقلل قدر الامكان من حجم الدمار بعد تاثير الزلزال، وخاصة بالنسبة للتحميل الدوري، كما هو الحال مثلا عندما يتعرض الإطار لتحميل الزلزال وبالتالي اجبار التصرف الانشائي للعمورد القوي والجسر الضعيف لتجنب انهيار المبنى. وقد تم مؤخرا الحيدث عن الزلزال المحتملة في مناطق منخفضة إلى معتدلة الزلزالية للمملكة العربية السعودية مخاوف من سلامة وضعف للمنشآت الخرسانية المسلحة، والتي لم يتم تصميمها حسب التعليمات المنصوص عليها في عملية التصميم الزلزالي. وتستند معظم المباني في هذه المناطق على التصميم ضد احمال الجاذبية والرياح والذي من شأنه أن يكون غير قابل للمقاومة في حالة حدوث الزلزال والتي يمكن أن تؤدي إلى خسائر في الأرواح والاضطراب الاقتصادي.

والهدف من هذه الدراسة هو التحقيق في سلوك المفاصل بين الجسر والعمود تحت تاثير الاحمال الدورية والساكنة عمليا. هذه المفاصل تمثل بناء المباني الموجودة في مناطق نشطة زلزاليا في المملكة العربية السعودية. وأيضا عن طريق استخدام النمذجة باستخدام برناج تحليل العناصر المحدودة و تشمل هذة النمذجة كل من نمذجة المفصل بدون استخام مادة الالياف الكربونبة والنمذجة عند تستخدام مادة الالياف الكربونية المستخدمة في المباني الخرسانية من اجل عملية تاهيلها ضد الزلازل.

وقد تبين من الدراسة مدى التقارب بين العمل التجريبي والنمذجة باستخام برنامج العناصر المحدودة, حيث ان استخدام مادة الالياف الكربونية زاد من قدرة استيعاب المفصل بشكل ملموس.

CHAPTER 1

INTRODUCTION

1.1   General

The Beam-Column Joint (BCJ) in reinforced concrete construction is considered the crucial zone in the reinforced concrete frame as it is the critical element subjected to large forces during severe ground shaking. Its behavior has a significant influence on the response of the structure, mainly with reference to its ductility and energy dissipating capability.

Since 1970's, design codes started enforcing stricter seismic provisions for the detailing of reinforcing bars in the joint regions as they remain extremely vulnerable during earthquakes and might result in structural collapses (Anderson, Mitchell et al. 1996), (Saatcioglu, Mitchell et al. 2001). BCJs deficiencies may be categorized to three classes. First, weak column/strong beam, which contradicts failure hierarchy of the design capacity concept; when plastic hinges form in the columns, the axial force causes a rapid degradation of the ability of the hinge to absorb energy while undergoing cyclic motion. Second, a weak beam/strong column - most favorable case since it is not associated with the loss of axial load carrying capacity, i.e. failure in the beam is less critical than that in the column. Finally, hinging in the joint, being at the point of intersection of the beam and column allows excessive rotations both in the beam and column in conjunction with a

loss of load carrying capacity of the column. Such a hazardous failure mechanism is unacceptable and must be prevented in design. Therefore, BCJs require special attention for proper design and detailing works.

A number of researchers e.g. (Parra-Montesinos, Peterfreund et al. 2005), (Parra-Montesinos and Wight 2001), have devoted significant efforts studying the behavior of joints under shear reversals, as well as on the development of design recommendations for ensuring adequate connection behavior in frame structures expected to undergo large inelastic deformations.

Current seismic design guidelines for RC BCJs (Joint ACI-ASCE Committee 352 – 2002, ACI 318-08) addresses three main aspects: i) confinement requirement, ii) evaluation of shear strength, and iii) anchorage of beam and column bars passing through their connection. Additionally, a strong column-weak beam behavior is desired, and frame members of regions expected to experience large reversed inelastic deformations. The joints need to be properly detailed to ensure sufficient ductility during earthquakes. The most important design criteria include safety of human lives and serviceability of essential facilities. Conventional structures are mostly designed for safety conditions, where earthquake energies are dissipated through the yielding of reinforcement and its inelastic deformation. Structures are allowed to undergo severe damage - this means saving lives at the expense of structures incurring huge economic losses. Now the vision has been broadened where the owners as well as designers no longer want to surrender their own creations/constructions. The seismic design of structures has evolved towards performance based design where there is a need for new structural members and systems that possess enhanced deformation capacity and ductility, higher damage tolerance,

concrete confinement, decreased or minimized residual crack sizes, recovered and reduced permanent deformations (Olsen and Billington 2011). If such a RC BCJs is built, this will allow the structural engineers to design connections with enhanced ductility exhibiting little damage and thus eliminating post-earthquake joint repairs.

In the past few decades, many investigations have been carried out to evaluate the performance of reinforced concrete structures subjected to seismic loading all over the world. For many reinforced concrete buildings and bridges, a significant majority of the structural failures could be attributed to inadequate seismic design of columns and the beam-column joints and/or the deterioration of concrete structures.

All the building structures before 1980's were mostly designed for the gravity load all over the world. These structures performed well under gravity loads but their performances are questionable under earthquake. Several recent earthquakes such as in Taiwan (1999), in Turkey (1999) and in Japan (2010) caused extensive building damage and collapse of RC structures because of old design and poor reinforcement detailing as shown in **Fig. 1.1**.

Shear failure of beam-column joints is defined as one of the causes of damage and collapse of these existing RC buildings due to poor reinforcement detailing within the beam-column joint region.

Figure 1.1: Damages Due to Earthquake in Japan Earthquake (2010) Taiwan Earthquake (1999) and Turkey Earthquake (1999)

This thesis research is currently under the collaborative research project between King Fahd University of Petroleum and Minerals (KFUPM) and Istanbul Technical University (ITU) in the area of seismic behavior of RC Structures to study the behavior of external beam-column joints with poor reinforcement detailing and retrofitting of these beam-column joints.

1.2   Need for this Research

1.2.1   Seismicity of KSA

In the past few decades, many investigations have been carried out to evaluate the performance of reinforced concrete structures subjected to seismic loading all over the world. For many reinforced concrete buildings and bridges, a significant majority of the structural failures could be attributed to the inadequate seismic design of columns and the BCJs and/or the deterioration of concrete structures.

Recently, there has been an increasing concern about the seismic activity along the western coast of the Kingdom. Several studies were conducted to estimate the level of the seismic risk in the Kingdom and seismic hazard analysis was performed. A zonation map, as shown in **Fig. 1.2**, was developed for the Kingdom, based on the Peak Ground Acceleration (PGA) values calculated for 50 years' service lifetime with 10% probability of being exceeded.
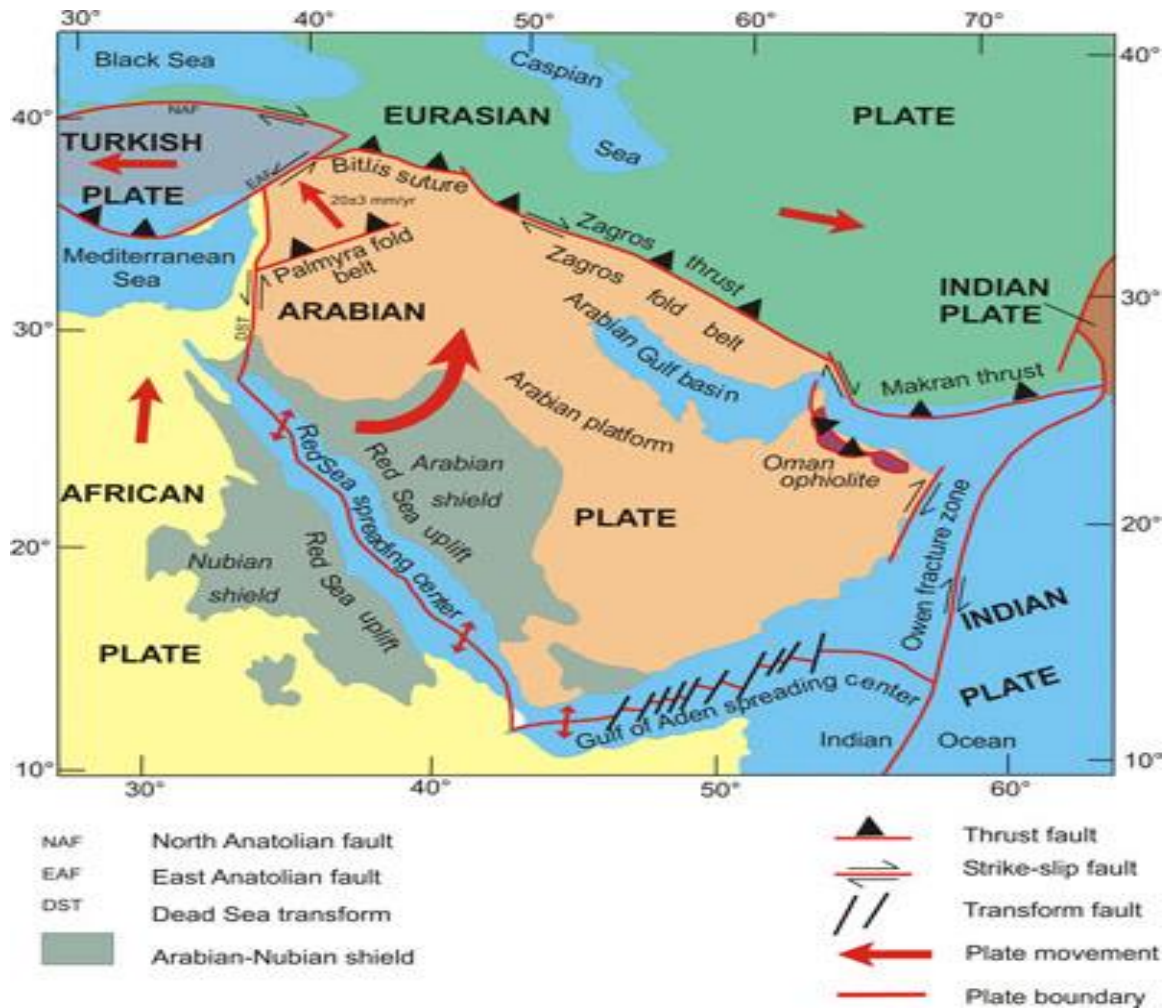
Figure 1.2: Seismic Zonation Map for the Kingdom

Following the Uniform Building Code (UBC 1991) model, the Kingdom was divided into four zones with Seismic Zone Numbers (SZN) of 0, 1, 2A and 2B as shown in **Table 1.1.**

Table 1-1 Seismic Zone Number (SZN) and Corresponding PGA According to UBC

SZN	PGA in g's
0	< 0.05
1	0.05 to 0.10
2A	0.10 to 0.15
2B	0.15 and above

The framework of ACI 318M-95 code was adopted for the design of reinforced concrete structures in the Kingdom. According to the ACI 318M table number R21.2.1, the zones of SZN = 0 and 1 are considered of 'No' and 'Low' risk levels, respectively. The zones of SZN = 2A and 2B are considered as areas with 'Moderate' risk level whereas the zones of SZN = 3 and 4 are considered to be 'High' seismic risk areas. Thus, according to the seismic zonation map, most of the Kingdom regions fall in the zone of no and low risk level. Areas along the western coast, especially in the northwest and southwest, are considered to be of a moderate risk level.

Some large cities in the Eastern Part of Saudi Arabia are located close to fault zones. As the population increases and new areas are developed, the seismic risk to human life and infrastructure increases. Geologists, in an interview with the Asharq Al Awasat, have explained that the cause of frequent earthquakes in recent years in the Arabian Peninsula can be attributed to the fact that the region is located near active seismic borders on both the north-eastern and western borders. They stated that the Arab plate which includes the

GCC states, Yemen, some parts of Iran and Greater Syria, collides with the Iranian plate (the Zagros Mountains) and the Turkish plate (the mountains of Anatolia). In turn, this causes the movement of the Arab plate by 2 cm annually causing an expansion to the Red Sea area and causing friction between the two plates in the eastern region of the Arab plate.

In September 2005, an earthquake measuring 3.7 on the Richter scale shook Mecca and caused panic amongst the citizens of Otaibah, a neighborhood situated near the Holy Mosque. Official statements regarding the intensity of the tremor contradicted each other and this led to a decision by the Saudi cabinet to assign the responsibility of monitoring seismic activity for the Saudi Geological Survey, which is to include all centers affiliated with King Abdul Aziz City for Science and Technology, King Abdul Aziz University, King Saud University and King Fahd University for Petroleum and Minerals under the umbrella of the Geological Survey. Following this, in the year 2006, in Jeddah, Asharq Al-Awsat reported an earthquake measuring 4.1 on the Richter scale that shook the city of Haradh in Eastern Saudi Arabia.

1.2.2   Buildings Built Prior to 1990s

In the Kingdom of Saudi Arabia, most of the existing buildings that were built in the sixties and mid-nineties were designed only for gravity and wind loads. These buildings particularly in the western region are prone to severe damage in case of an earthquake event because of poor detailing of BCJs of these existing buildings. BCJs in a reinforced

concrete moment resisting frame are crucial zones for the transfer of loads effectively between the connecting elements (i.e. beams and columns) in the structure.

Portions of columns that are common to beams at their intersections are called BCJs with some joints having limited shear force carrying capacity, especially if the compressive strength of concrete used is not very high when forces larger than these are applied during earthquakes, joints are severely damaged. Repairing damaged joint is difficult, and so the damage must be avoided by designing joint to resist earthquake effects.

Unsafe design and detailing within the joint region can jeopardize the entire structure, even if other structural members conform to the design requirements.

1.2.3 Need for Research

For the past three decades, extensive research has been carried out on studying the behavior of joints under seismic conditions through experimental and analytical studies. Various international codes of practice have been undergoing periodic revisions to incorporate the research findings into practice. New design and detailing aspects have been incorporated into the code to preclude joint failure. A vast body of research exists for retrofitting of BCJs in old concrete structures using carbon fibers (CFRP) and glass fibers (GFRP).

1.3   Objectives for this Research

The primary objective of this research was to investigate the behavior of Reinforced Concrete (RC) beam-column joints under cyclic load retrofitted by CFRP sheets.

The following investigations were carried out in order to meet the above objective:

To investigate the behavior of reinforced concrete (RC) BCJs under cyclic loading for various scenarios.

A. For non-retrofitted shear deficient RC BCJs using normal steel reinforcement using three different cases of reinforcement details in the joint:

- where the main beam steel is 12 mm bent out

- where the main beam steel 12 mm bent in

- where the main beam steel 18 mm bent in

B. For retrofitting existing BCJs that are designed to fail by shear failure of the joint using CFRP sheets with three different cases of reinforcement details in the joint:

- where the main beam steel is 12 mm bent out

- where the main beam steel 12 mm bent in

- where the main beam steel 18 mm bent in

C. Simulation of BCJ's in ABAQUS environment to predict the behavior and failure modes of joints for various scenarios for the six different scenarios mention

before. In this phase, the parameters of the model were calibrated by comparing

the numerical results to the experimental results.

CHAPTER 2

LITERATURE REVIEW

2.1 General

Carbon Fiber Reinforced Concrete (CFRP) retrofit technology has been introduced in the civil engineering area in the recent decades. For structural applications, CFRP is mainly to retrofit structurally deficient structural members with external application of CFRP sheet. CFRP can be bonded to reinforced concrete structural elements using various techniques such as external bonding, wrapping and near surface mounting. CFRP plates or sheets may be glued to the tension side of a structural member to provide flexural strength or glued to the web side of a beam to provide shear strength. CFRP sheets can also be wrapped around a beam to provide shear strength, wrapped around a column to provide confinement and thus increase the strength and ductility, and wrapped around the beam-column joint to close the tension crack due to tensile force at the joint.

2.2 Experimental Studies for Beam Column Joint and Retrofitting

The retrofitting of BCJs in old reinforced concrete structures using carbon fibers (CFRP) continues to be an active area of research in view of damage experienced in various parts of the world during recent earthquakes. In the recent years, research has concentrated on CFRP retrofitting of exterior, interior and corner BCJ's.

Currently, many researchers are experimentally investigating the behavior of beam-column joint retrofitted with CFRP. (Akguzel 2011) and (Antonopoulos and Triantafillou 2003) studied the Seismic performance of FRP retrofitted exterior RC beam-column joints under varying axial and bidirectional loading. (Parvin, Altay et al. 2009) studied the CFRP rehabilitation of concrete frame joints with inadequate shear and anchorage details the study involve full-scale experimental evaluation of carbon fiber-reinforced polymer CFRP rehabilitation for existing beam-column joints designed for gravity load with common pre-1970s deficient reinforcement details when subjected to cyclic loading as shown in **Fig. 2.1**.
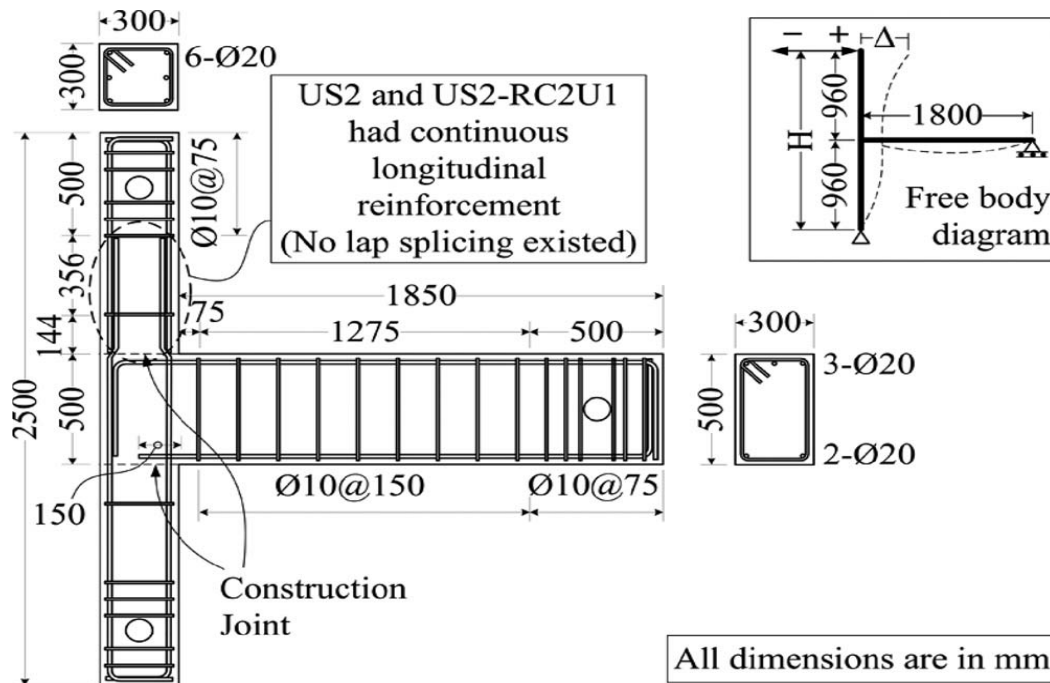
Figure 2.1: Reinforcement details and dimensions [Parvin, Altay et al. 2009]

(Hakuto, Park et al. 2000) studied the exterior and interior beam column joints which were designed as pre 70's specification with less reinforcement detailing in joint region and also tested one of the retrofitted interior beam-column joints to see the improved ductility of interior specimens as shown in **Fig. 2.2**. For exterior beam-column joints, they investigated difference of reinforcement detailing of longitudinal top and bottom beam bars end hooks in the joint. In old practices, the end hooks of beam bar in joint were bent up; and in the current practices, bars are bent down in the joint and the test shows the improvement in performance of joint with beam bars anchored according to current practice as shown in **Figs. 2.3 and 2.4**.
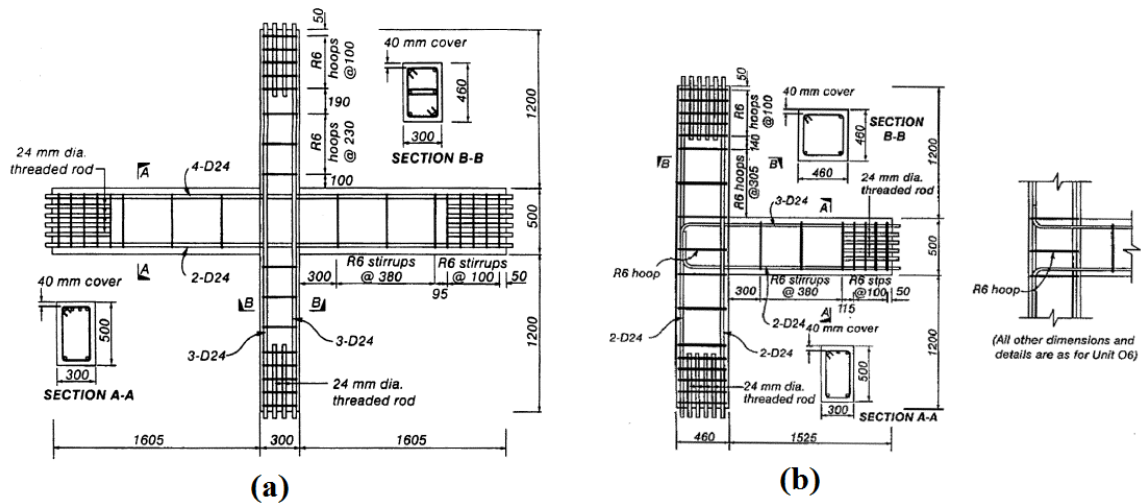
Figure 2.2: Interior and Exterior Beam Column Joints Size and Reinforcement Detailing [Hakuto, Park et al. 2000]
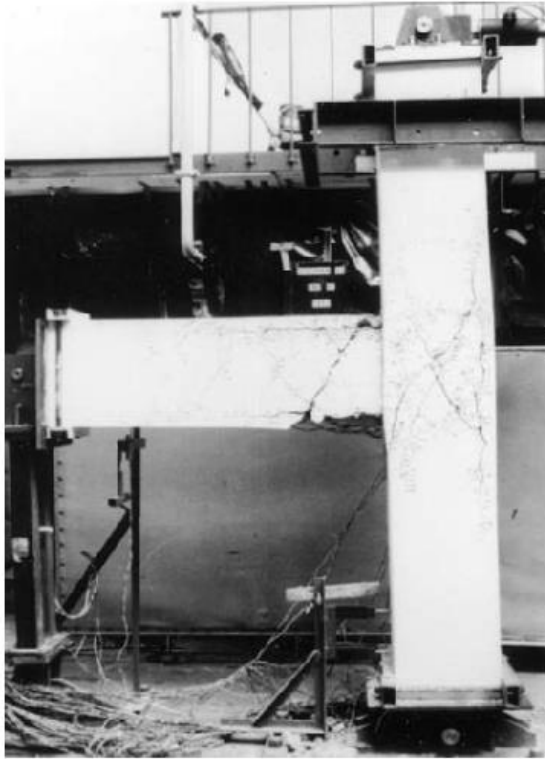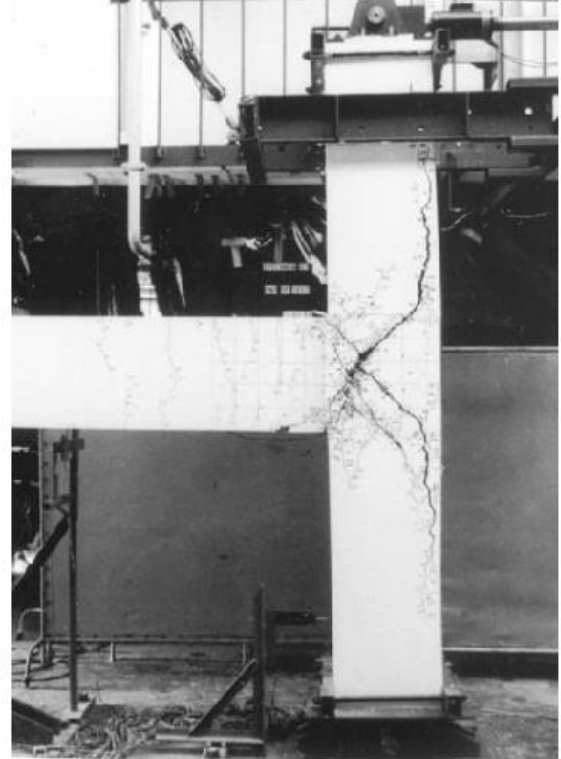
Figure 2.3: Crack Pattern for (a) Bent down and (b) Bent up Specimens [Hakuto, Park et al. 2000]
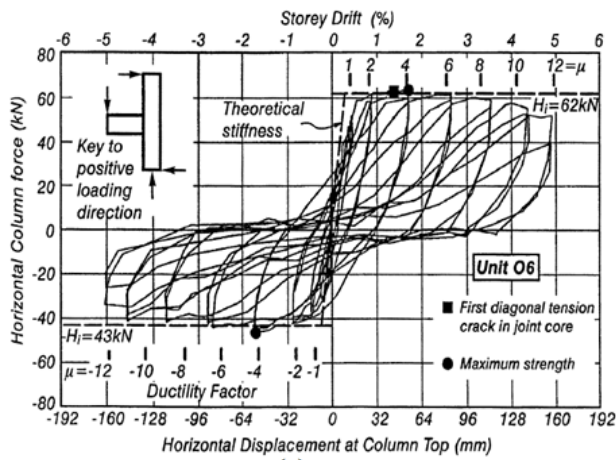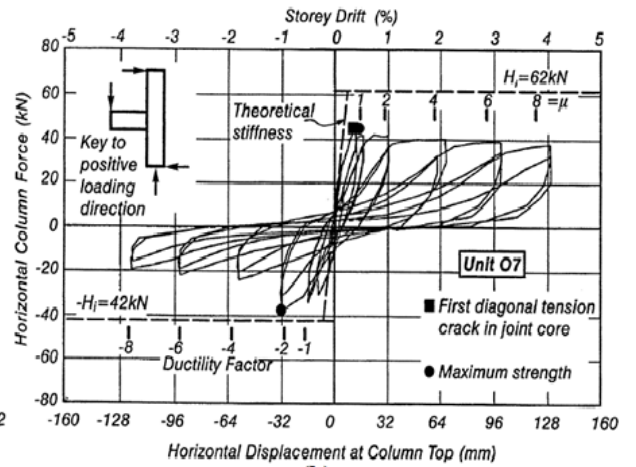
Figure 2.4: Horizontal Column Force versus Horizontal Displacement at Top of Column Relationship Measured
for (a) Bent down and (b) Bent up Specimen [Hakuto, Park et al. 2000]

15

(Ilki, Bedirhanoglu et al. 2010) study the behavior of FRP-Retrofitted joints built with plain bars and low-strength concrete as shown in **Fig. 2.5**. Two series of tests were conducted on eight full-scale exterior beam-column joint sub assemblages built with plain bars and low-strength concrete. No transverse reinforcement was present in the joint cores. In the first series of tests which included three specimens, the behavior of joints before Fiber-Reinforced Polymer (FRP) retrofitting was investigated. In the second series which included five specimens, the behavior of the FRP-retrofitted joints was investigated. The six specimens consisted of a column, an in-plane beam, a transverse beam, and a slab part; and two specimens were plane members without transverse beams and slabs. The utilized retrofitting scheme is easily applicable for actual exterior beam-column joints shown in **Fig. 2.6**, even in the presence of a transverse beam and a slab. Two types of strength limitation were observed for specimens in the first series. The strength of the specimen with beam longitudinal bars sufficiently anchored to the joint core was limited by the shear strength of the joint. The strengths of the other two specimens were limited by the slip of the beams' longitudinal bars at their anchorages. In the second series of tests, significantly better performance was obtained both in terms of shear strength and ductility provided that the slip of the beam bars was prevented. The strength and deformability characteristics of the tested reference and FRP-retrofitted joints are predicted with reasonable accuracy. The same algorithm is used for predicting the joint shear strength of specimens tested by other researchers, and satisfactory agreement is obtained between the predictions and test results. **Fig. 2.7** shows the compression for the control and retrofitted specimen.

Figure 2.5: Reinforcement details [Ilki, Bedirhanoglu et al. 2010]

Figure 2.6: Retrofitted scheme for the specimens [(Ilki, Bedirhanoglu et al. 2010]

17
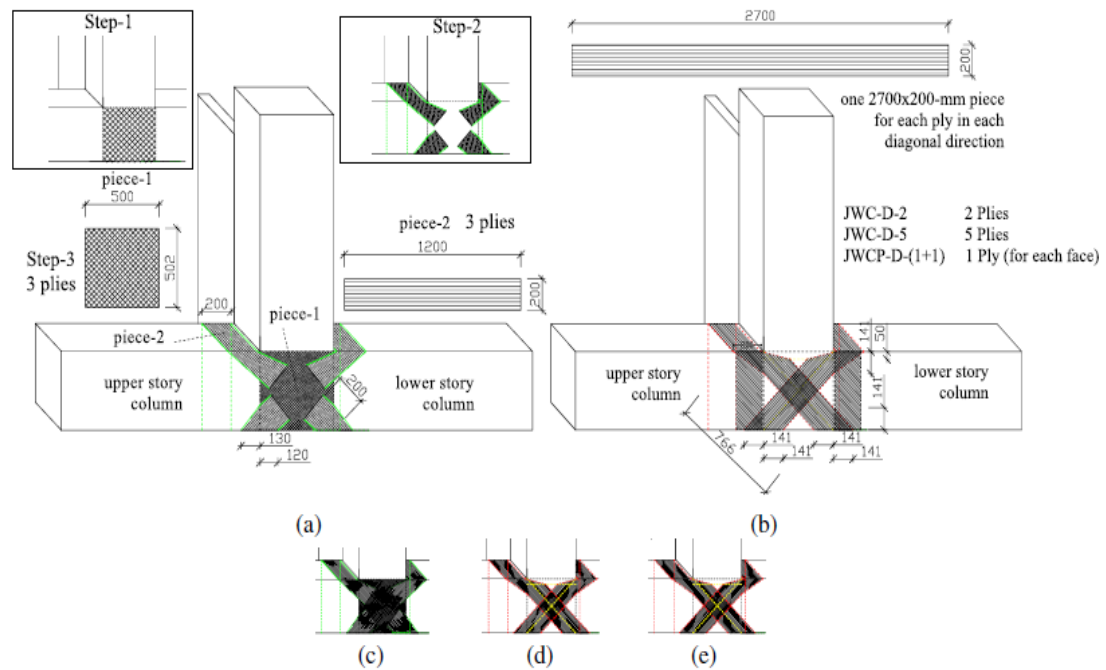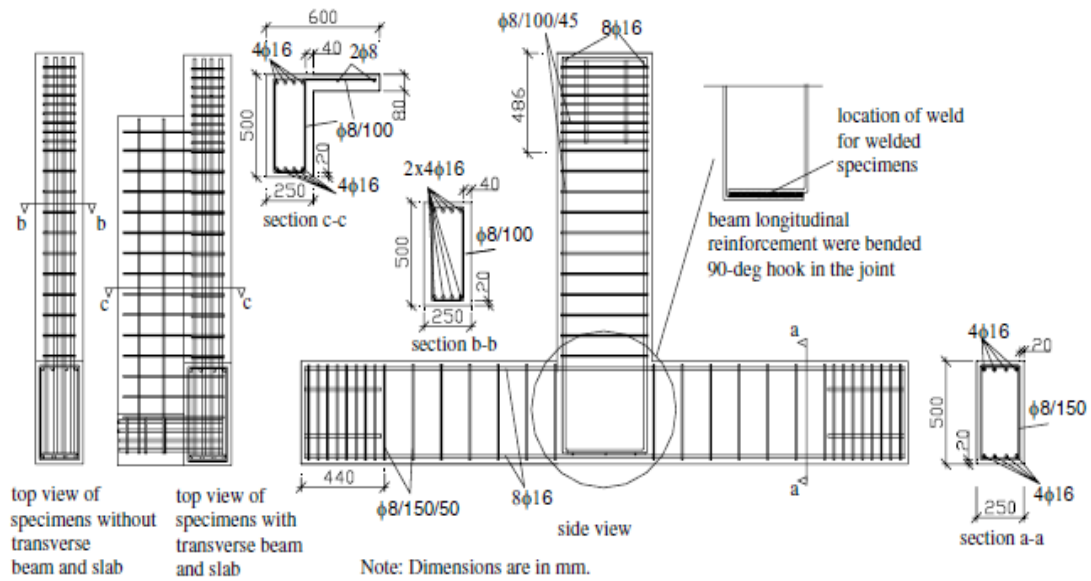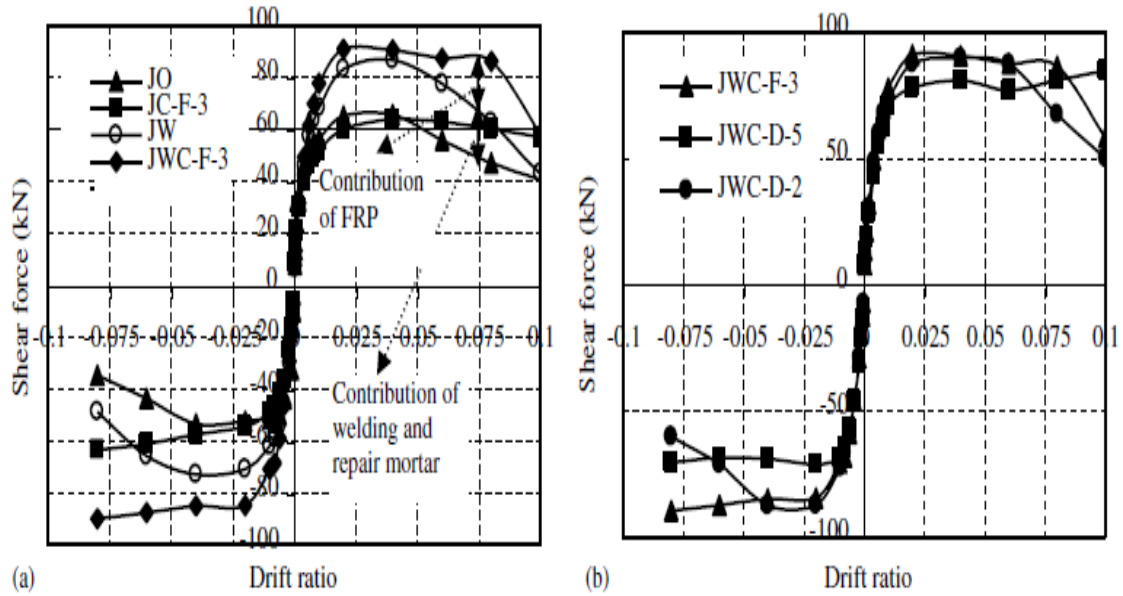
Figure 2.7: Comparison of envelopes of shear force–drift ratio relationships for control and retrofitted specimen [(Ilki, Bedirhanoglu et al. 2010]

(Pantelides, Clyde et al. 2000) tested two half scale corner beam column joints to investigate the diagonal tension failure in joint in the control specimen to see the increase in shear capacity of joint in retrofitted specimen as shown in **Fig. 2.8**. These specimens were tested under the quasi-static cyclic loading and their performance was examined in terms of peak lateral load capacity, ductility, drift, axial load bearing capacity of the column at high levels of drift, and in terms of crack widths. The behavior of the FRP composite retrofitted joint was found significantly improved in terms of lateral load capacity, ductility and axial load bearing capacity at high levels of drift as shown in **Fig. 2.9**. In addition, the joint shear strength of the FRP retrofitted joint was 45% higher than that of the control.
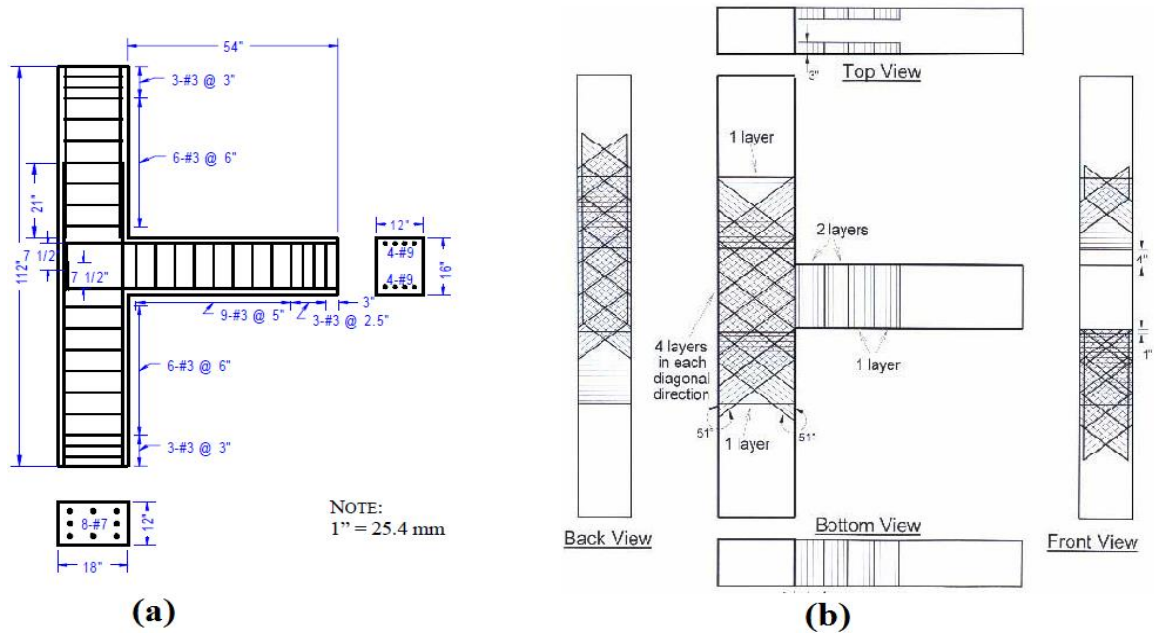
Figure 2.8: Specimen dimensions and reinforcement details (b) Composite retrofit layout [Pantelides, Clyde et al. 2000]
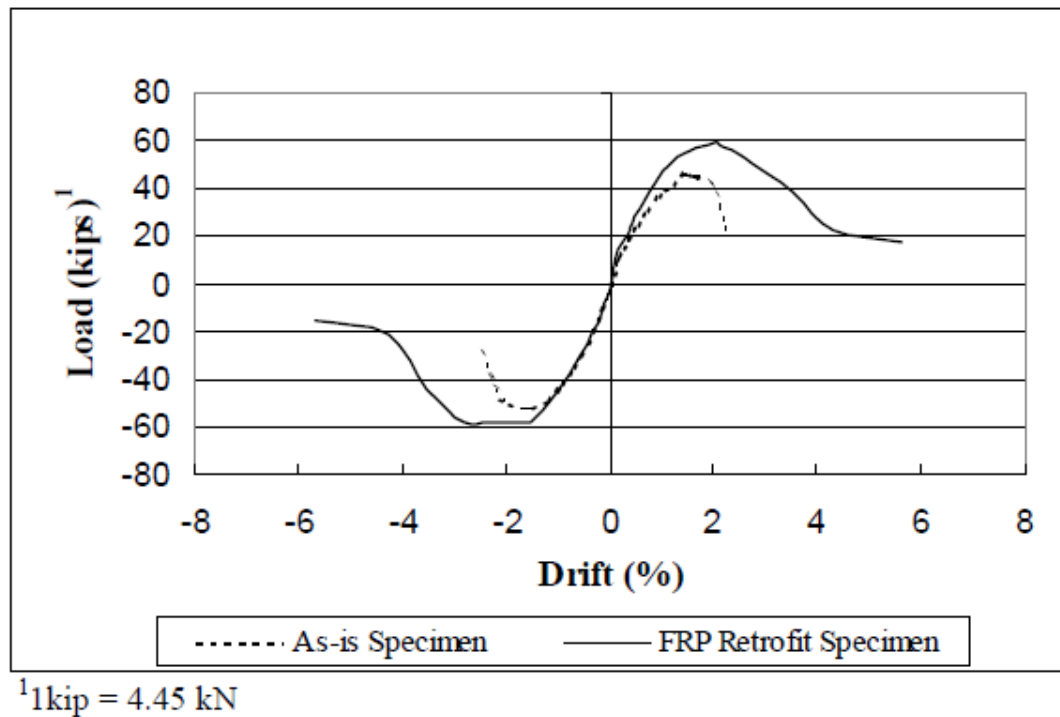
Figure 2.9: Backbone curve for as-is and FRP retrofit specimen [Pantelides, Clyde et al. 2000]

19

(Gencoglu and Mobasher 1993) investigated four half scale exterior beam-column joints under cyclic loading with constant load on the column of 90kN. One of the specimens was designed according to the ACI 318-02; two were rehabilitated with CFRP fabrics on the tension face of column and beam, and both column and beam were wrapped; and the last one was considered as control specimen as given in **Figs. 2.10 & 2.11(a)**. The test result indicates that the retrofitted specimens have more load carrying capacity, ultimate beam tip displacements and absorbed more total energy amount than ACI 318-02 design and control specimens as shown in **Fig. 2.11(b)**.
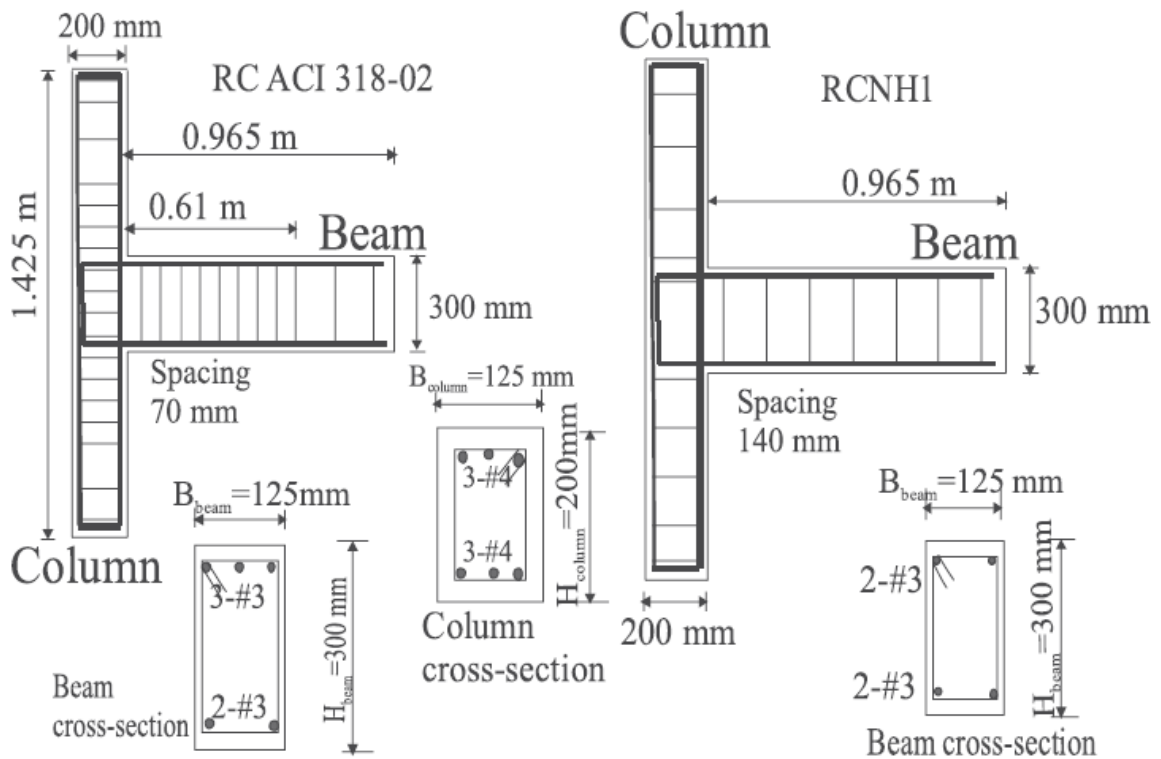
Figure 2.10: Reinforcement details of exterior beam-column joint specimens [Gencoglu and Mobasher 1993]
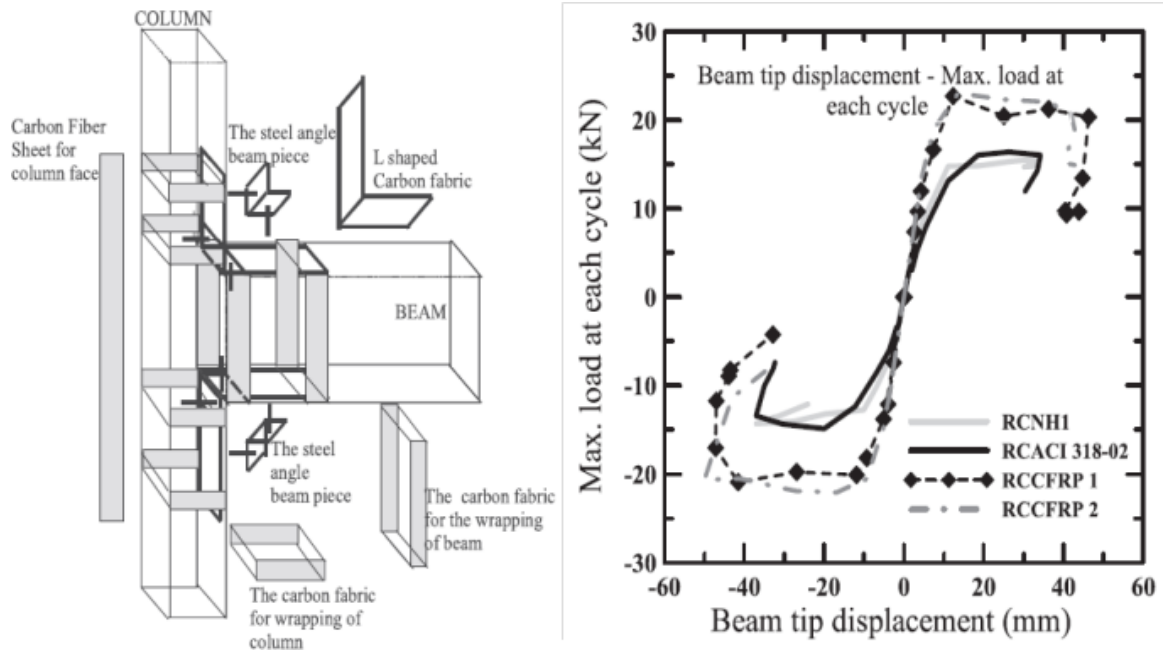
Figure 2.11: (a) Details of strengthening process by CFRP (b) The envelopes of beam tip displacement-cyclic loads of beam-column joint specimens [Gencoglu and Mobasher 1993]

(Le-Trung, Lee et al. 2010) studied eight 1/3 scale exterior reinforced concrete beam-column joints including a non-seismic, seismic and six retrofitted specimens with CFRP on different configuration as shown in **Figs. 2.12 and 2.13**, to find out the effective way of use of CFRP for strengthening the beam-column joints with CFRP to increase the lateral strength and ductility. According to the test results, the x-shape configuration of warping, the strip on the column and two layers of the CFRP sheets show better performance in terms of ductility and strength as shown in **Fig. 2.14**.

Figure 2.12: (a) Non-seismic and (b) Seismic details of the test specimens [Le-Trung, Lee et al. 2010]

a. NS and SD   b. RNS-1   c. RNS-2   d. RNS-3

e. RNS-4   f. RNS-5   g. RNS-6
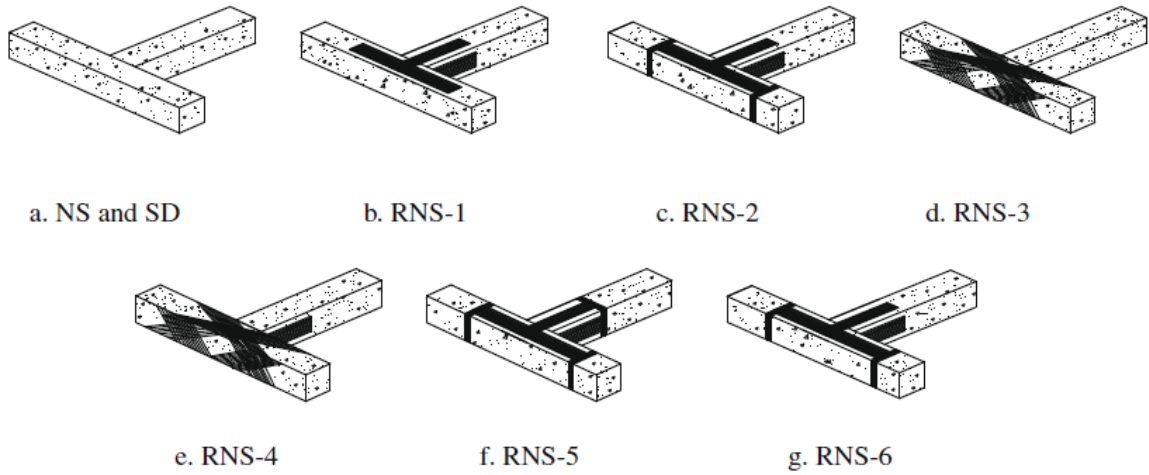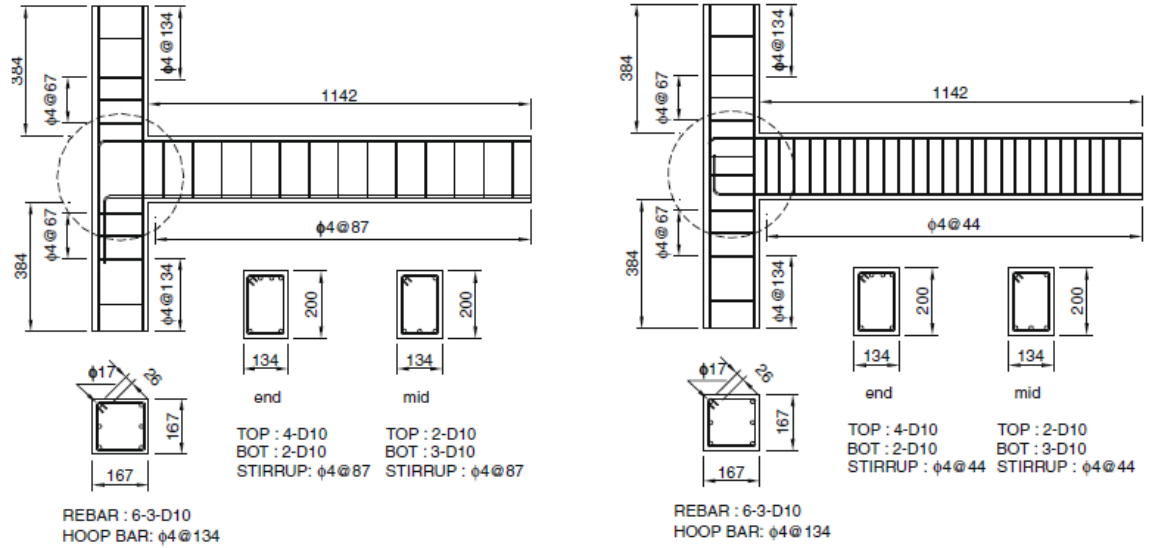
Figure 2.13: Description of all test specimens [Le-Trung, Lee et al. 2010]

22
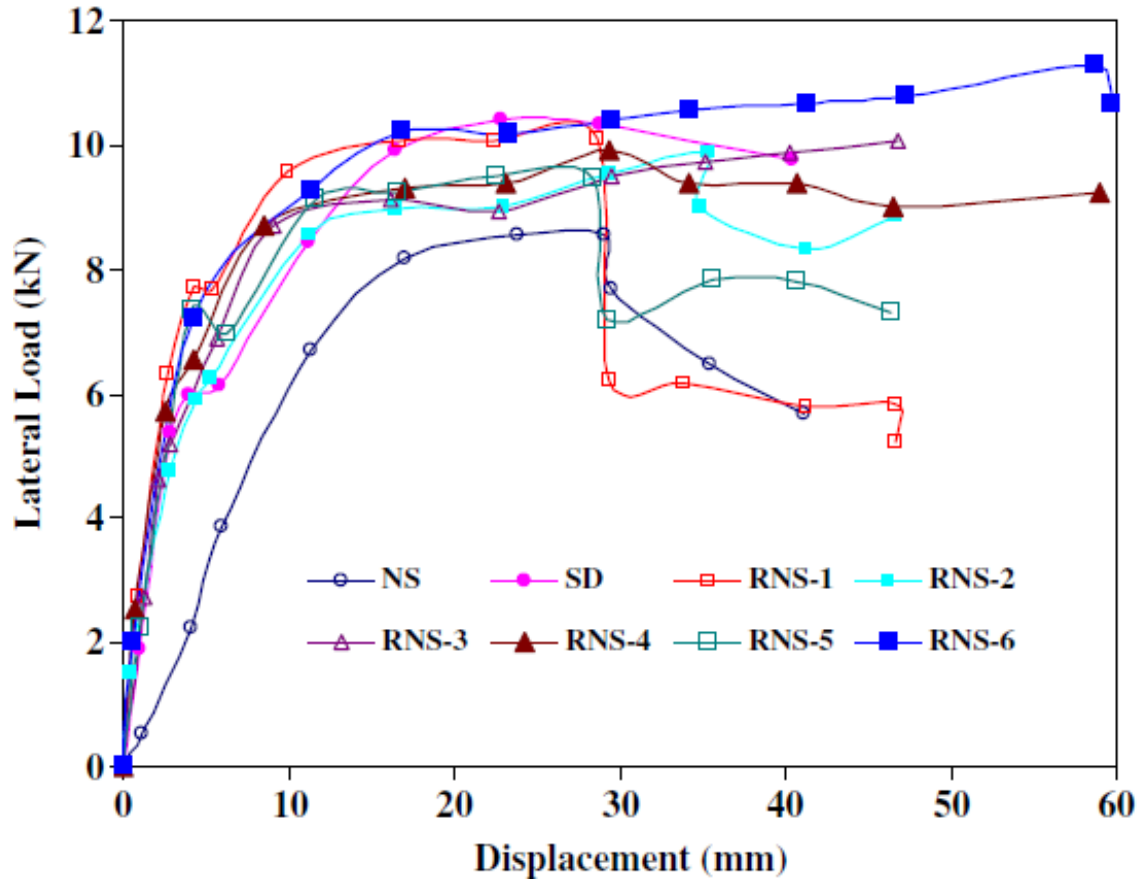
Figure 2.14: Positive lateral load versus Displacement envelop for all specimens [Le-Trung, Lee et al. 2010]

(Pampanin, Calvi et al. 2002) have investigated seismic behavior of six 2/3 scaled reinforced concrete beam-column joints designed for gravity load in which two were exterior knee joints, two exterior tee-joints and two interior cruciform joints using smooth bars with deficient anchorage hook-end bars and in-adequate detailing in the joint region as shown in **Fig. 2.15**. Experimental results showed the slippage of bars stress concentration at the end bars hook-end which results in concrete wedge at the joint in the exterior specimens as given in **Fig. 2.16**.
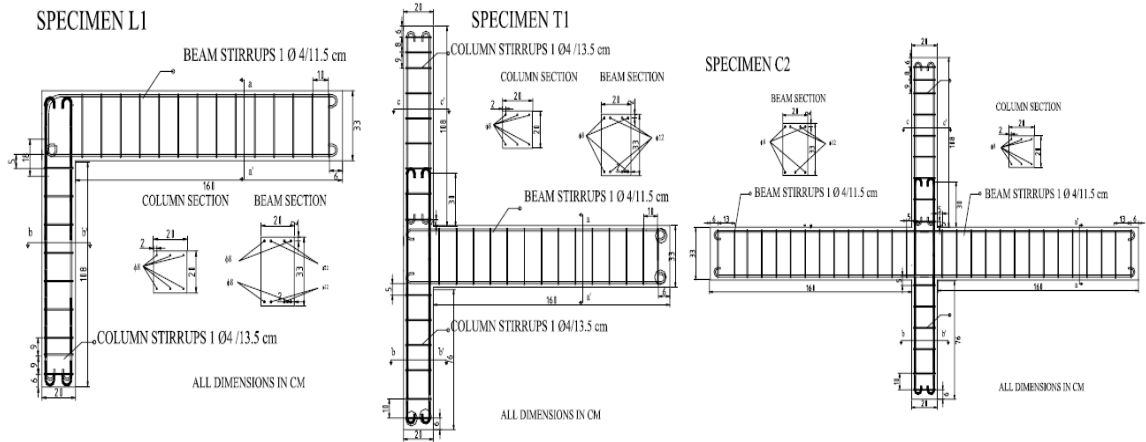
Figure 2.15: (a) Knee joint (b) Tee joint and (c) Interior joint sizes and reinforcement details [Pampanin, Calvi et al. 2002]
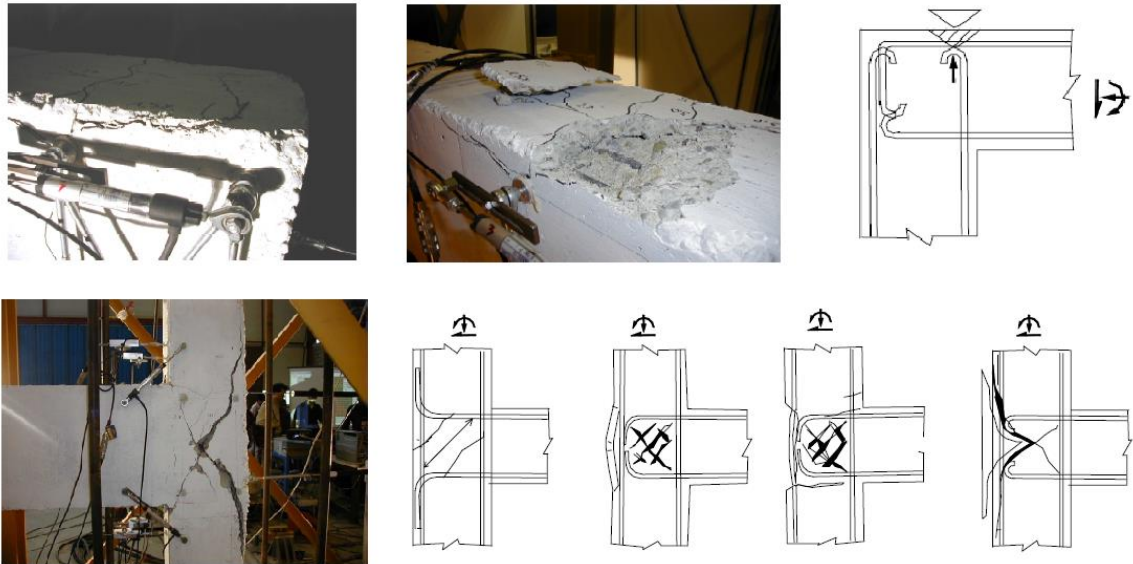
Figure 2.16: Knee and Tee joint failure mechanisms [Pampanin, Calvi et al. 2002]

(Ravi and Arulraj 2012) conducted an experimental investigation on influence of development length in retrofitted reinforced concrete beam-column joints. Nine controlled reinforced concrete beam-column joints specimens were cast, in which six specimens had design and details as per the code IS 456:2000. The remaining three specimens had design and details as per the code IS 13920:1993 as shown in **Fig. 2.17**. Retrofitting was done on failed specimens with details as per code IS 456:2000. Three specimens were wrapped with GFRP and remaining three with CFRP. Static load test was conducted on control and retrofitted specimens. They concluded that there was an increase in load carrying capacity by 14.5% and an increase in energy absorption capacity by 10% as the development length was increased based on code IS 13920:1993 as given in **Fig. 2.18**.
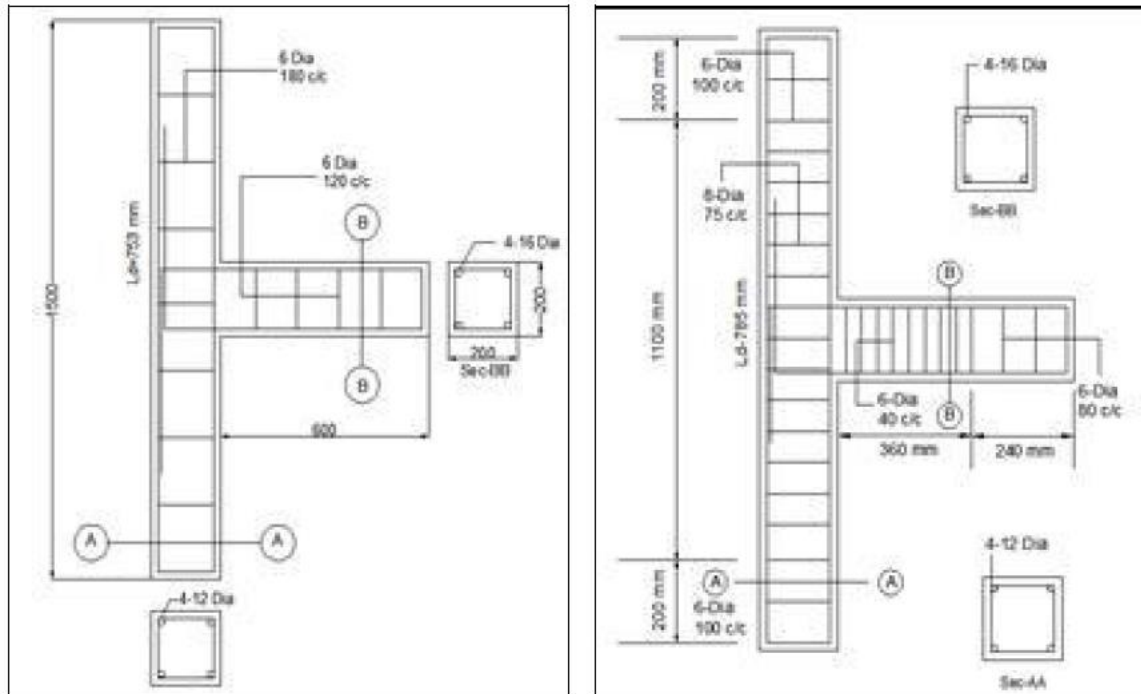
Figure 2.17: (a) IS 13920 and (b) IS 456 Specimens size and reinforcement details [Ravi and Arulraj 2012]
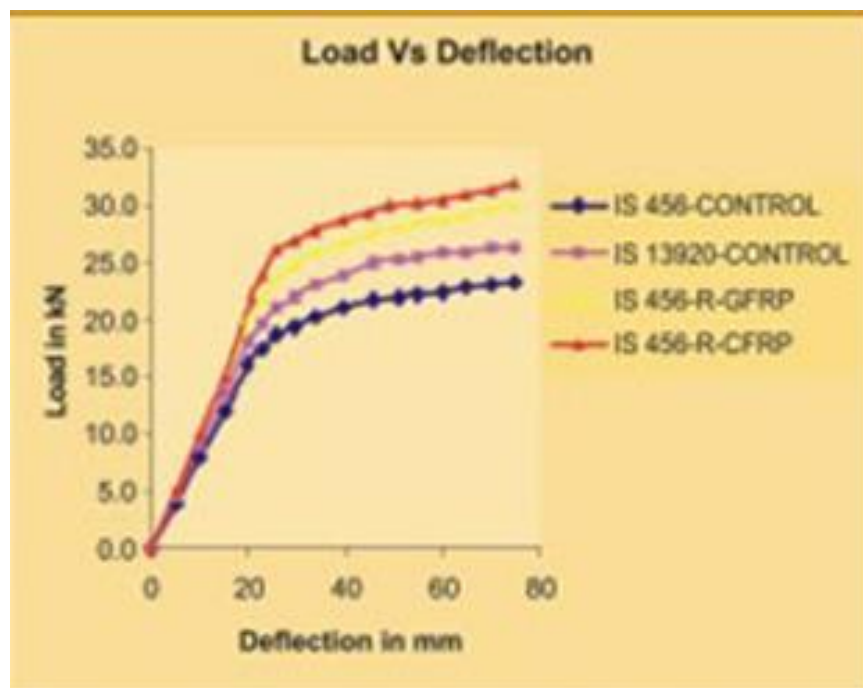
Figure 2.18: Load deflection curve for control and retrofitted specimens [Ravi and Arulraj 2012]

(El-Amoury and Ghobarah 2002) conducted the cyclic load test on the exterior beam-column joints designed only for gravity load without transverse reinforcement in the joint region, three reinforced concrete beam column joints were TO, TR1 and TR2, where TO is control and TR1 & TR2 were rehabilitated with GFRP as shown in **Figs. 2.19 & 2.20**. Results show that the joint rehabilitation eliminated the brittle joint failure and improved the bond conditions of beam top reinforcement, delayed slippage of bottom steel, increase the energy distribution of joints also improve the ductility and load carrying capacity of specimens as shown in **Fig. 2.21**.
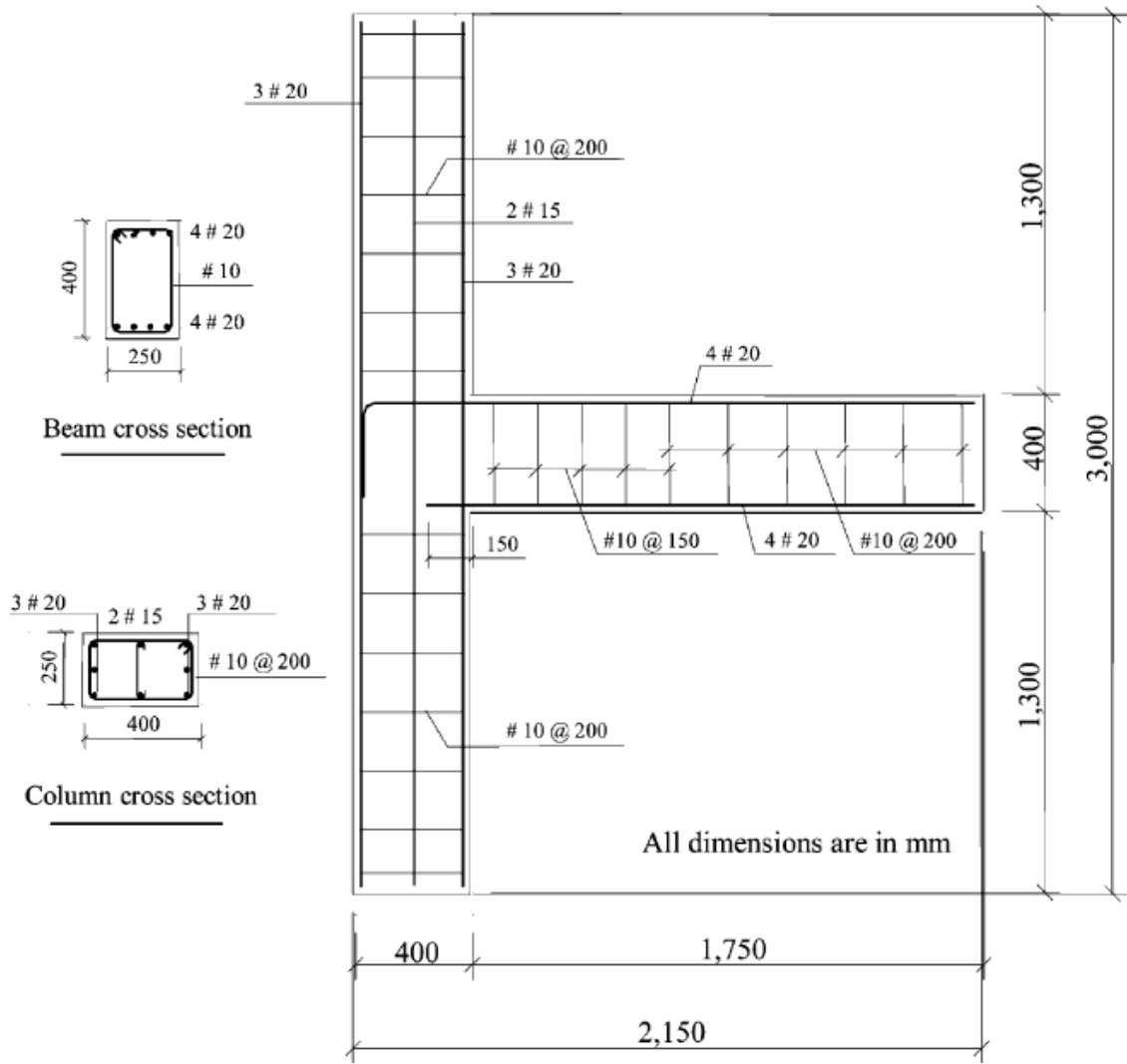
Figure 2.19: Specimen dimensions and reinforcement details [El-Amoury and Ghobarah 2002]

27
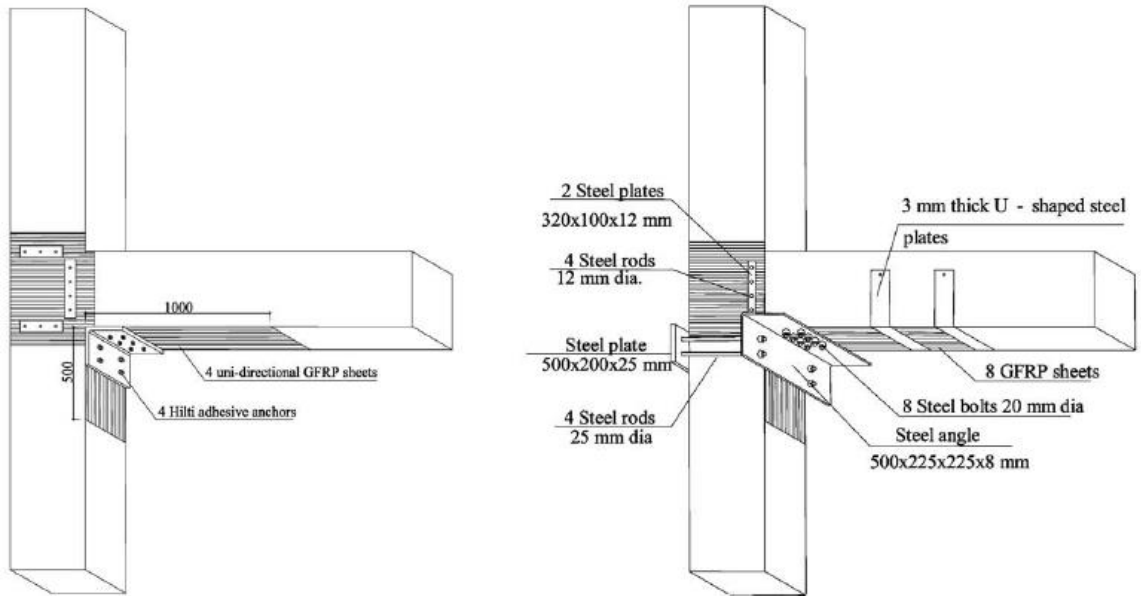
Figure 2.20: Retrofitting schemes: (a) Specimen TR1, (b) Specimen TR2 [El-Amoury and Ghobarah 2002]
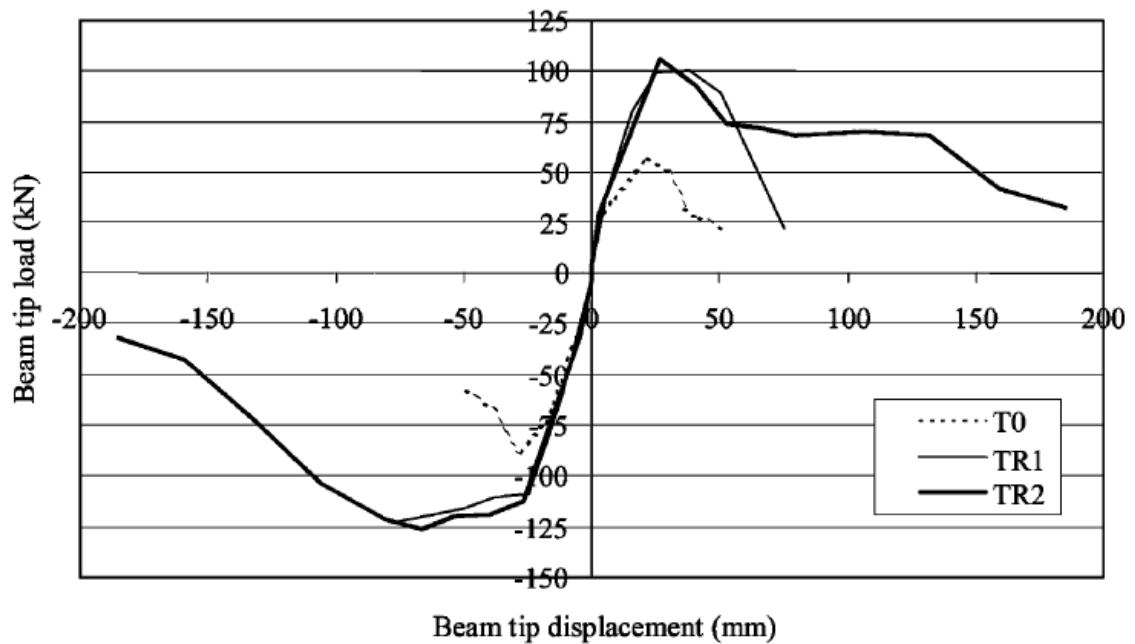
Figure 2.21: Hysteretic loop envelopes of the test specimens [El-Amoury and Ghobarah 2002]

28

(Braga, Gigliotti et al. 2009) studied the inelastic seismic behavior of reinforced concrete existing buildings with smooth bars and low strength concrete by testing four internal and exterior reinforced concrete beam-column joints under increasing cyclic horizontal displacement up to the failure. Results show the bond slips of longitudinal bars and shear failure in exterior as shown in **Fig. 2.22**.

Figure 2.22: T-Joint specimen: beam and joint panel cracks pattern at failure [(Braga, Gigliotti et al. 2009]

(Sasmal, Ramanjaneyulu et al. 2011) investigated the aspects of repair and retrofitting techniques adopted for reinforced concrete beam-column joint specimen under cyclic loading. Specimens were designed under seismic specification of Indian standard but without adopting ductile detailing (Non-Ductile) and repaired with epoxy mortar and grout using low viscous polymer and retrofitted using FRP wrapping and steel plate as shown in **Fig. 2.23**. The test results show that retrofitted specimens regain their stiffness and show that cumulative energy dissipation obtained from retrofitted specimens was almost 25% more than that of original specimen as shown in **Fig. 2.24**.
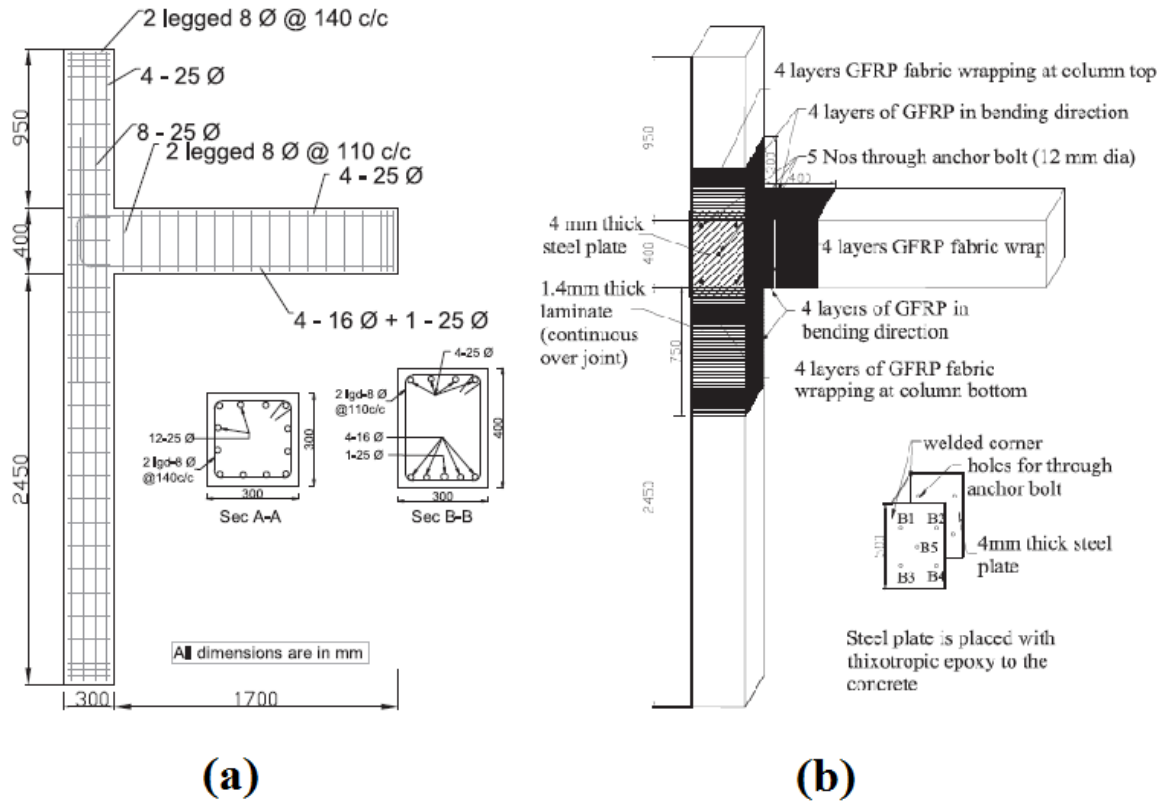
Figure 2.23: Reinforcement details of 'Non-Ductile' specimen and (b) Retrofitting scheme for damaged 'Non-Ductile' specimen [(Sasmal, Ramanjaneyulu et al. 2011]
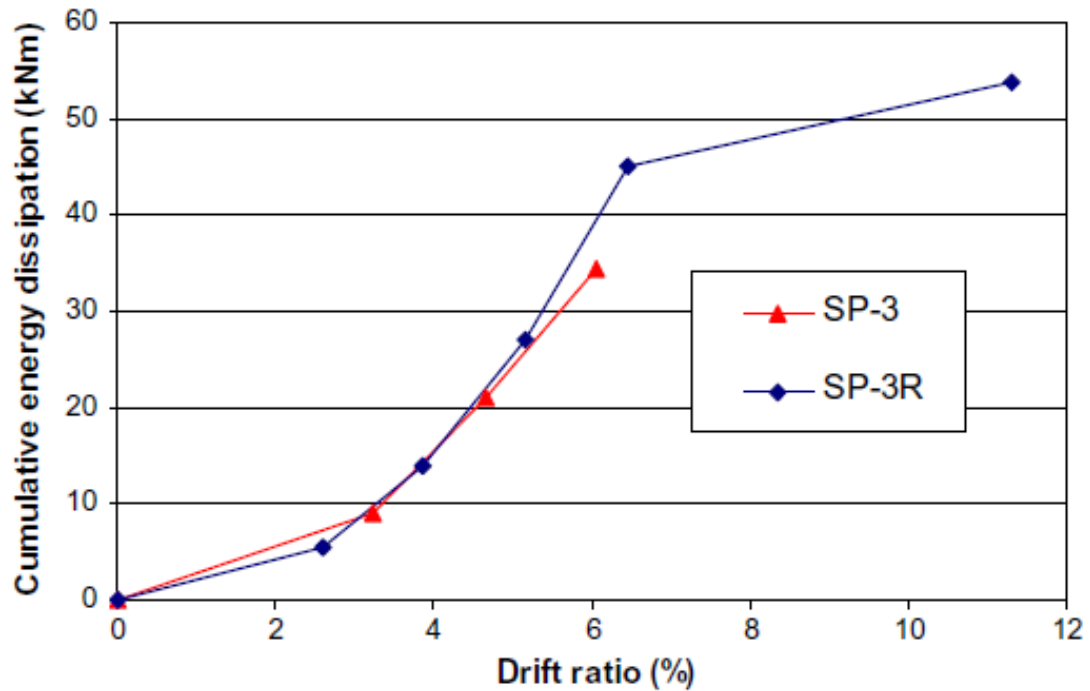
Figure 2.24: Comparison of Cumulative Energy Dissipation [(Sasmal, Ramanjaneyulu et al. 2011]

(Alsayed, Al-Salloum et al. 2010) have presented a practical technique for the seismic rehabilitation of poorly detailed beam-column corner joint using FRP composite sheets as shown in **Figs. 2.25 and 2.26**. A full scale corner beam-column sub-assemblage with inadequate joint shear strength and no transverse reinforcement in the joint is tested under reversed cyclic lateral load. The test results indicate improved shear capacity, ductility, higher load carrying capacity (**Fig. 2.27**) and slower stiffness degradation after FRP retrofit.
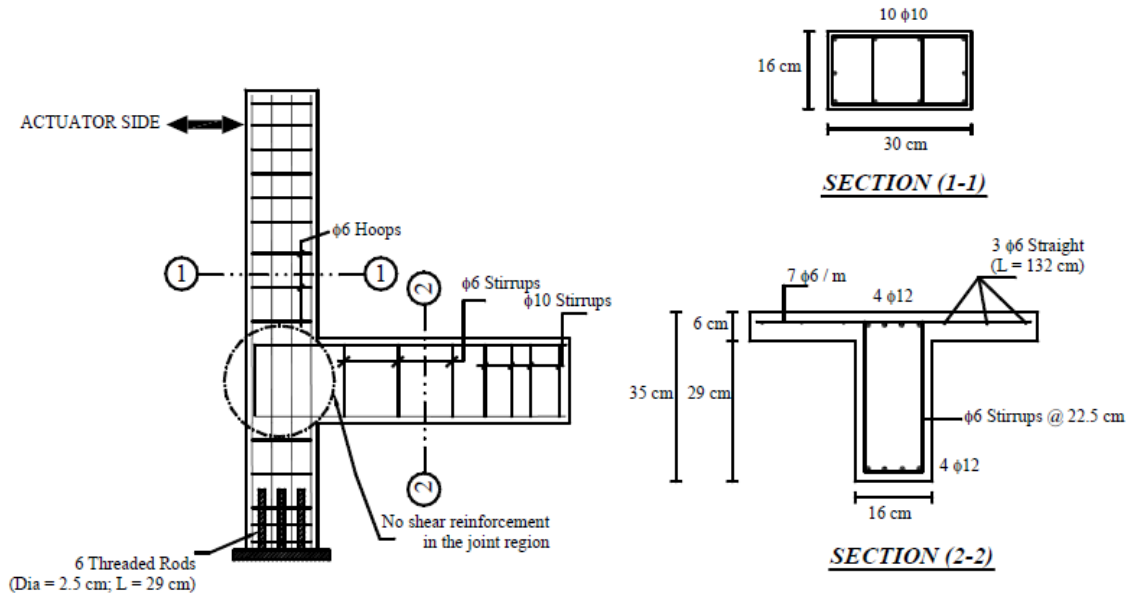
Figure 2.25: Reinforcement details of the As-Built specimen [Alsayed, Al-Salloum et al. 2010]

31
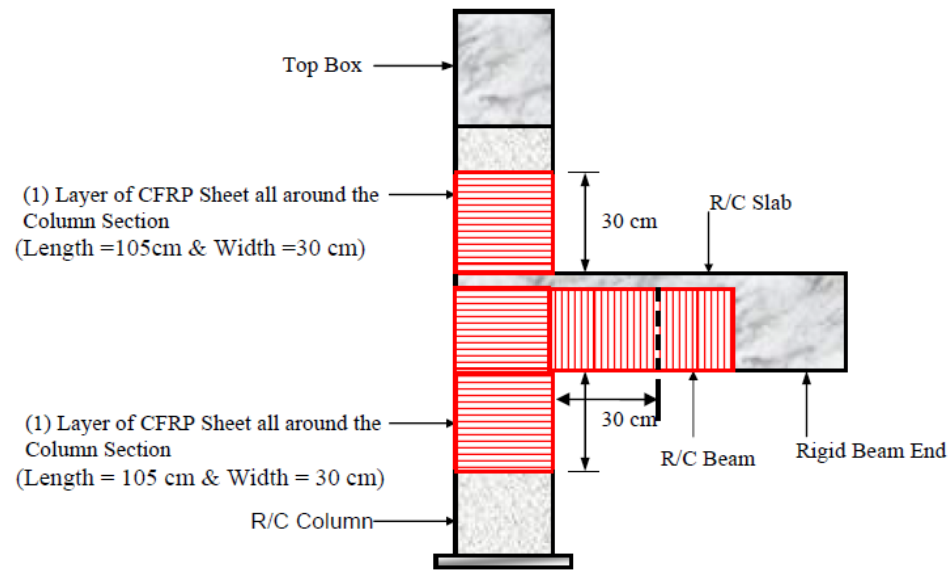
Figure 2.26: Final schematic representation of FRP scheme applied to As Built exterior joint [Alsayed, Al-Salloum et al. 2010]
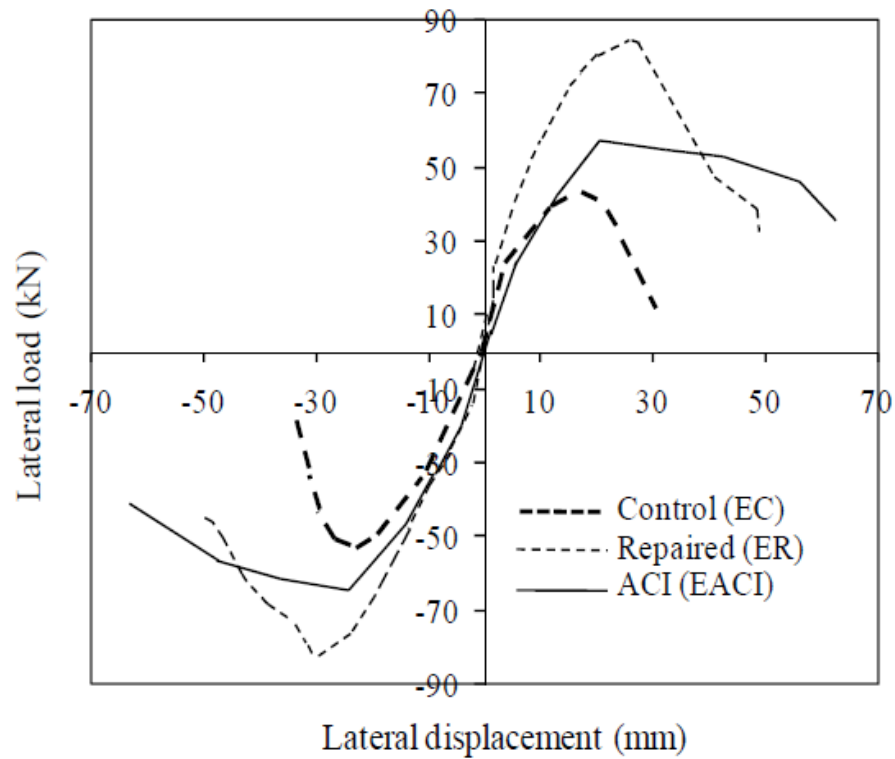
Figure 2.27: Envelopes of hysteretic plots for As-Built control, repaired and ACI based designed specimens [Alsayed, Al-Salloum et al. 2010]

2.3   Finite Element Studies in Beam-Column Joint

A number of experimental and analytical studies have been reported in the literature recently. The research has concentrated on CFRP retrofitting of exterior, interior and corner BCJ's performed experimental and numerical investigation on RC, wide beam-column joints when subjected to seismic loads. The experimental study was conducted by subjecting three full-scale wide exterior beam-column specimens to simulate seismic load. The experimental results were then used to validate a three-dimensional 3D-nonlinear finite-element model. Many researcher investigate the response of beam-column joints utilizing finite element software (Birely, Lowes et al. 2012). (Niroomandi, Maheri et al. 2010) utilized finite element analysis to study the behavior of beam column joint retrofitted by FRP sheet. (Baluch, Ahmed et al. 2013) performed a nonlinear finite element analysis of non-seismically detailed reinforced concrete beam-column connections with low concrete compressive strength. They tested half-scale non-ductile reinforced concrete beam-column joints. (Alhaddad, Siddiqui et al. 2011) investigated a numerical study to investigate the seismic behavior of FRP upgraded RC exterior beam-column joints. (Ibrahim and Mahmood 2009) presented an analysis model for reinforced concrete beams externally reinforced with Fiber Reinforced Polymer (FRP) laminates using finite elements in an ANSYS environment. The finite element models are developed using a smeared cracking approach for concrete and three dimensional layered elements for the FRP composites. The results obtained from the ANSYS finite element analysis are compared with the experimental data for six beams.

(Patil and Manekari 2013) model, Reinforced Beam-Column Joint Subjected to Monotonic Loading using ANSYS software as shown in **Fig. 2.28**. In this study, various

33

parameters are studied for monotonically loaded exterior and corner reinforced concrete beam-column joint. The corner as well as the exterior beam-column joint is analyzed with varying stiffness of beam-column joint. The behavior of exterior and corner beam-column joint subjected to monotonic loading is different. Various graphs like load vs. displacement (deformations), maximum stress, stiffness variations (i.e. joint ratios of beam-column joints) are plotted.
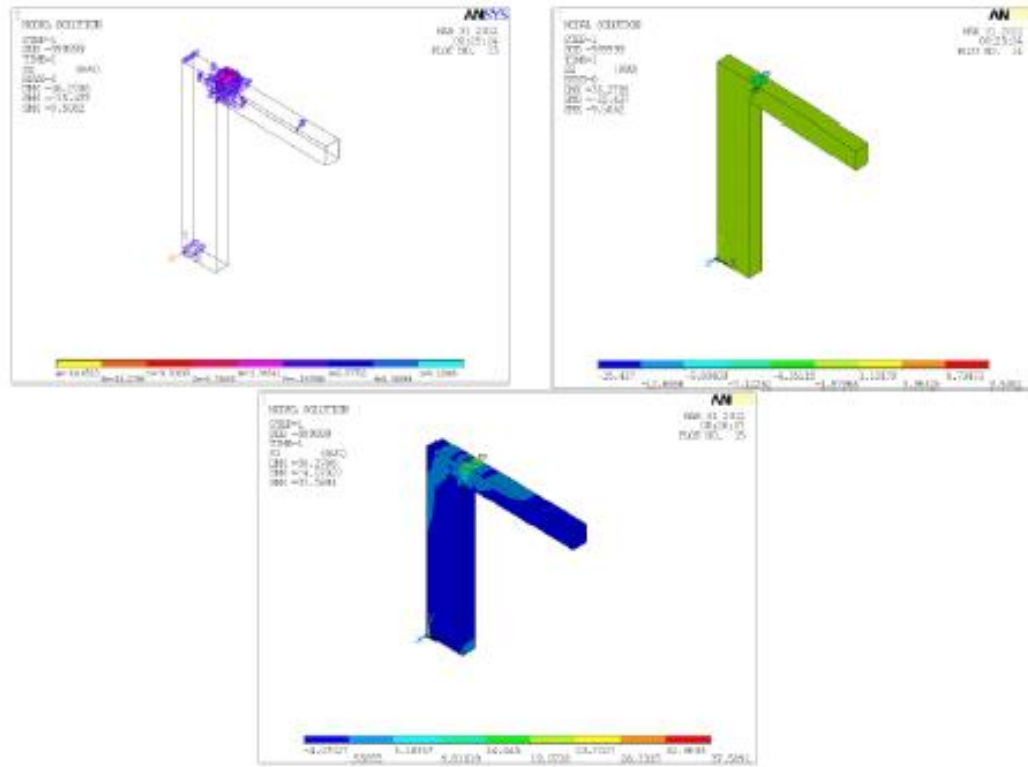
Figure 2.28: Modeling of corner beam-column joints in the ANSYS [Patil and Manekari 2013]

(Mostofinejad and Talaeitaba 2006) modeled and analyzed the non-linearly of the reinforced concrete beam-column joint with FRP overlays in ANSYS as shown in **Fig. 2.29(a)**. The model consists of the effect of anchorage slip and anchorage extension of steel. Results indicate the good match in the experimental and model prediction as shown in **Fig. 2.29(b)**.
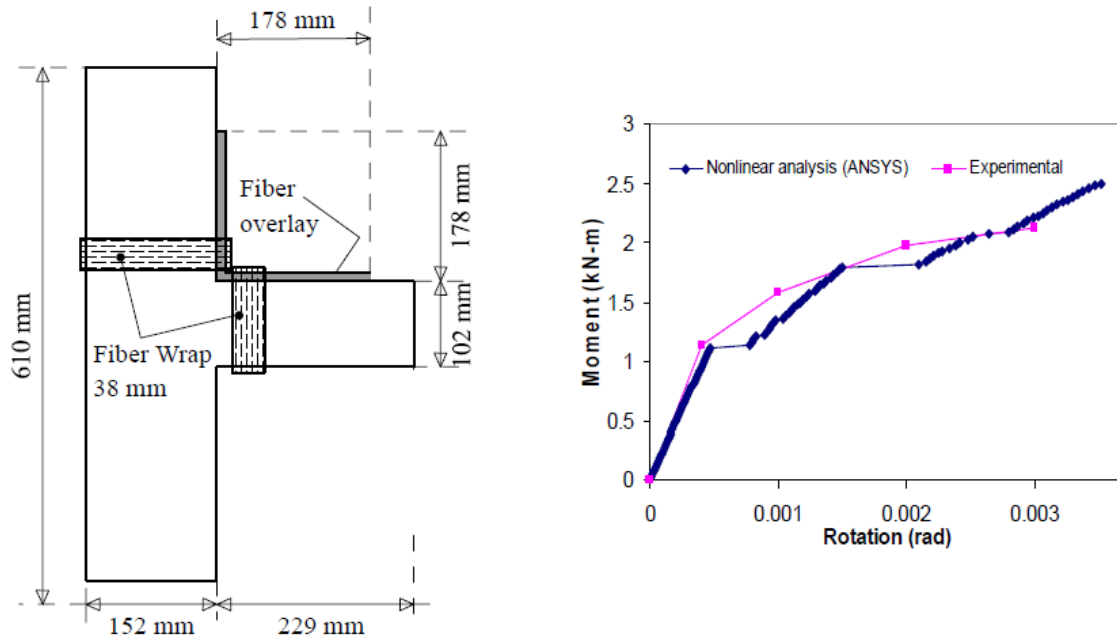
Figure 2.29: (a) FRP strengthening plan and (b) Moment-rotation curve for the joint [Mostofinejad and Talaeitaba 2006]

(Ravi and Arulraj 2010) modeled and analyzed three specimens using ANSYS in which one of the specimens has the seismic detailing and other two have non-seismic detailing for reinforcement. One of the non-seismic detail specimens were retrofit with CFRP as shown in **Fig. 2.30(a) and 2.30(b)**. In this study, the performance of exterior beam-column joints was compared with control specimen as shown in **Fig. 2.31**.
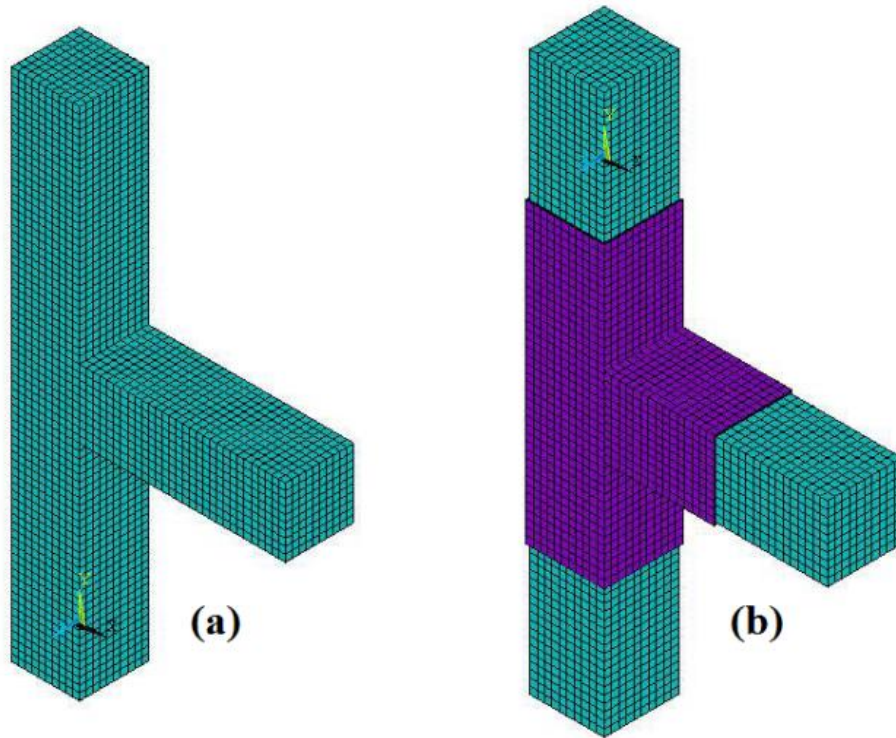
Figure 2.30: (a) Typical meshed (b) Typical meshed control specimen retrofitted specimen [Ravi and Arulraj 2010]
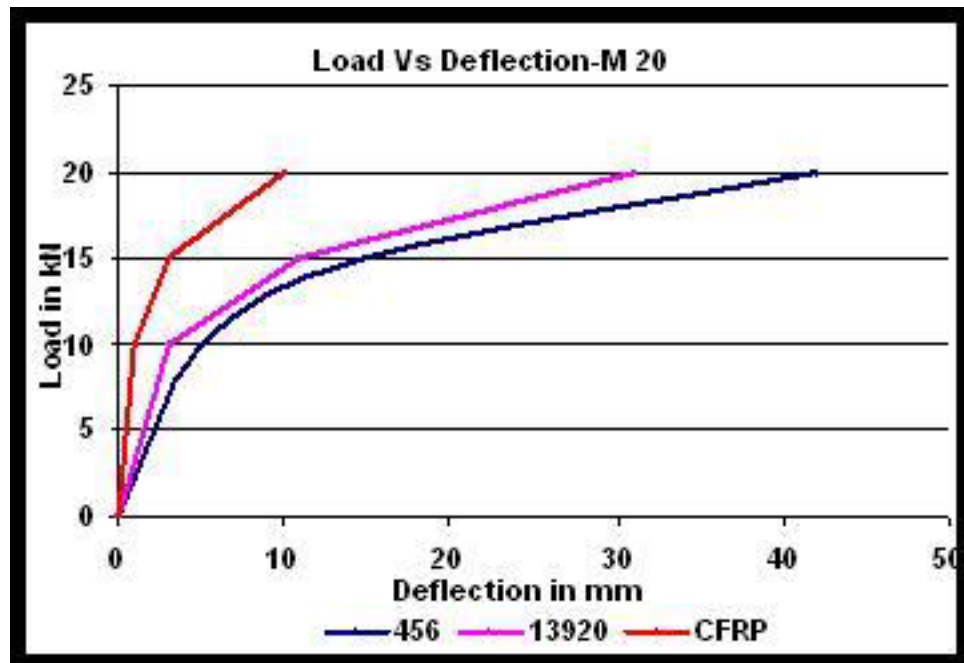
Figure 2.31: Load deflection curve for the retrofitted specimen control and retrofitted specimen [Ravi and Arulraj 2010]

(Bindhu and Jaya 2010) tested four beam-column joints in two groups, group A comprises of two joints with reinforced detailing as per Indian construction practice code IS 456:2000, and group B comprises of two specimens having additional cross bearing reinforcement for joint detail with the same IS 456:2000 as shown in **Fig. 2.32**. Finite element program ANSYS was used to model and analyze these specimens to validate the experimental results as given in **Fig. 2.33**.
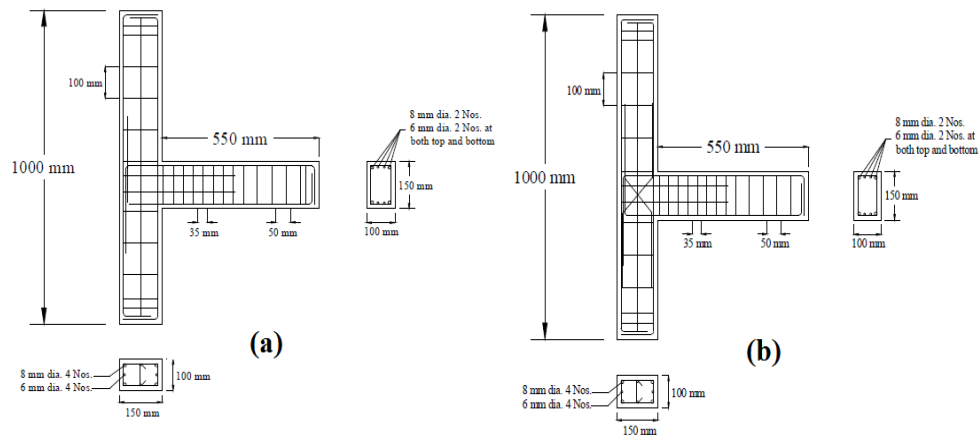
Figure 2.32: Reinforcement details of the specimens (a) Group A (As per IS: 456-2000) (b) Group B (As per IS: 456-2000 with Non-conventional reinforcement) [Bindhu and Jaya 2010]
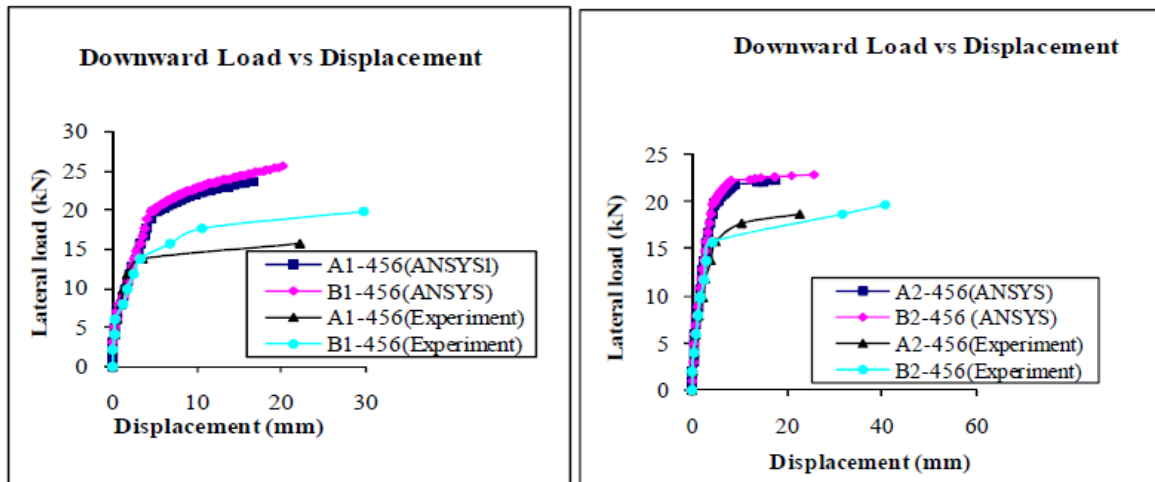
Figure 2.33: Comparison of load-displacement relations of models and specimens [Bindhu and Jaya 2010]

37

(Deaton 2013) investigated the behavior of nonseismically detailed reinforced concrete exterior beam-column joints subjected to bidirectional lateral cyclic loading using nonlinear finite element analysis. The simulated joints included: a one-way exterior joint, a two-way beam-column exterior corner joint, and a series of two-way beam-column-slab exterior corner joints with varying degrees of seismic vulnerability. The two-way corner joint specimens were evaluated under simultaneous cyclic bidirectional lateral and cyclic column axial loading. For each specimen, the ability of the prototype model to capture the strength, stiffness degradation, energy dissipation, joint shear strength, and progressive failure mechanisms (e.g. cracking) was demonstrated.

2.4 Carbon Fiber Reinforced Concrete (CFRC) Sheet and Adhesive Material

2.4.1 CFRP Sheet

Carbon Fiber Reinforcement Polymer (CFRP) has a strong and light fiber-reinforced polymer that contains carbon fibers CFRP has many uses such as:

- Increasing the load capacity of structures which includes slabs, beams, and bridges for shear and bending, or columns.

- Improving capacity of damaged elements such as steel reinforcement corrosion, and vehicle impact.

- Useful in service improvements such as reduced deflection and crack width reduction.

The characteristic of CFRP has some advantages such as:

- Very high strength.

- Flexibility of surface geometry (Beams, columns, chimneys, piles, walls, silos)

- Lightweight and low density.

- Non-corrosive.

- Combinations of high strength and modulus of elasticity available.

- Excellent durability.

- Easy to install, especially overhead.

- Economical, compared to traditional techniques.

- CFRP bonded to the concrete slab over the negative moment region. A mid-strength carbon fibers with fiber orientation of 0° (Unidirectional) was selected.

- This fiber has a fiber density of 1.8g/cm^3, the tensile strength is 3800 N/mm^2 and elongation at break is 1.8%. The tensile E-modulus is 63 KN/mm^2. **Fig. 2.34** shows the stress-strain diagram for CFRP.
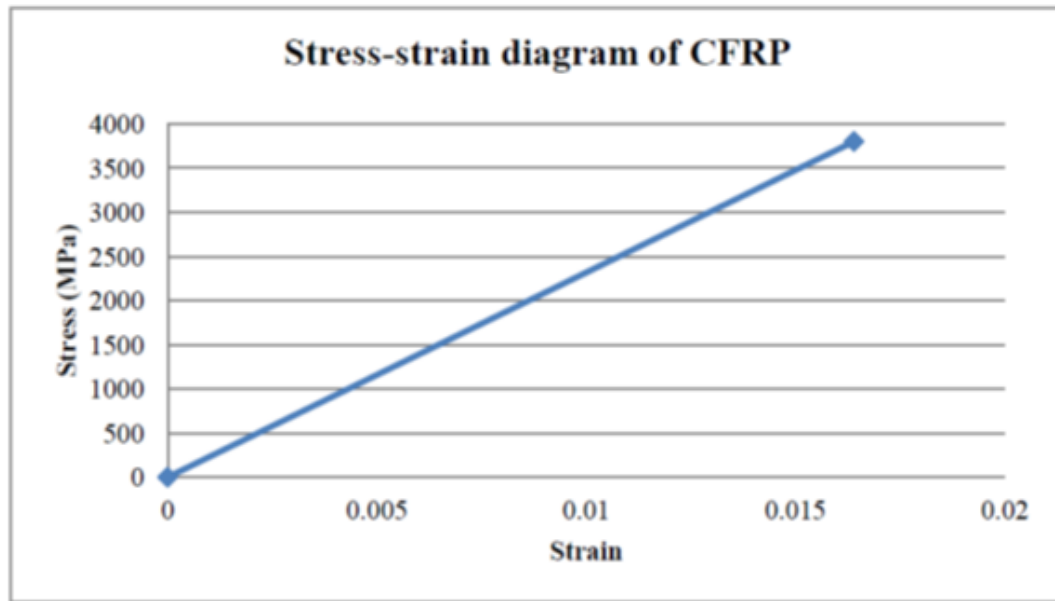
Figure 2.34: Typical Stress-strain diagram for CFRP

2.4.2 Adhesive Materials

Adhesive materials (epoxy) are used to make the interaction between structural elements and CFRP. Many types of adhesive materials could be used to connect concrete with CFRP such as 2-part epoxy impregnation resin, and adhesive for bonding reinforcement. 2-part epoxy impregnation resin has some properties that make it proper for connecting CFRP with concrete such as:

- Easy mix and application by trowel and impregnation roller.
- Manufactured for manual saturation methods.

- Excellent application behavior to vertical and overhead surfaces.

- High mechanical properties.

- No separate primer required.

- Solvent free.

- CFRP bonded to the concrete slab using 2-part epoxy impregnation resin. The tensile strength of this material is 30 N/mm^2 and elongation at break is 0.9%. The flexural elastic modulus is 3800 N/mm^2, and Tensile E-modulus is 4500 N/mm^2, and the shear strength of epoxy is 22 N/mm^2.

CHAPTER 3

THEORETICAL PRELIMINARIES

3.1   Mechanistic Analysis

3.1.1   Mode of Failure of Beam – Column Joint

The behavior of a beam-column joint region in a reinforced concrete structure is not easily understood. Number of adjoining members with complex stress fields converges at one point. Flexural moments and shear stresses are transferred into the joint from the beam and axial, and shear stresses are transferred into the joint region from the column. To understand joint forces, we need to know the loading on beams and columns.

3.1.2   Loading on Beams and Columns

Under lateral loading (as in the case of seismic loading), an assumption is made that inflection points occur at the midpoint between floors are in the column where the bending moment is zero; moment within the top and bottom story columns at the beam-column joint is the same as the moment at the end of the beam, M_n.

The moment reaction at the joint interface, M_n equation [3.1]:

$$M_n = P \times l_p \tag{3.1}$$

Where:

P is the load

l_p is the distance from the tip of the beam where the load is applied to the column face as shown in **Fig. 3.1**.

The shear force in the column can be calculated by equation [3.2].

$$V_c' = \frac{M_n}{l_{pc}} \qquad\qquad [3.2]$$

Where:

V'_c is the shear force in the column, and l_{pc} is the distance between column inflection points as given in **Fig. 3.1**.
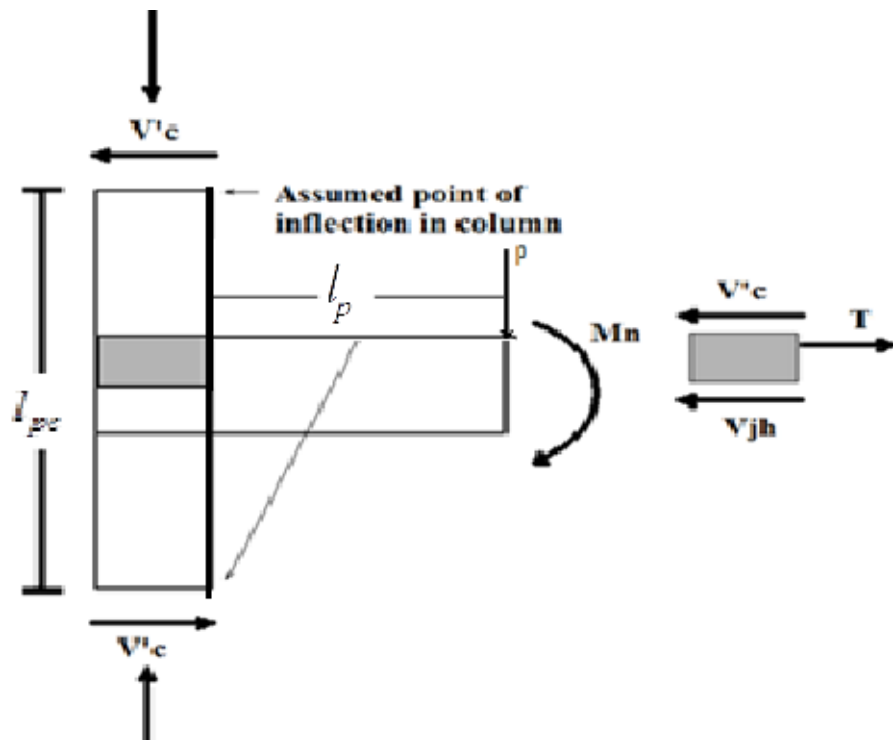
Figure 3.1: Forces in beam-column joints

43

Fig. 3.1 shows that the horizontal shear force in the joint is a combination of the shear carried down through the column and tensile force in the beam reinforcement framing into the joint as given by equation [3.3].

$$V_{jh} = T - V_c'$$

[3.3]

Where:

T is equal to the tensile force in the beam longitudinal reinforcement and V'$_c$ is the total shear in the column above the joint.

The strength of the beam-column joint is governed by the shear strength and this shear is the combination of horizontal shear force V_{jh} and vertical shear force as shown in **Fig. 3.2** considering the free body diagram in mid-width of the joint of the vertical shear force V_{jv} is given in equation [3.4].

$$V_{jv} = T' + C_c'' + C_s'' - V_b$$

[3.4]
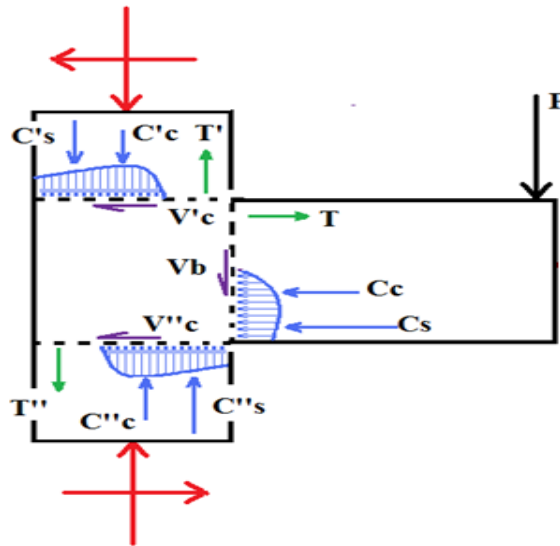
Figure 3.2: Stresses in beam-column joints

44

3.1.3 Exterior Beam-Column Joint Shear Strength Requirement

Instead of using horizontal and vertical joint shear forces and stresses, the principal tensile stress is used as an index in determining the joint shear capacity as shown in **Fig. 3.3**.
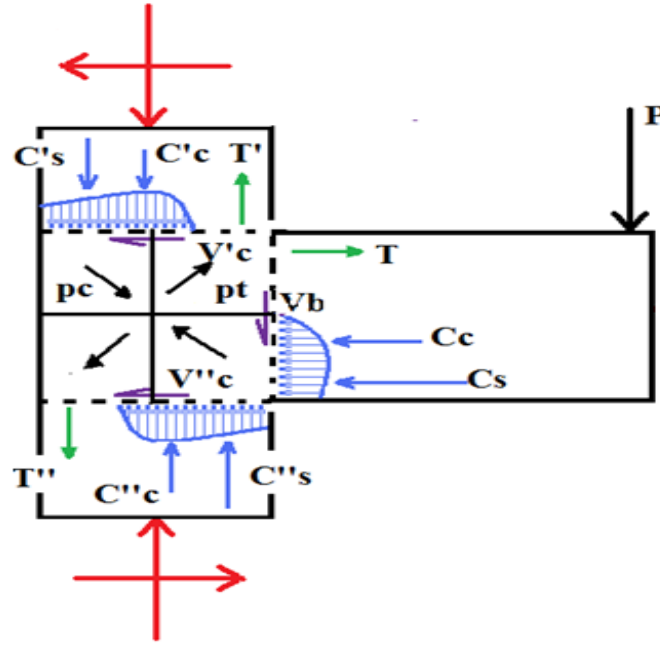
Figure 3.3: Principle tensile stresses in beam-column joints

From Mohr's circle, the principle tensile stress in the joint is expressed as:

$$\sigma_{1,2} = \frac{\sigma_x + \sigma_y}{2} \pm \sqrt{\left(\frac{\sigma_x - \sigma_y}{2}\right)^2 + \tau_{xy}^2} \qquad [3.5]$$

Where:

σ_x = stress on plane parallel to the longitudinal axis of the member which is equal to the axial stress (σ_a) on the column; σ_y = normal stress plane perpendicular to the axis of

member, which is zero for the joint; and τ_{xy} = shear stress which is equal to v_{jh}, so, for the

exterior joints, equation [3.6] can be written as:

$$\sigma_1 = \frac{\sigma_a}{2} + \sqrt{\left(\frac{\sigma_a}{2}\right)^2 + v^2_{jh}}$$ [3.6]

Where:

σ_a = column axial stress (N/A_g)   (negative when N compression)

v_{jh} = horizontal shear stress (v_{jh}/A_j)

3.1.4 Failure Mode for Exterior Beam-Column Joint

If principle tensile stress of joint (σ_1) becomes equal to the tensile strength of concrete f_t, this will result in a diagonal crack in the joint. When the loading is reversed, a crack in the other diagonal direction will result, leading to X-shaped cracking in the joint **Figs. 3.4 and 3.5**.
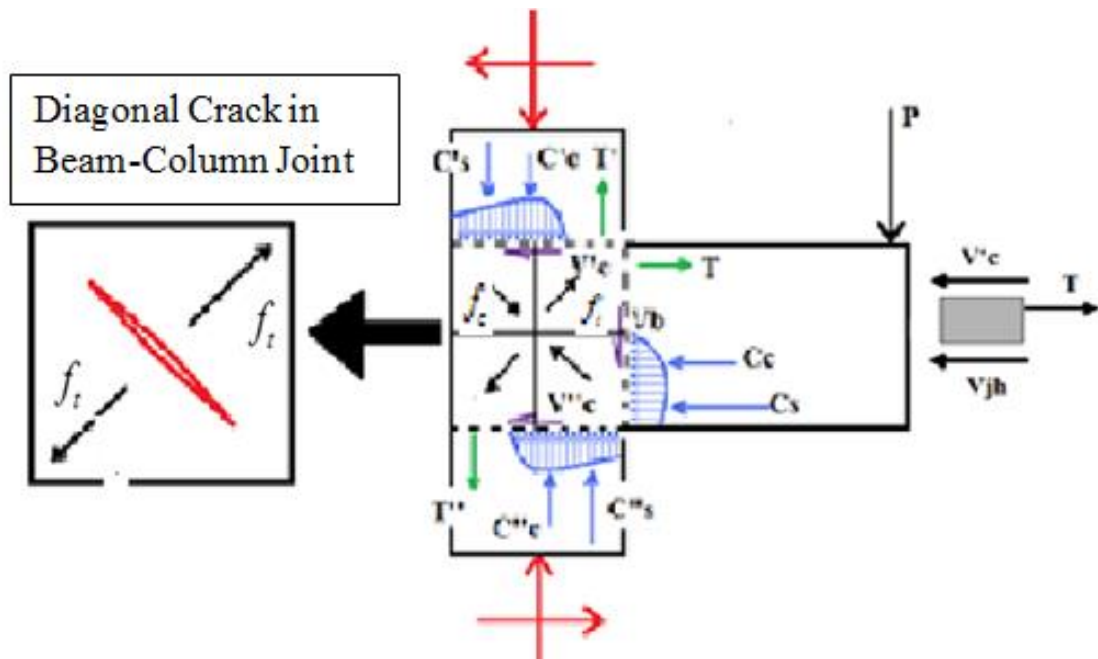
Figure 3.4: Diagonal crack in beam-column joints
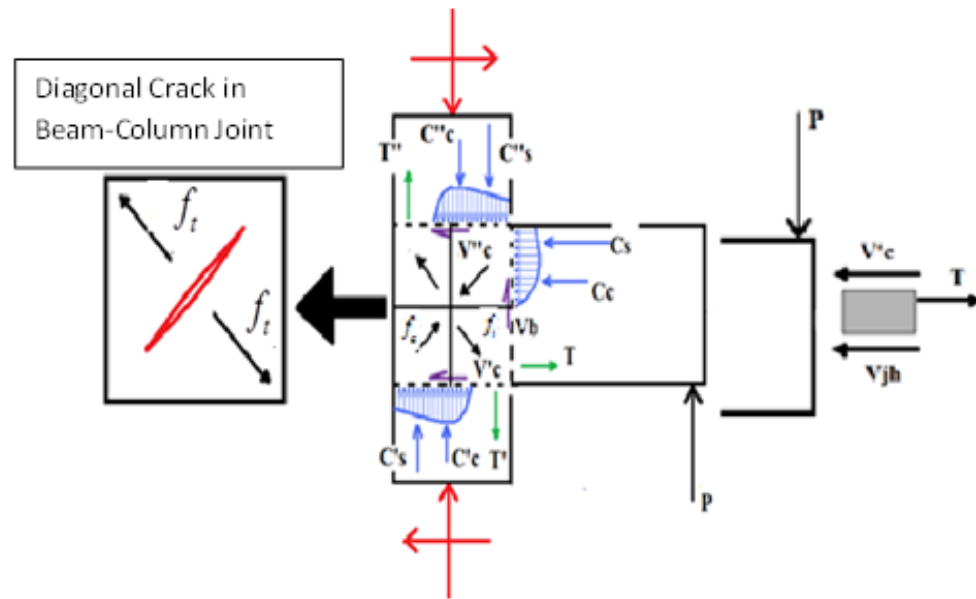
Figure 3.5: Diagonal crack in beam-column joints on load reversal

The force acting on exterior BCJ is shown in **Figs. 3.4 and 3.5**.

The shear force in the joint gives rise to diagonal cracks thus requiring proper detailing of the joint. The detailing patterns of longitudinal reinforcements of beam significantly affect joint efficiency. Some of the detailing patterns for exterior joints are shown in **Fig. 3.6(b)** and **Fig. 3.6(c)**. The bars if bent away from the joint core **Fig. 3.6(b)** result in efficiencies of 25-40% while those passing through and anchored in the joint core **Fig. 3.6(c)** shows 85-100% efficiency. However, the stirrups should also be provided to confine the concrete core within the joint.
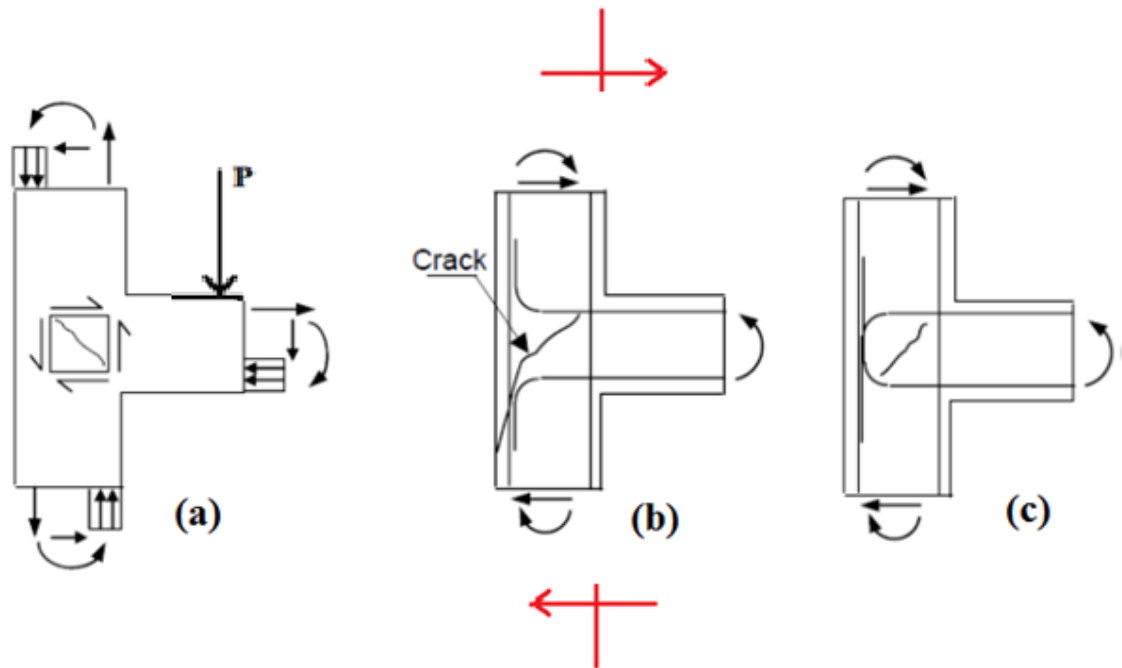
Figure 3.6: (a) Forces in exterior beam-column joint (b) Exterior joint with Bent up bar (c) Exterior joint with Bent in bar

3.2 Theoretical Consideration of Shear Strength of BCJ using CFRP

Beam shear force (V), column axial force (N), resulting shear (τ_v), and axial stresses (σ_N) in the joint, and corresponding principal stresses ($\sigma 1$ and $\sigma 2$) in the joint core are given in **Fig. 3.7(a)**. The Mohr circle for these stresses is shown in **Fig. 3.7(b)**. Since, there is no shear reinforcement in the joint, for reference specimens, shear failure is assumed to correspond to the formation of a diagonal crack in the joint. Diagonal crack is assumed to form when principal tensile stress reaches the tensile strength of concrete. Consequently, shear failure of the joint is a function of the tensile strength of the concrete. Frequently, concrete tensile strength, $f_{ct} = (\sigma 1)$, is related to splitting cylinder tension tests and it was found to be approximately proportional to $\sqrt{f'_c}$. Therefore, concrete tensile strength is expressed as $f_{ct} = c\sqrt{f'_c}$, where C is a constant (ACI 318-02 2008 suggests a C value of 0.5). Thus, considering the level of compressive strength of concrete, coefficient C is assumed as 0.5 for calculating the concrete tensile strength. Principal stresses under normal and shear stresses can be calculated by using Eq. [3.7], according to Mohr's theorem.
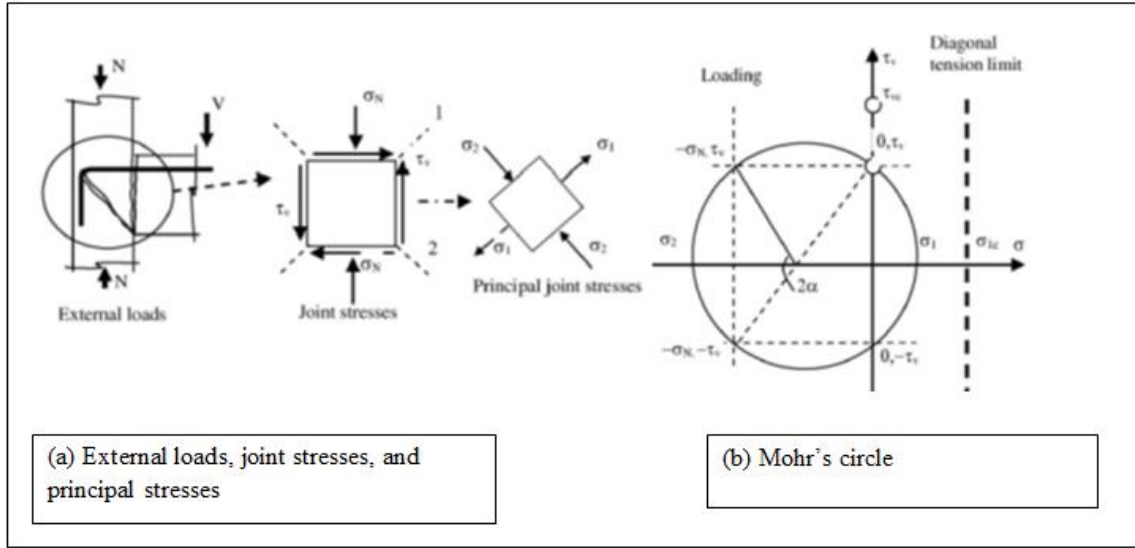
Figure 3.7: (a) External loads, joint stresses, and principal stresses; (b) Mohr's circle

$$\sigma_{1,2} = \frac{\sigma_x + \sigma_y}{2} \pm \sqrt{\left(\frac{\sigma_x - \sigma_y}{2}\right)^2 + \tau^2_{xy}} \qquad [3.7]$$

Where σ_x = stress on plane parallel to the longitudinal axis of the member which is equal to the axial stress (σ_N) on the column; σ_y = normal stress on plane perpendicular to the axis of the member, which is zero for the joint; and τ_{xy} = shear stress. For the tested joints, Eq. [3.7] can be rewritten as Eq. [3.8]. The shear stress is a function of principal tensile stress ($\sigma 1$), and can be obtained by Eq. [3.9] by making use of Eq. [3.8]. Assuming failure occurs when $\sigma 1$ reaches the tensile strength of concrete, the shear strength of the joint can be calculated by Eq. [3.10], where $\sigma_N = \frac{N}{A_g}$ and Ag = gross cross-sectional area of the column. The contribution of concrete to the shear capacity of the joints of the reference specimens can then be calculated by Eq. [3.11], where d = effective depth of the column. The joint shear strengths of the reference specimens depend only on the contribution of concrete because there is no shear reinforcement in the joint core

$$\sigma_{1,2} = \frac{\sigma_N}{2} \pm \sqrt{\left(\frac{\sigma_N}{2}\right) \pm \tau^2{}_v} \qquad [3.8]$$

$$\tau_v = \sigma_1 \sqrt{\left(1 - \frac{\sigma_N}{\sigma_1}\right)} \qquad [3.9]$$

$$\tau_{vc} = 0.5\sqrt{f'_c} \sqrt{\left(1 + \frac{N}{0.5\sqrt{f'_c} A_g}\right)} \qquad [3.10]$$

$$V_c = \tau_{vc} \times b \times d \qquad [3.11]$$

Shear capacity of the CFRP-retrofitted joints is calculated by using truss analogy (Priestley 1996). The shear capacity of the joint is assumed to be the sum of the contribution of the concrete and the CFRP. The shear force, which is resisted by the CFRP in the direction of the fibers (diagonal to beam axis) can be calculated by Eq. [3.12]. In this equation, ε_{fe} is the effective strain of the CFRP sheets, which is assumed to be the minimum of 0.004 or 0.5 ε_{frpult}, as suggested by different codes (ACI 440 2008; CSA S806-02 2002). E_f and A_f = modulus of elasticity and effective cross-sectional area of the CFRP sheets in diagonal direction; and ε_{frpult} = ultimate strain value given by the manufacturer. The contribution of CFRP sheets to the shear capacity in a horizontal or vertical direction can be calculated by Eq. [3.13], and the total shear capacity of the retrofitted joint (V_t) can be calculated by Eq. [3.14].

$$F_{CFRP} = \varepsilon_{fe} \times E_f \times A_f \qquad [3.12]$$

$$V_{CFRP} = F_{CFRP} \times \sin 45° \qquad [3.13]$$

$$V_t = V_c + V_{CFRP} \qquad [3.14]$$

CHAPTER 4

EXPERIMENTAL INVESTIGATIONS

4.1   Introduction

In this study, several experimental tests have been carried out including concrete

mechanical properties test, steel tensile test and complete beam-column joint under

monotonic and cyclic loading. The tests conducted in this study are as follows:

1. Mechanical properties tests of concrete.

2. Mechanical properties tests of steel bar.

3. Full-scale beam-column joint test.

The data found from the above-mentioned tests will be used in the numerical simulation.

The flow chart of the experimental and numerical programs is shown in **Fig. 4.1**.

4.2 Mechanical Properties of Concrete

Concrete used in the specimens is ready mixed with the required strength of 30 MPa with 110 mm slump and with 25 mm maximum size aggregate. Specimens were cast in the KFUPM lab and in a construction company at Dammam. Nine cylinders of 150 x 75 mm were cast and compression tests were performed in the lab to determine the concrete strength at the time of testing of specimens.

Three main tests have been conducted to sandstone material. These tests include:

- Compression tests
- Tension tests

The procedures and details of all tests were based on ASTM specifications.
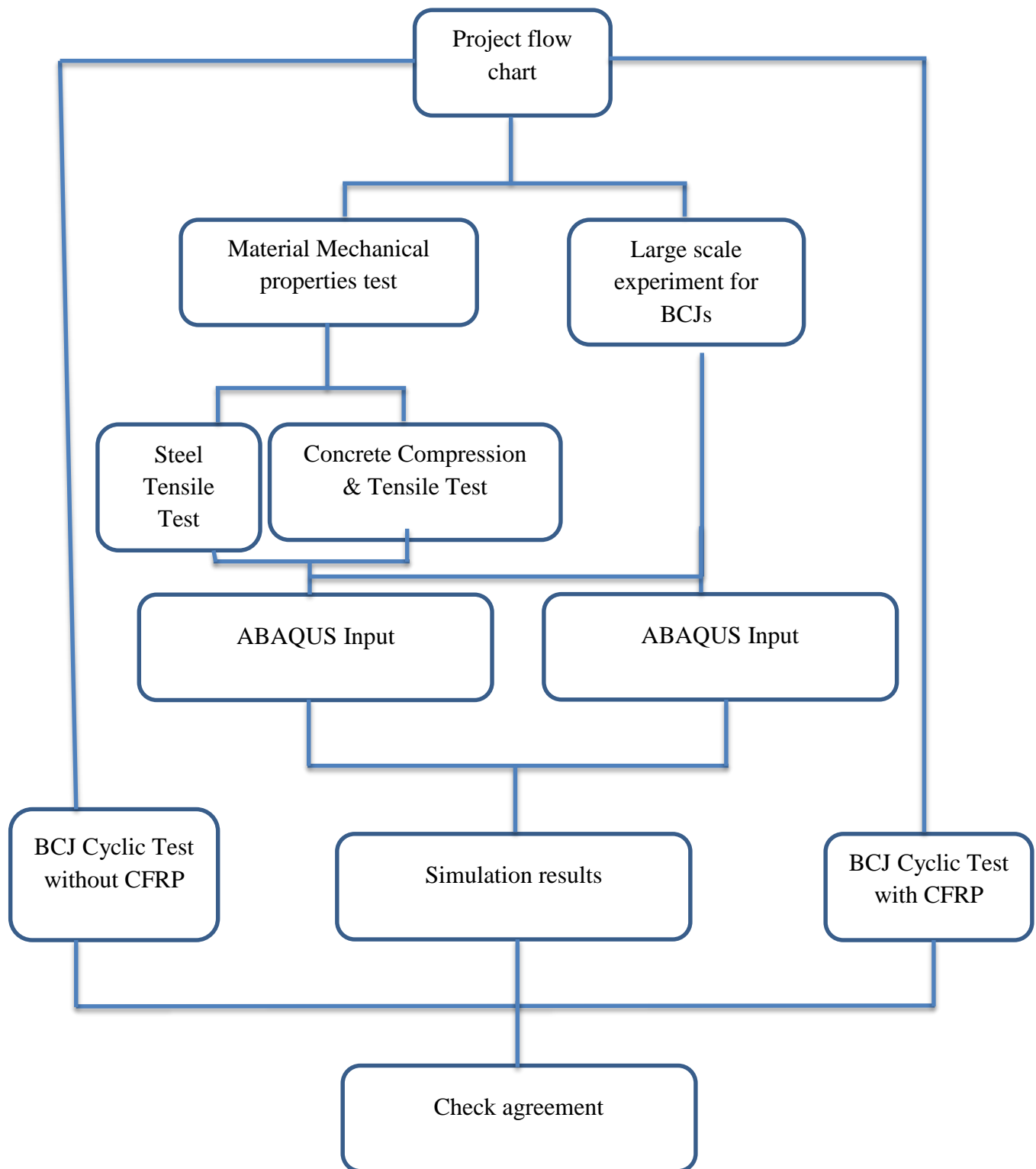
Figure 4.1: Flow chart of the experimental investigation and modeling

4.2.1 Concrete Compression Test

For compression test, three cylindrical specimens 75x150 mm as shown in **Fig. 4.2** were used to find the compressive behavior of the concrete material, and in order to get the full stress strain curve for concrete under compression, low rate load were applied using strain gauge in vertical and horizontal direction. The setup for the compression test is shown in **Fig. 4.4**. The stress-strain curve for the three cylinders is shown in **Fig. 4.5**. The average compressive strength is 34 MPa, and the modulus of elasticity is 29,000 MPa. In order to measure the workability of the concrete, a slump test was conducted and the slump was 110 mm as shown in **Fig. 4.3**. In order to include the data for evolution of uniaxial stress and damage with increment in plastic strain for concrete and reinforcing steel, **Fig. 4.6** shows the stress-plastic strain data for concrete in compression obtained from the tests conducted.
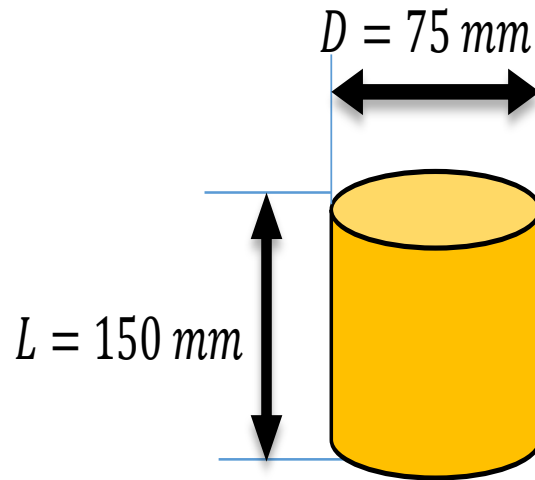
Figure 4.2: Dimensions of cylinders test under uniaxial compression

Figure 4.3: Slump test for fresh concrete

Figure 4.4: Cylinder test for concrete compressive strength
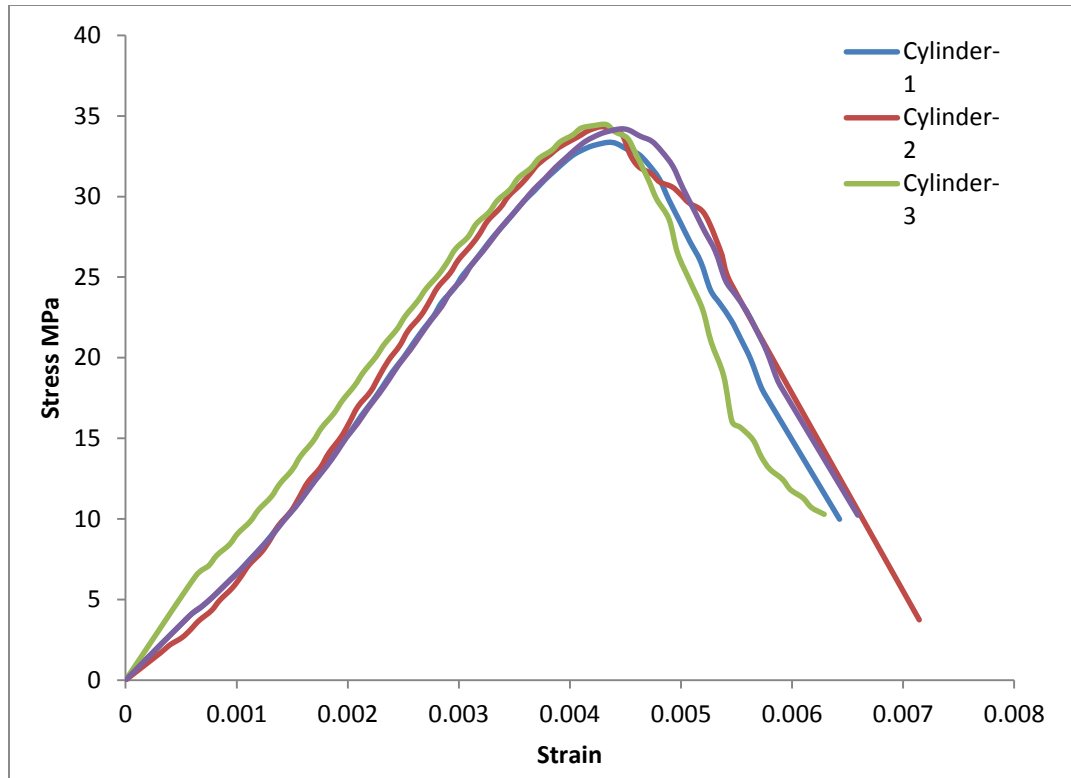
Figure 4.5: Stress-Strain curve for concrete under compression
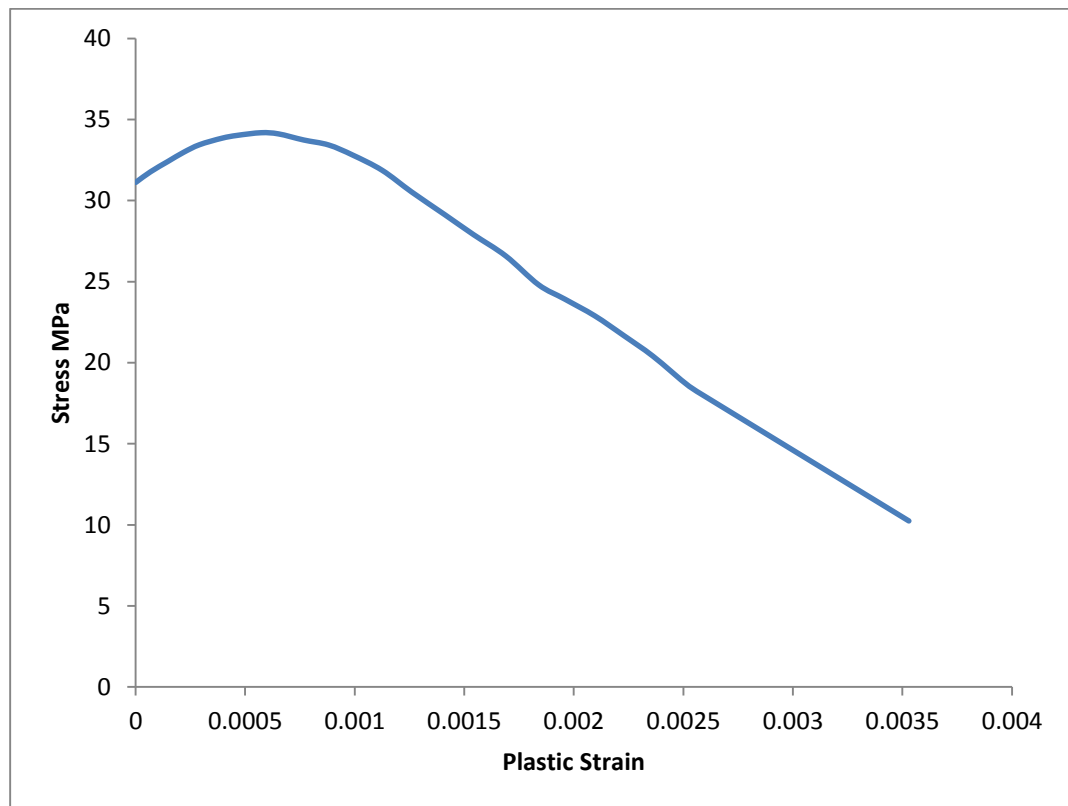
Figure 4.6: Stress-plastic strain curve for concrete under compression

58

4.2.2 Concrete Tensile Test

In tension test, split test has been adopted.

4.2.2.1 Split Tension Tests

This test is a standard test used to find indirectly the tensile strength of cylinder specimens. ASTM-D3967 and C496 cover testing apparatus, specimen preparation, and testing procedures for determining the splitting tensile strength. As shown in **Figs. 4.7 & 4.8**, the dimension of the specimen and the test setup are shown.
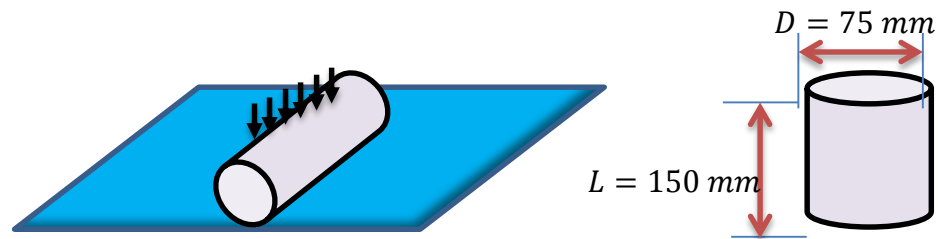
Figure 4.7: Depiction of concrete cylinder used in split test

Figure 4.8: Concrete specimen under split test.

Splitting tensile strength can be calculated by the following equation:

$$f_t = \frac{2P}{\pi l d}$$ [4.1]

Where:

P: applied load (39.4 kN)

L: length of cylinder (150 mm)

D: diameter of specimen (75 mm)

From the result of the split test, the tensile stress is equal to 2.2 MPa, and tensile strength for concrete can be calculated from the following formula:

$$f_t = 0.33\sqrt{f_c'} = 1.81\,\text{MPa}$$ [4.2]

The stress-strain curve reveals that the sandstone behavior is very brittle under uniaxial tension test. Typical result of direct tension test is shown in **Fig. 4.9**.
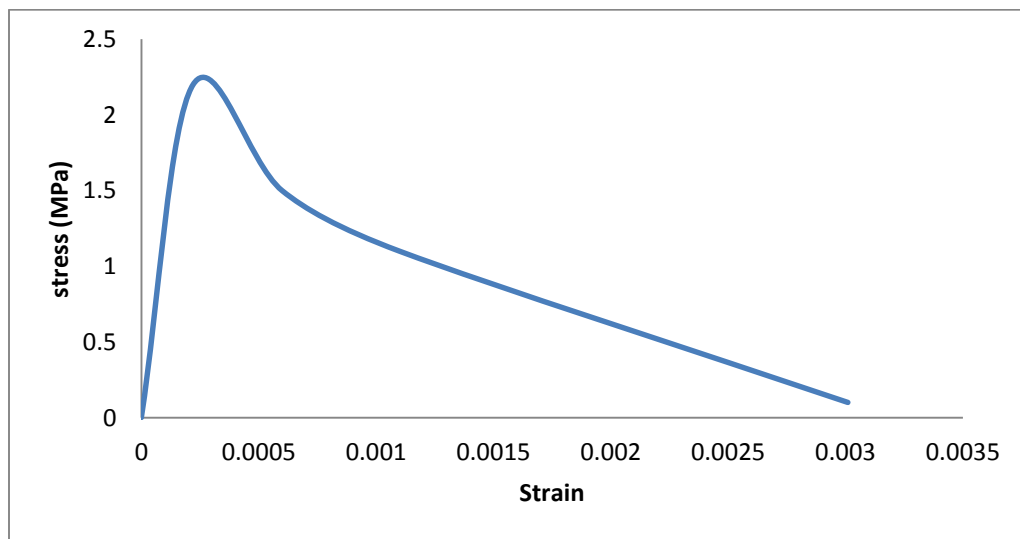
Figure 4.9: Stress-Strain curve of concrete

4.3   Steel Tensile Strength

In all three specimens, longitudinal and transverse reinforcement were 12 mm, 18 mm diameter and 8 mm diameter were used. Tensile test was carried out to determine the actual tensile strength of reinforcement. The properties of the reinforcements are summarized in **Table 4.1** and stress-strain curves are given in **Fig. 4.10** while the stress inelastic strain for the steel is given in **Fig. 4.11**. The actual tensile strength f_y of the reinforcement was used in the calculation of nominal moment capacity M_n of the beam for each specimens.

Table 4-1: Mechanical Properties of Reinforcement

Reinforcements	Diameter (mm)	Fy (MPa)
Φ12	12	568
Φ18	18	593
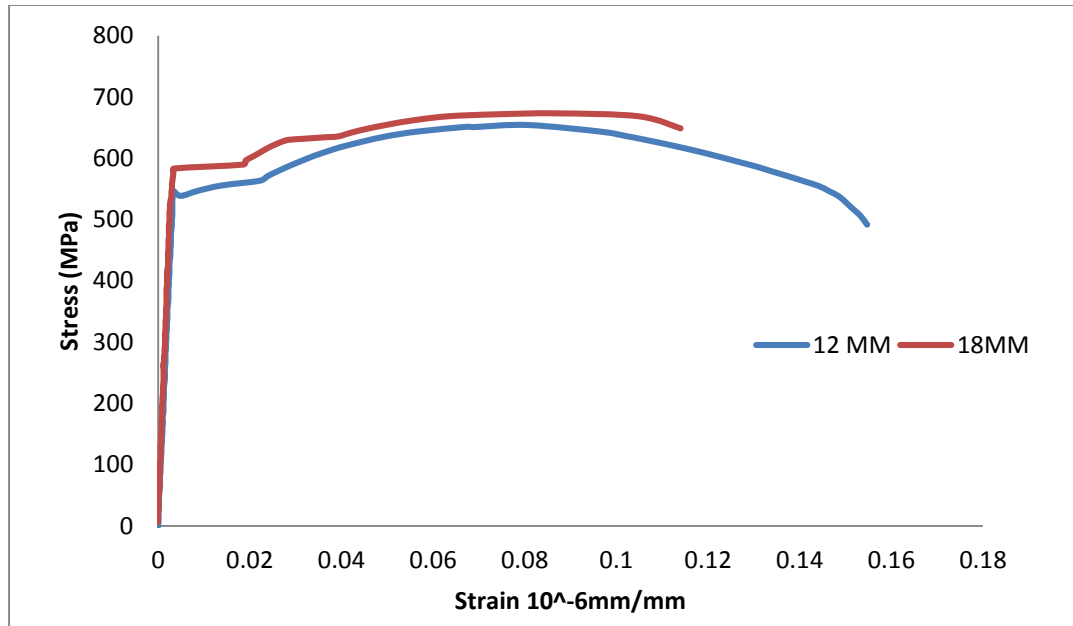
Figure 4.10: Stress-Strain graph for 18 mm diameter reinforcement
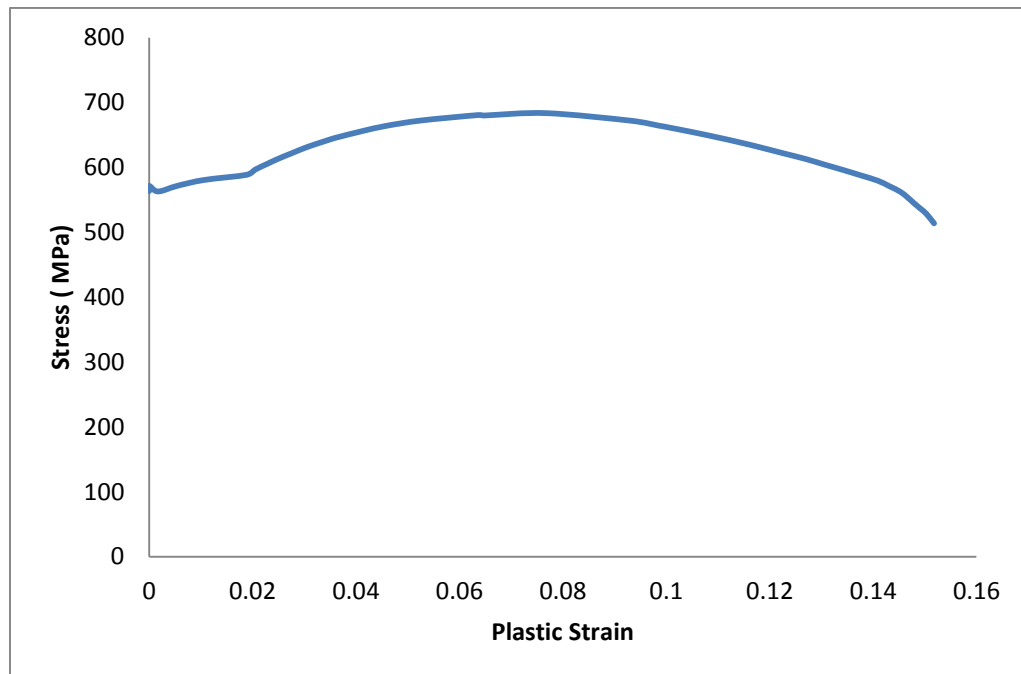
Figure 4.11: Stress-Plastic strain for steel

4.4   Test Setup and Preparation

In order to investigate the behavior of reinforced concrete deficient shear beam-column joints retrofitted with CFRP sheet, experimental test was carried out on thirteen different kinds of specimens with inadequate joint shear strength and no transverse reinforcement in the joint. The difference between these specimens is the detailing of bent of the longitudinal reinforcement of beam in the joint and the existing of CFRP sheet as shown in **Fig. 4.12**. The difference and details of all eight specimens are given in **Tables 4.2 and 4.3** for the monotonic and cyclic tests, respectively to see the comparison of these eight non-seismically detail beam-column joints specimens as tested under cyclic loading up-to failure.

Table 4-2: Specimens Details for Monotonic Test

S. No.	No. of Specimens	Specimens	Details	Test Method
1	1	BCJ-12MM-Bent Up	Beam bars bent out in column having 12mm diameter	Monotonic
2	1	BCJ-12MM- Bent In	Beam bars bent in joint having 12mm diameter	Monotonic
3	1	BCJ-18MM – Bent In	Beam bars bent in joint having 18mm diameter	Monotonic
4	1	BCJ 12MM – Bent Up with CFRP	Beam bars bent out in column having 12mm diameter retrofitted with CFRP	Monotonic
5	1	BCJ-12MM - Bent In with CFRP	Beam bars bent in joint having 12mm diameter retrofitted with CFRP	Monotonic
6	1	BJI-18MM – Bent In with CFRP	Beam bars bent in joint having 18mm diameter retrofitted with CFRP	Monotonic

Table 4-3: Specimens Details for Cyclic Test

S. No.	No. Specimens	Specimens	Details	Test Method
1	1	BCJ-12MM-Bent Up	Beam bars bent out in column having 12mm diameter	Cyclic
2	1	BCJ-12MM- Bent In	Beam bars bent in joint having 12mm diameter	Cyclic
3	1	BCJ-18MM – Bent In	Beam bars bent in joint having 18mm diameter	Cyclic
4	1	BCJ 12M – Bent Up with CFRP	Beam bars bent out in column having 12mm diameter retrofitted with CFRP	Cyclic
5	2	BCJ-12MM - Bent In with CFRP	Beam bars bent in joint having 12mm diameter retrofitted with CFRP	Cyclic
6	1	BJI-18MM – Bent In with CFRP	Beam bars bent in joint having 18mm diameter retrofitted with CFRP	Cyclic

(a)Bent out Details for Beam Longitudinal Reinforcement

(b) Bent in Details for Beam Longitudinal Reinforcement
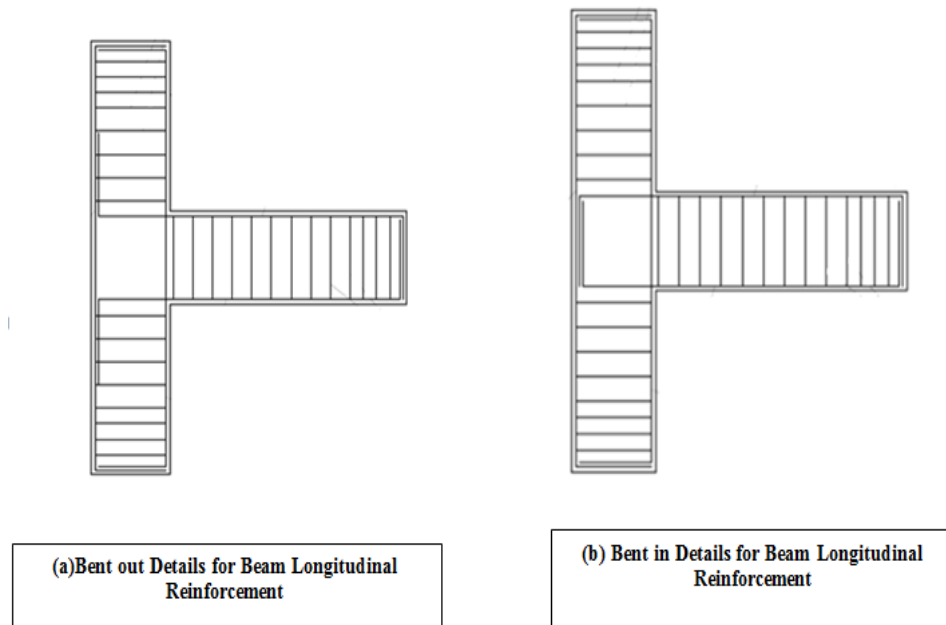
Figure 4.12: Specimens details

4.5 Specimens Details

4.5.1 Beam-Column Dimensions and Reinforcement Details

The configuration for beams and columns of the specimens were produced with same dimensions 250 mm x 300 mm, the cantilever length of beam was 900 mm and the height of column was 1400 mm. Dimensions were selected to represent approximately average sized beam-column joint, and were further limited by the dimensions of existing testing frame as given in **Fig. 4.13**.

Figure 4.13: Existing frame in KFUPM bab

Amount of longitudinal reinforcement was constant for BCJ-12 mm – Bent Up and BCJ-12mm – Bent In specimens as shown in **Figs. 4.14 and 4.15**. Six bars of 12 mm diameter were used in the column for longitudinal reinforcement and 8 mm diameter closed ties at a spacing of 75 mm, were used as transverse reinforcement. For beams, three bars of 12 mm diameter were used for both the top and bottom longitudinal reinforcement and 8 mm diameter closed stirrups with spacing of 75 mm were used for transverse reinforcement in the beam except for BCJ-18 mm – Bent In specimen in which all the main reinforcement used was of 18 mm diameter while there was no transverse reinforcement provided in the joint region in all the specimens. This design resulted for BCJ-12 mm – Bent Up and BCJ-12 mm – Bent In in a column and beam flexure strength of 84.61 kN-m and 53.56 kN-m and for BCJ-18 mm – Bent In, the designed column and beam flexure strength was 164.355 kN-m and 124.00 kN-m, Detailed calculations for column and beam flexure strength are included in **Appendix**. Details of specimen's geometry and reinforcement are given in **Figs. 4.14, 4.15 and 4.16**.

Figure 4.14: Geometric and reinforcement details for BCJ-12 mm - Bent Up

Figure 4.15: Geometric and reinforcement details for BCJ-12 mm – Bent In

Figure 4.16: Geometric and reinforcement details for BCJ-18 mm – Bent In

4.5.2 Strain Gauges

Total of 12 strain gauges were installed in each specimen in the selected position in the beam-column and joint reinforcement as shown in **Fig. 4.17**. Two gauges were placed on front face of the center reinforcement above and below the joint region, and one gauge was placed on each lateral tie just above and below the joint region, and two gauges were placed on the center beam reinforcement top and bottom, one in joint and on just after joint interface. Before the bonding of strain gauges, surface was prepared on the reinforcement as shown in **Fig. 4.18**, and the adhesives were used to paste the gauges on the reinforcement surface and then wrapped with the tape as shown in **Fig. 4.19**.
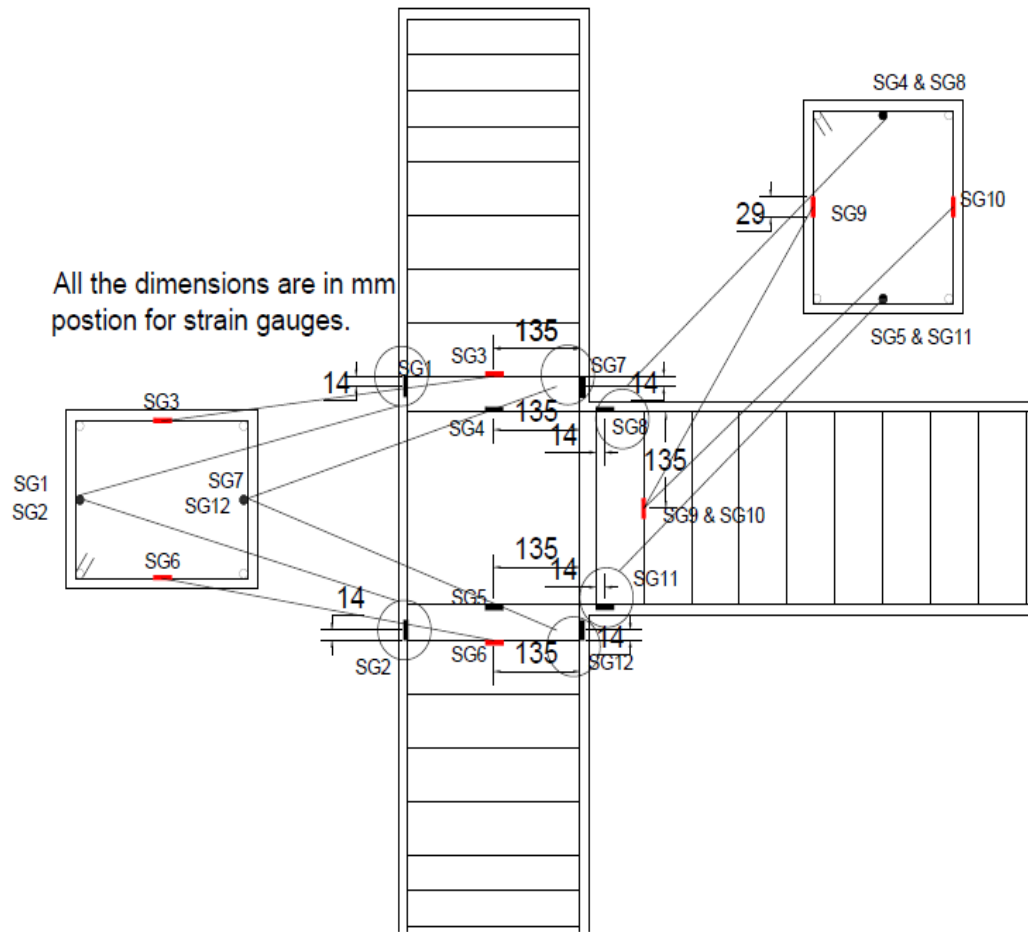
Figure 4.17: Locations for strain gauges for reinforcement

70

Figure 4.18: Surface preparation for installation of strain gauges

Figure 4.19: Installation of strain gauges and check the voltage reading

4.6 Casting of Beam-Column Joint at KFUPM Lab and Dammam

Two sets of casting were done to prepare the BCJs specimens. The casting of beam-column joints wooden form work was used and the reinforcing cage was set into the form work as shown in **Fig. 4.20.** The joints of the form work were sealed to prevent water seeping out after the installation of strain gauges on the reinforcement the specimens casted and for casting the concrete mix was batched and delivered in the mixer truck to KFUPM lab. All the concrete was placed in the wheel barrow and then shoved in the form work. After the concrete work, a trowel was used to make the smooth surface of the specimens which were then covered with the wetted burlap for curing and later covered by plastic tarp to maintain the moisture level as shown in **Fig. 4.21.** Second set of casting was done in Dammam; all the concrete was placed by pumping in the form work. After the concrete work, the trowel was used to make the smooth surface of the specimens which were then covered with the wet burlap for curing and later covered by plastic tarp to maintain the moisture level as shown in **Fig. 4.22.** After the casting processes, the check for the strain gauge was conducted to make it sure that all the wires were in good condition as shown in **Fig. 4.23**.

Figure 4.20: Casting specimen at KFUPM lab

Figure 4.21: Specimens covered with wet burlap for curing

Figure 4.22: Casting specimen in Dammam

Figure 4.23: Checking the voltage of wire after casting

4.7   Testing Arrangements for the Specimens

Specimens were tested in a self-reacting steel loading, additional clamping system was provided to the frame to hold the specimen at the top and bottom of column and at the tip of beam to apply the load from hydraulic jack as given in **Fig. 4.24.** Two hydraulic jacks were used for application of loads. One hydraulic jack (A) of 30 ton at the top of the column for constant axial load and the other, hydraulic jack (B) of 10 ton at the tip of the beam for cyclic loading on the beam as shown in **Fig. 4.25.**
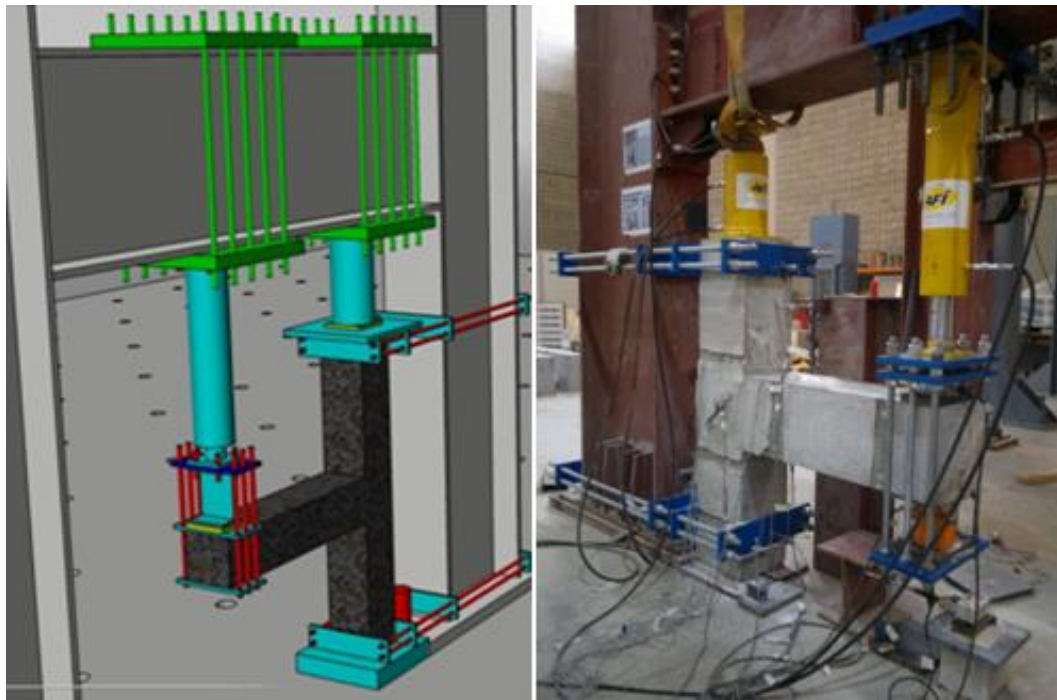
Figure 4.24: Additional clamping system to hold the specimens during the test
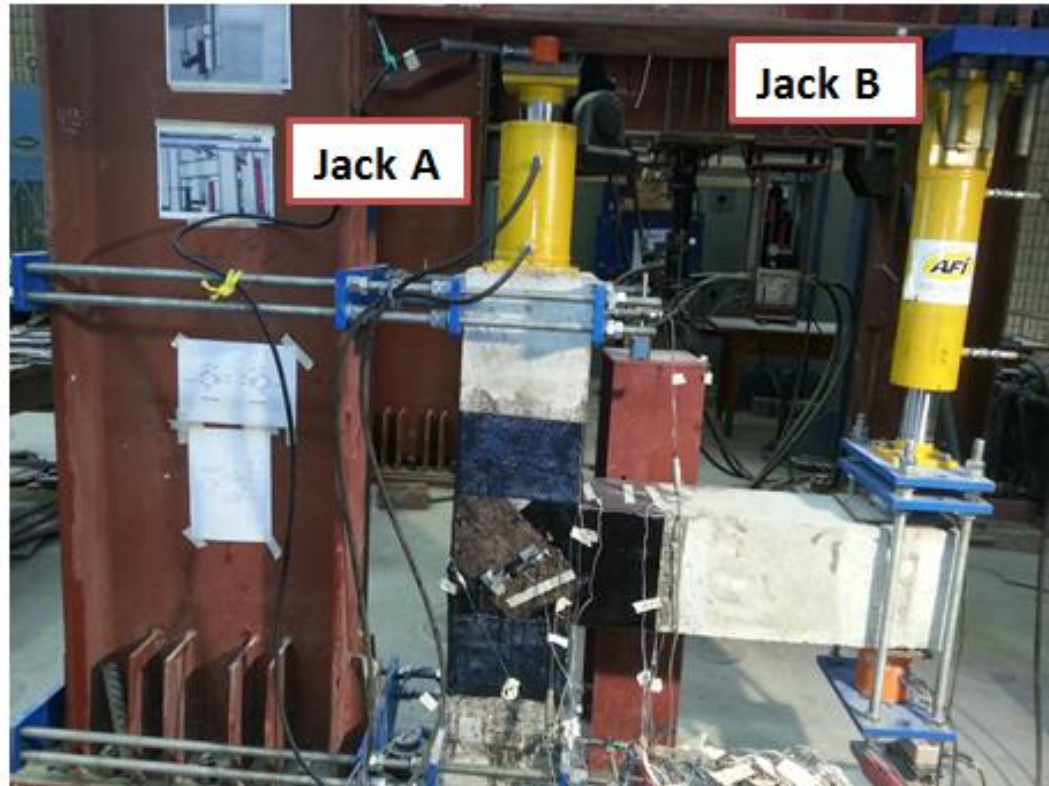
Figure 4.25: Hydraulic jacks used for testing of beam-column joints

4.8   Instruments for Monitoring Test

Load cells, LVDT's and concrete surface stain gauges were also installed to the specimens during the test to monitor the load stresses and deflections. Regarding the load cells, one Load Cell (LC3) of 20 ton capacity was installed at the top of the column, and two load cells (LC1 and LC2) of 100 ton capacity were installed at the top and bottom of the tip of beam as shown in **Fig. 4.26**.

LVDT's (Face 1 = J1 and Face 2 = J2) were installed at the joint region to observe the diagonal crack openings. Two LVDT's (C1 and C2) were also installed at the top and bottom of the column to see the movements, and one string type LVDT (patriot B2) was installed at the tip of the beam to measure the deflections during the tests of specimens. Concrete surface strain gauges were pasted on the compression and tension side of beam and column to observe the strains on the surface of the concrete as given in **Fig. 4.27**.
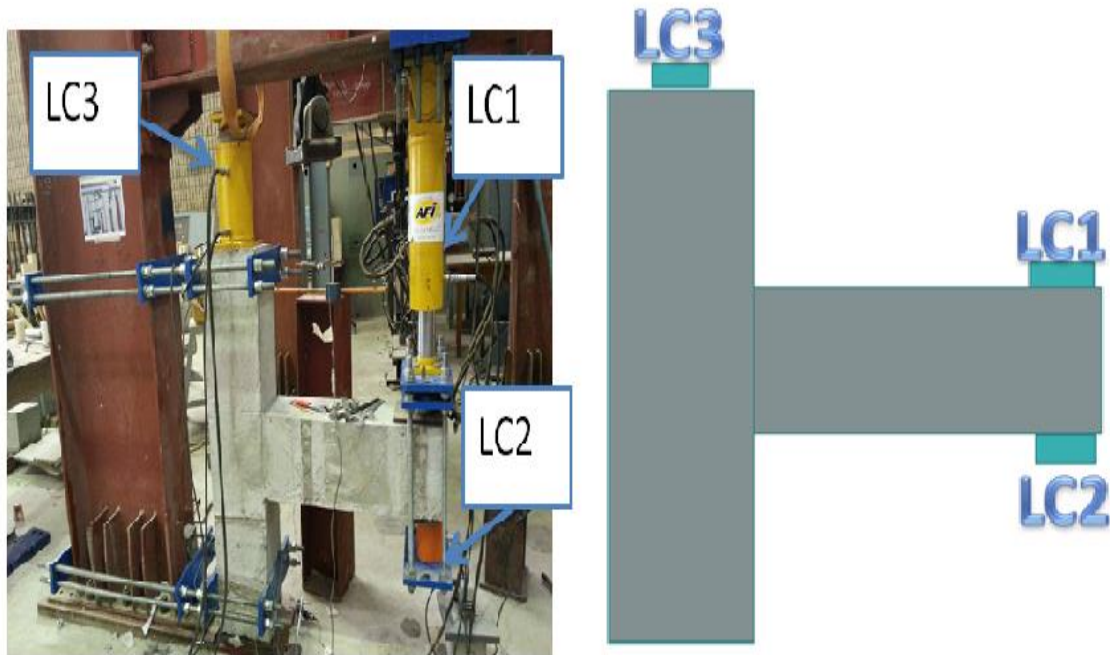
Figure 4.26: Concrete surface-strain gauges LVDT and load cells
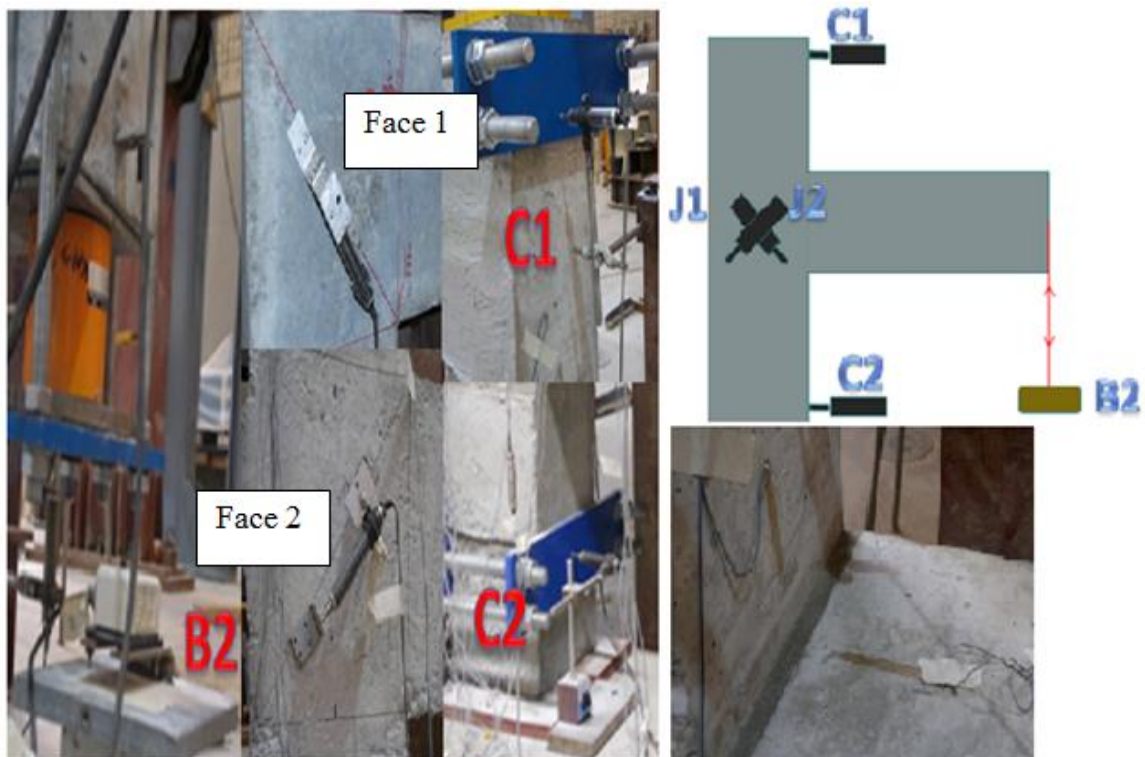
Figure 4.27: Positions for LVDT's and strain gauges attached to the specimens during the test

4.9 Test Program for the Specimens

4.9.1 Testing for Non- Retrofitting Beam-Column Joint

Exterior beam-column joints were tested under displacement control method. Two types of loadings were applied to the specimens as shown in **Fig. 4.28**. A constant axial load on column (150 kN) and increasing displacement at the tip of the beam on both push and pull side up-to the failure of specimens. The pattern of the cyclic load during the test is shown in **Fig. 4.29** and **Table 4.3**. Photo graphs of the specimens were taken throughout the testing process and the cracks developed during the test were noted. Three types of data were collected in the experiments. They were the loads and displacement at the beam tip and the strain values at the selected location of reinforcement in each specimen.
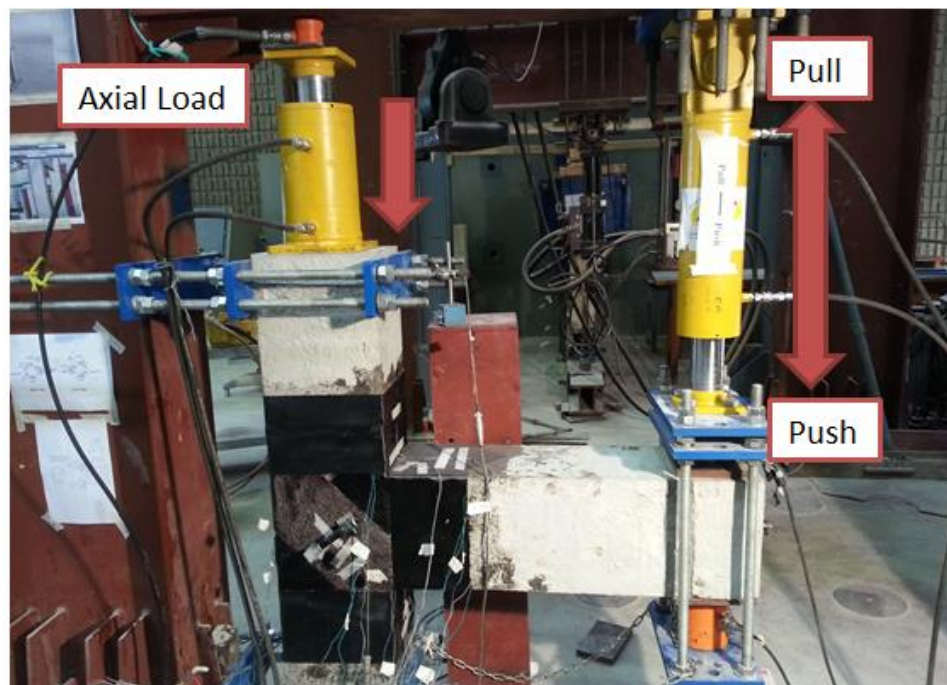
Figure 4.28: Testing procedure for beam-column joints

The numerical modeling of BCJ without strengthening was carried out during the period of this progress report. Load-deformation curves comparing experimental and finite elements results are shown below. Also, the stresses in the joints and modes of failure and cracks patterns are shown.

Table 4-4: Cyclic Load Pattern during the Test

Cyclic Loading			
No.	Drift Ratio	Push	Pull
	%	mm	mm
1	0.288%	2.6	-2.6
2	0.6%	5.4	-5.4
3	1.11%	10	-10
4	1.66%	15	-15
5	2.22%	20	-20
6	2.77%	25	-25
7	3.33%	30	-30
8	4.44%	40	-40
9	5.55%	50	-50
10	7.22%	65	-65
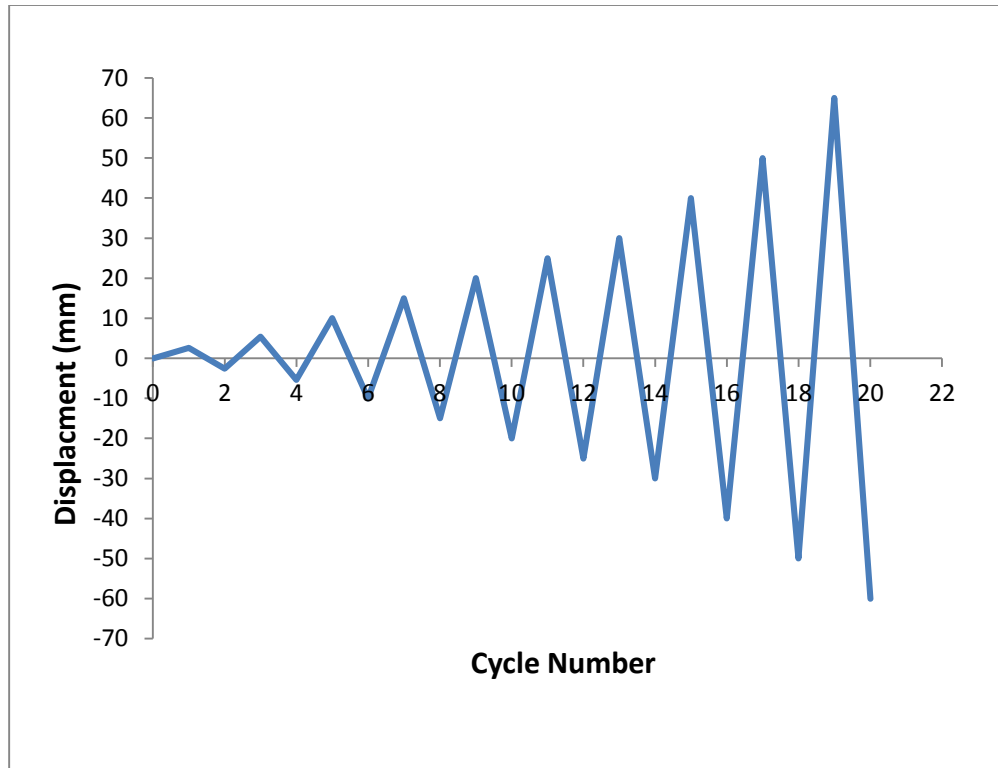
Figure 4.29: Cyclic load pattern applied during the test

4.10 Testing for Retrofitting Beam-Column Joint with CFRP Sheet Strengthening of Beam-Column Joint

As mentioned before, beam-column joint when subjected to cyclic loading, experiences some damage. To avoid severe damage, a retrofitting process has to be carried out for the beam-column joint. Several types of retrofitting materials and techniques have been adopted and studied by various researchers. One of the most common types of reinforcement is the CFRP (Carbon-Fiber-Reinforced Polymer). This material has a high tensile strength capacity which helps the structure regain strength. In this study, CFRP strengthening process for beam-column joint has been adopted and experimentally tested. One layer of CFRP sheet was wrapped diagonally to the beam-column joint. The CFRP sheet was attached to the surface using Sika-Dur 300 Epoxy **Fig. 4.30**.

Figure 4.30: Sika-Dur 300 Epoxy

Beam-column joints in old buildings without transverse reinforcement and subjected to cyclic loading result in diagonal cracking in the joint region. To avoid damage, these joints need to be retrofitted. Several types of retrofitting materials and techniques have been adopted and studied by various researchers. CFRP (Carbon-Fiber-Reinforced Polymer) is now being extensively used in retrofitting of reinforced concrete structures. CFRP has high tensile strength capacity which can be exploited for enhancing the capacity of beam-column joints subjected to diagonal tensile stresses under seismic loads. In the experimental program conducted, one layer of CFRP sheet was wrapped diagonally to the beam-column joint. The schematic applications for CFRP on BCJs are shown in **Fig. 4.31**. The CFRP sheet used in this study is a SikaWrap-230C which is a woven carbon fiber fabric recommended for structural strengthening and improved seismic performance. The SikaWrap-230C uses mid-strength unidirectional carbon fibers. The 200 mm wide CFRP sheet having a thickness of 0.12 mm was impregnated with Sikadur-330 epoxy and applied to the joints in diagonal direction and extended to the beams and columns as shown in **Fig. 4.32**. The CFRP strengthened beam-column joints were tested after 7 days.
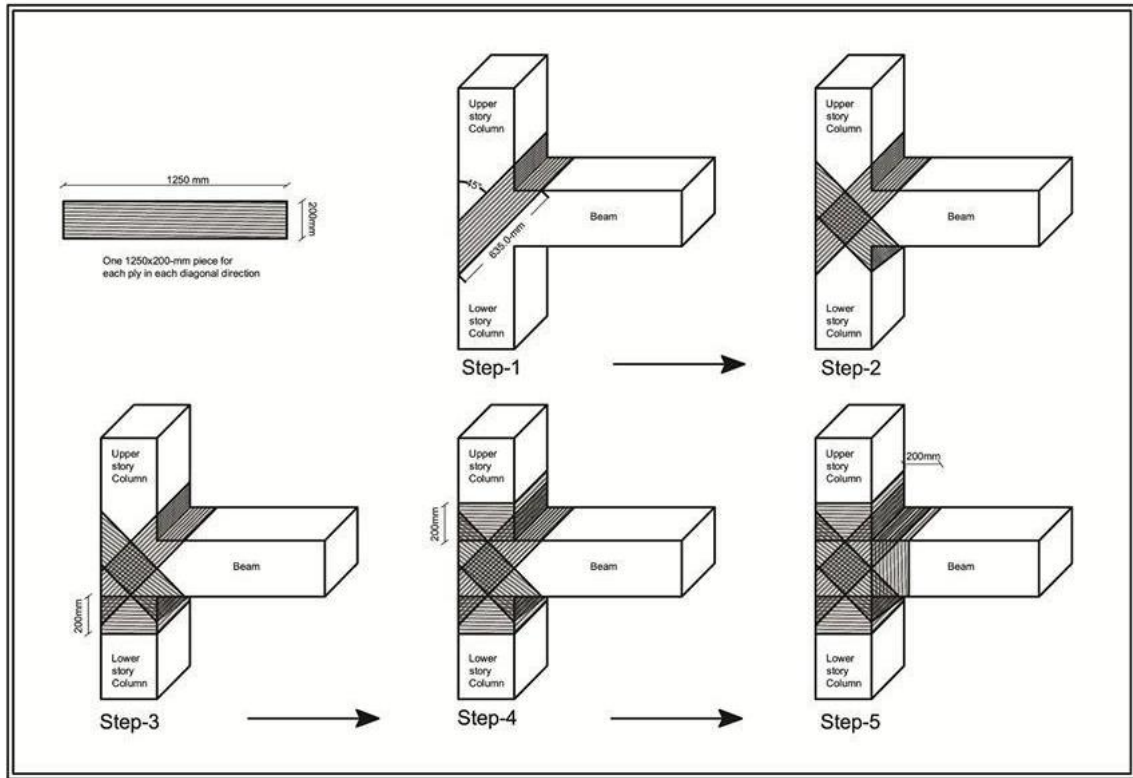
Figure 4.31: Sequential scheme for applying the CFRP sheet

Figure 4.32: Sequence applying the CFRP sheet

CHAPTER 5

EXPERIMENTAL TEST RESULTS

5.1   Monotonic Test Result for BCJ – Bent Up – 12MM

BCJ-Bent Up - 12MM specimen has the bent up detailing in the joint region with 12 mm diameter flexural reinforcement for beam and column. For the control specimen, the load verses displacement graph shows that the maximum load and displacement reached 71.2 kN and 17.5, as shown in **Fig. 5.1**. The first crack formed in the specimen was flexural crack near the beam-column interface at the load of 26 kN and 2.8 mm. The subsequent flexural crack in the beam happened at 38 kN and 5.6 mm. The first diagonal crack at the joint region was formed at the load of 57 kN and 11.7 mm. The diagonal crack extended at load of 60 kN and 49 mm. In the last step of the test, the beam-column interface of the specimen was totally damaged and crushed, concrete cover spalled off from one side of the joint, and a wide flexural crack occurred. The reinforcement was totally visible to the naked eye. The failure in this specimen was totally flexural and the residual displacement of the beam can be seen clearly as shown in **Fig. 5.2**.

For the retrofitted specimen, the load verses displacement graph shows that the maximum load reached was 84.1 kN and 27.63 mm as shown in **Fig. 5.1**. The first crack formed in the specimen was flexural crack at distance from the BCJ interface at load 48 kN and displacement 6.4 mm. The second flexural crack occurs at BCJ interface at load 74 kN and displacements 14.2 mm. The first rupture of CFRP sheet in weak direction occurred at load 80 kN and displacement 21.7 mm. The rupture of CFRP sheet in strong direction

occurs at load 79 kN and displacement 30.3 mm as shown in **Fig. 5.3**. The maximum strain at the time of rupture of CFRP was 0.003894 µs. The retrofitted sample enhances the load displacement response of the BCJ for 19.7%.
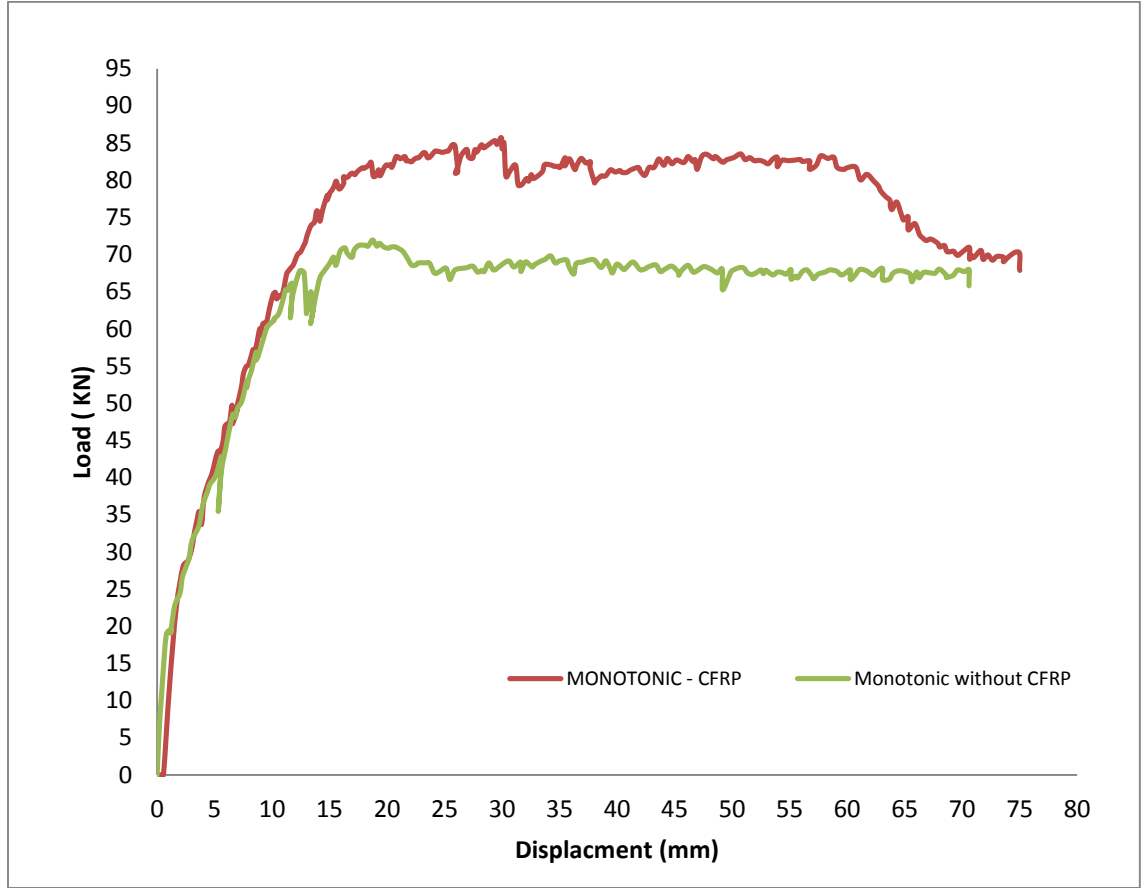
Figure 5.1: Load verses displacement graph for specimen BCJ- Bent Up - 12MM

first Flexural crak at 26 KN

Flexural crak in beam at 38 KN

First diagonal crak in joint at 57

Figure 5.2: Crack pattern specimen BCJ-12MM- without CFRP

First flexural crack in beam at 48KN

Flexural crack in BCJ interface at 74 KN

Rupture of CFRP in weak direction at 80KN and 14.2mm

Rupture of CFRP in strong direction at 80KN and 21.7mm

Figure 5.3: Crack pattern specimen BCJ-12MM- with CFRP

The graphs are plotted for both sides of joint crack openings as shown in **Figs. 5.4 and 5.5**, both the LVDTs shows that the displacements start in the push direction when the cracks start increasing.
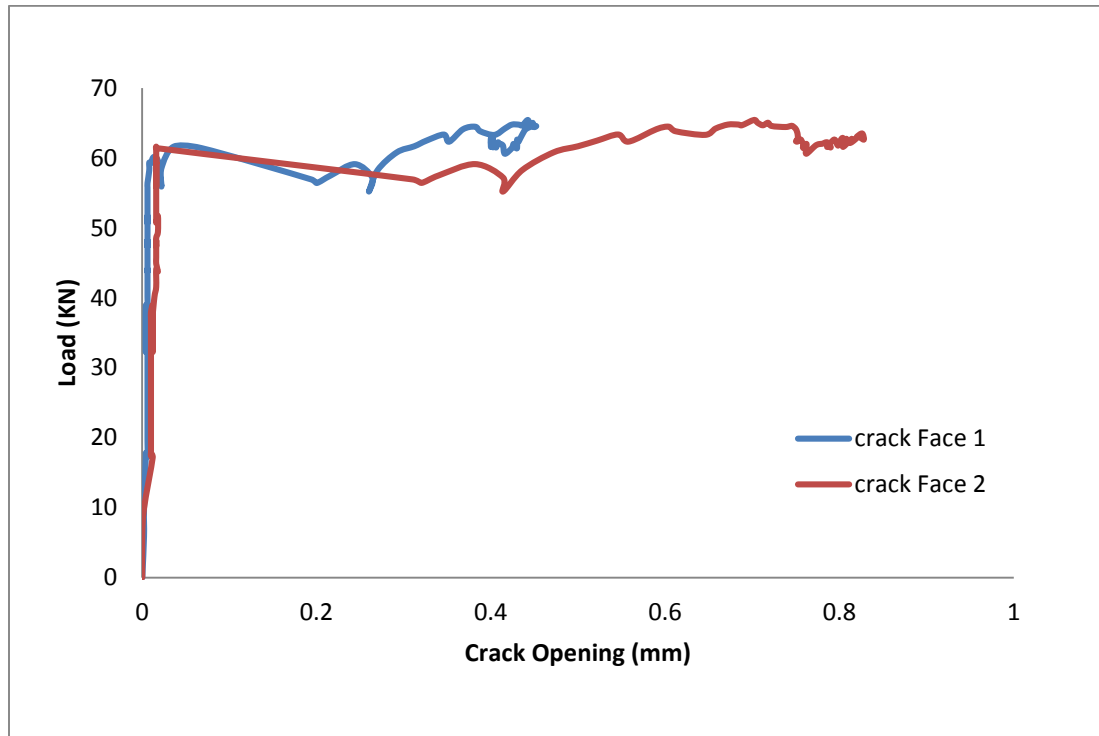
Figure 5.4: Load verses crack opening graph for LVDT for BCJ-12MM-Bent Up without CFRP
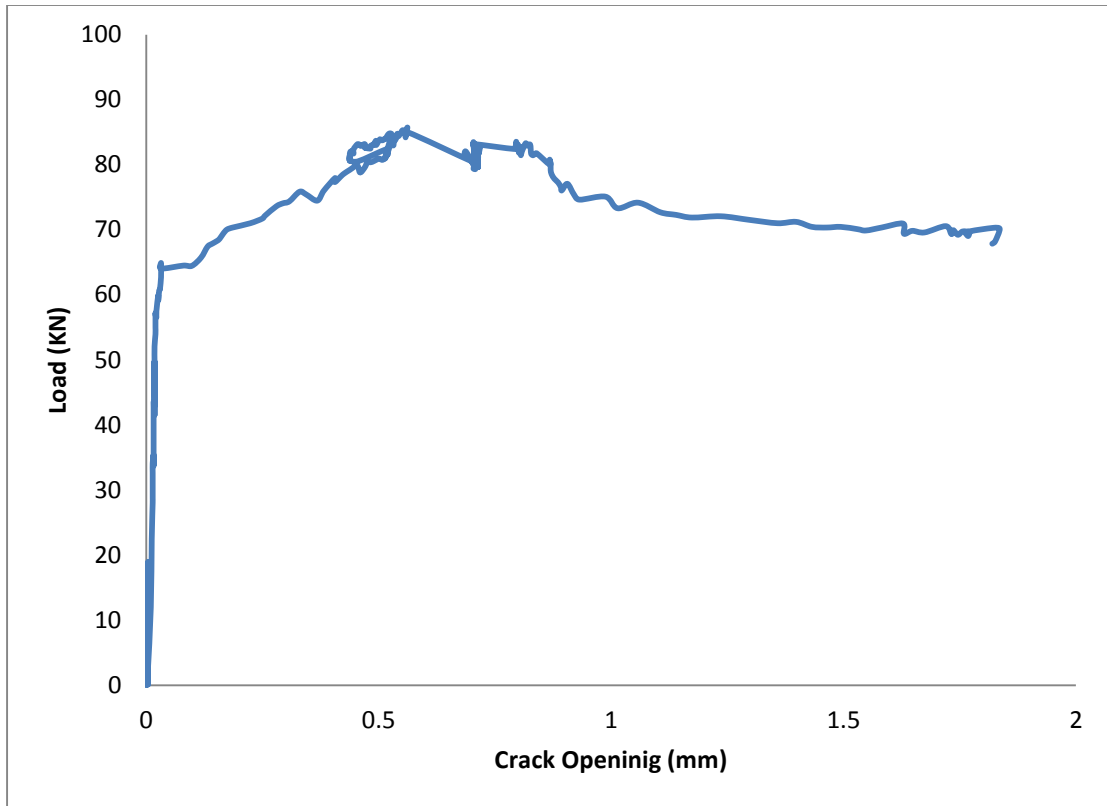
Figure 5.5: Load verses crack opening graph for LVDT for BCJ-12MM-Bent Up with CFRP

Strain gauges were installed to monitor the strains in the reinforcement; **Fig. 5.6** shows the graph between load and strains in the steel for top and bottom reinforcement of beam in the specimen which includes the joint regions and the interface of the BCJ without using CFRP.
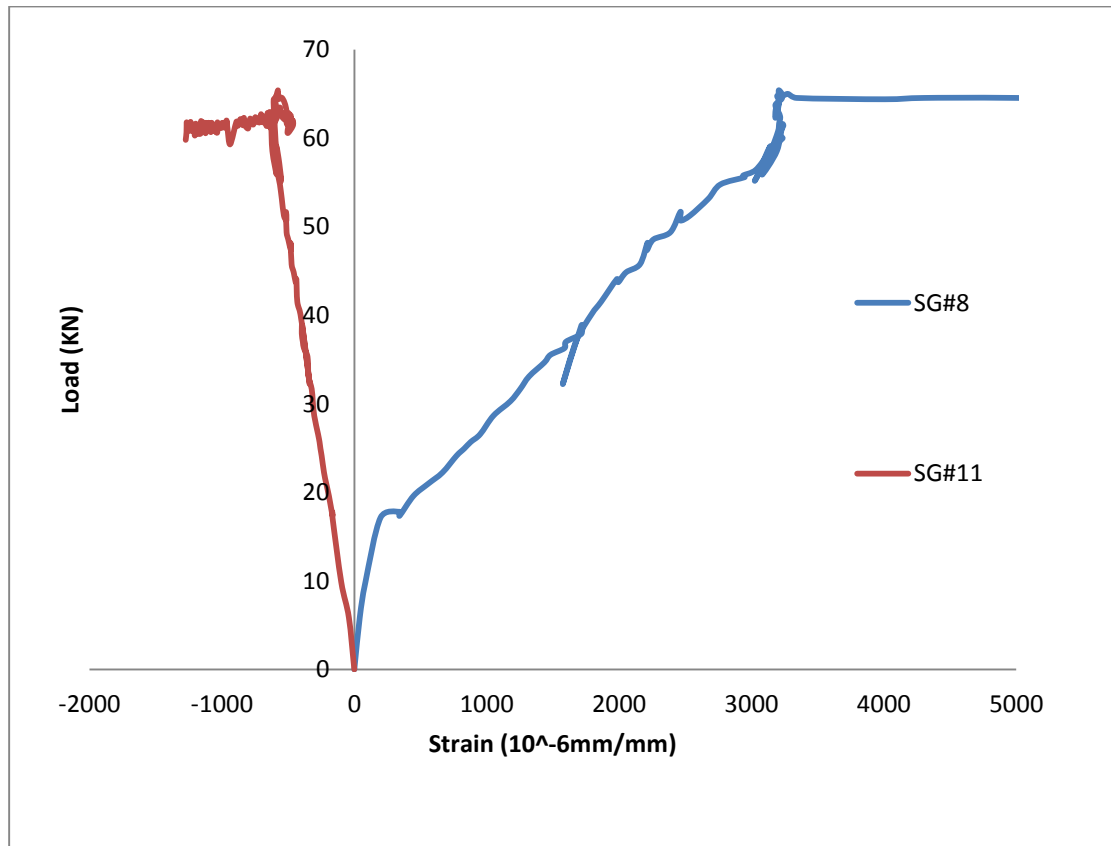
Figure 5.6: Load verses strain graph for top and bottom beam reinforcement for BCJ-12MM-Bent Up without CFRP

Strain gauges were also installed for BCJ-18MM-with CFRP to monitor the strains in the reinforcement. **Fig. 5.7** shows the graph between load and strains in the steel for top and bottom reinforcement of beam in the specimen which includes the joint regions and the interface of the BCJ using CFRP.
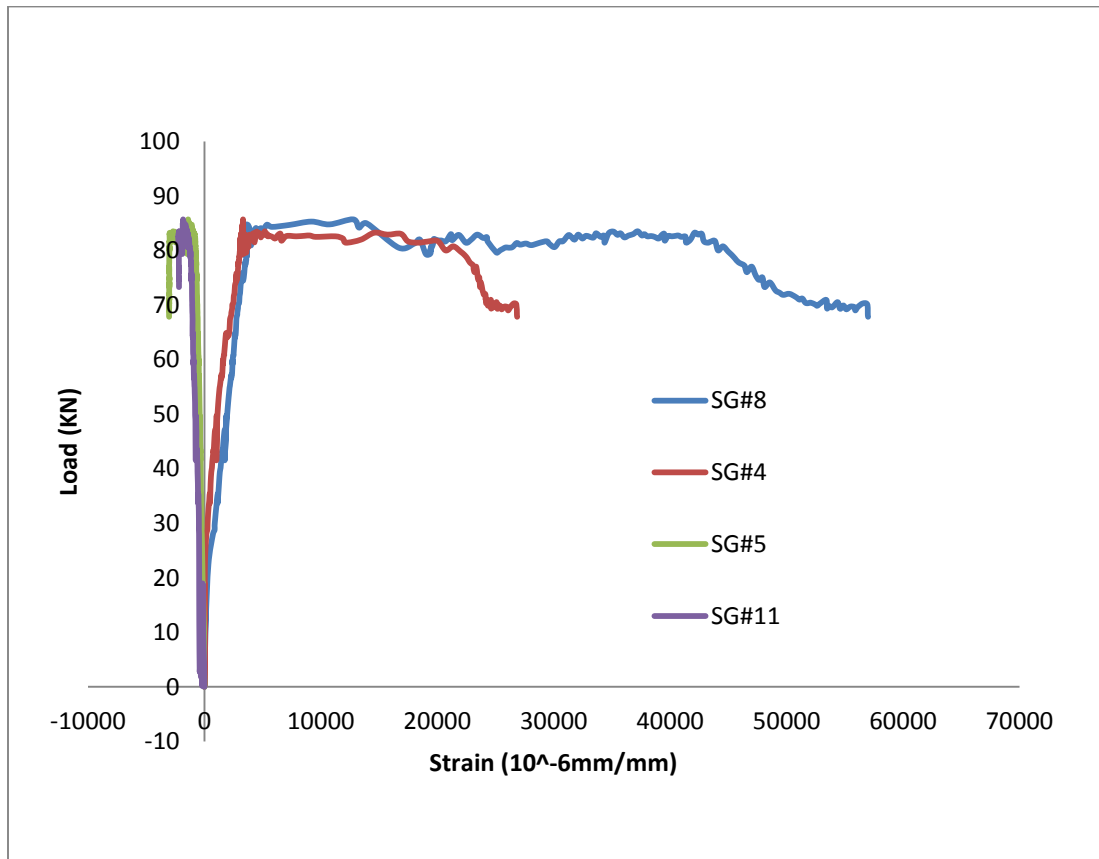
Figure 5.7: Load verses strain graph for bottom beam reinforcement for BCJ-12MM-Bent Up with CFRP

In order to measure the strain for CFRP sheets, strains gauges were installed on both sides of the face of the joint and the load and the strain in the CFRP sheet in the strong direction were plotted as shown in **Fig. 5.8**.
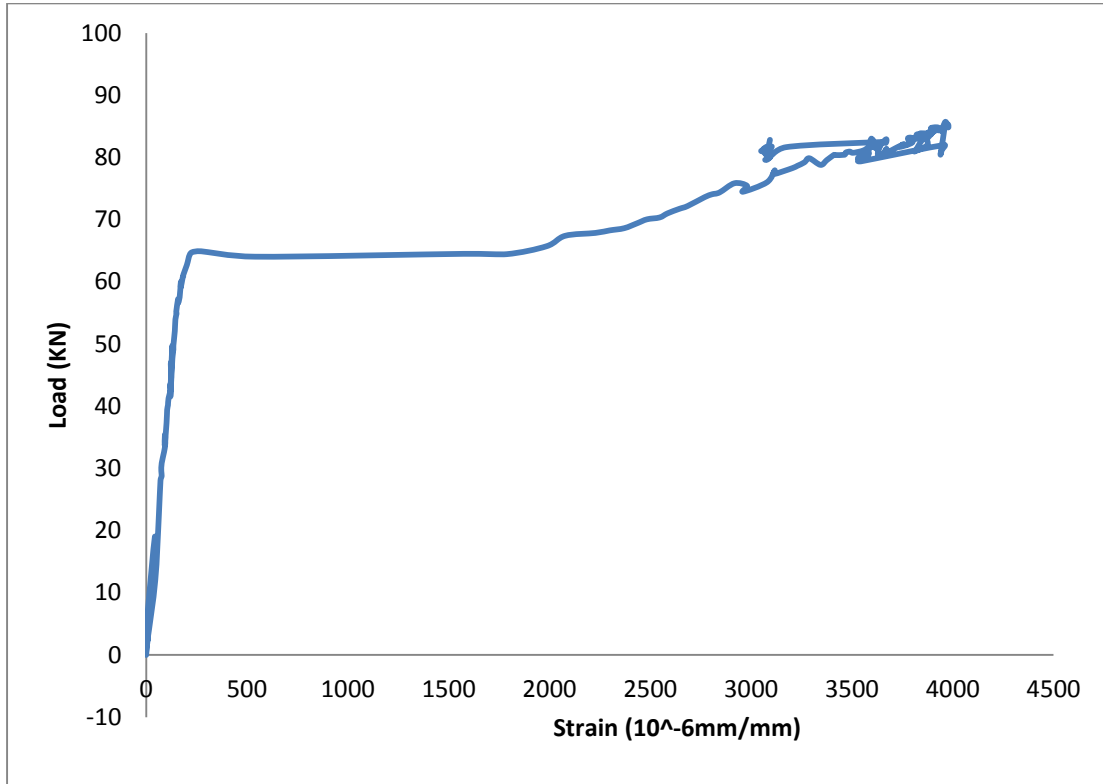
Figure 5.8: Load verses strain graph for CFRP sheets

5.2   Monotonic Test Result for BCJ – Bent In – 12MM

BCJ-Bent In - 12MM specimen has the bent in detailing in the joint region with 12 mm diameter flexural reinforcement for beam and column. For the control specimen, the load verses displacement graph shows that the maximum load and displacement reached was 74 kN and 26.8 as shown in **Fig. 5.9**. The first crack formed in the specimen was flexural crack near the beam-column interface at the load of 24 kN and 2.2 mm. The first crack in the beam happened at 38 kN and 5.3 mm. The first diagonal crack at the joint region was formed at the load of 53 kN and 8.53 mm. The diagonal crack extended at load of 68 kN and 14.315 mm. In the last step of the test, the beam-column interface of the specimen was totally damaged and crushed, concrete cover spall off from one side of the joint, and a wide flexural crack occurred. The reinforcement was totally visible to the naked eye. The failure in this specimen was totally flexural and the residual displacement of the beam can be scene clearly as shown in **Fig. 5.10**.

For the retrofitted specimen, the load-displacement graph shows that the maximum load reached was 85.3 kN with corresponding tip displacement of 14.7 mm as shown in **Fig. 5.9**. The first visible crack formed in the specimen was a flexural crack at some distance from the BCJ interface at load 24 kN and displacement 2.7 mm. The second flexural crack occurred at BCJ interface at load 42 kN and displacement 5.6 mm. The first rupture of CFRP sheet in weak direction occurred at load 66 kN and displacement 10.7 mm. After that, the rupture of CFRP sheet in strong direction occurred at a load of 66 kN and displacement 29.7 mm, as shown in **Fig. 5.11** the maximum strain at the time of rupture of CFRP was 0.013929 µs. The retrofitted samples enhanced the load displacement response of the BCJ for 12.8%.

97
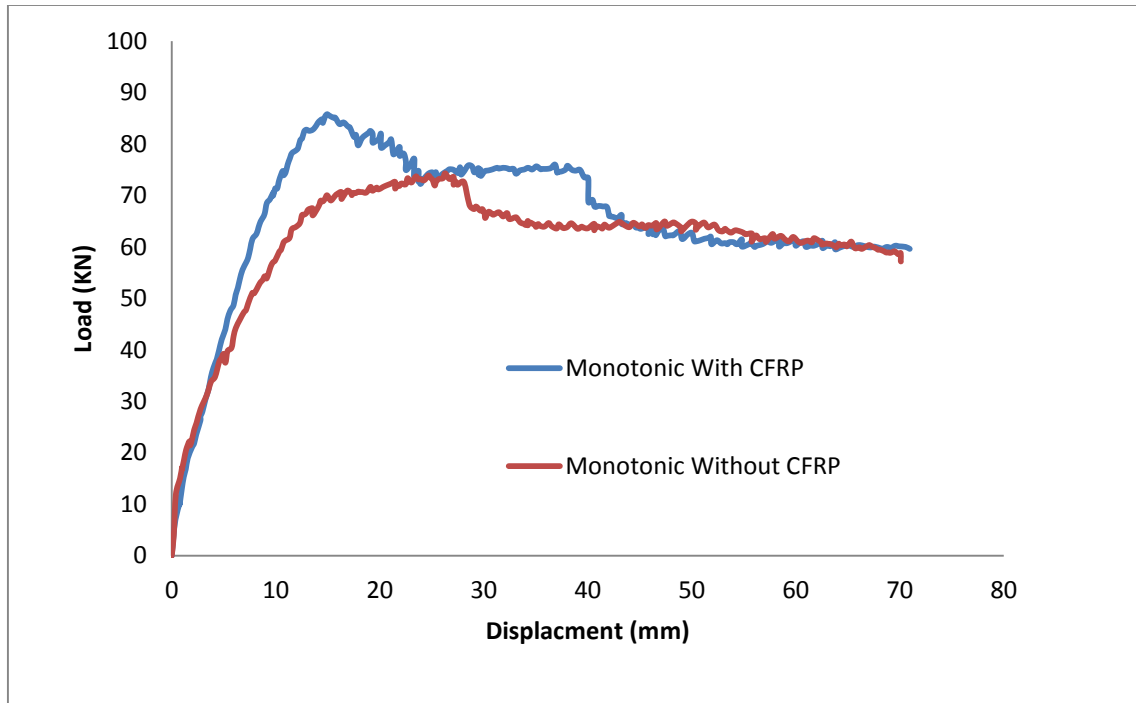
Figure 5.9: Load verses displacement graph for specimen BCJ- Bent In - 12MM
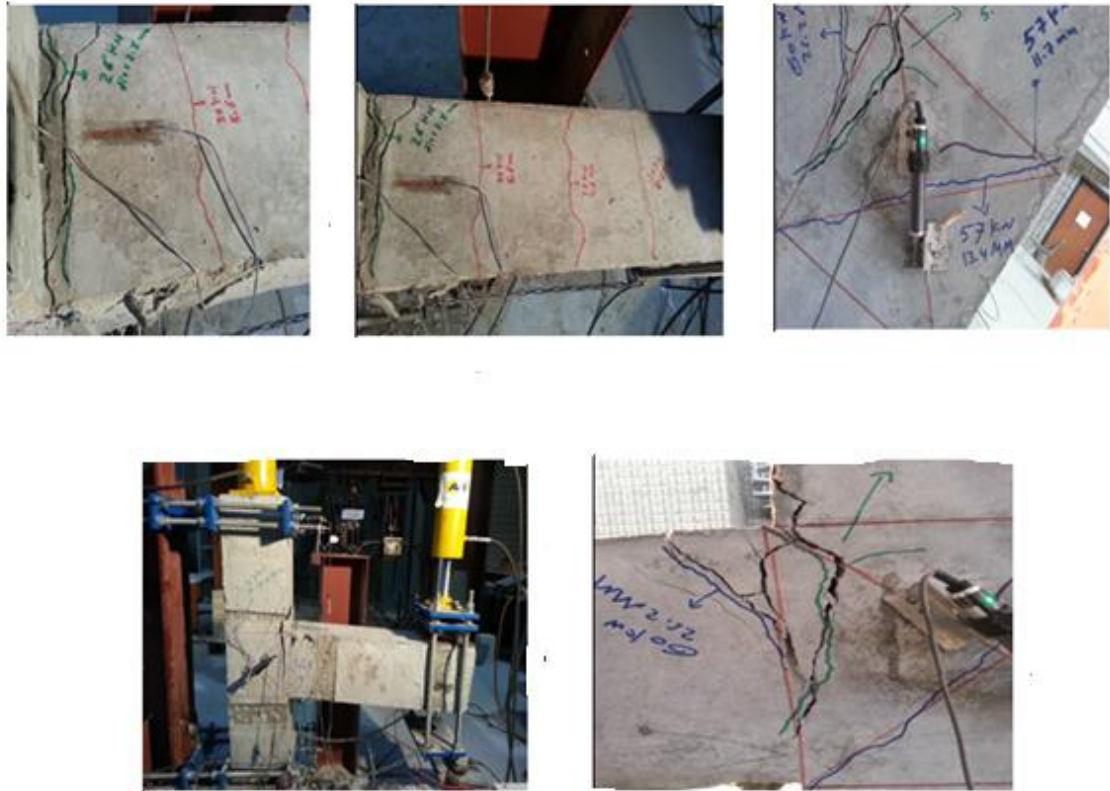
Figure 5.10: Crack pattern specimen BCJ-12MM- without CFRP

98

Figure 5.11: Crack pattern specimen BCJ-12MM- with CFRP

The graphs are plotted for both sides of joint crack openings as shown in **Figs. 5.12 and 5.13**; both the LVDTs show that the displacements start in the push direction when the cracks start increasing.
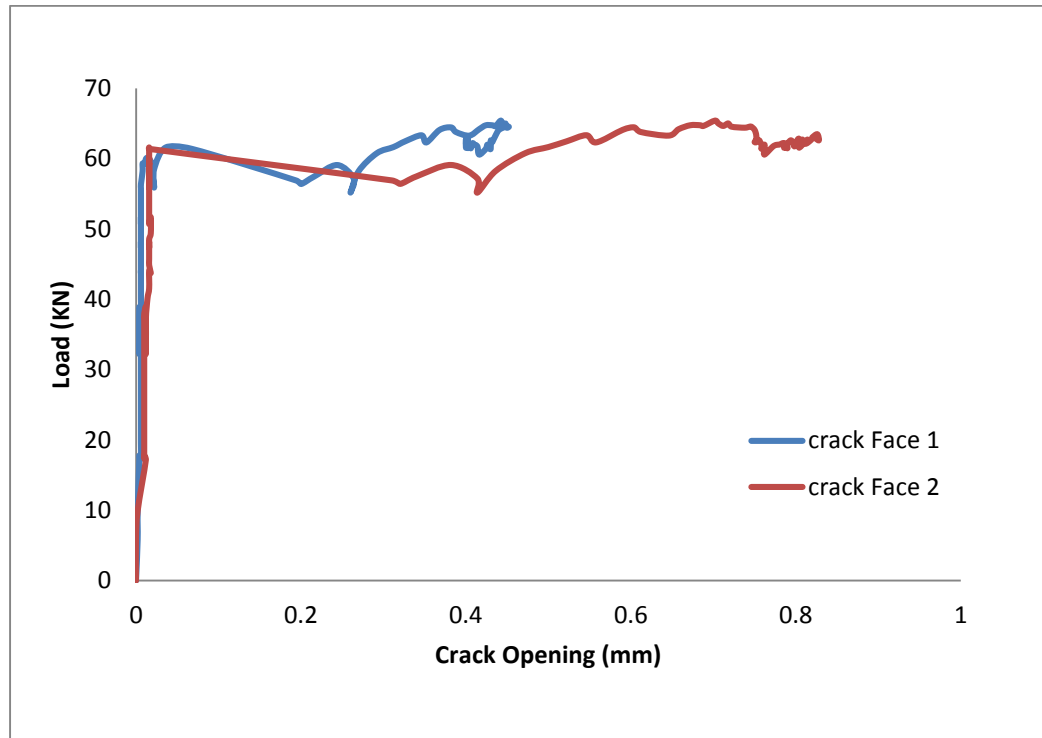
Figure 5.12: Load verses crack opening graph for LVDT for BCJ-12MM-Bent Up without CFRP
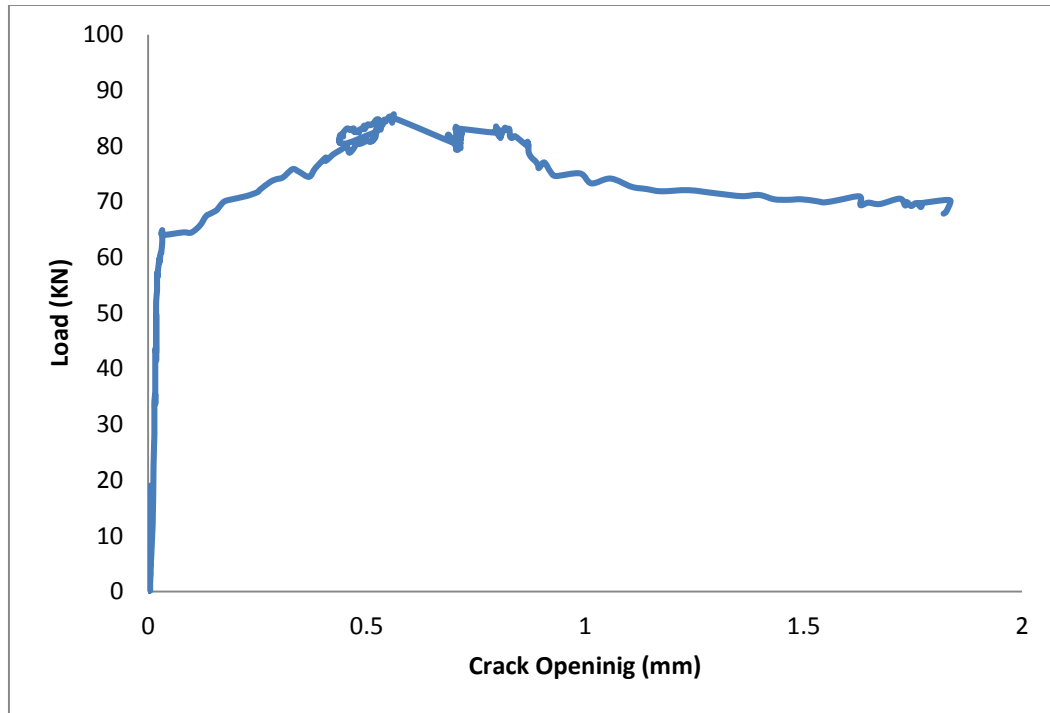
Figure 5.13: Load verses crack opening graph for LVDT for BCJ-12MM-Bent Up with CFRP

Strain gauges were installed to monitor the strains in the reinforcement; **Fig. 5.14** shows the graphs between load and strains in the steel for top and bottom reinforcement of beam in the specimen which includes the joint regions and the interface of the BCJ without using CFRP.
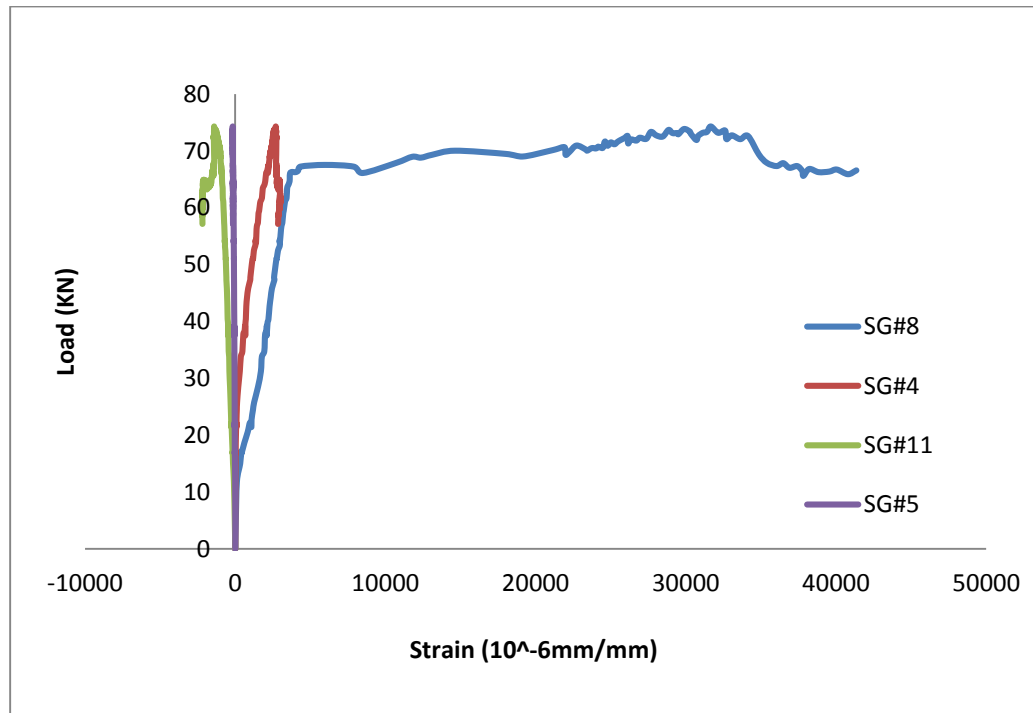
Figure 5.14: Load verses strain graph for top and bottom beam reinforcement for BCJ-18MM-without CFRP

Strain gauges were also installed for BCJ-18MM-With CFRP to monitor the strains in the reinforcement; **Fig. 5.15** shows the graphs between load and strains in the steel for top and bottom reinforcement of beam in the specimen which includes the joint regions and the interface of the BCJ using CFRP.

Figure 5.15: Load verses strain graph for bottom beam reinforcement for BCJ-12MM-Bent In with CFRP

In order to measure the strain for CFRP sheets, strain gauges were installed on both sides of the face of the joint and the load and the strain in the CFRP sheet in the strong direction were plotted as shown in **Fig. 5.16**.

Figure 5.16: Load verses strain graph for CFRP sheets

5.3   Monotonic Test Result for BCJ – Bent In – 18MM

BCJ-Bent In - 18MM specimen has the Bent In detailing in the joint region with 18 mm diameter flexural reinforcement for beam and column. For the control specimen, the load verses displacement graph shows that the maximum load and displacement reached was 97.23 kN and 17.48, as shown in **Fig. 5.17**. The first crack formed in the specimen was flexural crack near the beam-column interface at the load of 37.1 kN and 3.5 mm. The first diagonal crack at the joint region was formed at the load of 50 kN and 5.5 mm. The diagonal crack extended at load of 90 kN and 14.9 mm. In the last step of the test the beam-column joint of the specimen was totally damaged and crushed, and a wide joint crack occurred as shown in **Fig. 5.18**.

For the retrofitted specimen, the load verses displacement graph shows that the maximum load reached was 118.3 kN and 19.79 mm as shown in **Fig. 5.17**. The first crack formed in the specimen was flexural crack at distance from the BCJ interface at load 62 kN and displacement 5.2 mm. More flexural cracks occurred at the beam at load 94 kN and displacements 11 mm. The first rupture of CFRP sheet in weak direction occur at load 112 kN and displacement 21.2 mm. After that the rupture of CFRP sheet in strong direction start to occur at Load 94 kN and displacement 34.4 mm as shown in **Fig. 5.19**. A full rupture of CFRP sheet occurs at load 76 kN and displacement 43.9 mm. The maximum strain at the time of rupture of CFRP was 0.005336 μs. The retrofitted sample enhances the load displacement response of the BCJ for 20.78%.
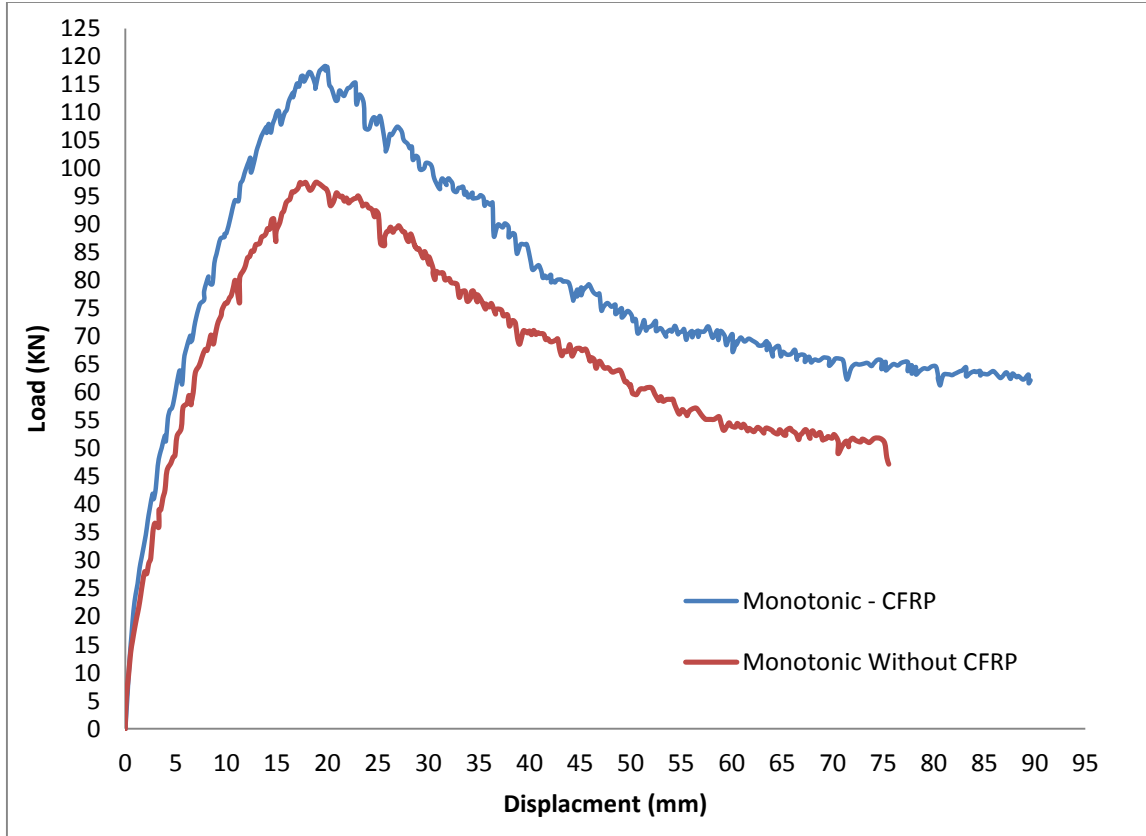
Figure 5.17: Load verses displacement graph for specimen BCJ- Bent In - 18MM
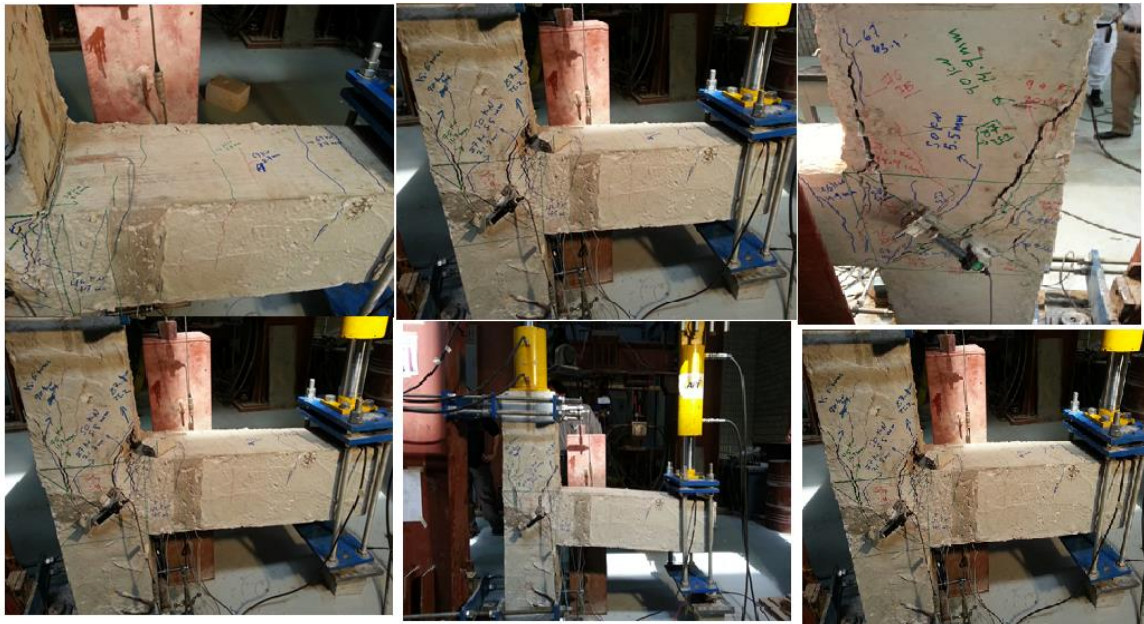
Figure 5.18: Crack pattern specimen BCJ-18MM-Bent In without CFRP

106

Figure 5.19: Crack pattern Specimen BCJ-18MM- Bent In with CFRP

To observe the opening in the joints LVDTs were installed diagonally to the joint on both

the sides, opposite to each other as shown in **Fig. 5.20**.
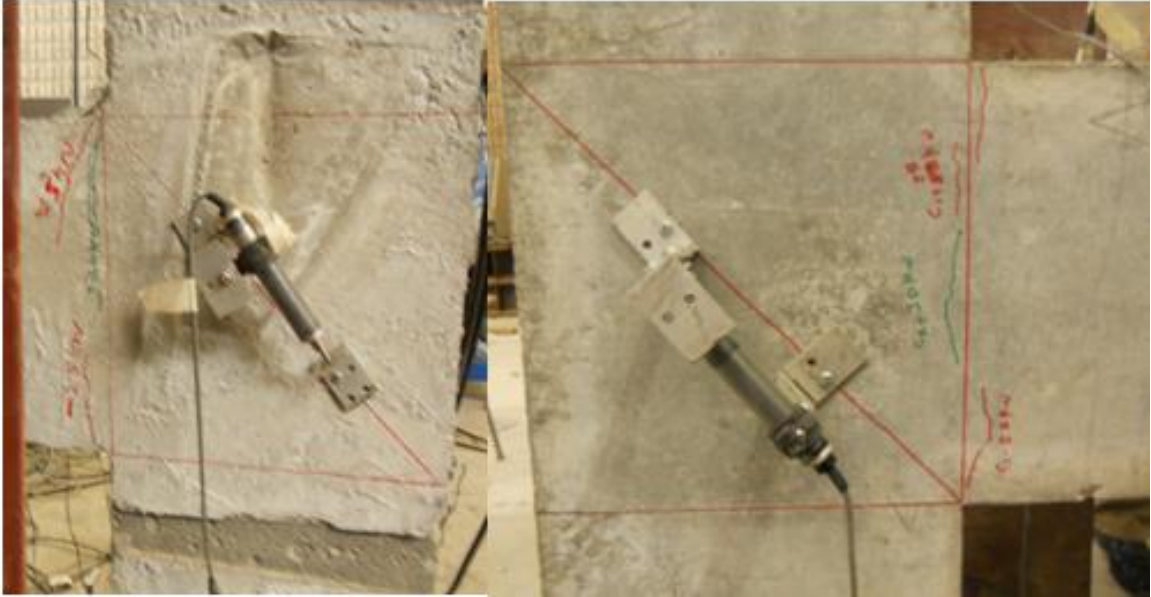
Figure 5.20: Position of LVDT's in joint to observe diagonal cracks

The graphs are plotted for both sides of the joint crack openings as shown in **Fig. 5.21**, Both the LVDTs show that when the displacements started in the push direction the cracks started to increase.

Figure 5.21: Load verses crack opening graph for LVDT face I

Strain gauges were installed to monitor the strains in the reinforcement; **Fig. 5.22** shows the graphs between load and strains in the steel for top and bottom reinforcement of beam in the specimen which includes the joint regions and the interface of the BCJ without using CFRP.
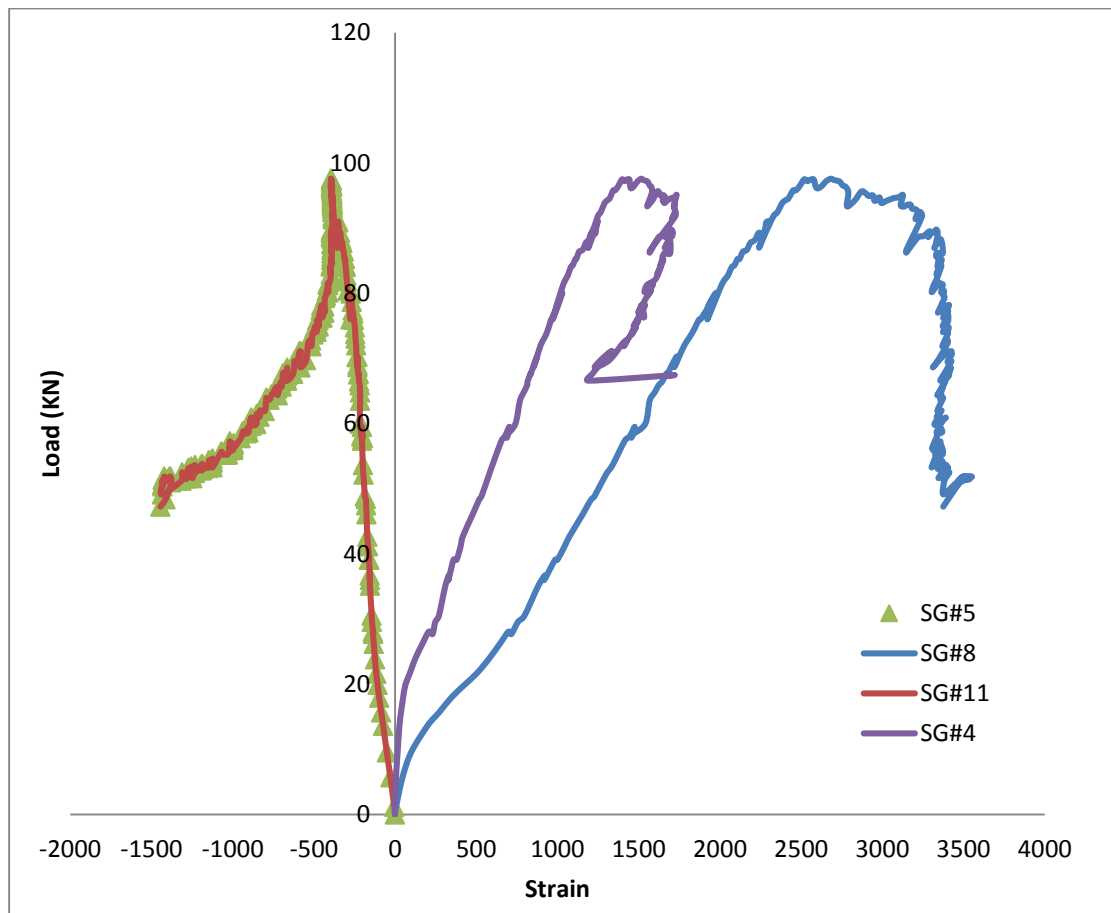
Figure 5.22: Load verses strain graph for top and bottom beam reinforcement for BCJ-18MM-without CFRP

Strain gauges were also installed for BCJ-18MM-With CFRP to monitor the strains in the reinforcement; **Fig. 5.23** shows the graphs between load and strains in the steel for top and bottom reinforcement of beam in the specimen which includes the joint regions and the interface of the BCJ using CFRP.

Figure 5.23: Load verses strain graph for bottom beam reinforcement for BCJ-18MM with CFRP

In order to measure the strain for CFRP sheets, strain gauges were installed in both faces of the joint and the load and the strain in the CFRP sheet in the strong direction were plotted as shown in **Fig. 5.24**.

Figure 5.24: Load Verses Strain Graph for CFRP sheets

5.4   Cyclic Load

5.4.1   Cyclic Test Result for Type BCJ- Bent Up-12MM

For the control specimen, the load verses displacement graph shows that the maximum load and displacement reached in push direction was 67.2 kN and 18.88 mm displacement, and the maximum load in pull direction was 68.8 kN and 12.07 mm as shown in **Fig. 5.25**. The first crack formed in the specimen was at the beam-column interface during the first cycle both at the top and bottom during the push and pull displacement. The cracking load was 25 kN (push) and 2.2 mm, and 20 kN (pull). The first diagonal crack at the joint region appeared in the third push cycle at a load of 53 kN and 6.488 mm, which extended at a load of 66 kN in the fourth cycle. In the last two cycles, the beam-column interface of the specimen was totally damaged and crushed, concrete cover spalled off from one side of the joint and the reinforcement was visible. The mode of failure in the specimen was initial flexural failure at the beam-column interface followed by a diagonal shear crack in the joint as shown in **Fig. 5.26**. For the retrofitted specimen, the load verses displacement graph shows that the maximum load reached in push direction was 76.13 kN and 19.95 mm, and the maximum load in pull direction was 67.7 kN, and 18.767 mm as shown in **Fig. 5.27**. The first crack formed in the specimen was a flexural crack away from the BCJ interface at a displacement 5.4 mm. This was followed by a flexural crack at the BCJ interface. The first rupture of CFRP sheet in weak direction occurred at a load of 72 kN in the push cycle. After this a rupture of CFRP sheet in strong direction occurred at a load of 46 kN and displacement 40 mm as shown in **Fig. 5.28**. The maximum strain at the time of rupture of CFRP was 0.05364.

The CFRP retrofitting resulted in 10.62% increase in the load capacity.

Figure 5.25: Load verses displacement graph for specimen BCJ-12MM-Bent Up
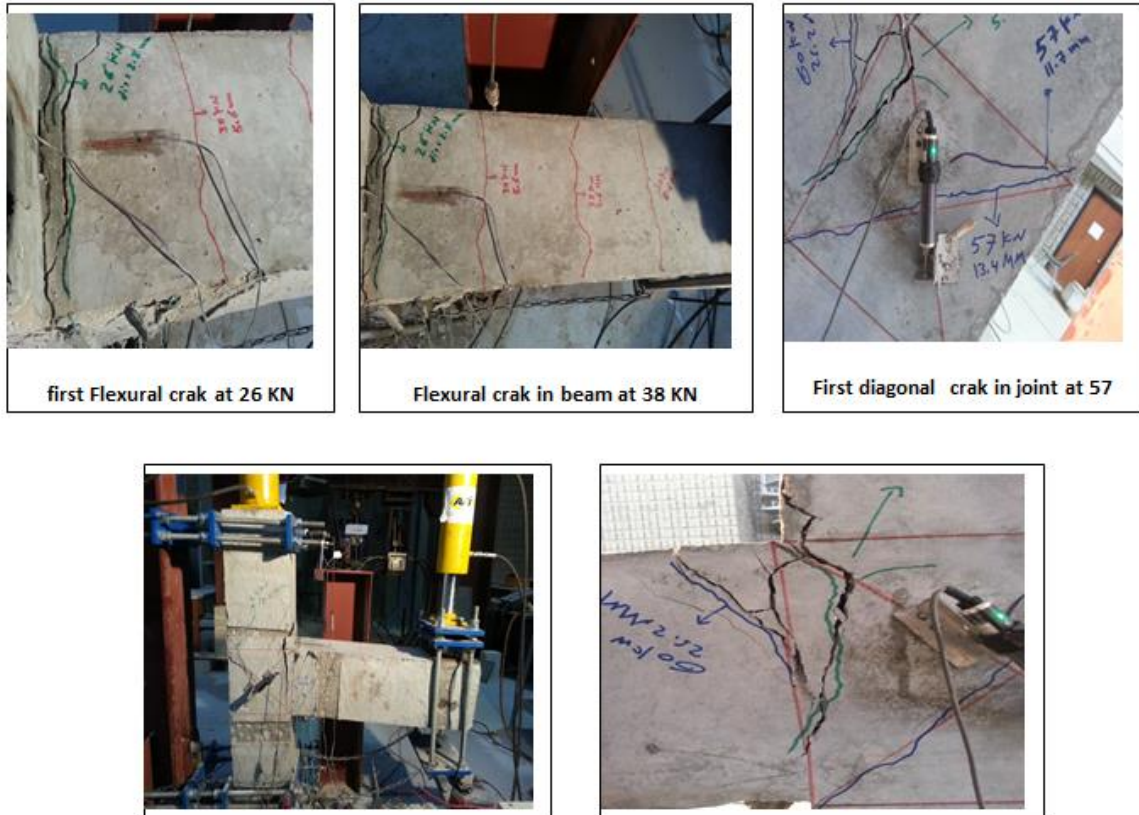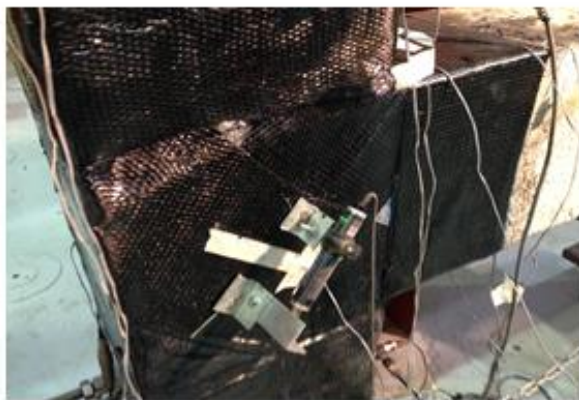

Figure 5.26: Crack pattern for specimen BCJ-12MM-Bent Up without CFRP

114

Fisrt flexural crack in beam at 48KN
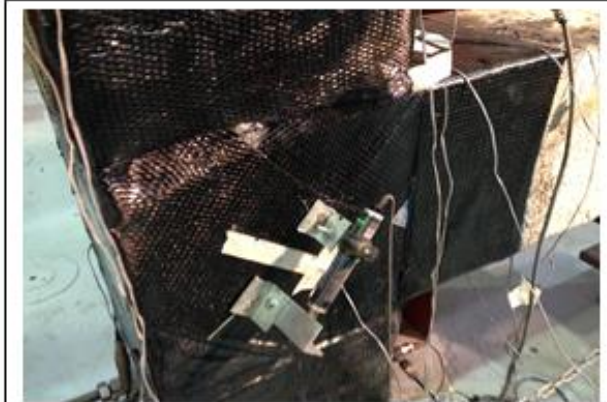
Flexural crack in BCJ interface at 74 KN

Rupture of CFRP in weak direction at 80KN and 14.2mm

Rupture of CFRP in strong direction at 80KN and 21.7mm

Figure 5.27: Crack pattern for specimen BCJ-12MM-Bent Up with CFRP

In type BCJ-12MM specimen during the testing, the first crack was found in the first cycle in the push direction on two places; one at the beam-column joint interface and second little away from the joint in the beam and both of the cracks were flexural cracks at the load of 25 kN and the displacement of 2.2 mm, the first diagonal crack found in the joint at third cycle in push direction at load of 53 kN and at the displacement of 6.844 mm as shown in **Fig. 5.28**.

Figure 5.28: Location of first crack at beam-column interface and in joint for specimen BCJ-12MM-Bent Up

During the cyclic load test, the cracks start from the beam-column joint interface and reached towards the joint as the load cycle increased in the entire load cycling process. It was observed that the cracks were opened and closed, opposite to their loading directions and the diagonal cracks were widen up to 3 mm at the sixth cycle in push direction at 66 kN. In this specimen, same diagonal cracks were found in both push and pull direction as it was found in the type J-BI-12 specimen but the difference was, these diagonal cracks reached to the columns and severe shear X cracks were formed as shown in **Figs. 5.29, 5.30 and 5.31**.
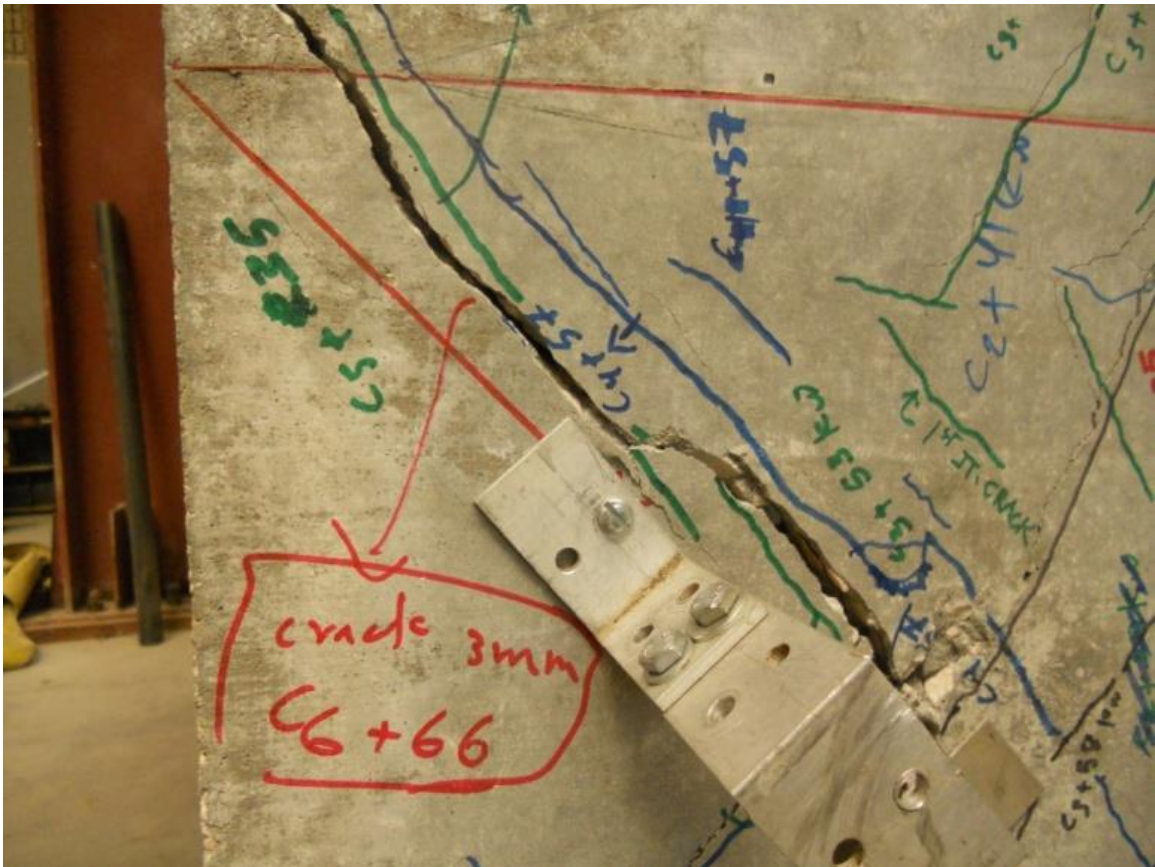
Figure 5.29: Widening up of shear diagonal crack in joint for specimen BCJ-12MM-Bent Up

Figure 5.30: Formation of crack in joint during cyclic load test in specimen BCJ-12MM-Bent Up
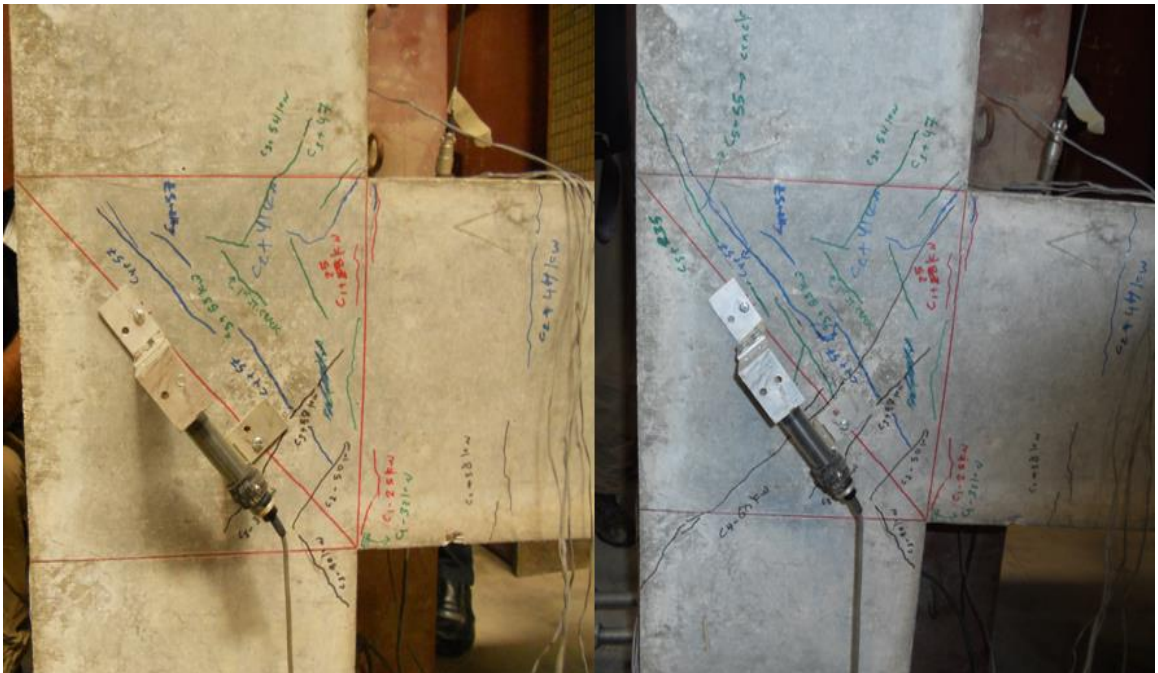
Figure 5.31: Formation of crack in joint during cyclic load test in specimen BCJ-12MM-Bent Up

The entire failure of the specimens was in shear of the joints. The concrete of the joint was spilled off from the surface and there was severe damage at the back side of the joint. At the failure, joint was totally crushed and the reinforcement was totally visible and the residual displacement remained in the beam which was visible to the naked eye as shown in **Figs. 5.32 and 5.33**.

Figure 5.32: Failure of specimen BCJ-12MM-Bent Up

Figure 5.33: Crushing of joint and residual displacement in beam of specimen BCJ-12MM-Bent Up

To observe the opening in the joints, LVDTs were diagonally installed as mentioned before in the Monotonic Test, to the joint on both the sides opposite to each other.

The graphs are plotted for both sides of joint crack openings as given in **Figs. 5.34 and 5.35**. Both the LVDTs show that when the displacements start in the push direction the cracks start increasing, and reduce as the displacement reduces. This condition was same for the pull side displacement but the behavior was vice versa as it was in push direction, tension side converts into compression and compression side converts into tension.
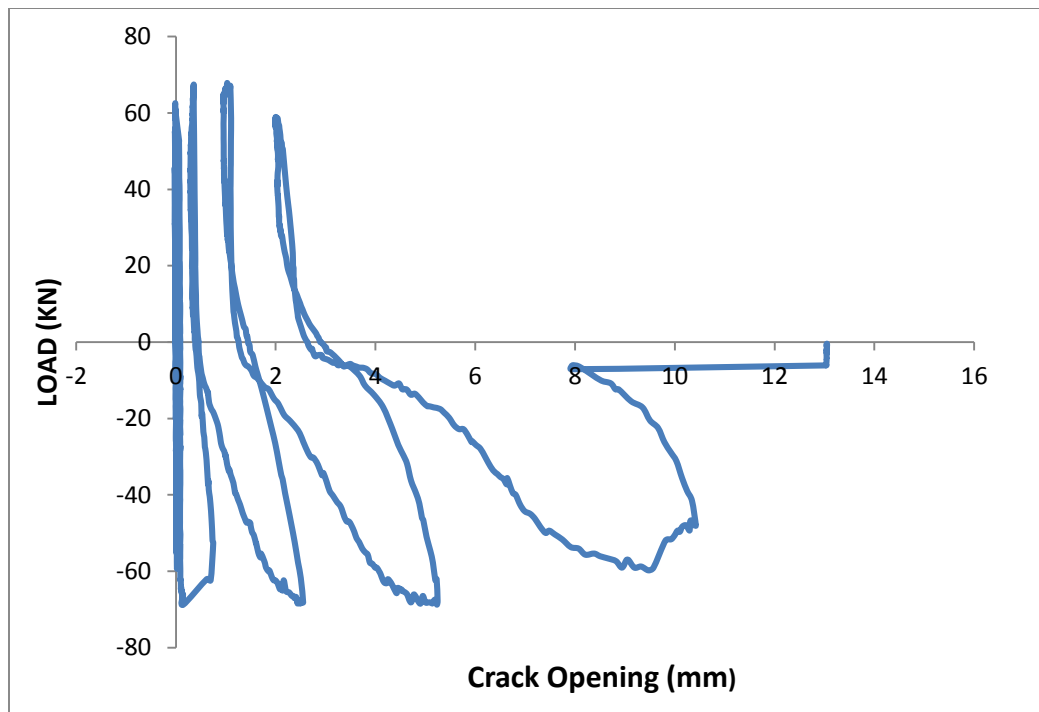
Figure 5.34: Load verses crack opening graph for LVDT Face 1
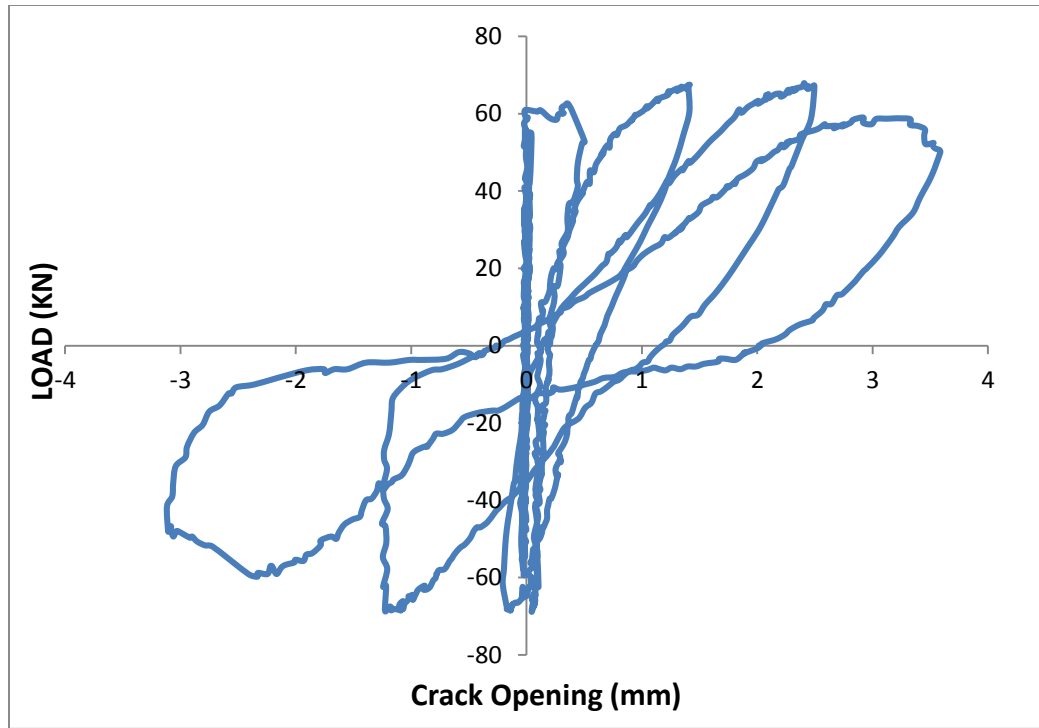
Figure 5.35: Load verses crack opening graph for LVDT Face 2

Strain gauges were installed to monitor the strains in the reinforcement. **Figs. 5.36 and 5.37** show the graphs between load and strains in the steel for top and bottom reinforcement of beam in the specimen which shows the cyclic behavior according to the cyclic test of beam-column joints.

Figure 5.36: Load verses strain graph for top beam reinforcement

Figure 5.37: Load verses strain graph for bottom beam reinforcement

For the retrofitted specimens, the graphs are plotted for both sides of the joint crack openings as given in **Fig. 5.38**. Both the LVDTs show that when the displacements starts in the push direction the cracks start increasing.

Figure 5.38: Load verses crack opening for BCJ-12MM-Bent Up with CFRP

Strain gauges were installed to monitor the strains in the reinforcement. **Fig. 5.39** shows the graphs between load and strains in the steel for top and bottom reinforcement of beam in the specimen which includes the joint regions and the interface of the BCJ using CFRP.

Figure 5.39: Load verses strain graph for top and bottom beam reinforcement for BCJ-18MM-with CFRP

126

In order to measure the strain for CFRP sheets, strain gauges were installed in both faces of the joint and the load and the strain in the CFRP sheet in the strong direction were plotted as shown in **Fig. 5.40.**

Figure 5.40: Load verses strain graph for CFRP sheets

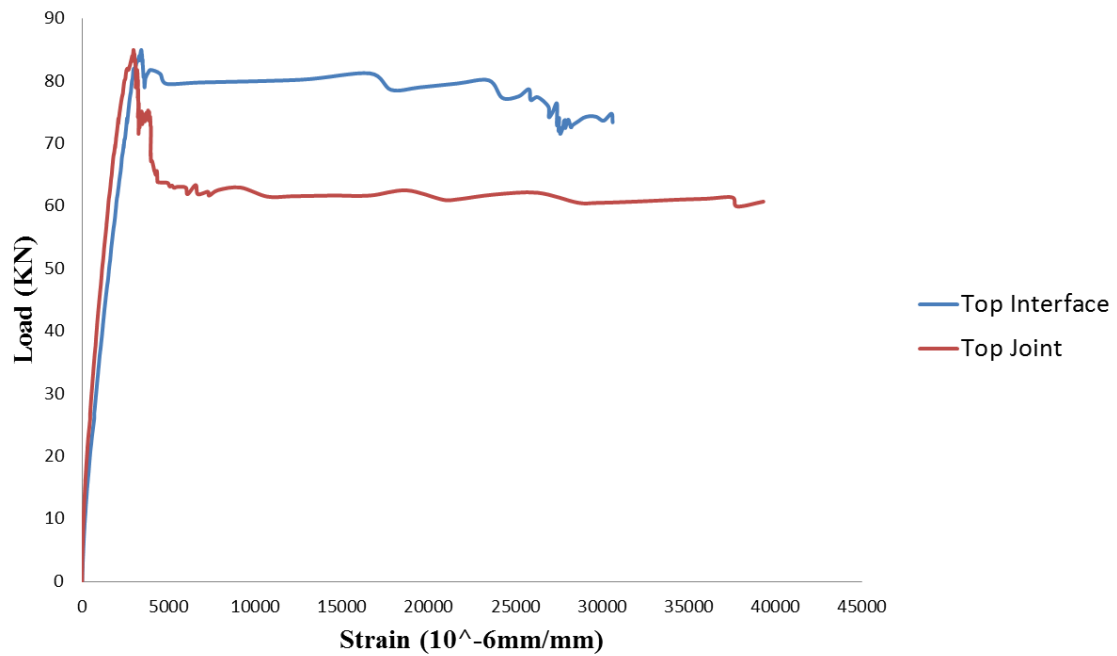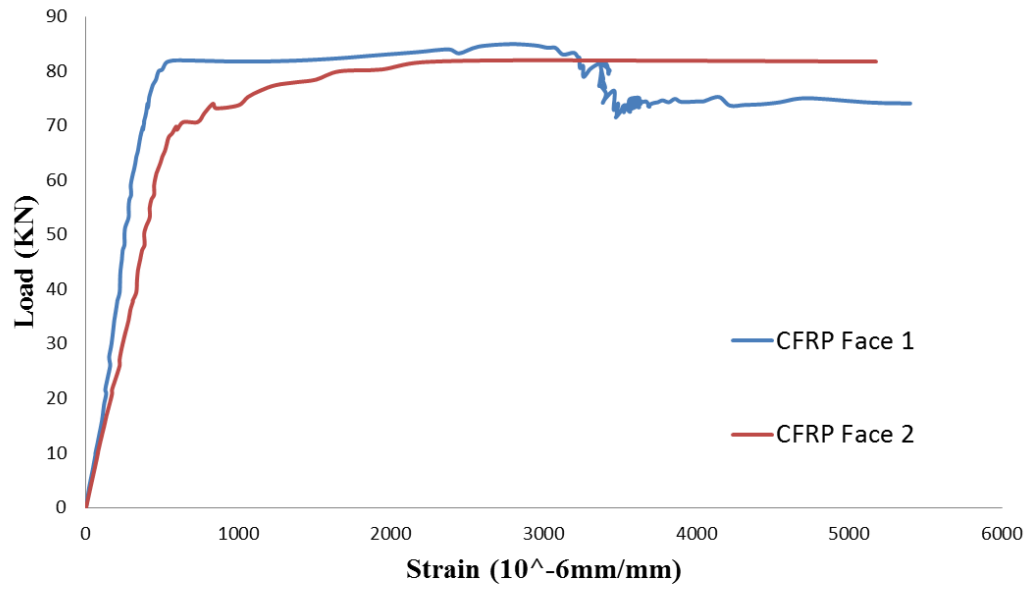### 5.4.2 Cyclic Test Result for BCJ – Bent In -12MM

For the control specimen, the load verses displacement graph shows that the maximum load and displacement reached in push direction was 67.8 kN and the maximum load in pull direction was 69.4 kN as shown in **Fig. 5.41**. The first crack formed in the specimen was a crack at the beam-column interface during the first cycle, both at the top and bottom during the push and pull displacement. The cracking load was 25 kN (push) and 20 kN (pull). The first diagonal crack at the joint region appeared in the third push cycle at a load of 53 kN which extended at a load of 66 kN in the fourth cycle. In the last two cycles the beam-column interface of the specimen was totally damaged and crushed, concrete cover spalled off from one side of the joint and the reinforcement was visible. The mode of failure in the specimen was initial flexural failure at the beam-column interface followed by a diagonal shear crack in the joint as shown in **Fig. 5.42**. For the retrofitted specimen, the load verses displacement graph shows that the maximum load reached in push direction was 73.2 kN and the maximum load in pull direction was 70.3 kN as shown in **Fig. 5.43**. The first crack formed in the specimen was a flexural crack away from the BCJ interface at a displacement 5.4 mm. This was followed by a flexural crack at the BCJ interface. The first rupture of CFRP sheet in weak direction occurred at a load of 72 kN in the push cycle. After this, a rupture of CFRP sheet in strong direction occurred at a load of 70 kN and displacement 30.3 mm as shown in **Fig. 5.44**. The maximum strain at the time of rupture of CFRP was 3182μs. The CFRP retrofitting resulted in 10% increase in the load capacity.
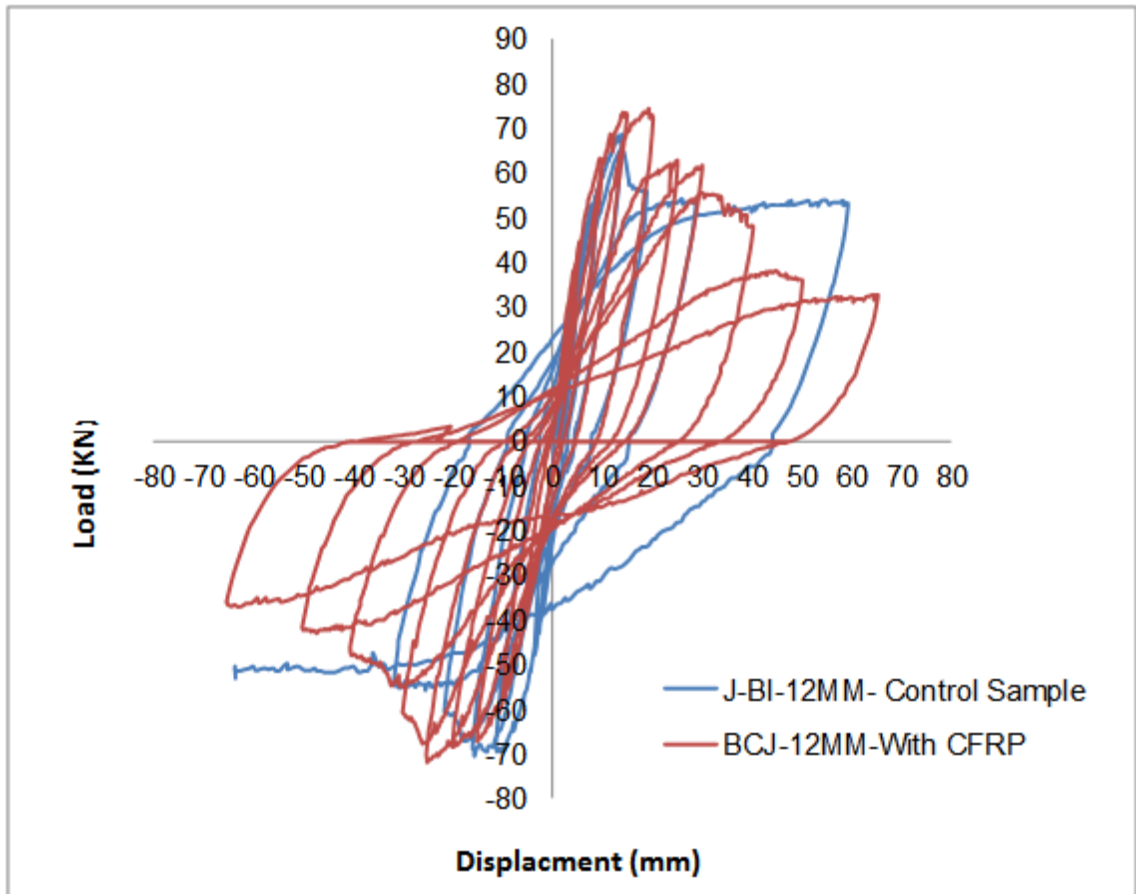
Figure 5.41: Load verses displacement graph for specimen BCJ-12MM

Figure 5.42: Crack pattern for specimen BCJ-12MM- without CFRP

129

Figure 5.43: Crack pattern for specimen BCJ-12MM- with CFRP
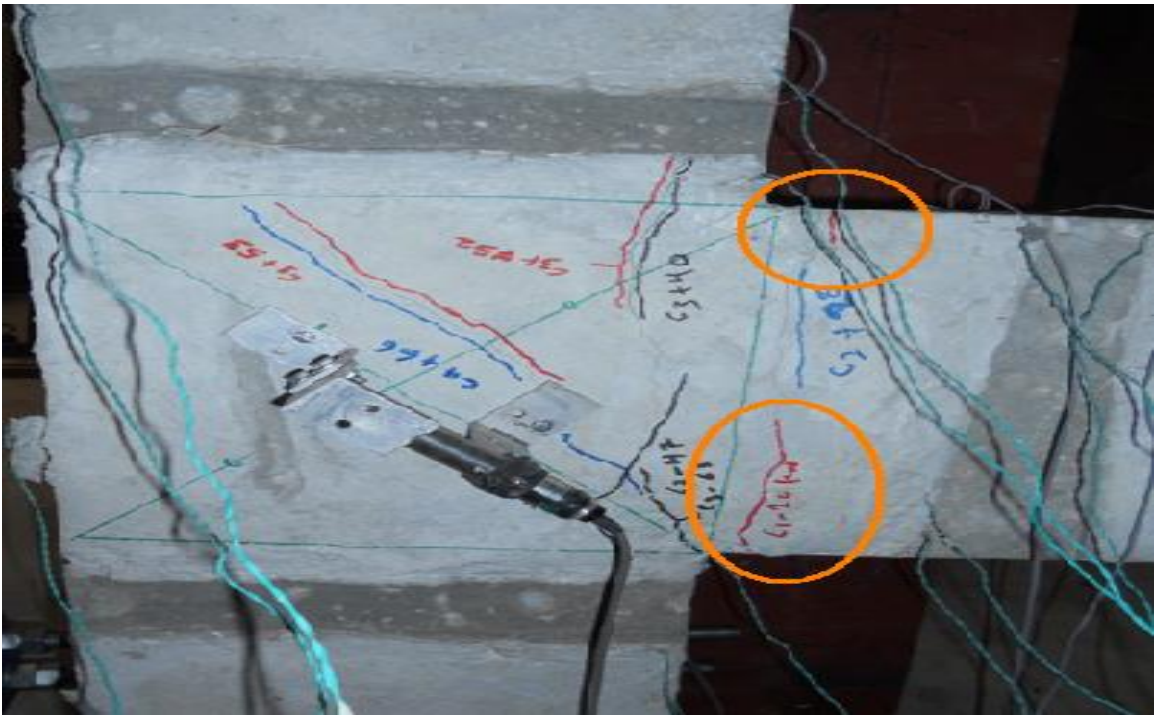
Figure 5.44: First flexural crack for specimen BCJ-12MM-Bent In

The first diagonal crack at the joint region was formed in the third cycle at the push side at the load of 53 kN and the diagonal crack extended at load of 66 kN in the fourth cycle when displaced in push direction as shown in **Fig. 5.45**.
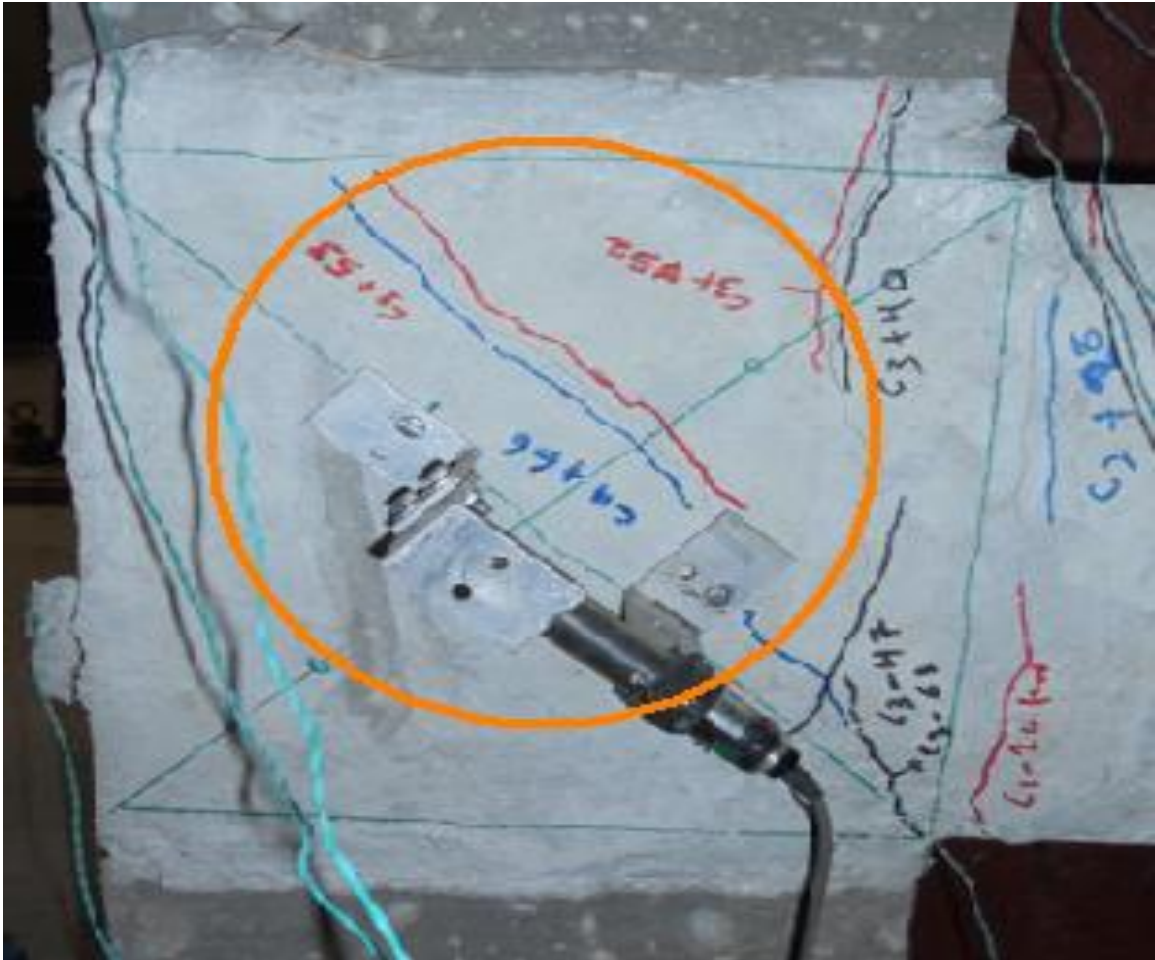
Figure 5.45: First diagonal crack in joint for specimen BCJ-12MM-Bent In

In the last two cycles, the beam-column interface of the specimen was totally damaged and crushed, concrete cover spalled off from one side of the joint, the reinforcement was totally visible to the naked eye. The failure in this specimen was totally flexural and the residual displacement of the beam can be seen clearly as shown in **Figs. 5.46, 5.47 and 5.48**.

Figure 5.46: Crushing of concrete near beam-column interface for specimen BCJ-12MM-Bent In

Figure 5.47: Spilling of concrete in joint region for specimen BCJ-12MM-Bent

Figure 5.48: Residual displacement in beam for specimen BCJ-12MM-Bent In

LVDTs were installed at the joint region diagonally on both sides to observe the crack opening during the push and pull loading as shown in **Figs. 5.49 and 5.50**. The graphs were plotted between the load and diagonal crack openings in the joint as given in **Figs. 5.51 and 5.52.**
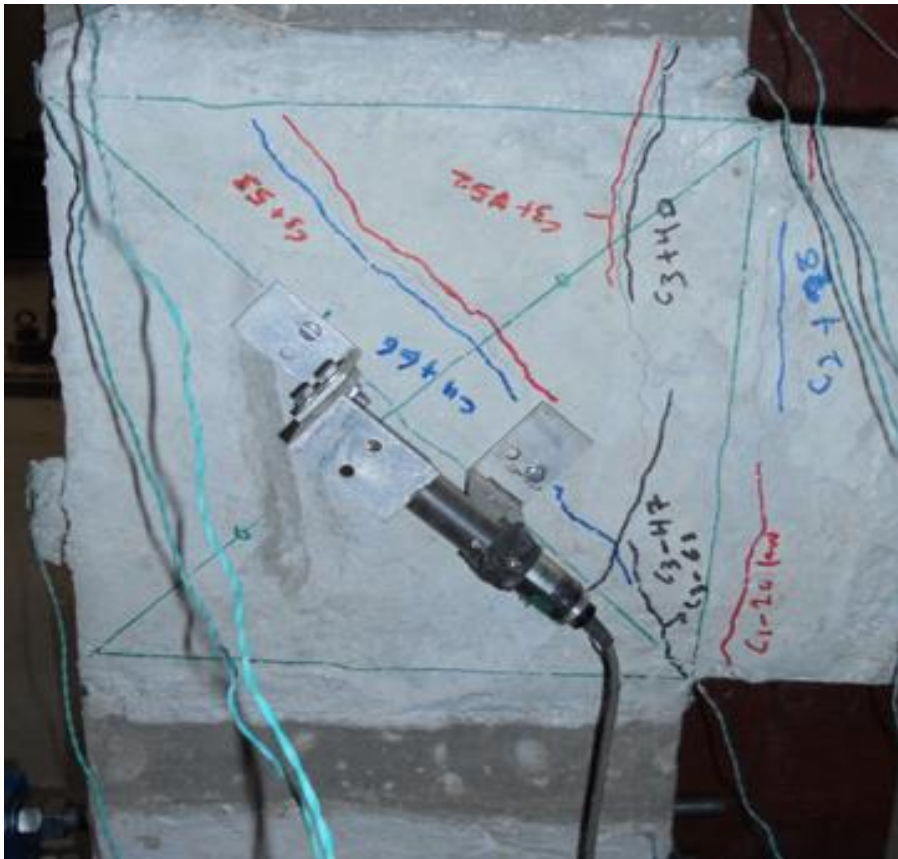
Figure 5.49: Position of LVDT J1 in joint to observe diagonal crack

Figure 5.50: Position of LVDT J2 in joint to observe diagonal crack
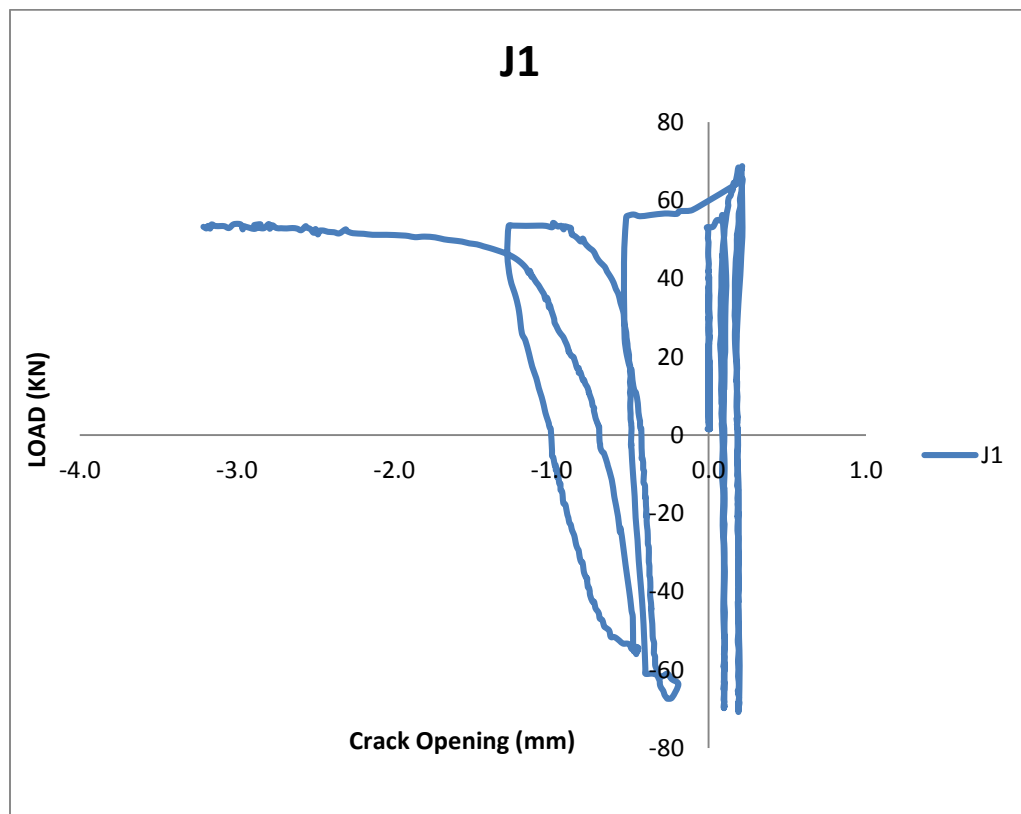
Figure 5.51: Load verses crack opening graph for LVDT J1
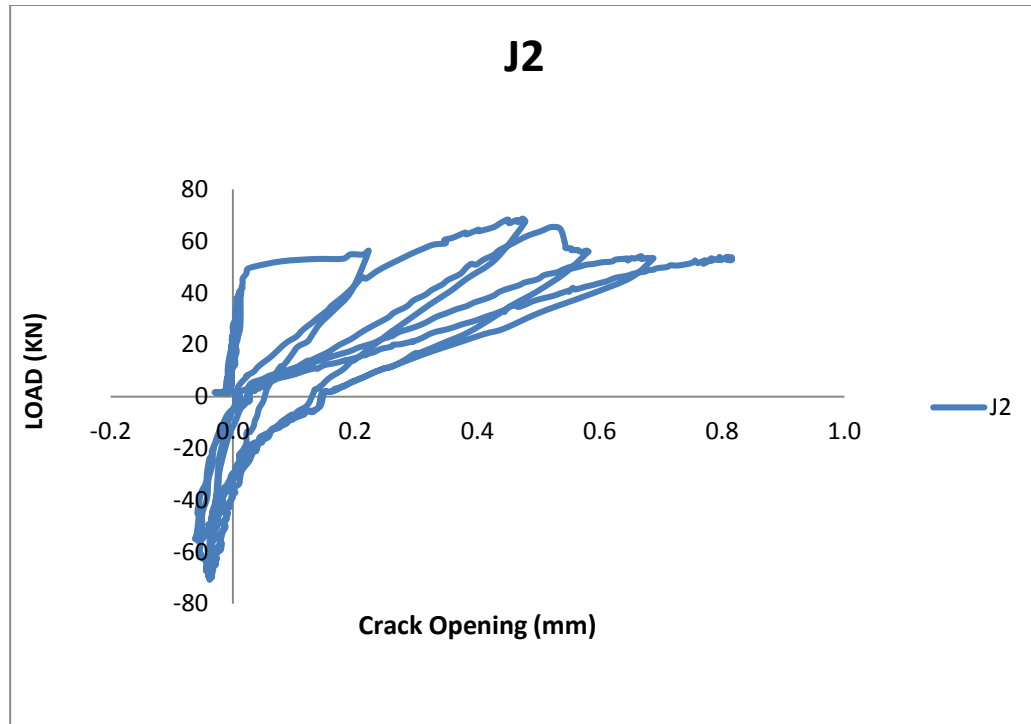
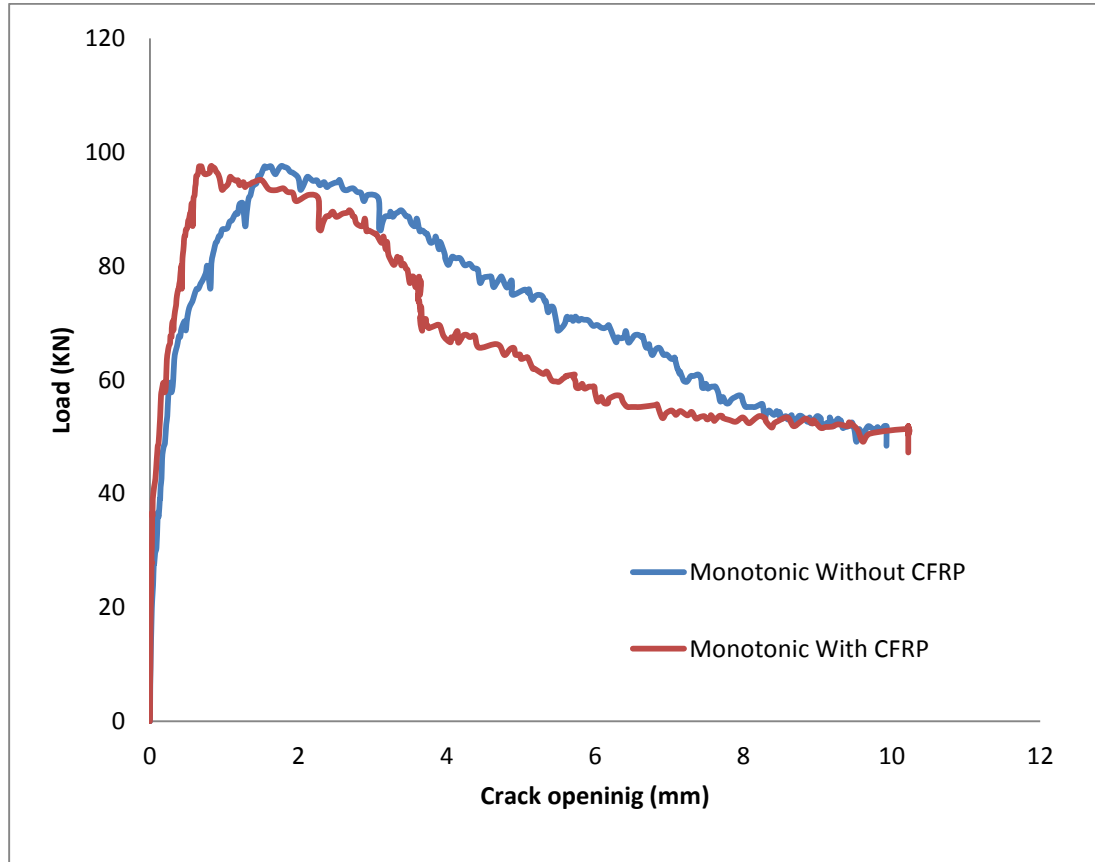**Figure 5.52: Load verses crack opening graph for LVDT J2**

Strain gauges were installed to observe the strains in the reinforcement on the selected positions, and graphs were plotted between the load and strains in the reinforcements as shown in **Figs. 5.53 and 5.54**. Graphs for SG8 and SG11 show the strains for the beam top and bottom reinforcements; **Figs. 5.53 and 5.54** clearly show the compression and tension behavior of steel during the push and pull cyclic displacement of beam.
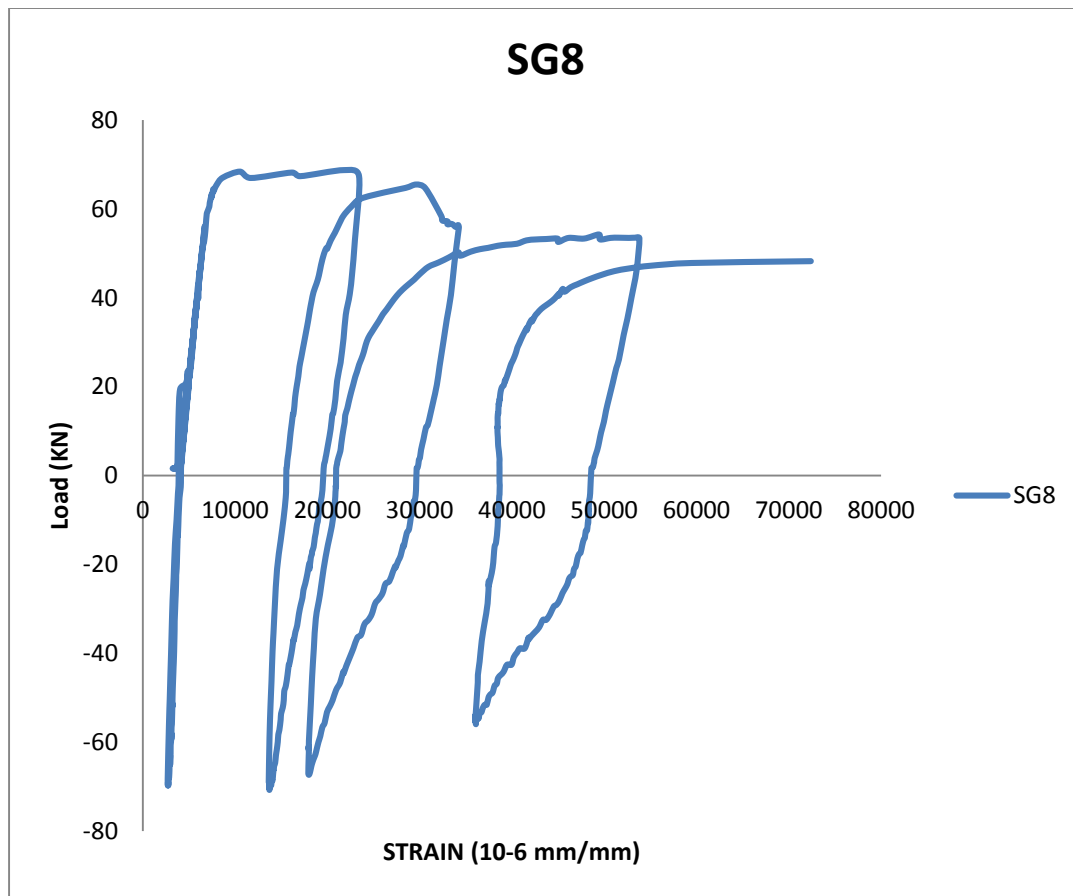
Figure 5.53: Load verses strain graph for top beam reinforcement
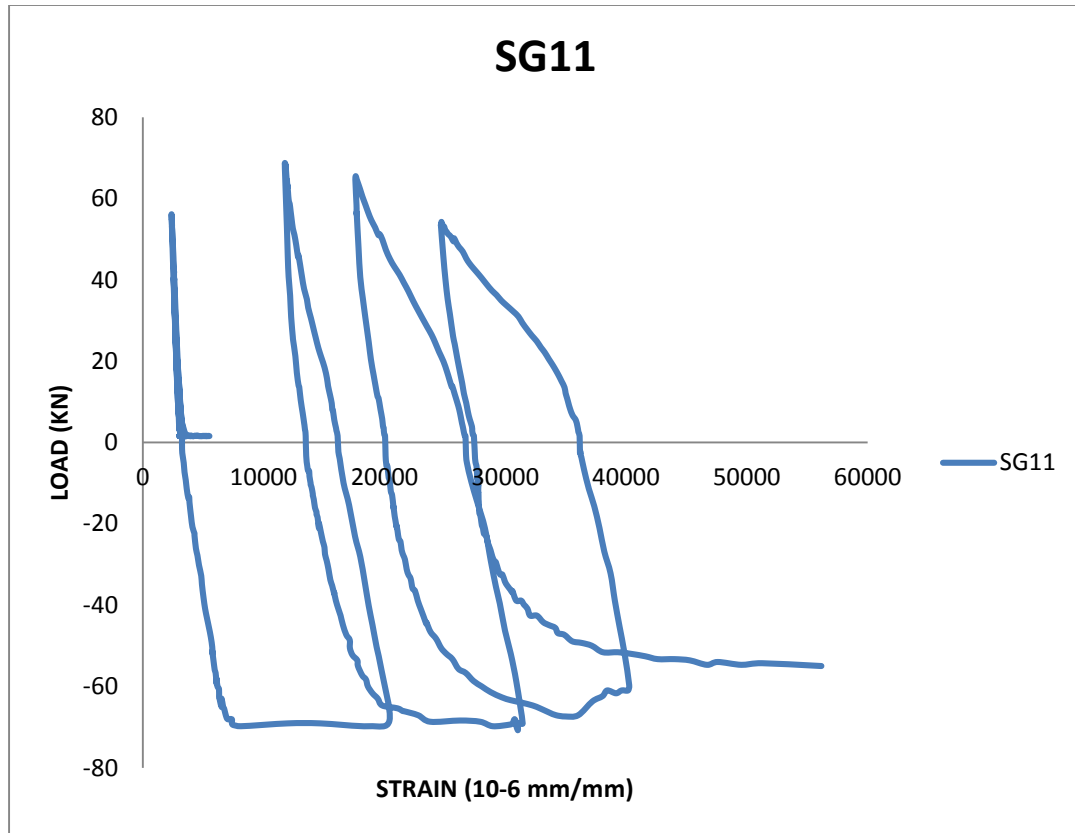
Figure 5.54: Load verses strain graph for bottom beam reinforcement

For the retrofitted specimens, the graphs are plotted for both sides of joint crack openings as given in **Fig. 5.55**; both the LVDTs show when the displacements start in the push direction, the cracks start increasing.
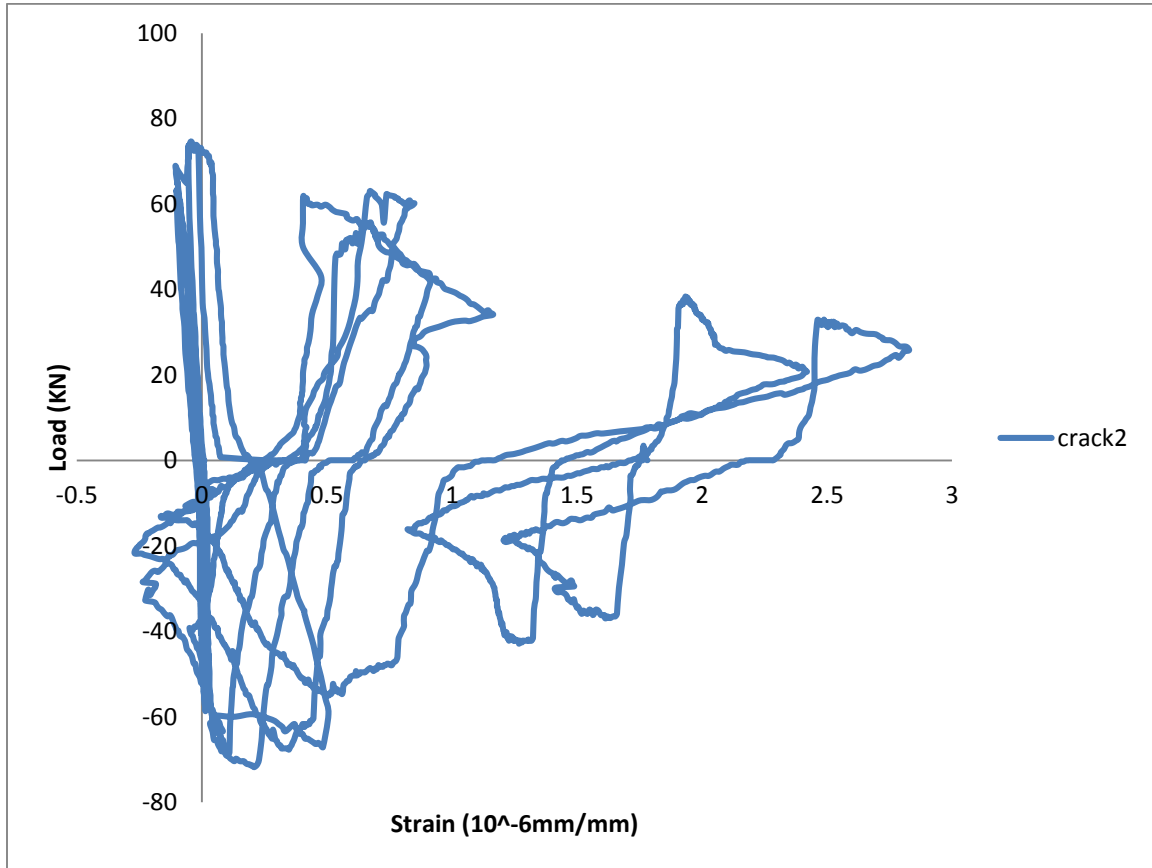
Figure 5.55: Load verses crack opening for BCJ-12MM-Bent In with CFRP

Strain gauges were installed to monitor the strains in the reinforcement; **Fig. 5.56** shows the graphs between load and strains in the steel for top and bottom reinforcement of beam in the specimen which includes the joint regions and the interface of the BCJ using CFRP.
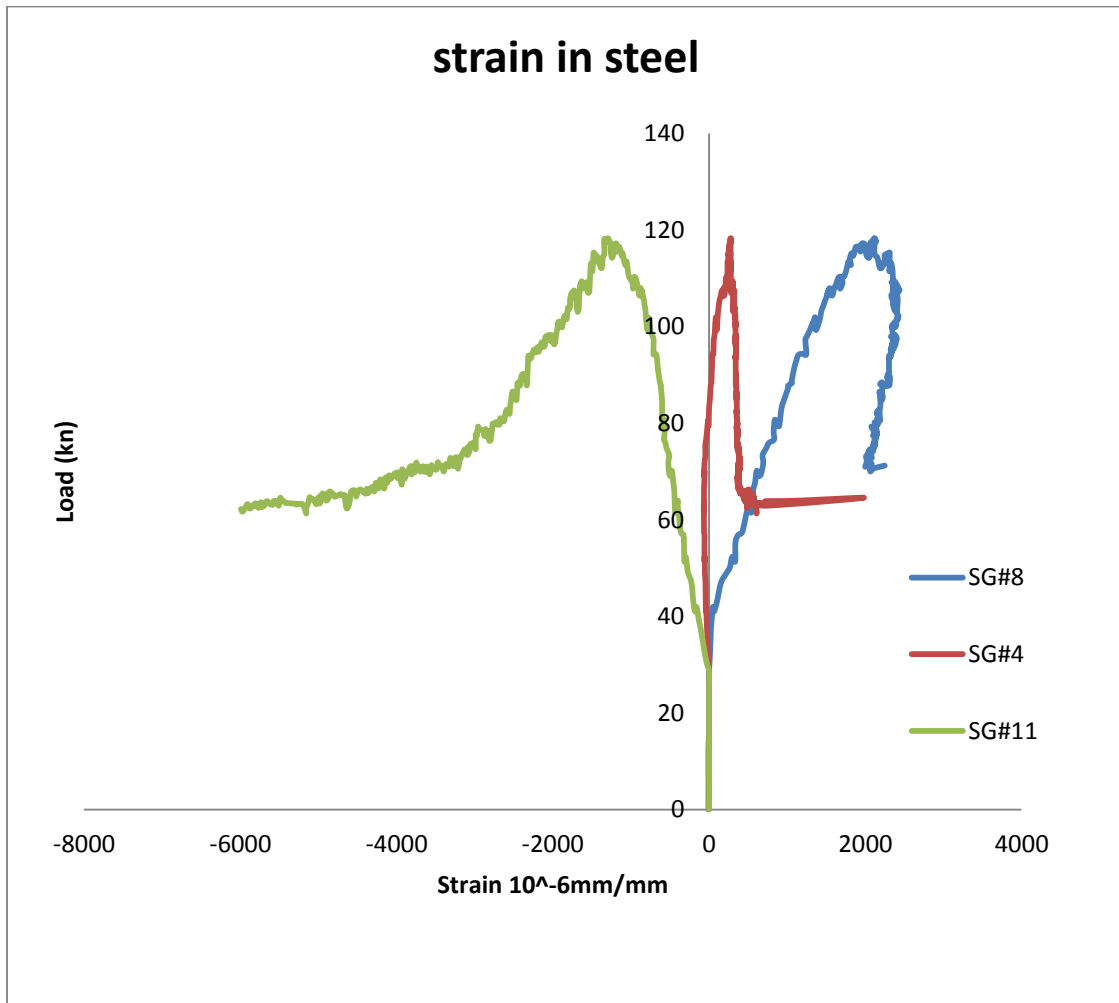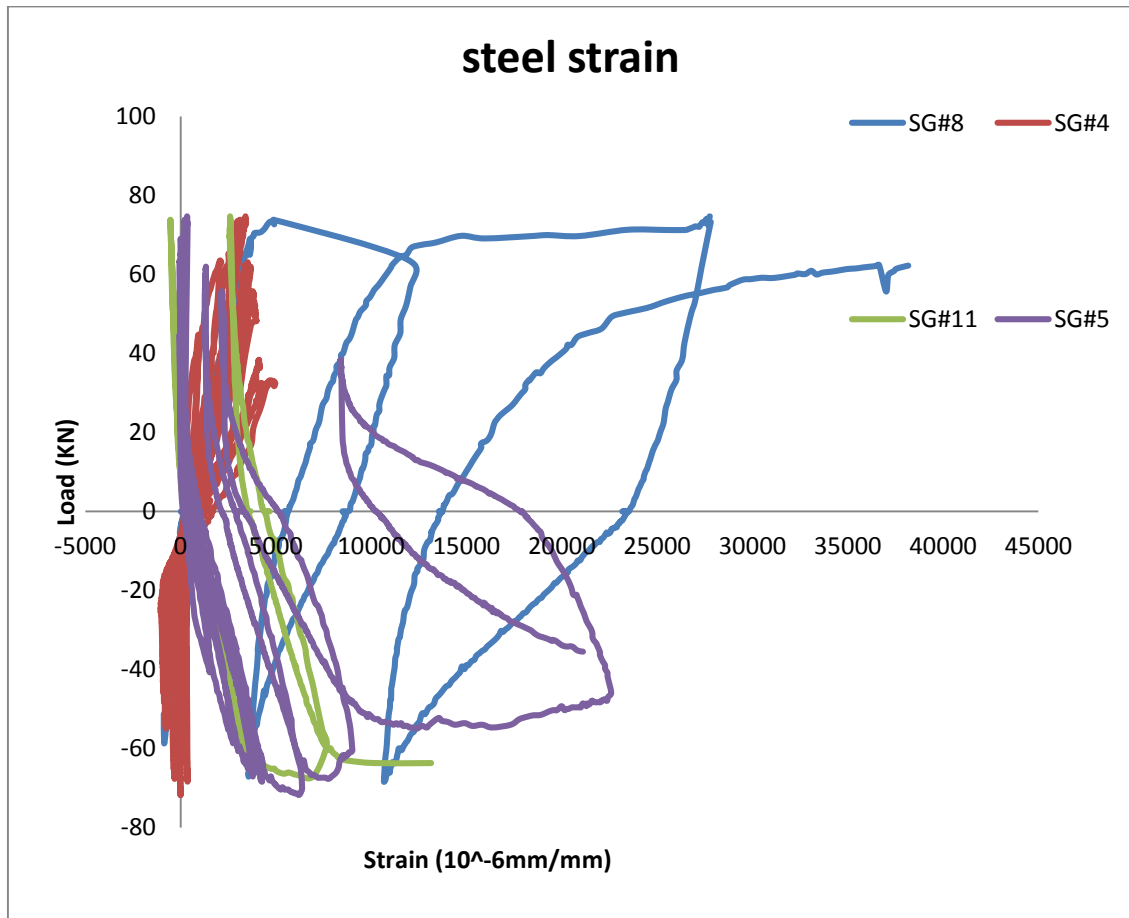

Figure 5.56: Load verses strain graph for top and bottom beam reinforcement for BCJ-12MM-Bent In with CFRP

In order to measure the strain for CFRP sheets, strain gauges were installed in both faces of the joint and the load and the strain in the CFRP sheet in the strong direction were plotted as shown in **Fig. 5.57**.
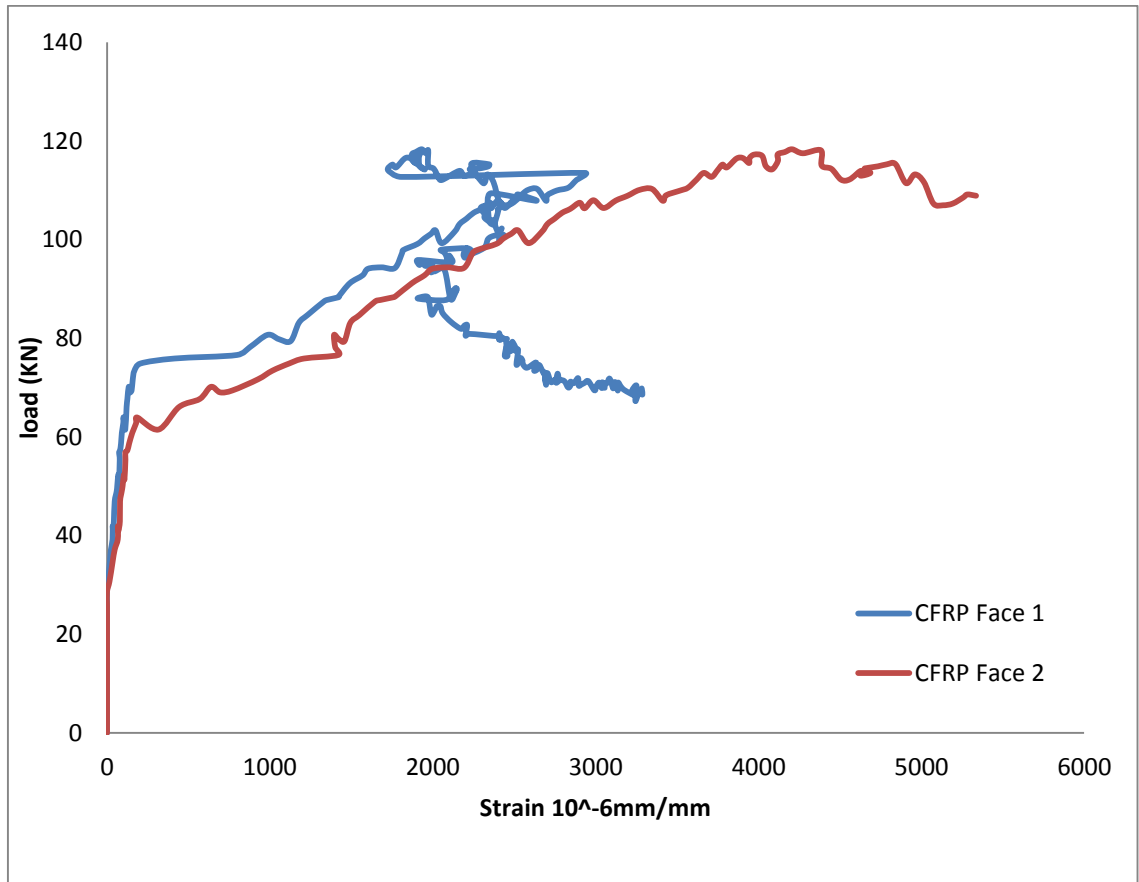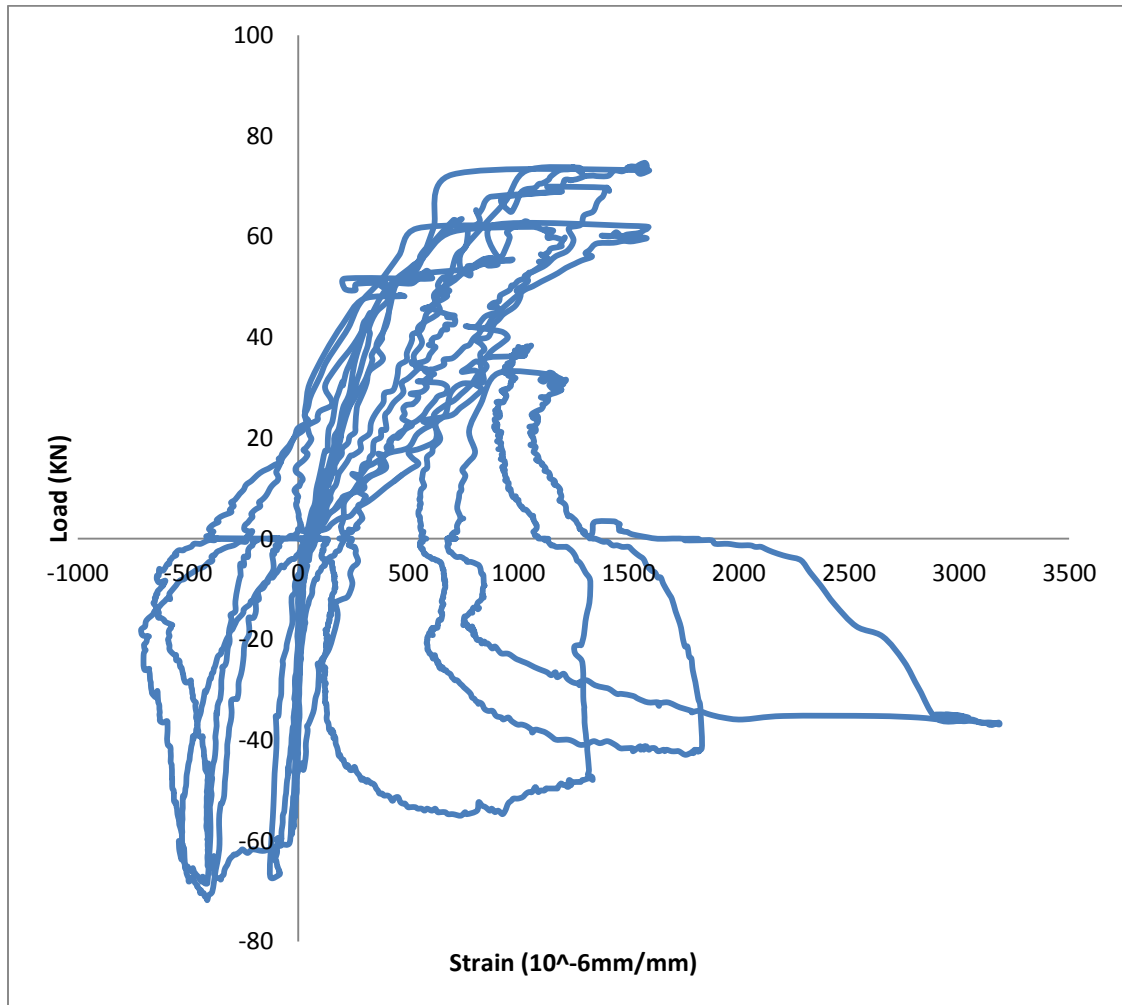

Figure 5.57: Load verses strain graph for CFRP sheets

5.4.3 Cyclic Test Result for BCJ-18MM

The load verses displacement graph for retrofitted and non-retrofitted specimen is shown in **Fig. 5.58**. The maximum load in push and cycle was 99 kN and 100.3 kN, respectively. The first flexural crack was formed near the beam-column interface at 45 kN at a displacement of 3.3 mm. Diagonal crack in the BCJ appeared at a load of 60 kN and a displacement 5.59 mm in the push cycle. The diagonal cracks progressed towards the center with increasing load and displacements. During the pull cycle, diagonal joint cracks were also formed in the opposite direction as shown in **Fig. 5.59**. These diagonal cracks on both sides of the column widened up during the successive pull-push cycles. During the last two cyclic loads, concrete on the beam-column interface was crushed and spalled off on the both sides. For the retrofitted specimen, the load verses displacement graph shows that the maximum load in the push, and cycles were 124.7 kN and 92.9 kN, respectively as shown in **Fig. 5.58**. The first crack formed away from the BCJ interface at 48 kN. The CFRP sheet ruptured in weak direction at 124 kN in push cycle. The rupture of CFRP sheet in strong direction occurred at 85 kN as shown in **Fig. 5.60**. The maximum strain at rupture of CFRP was 5860μs. A load capacity enhancement of 27.5% was observed.
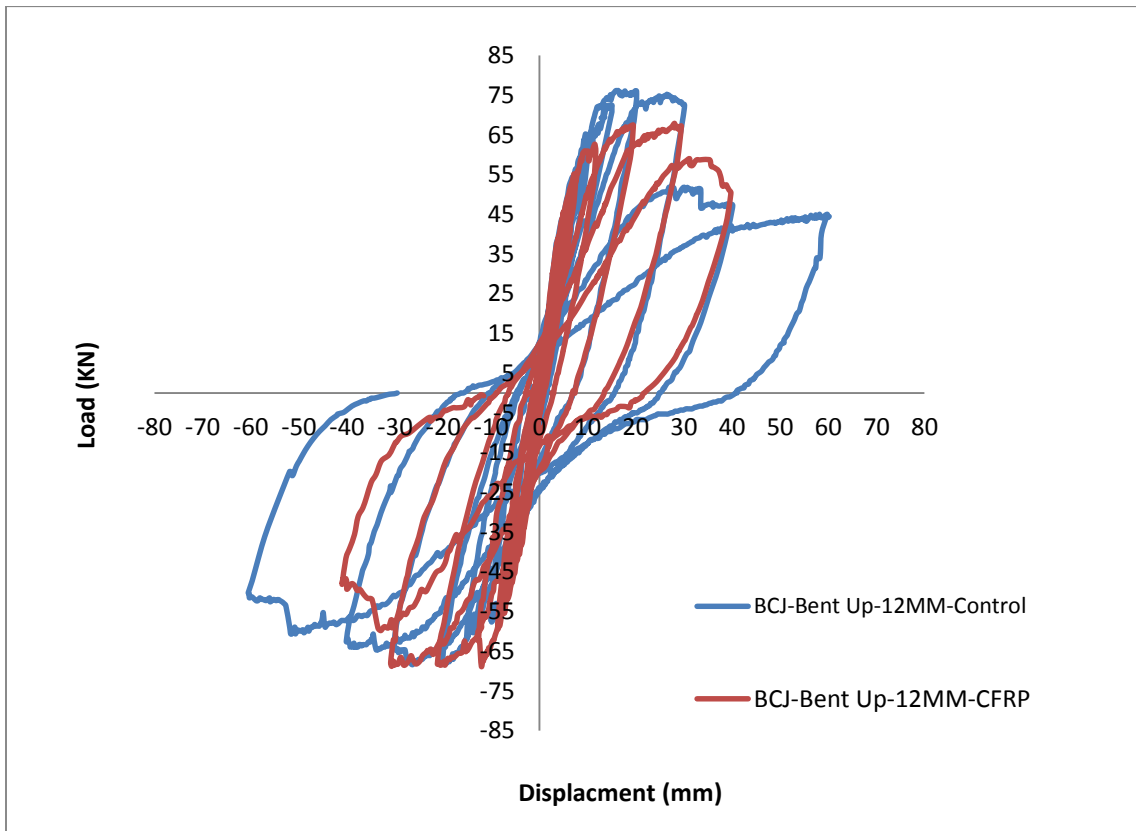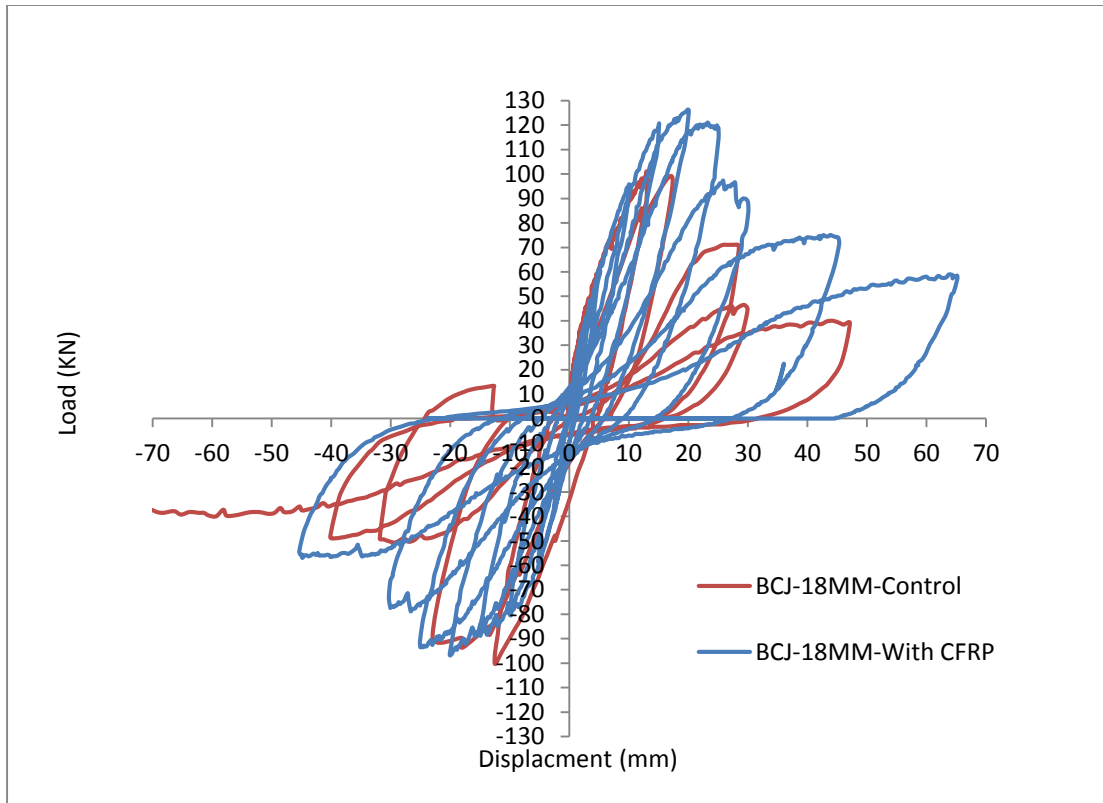
Figure 5.58: Load verses displacement graph for specimen BCJ-18MM

Figure 5.59: Crack pattern specimen BCJ-18MM- without CFRP

143

Figure 5.60: Crack pattern specimen BCJ-18MM- with CFRP

The first flexural crack was found in the first cycle in the push down direction near the beam-column interface at 45 kN and displacement of 3.3 mm and when the load and displacement reached to 60 kN and 5.59 mm, the diagonal crack in the joint appeared as shown in **Fig. 5.61** and diagonal cracks in the joints move towards the center with the increasing load and displacements, the maximum load reached in the push direction was 96.98 kN.

Figure 5.61: First flexural crack for specimen BCJ-18MM

When the specimen was displaced in pulling direction, cracks were formed in the bottom of the beam at 58 kN load. Diagonal joint cracks were also formed in the opposite direction to the previous joint cracks as shown in **Fig. 5.62**.

Figure 5.62: First diagonal crack in joint for specimen BCJ-18MM

The cracks were also formed on the back side of the column and all the cracks were widened up during the pull-push loading process. Because of these wide cracks, the stiffness of the specimen reduced as shown in load and displacement relationship plot. During the last two cyclic loads, concrete on the beam-column interface was crushed and joint surfaces start to spall off on the both sides of the joint and the reinforcements were visible to the naked eye as shown in **Figs. 5.63 and 5.64**. In the end, the reinforcement had yielded, joint was completely failed and significant residual displacement was observed.

Figure 5.63: Formation of crack in joint during cyclic load test in specimen BCJ-18MM

Figure 5.64: Spilling of concrete in joint region for specimen BCJ-18MM

LVDTs were placed diagonally in the joint region to observe the tension crack openings in the joints and the graph was plotted for load and opening as given in **Figs. 5.65 and 5.66**. It can be seen from the graph, when the displacement starts in the push direction the cracks start increasing, and reduce as the displacement reduces. This condition was same for the pull side displacement but the behavior was vice versa as it was in push direction. Tension side converts into compression and compression side converts into tension and the cracks were seen on both directions in the joint in the form of X as shown in **Fig. 5.67** and this X crack was also observed in the core of concrete joint.

Figure 5.65: Position of LVDT J1 in joint to observe diagonal crack
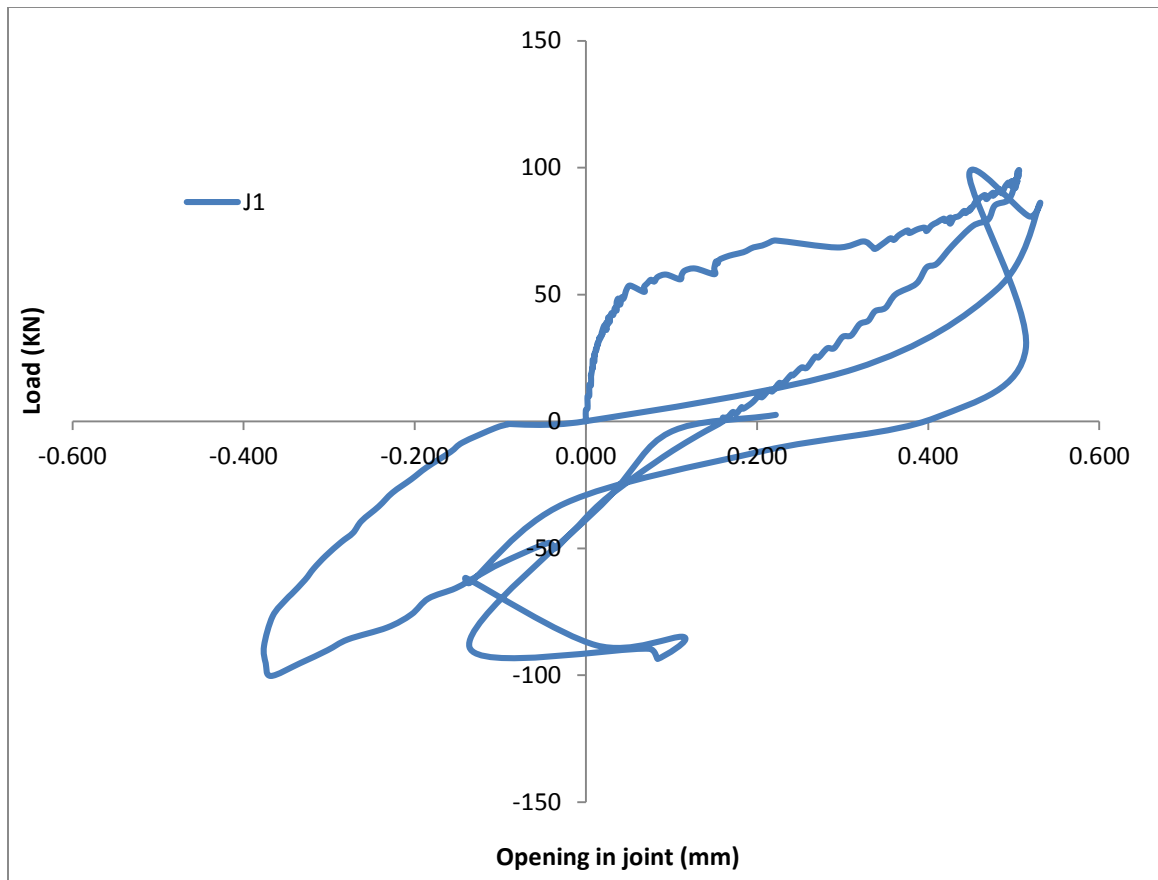
Figure 5.66: Load verses crack opening for BCJ-18MM-without CFRP
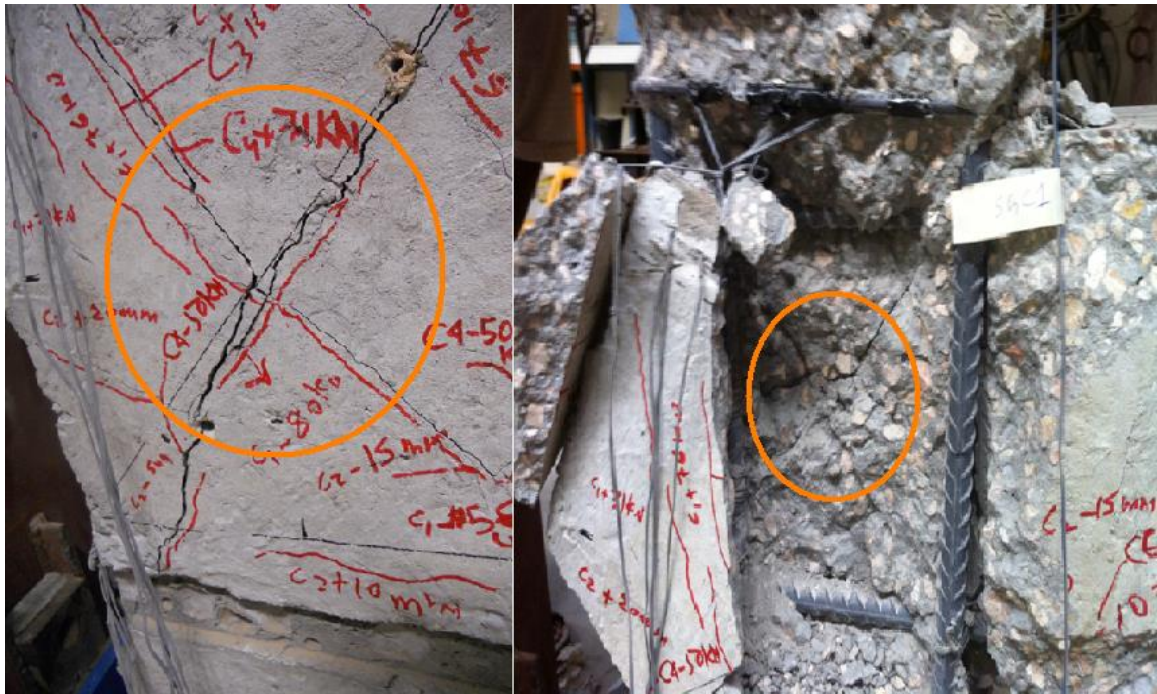
Figure 5.67: Diagonal X crack failure in joint core

150

Strain gauges were installed in the reinforcement to observe the strain in the steel during the test. Strain gauges SG8 and SG11 were located at the top and bottom reinforcement of beam near the beam-column interface. It is clear from **Figs. 5.68 and 5.69**, when the displacement was applied in the push direction to the specimen, the top reinforcements of the beam face of the tension while the bottom reinforcements were facing compression and the opposite conditions were observed when the specimen was displaced in pull direction.
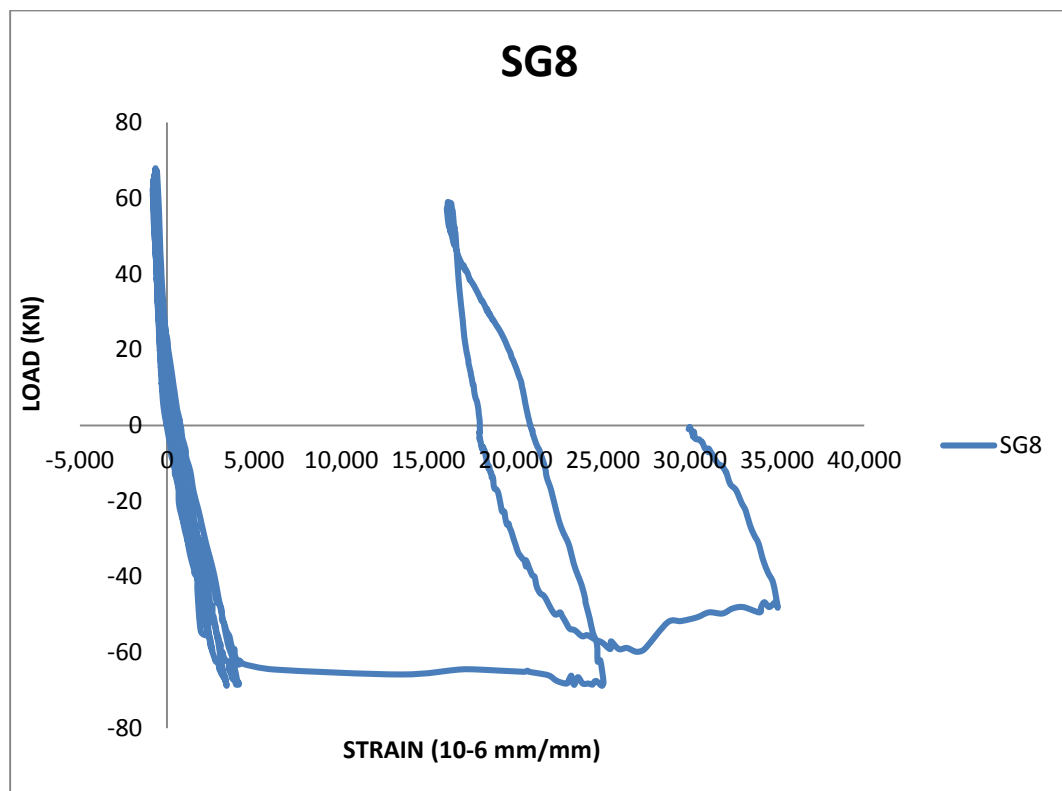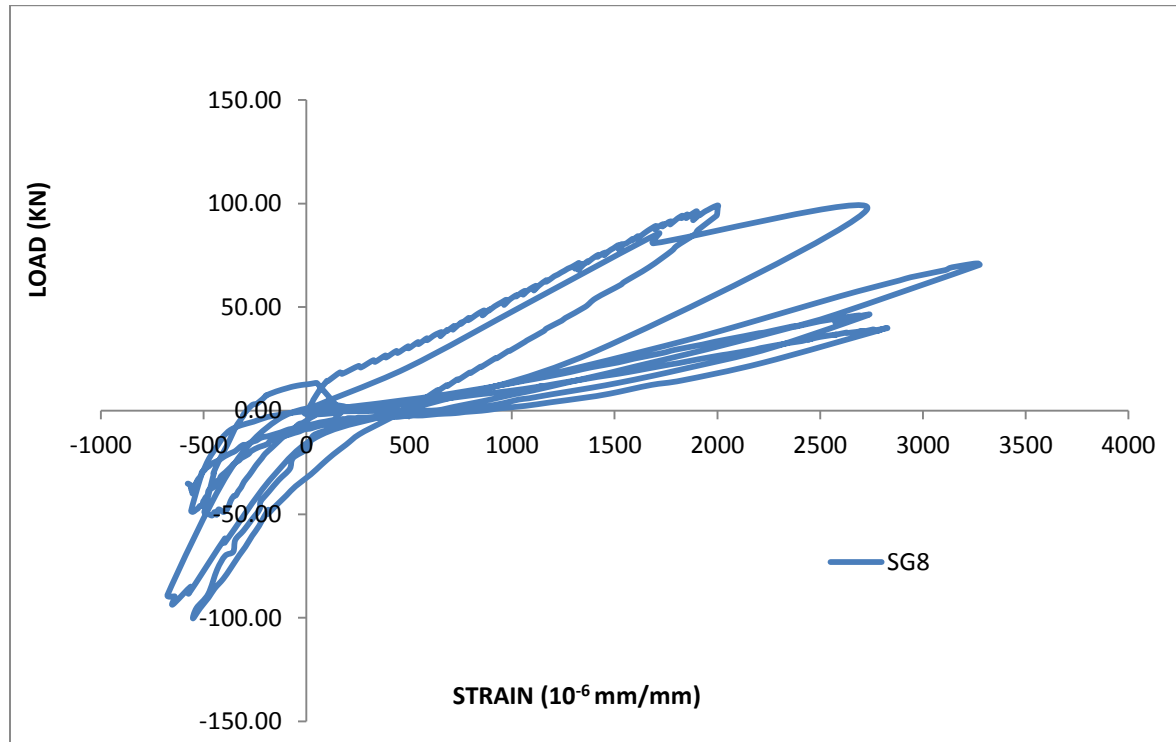

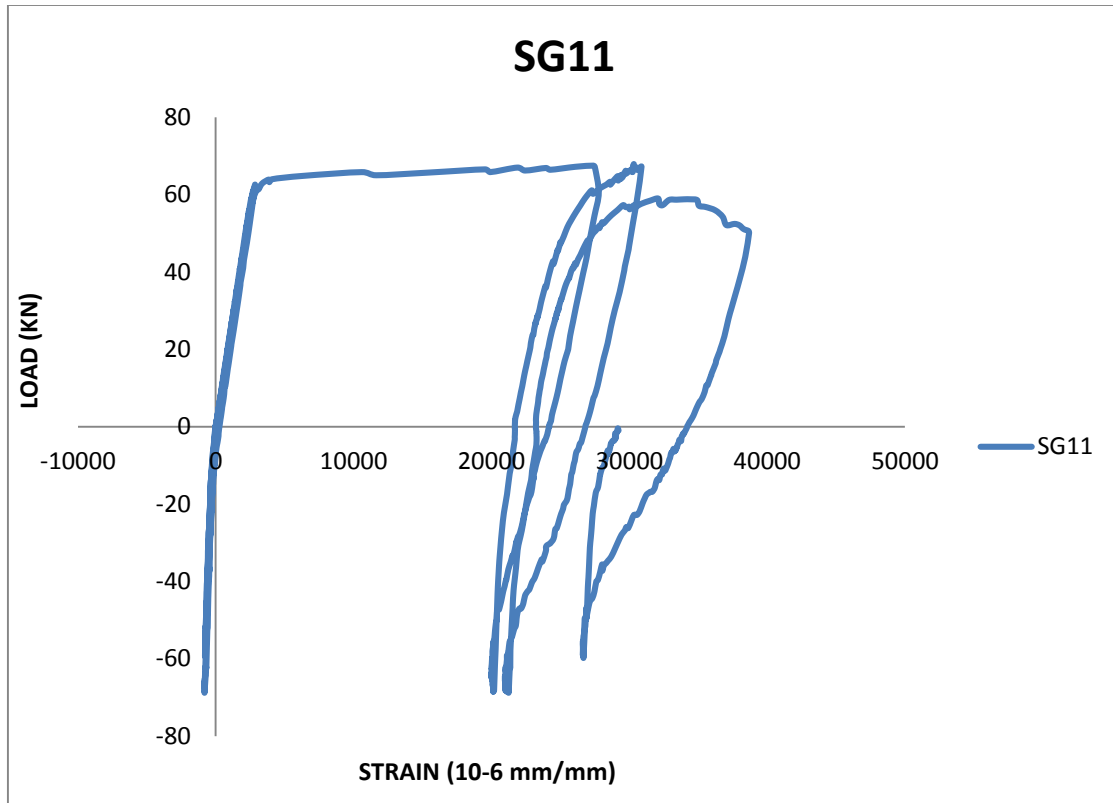**Figure 5.68: Load verses strain graph for top beam reinforcement**
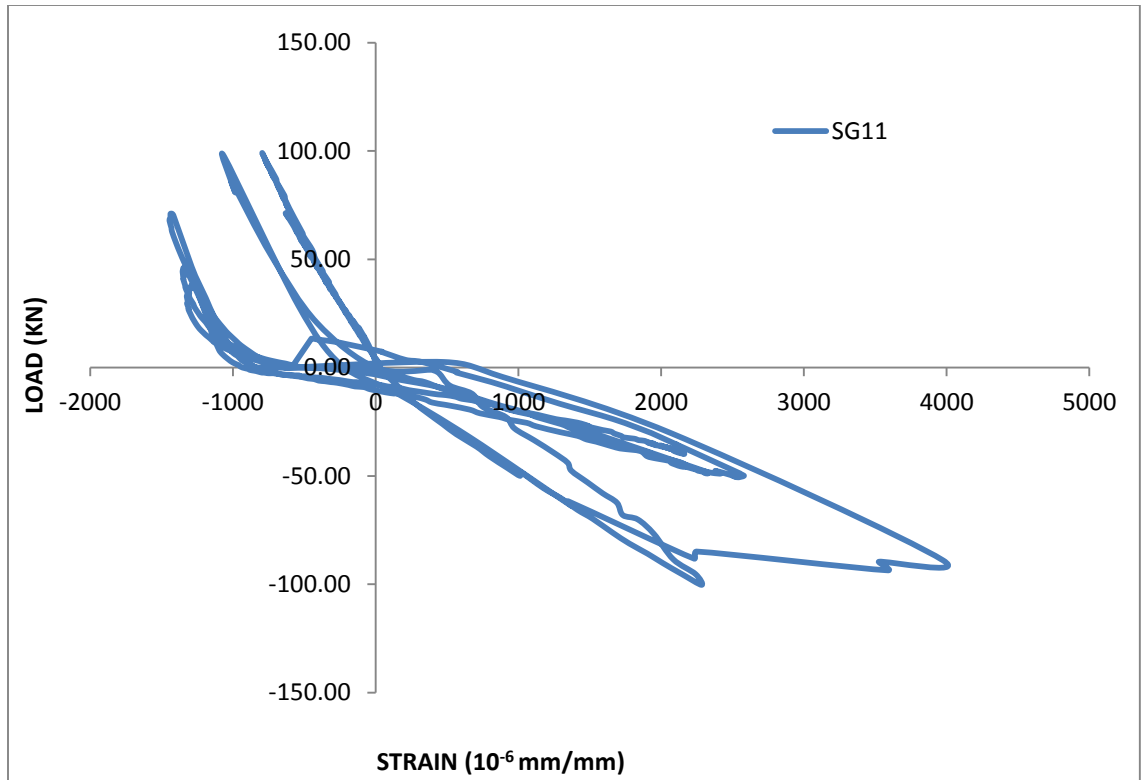
Figure 5.69: Load verses strain graph for bottom beam reinforcement

For the retrofitted specimen, the graphs are plotted for both sides of joint crack openings as given in **Fig. 5.70**. Both the LVDTs show that when the displacements start in the push direction, the cracks start increasing.
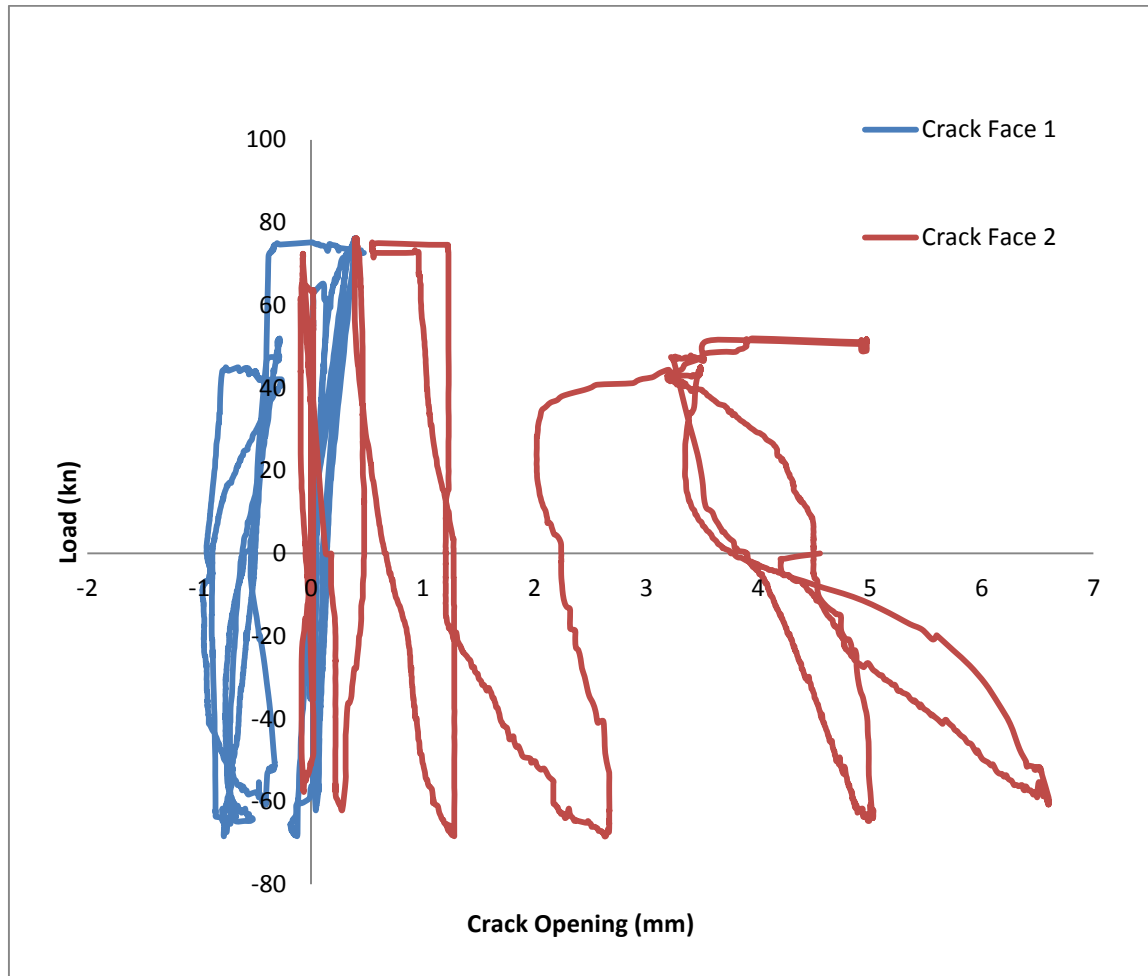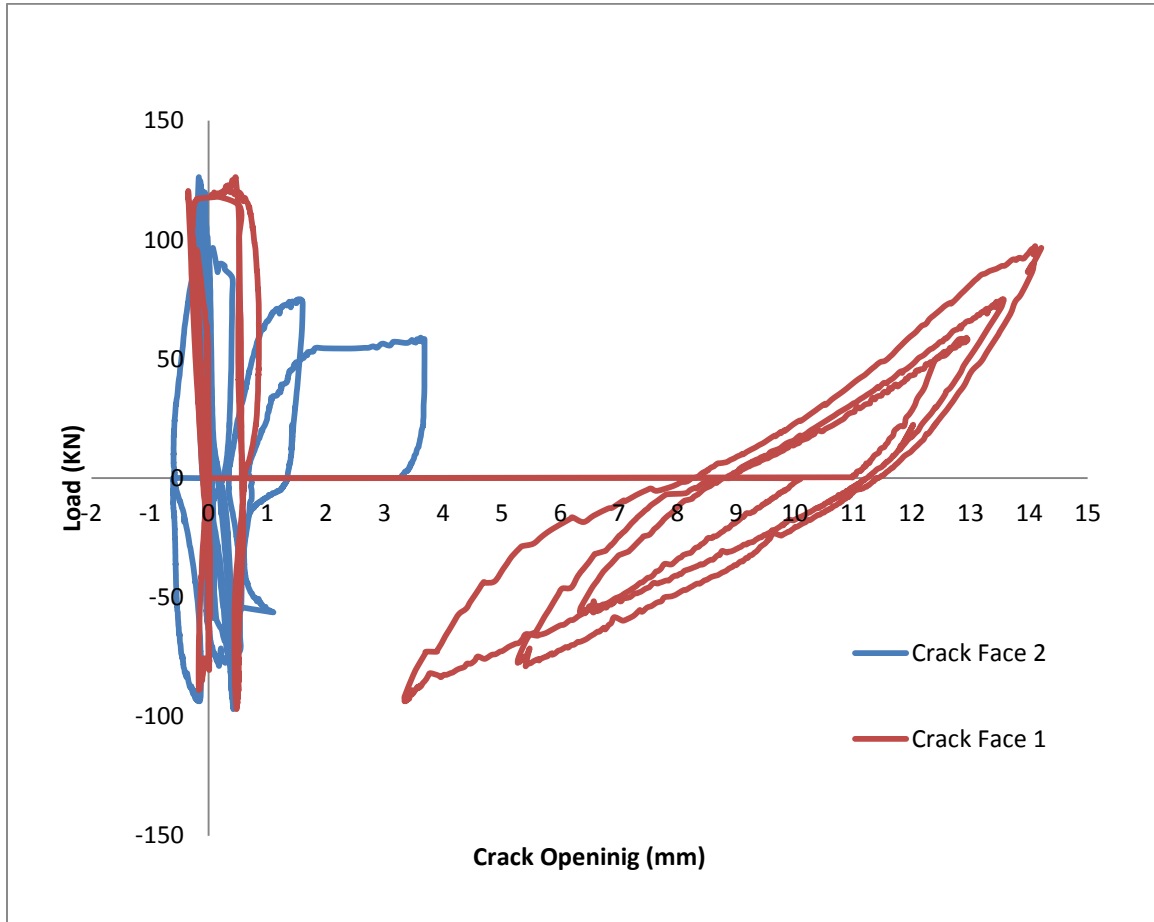

Figure 5.70: Load verses crack opening for BCJ-18MM- with CFRP

Strain gauges were installed to monitor the strains in the reinforcement; **Fig. 5.71** shows the graphs between the load and strains in the steel for top and bottom reinforcement of beam in the specimen which includes the joint regions and the interface of the BCJ using CFRP.
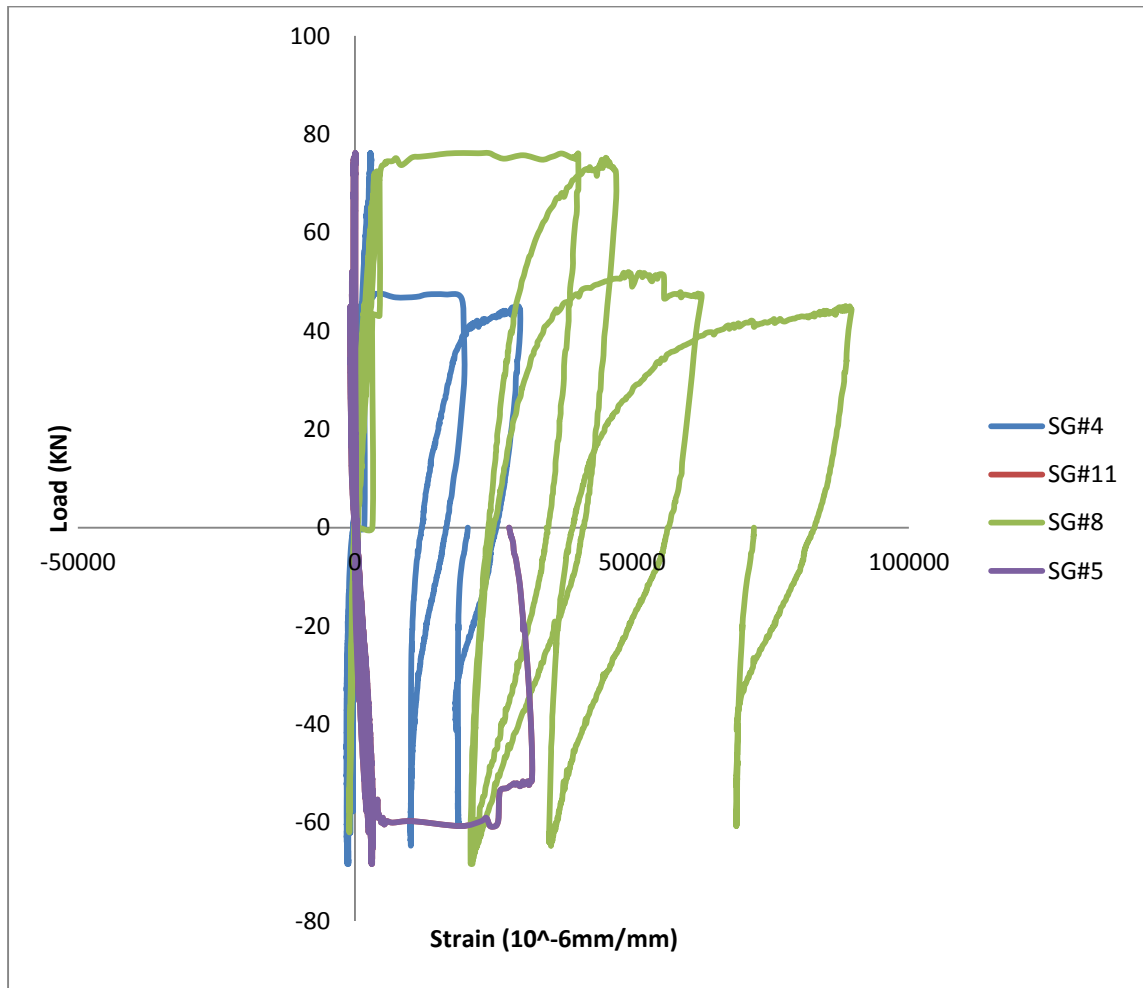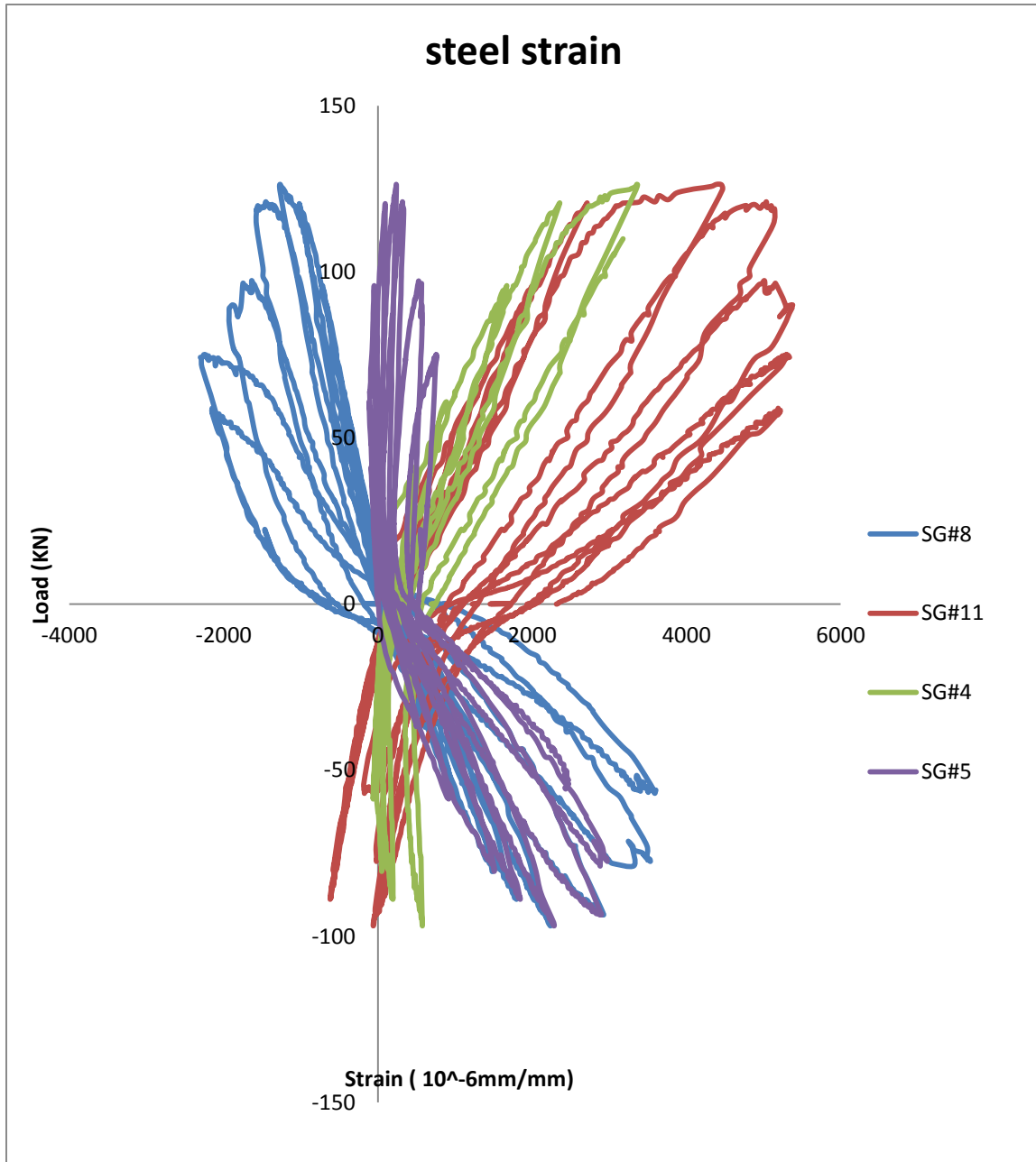

Figure 5.71: Load verses strain graph for top and bottom-beam reinforcement for BCJ-18MM-with CFRP

In order to measure the strain for CFRP sheets, strain gauges were installed in both faces of the joint and the load and the strain in the CFRP sheet in the strong direction were plotted as shown in **Fig. 5.72**.
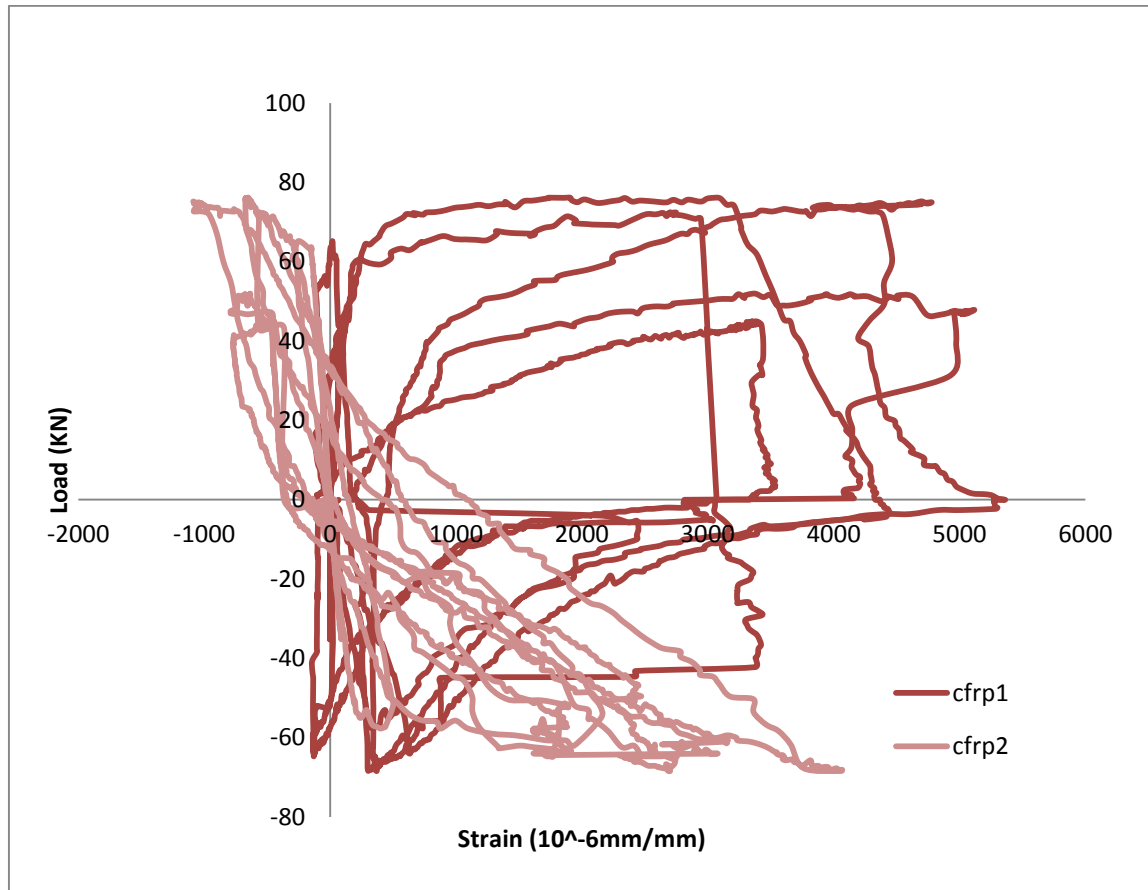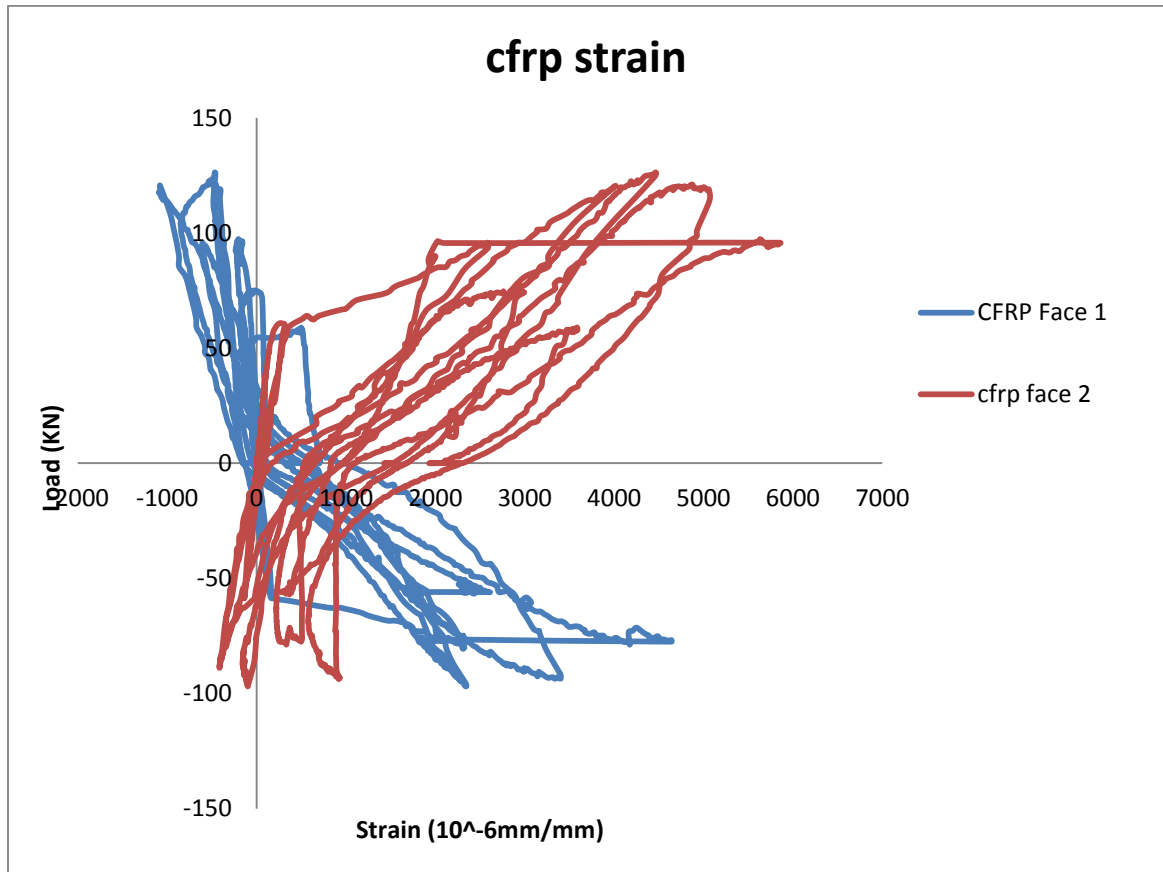

Figure 5.72: Load verses strain graph for CFRP sheets

5.5   Comparison of Load Displacement Response of all Specimens

For the monotonic test, it is clear that the BCJ-12MM Bent Up and BCJ-12MM-Bent-In fail under flexure while the BCJ-18MM-Bent-In fails due to the shear failure at the joint as shown in **Figs. 5.73 and 5.74**.
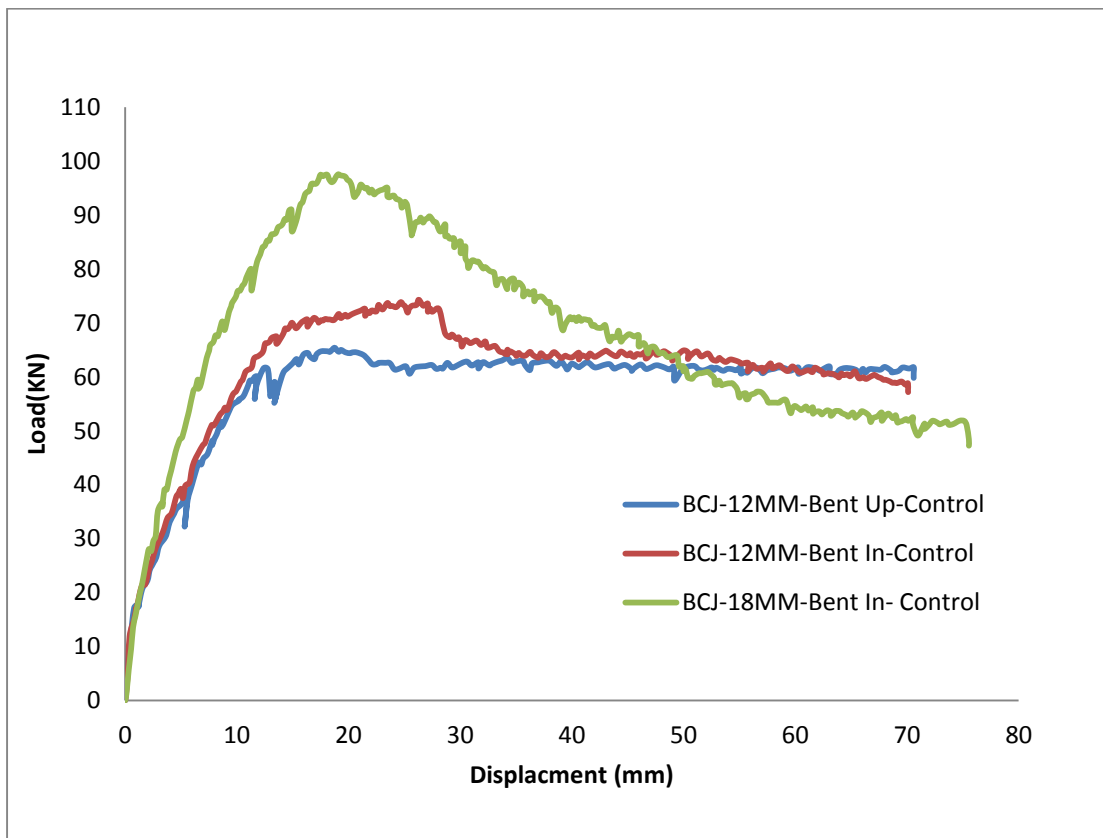
Figure 5.73: Comparison of load deflection response of all specimens without CFRP
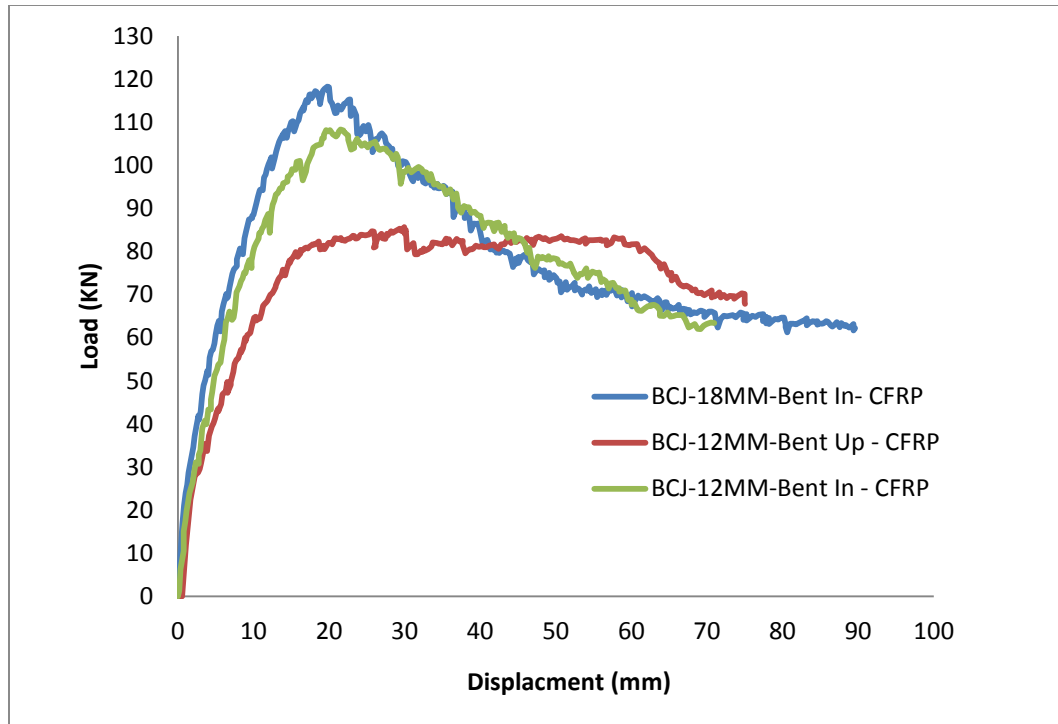
Figure 5.74: Comparison of load deflection response of all specimens with CFRP

For the cyclic test, the hysteresis for all the specimens was plotted in **Figs. 5.75 and 5.76** which show the difference of behavior for each specimen. Specimen BCJ-18MM has more flexural capacity than BCJ-12MM- Bent-Up and BCJ-12MM- Bent-In, whereas BCJ-12MM- Bent-In has approximate same flexural capacity as BCJ-12MM- Bent-Up but it shows the stiffer behavior both in push and pull directions.
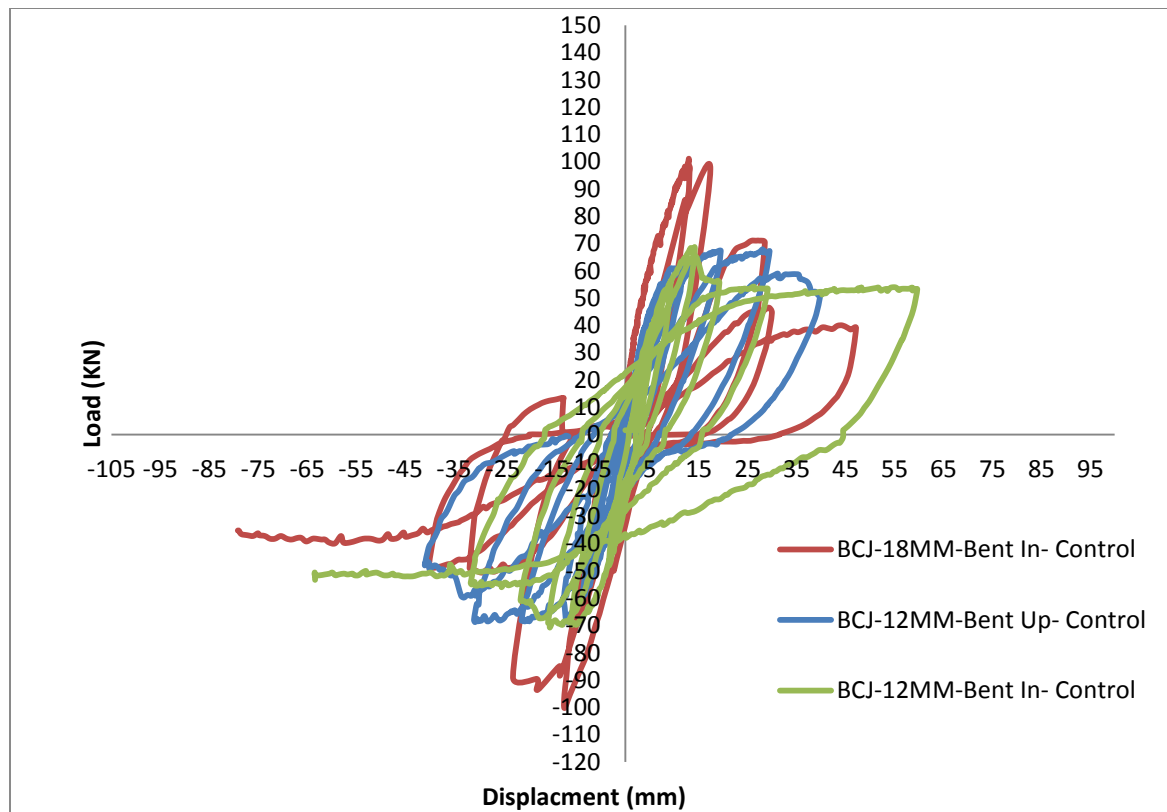
Figure 5.75: Comparison of hysteresis envelope of all control specimens
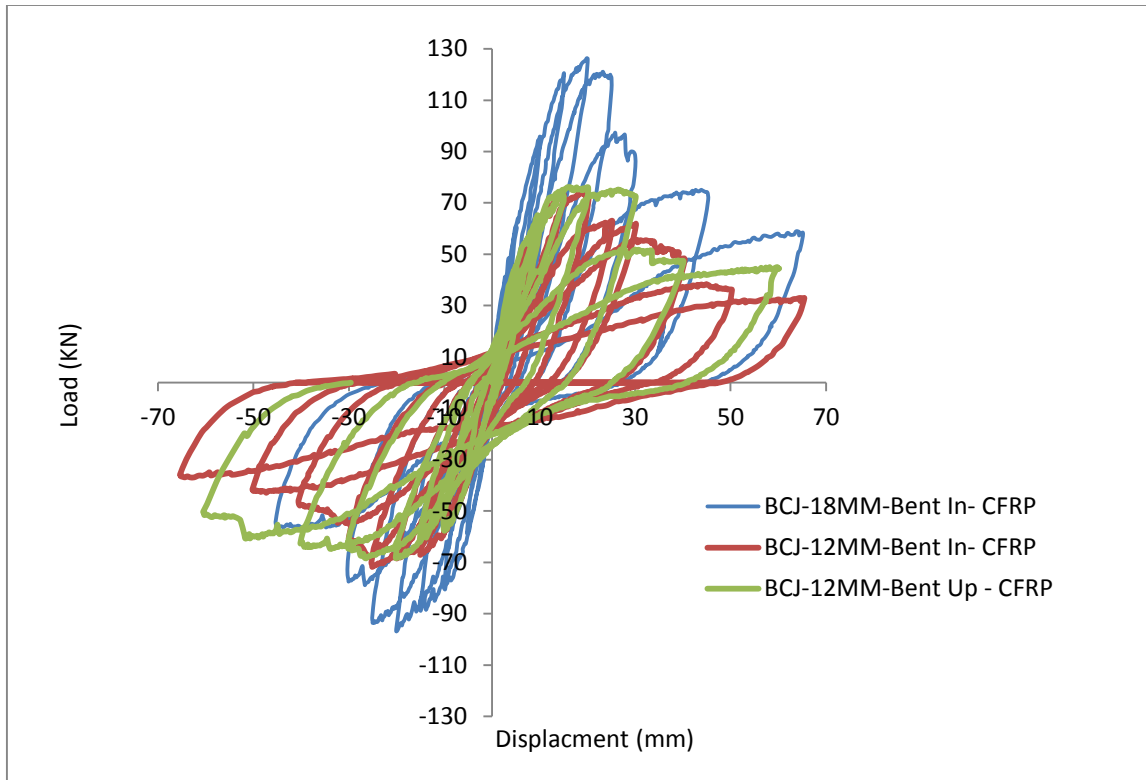
Figure 5.76: Comparison of hysteresis envelope of all retrofitted specimens

159

Envelop of the hysteresis for all the specimens were plotted in **Figs. 5.77 and 5.78** which shows the difference of behavior for each specimen. Specimen BCJ-18MM-Bent In has more flexural capacity than BCJ-12MM-Bent Up and BCJ-12MM-Bent In, whereas BCJ-12MM-Bent In has approximate same flexural capacity as BCJ-12MM-Bent Up but it shows the stiffer behavior both in push and pull directions.
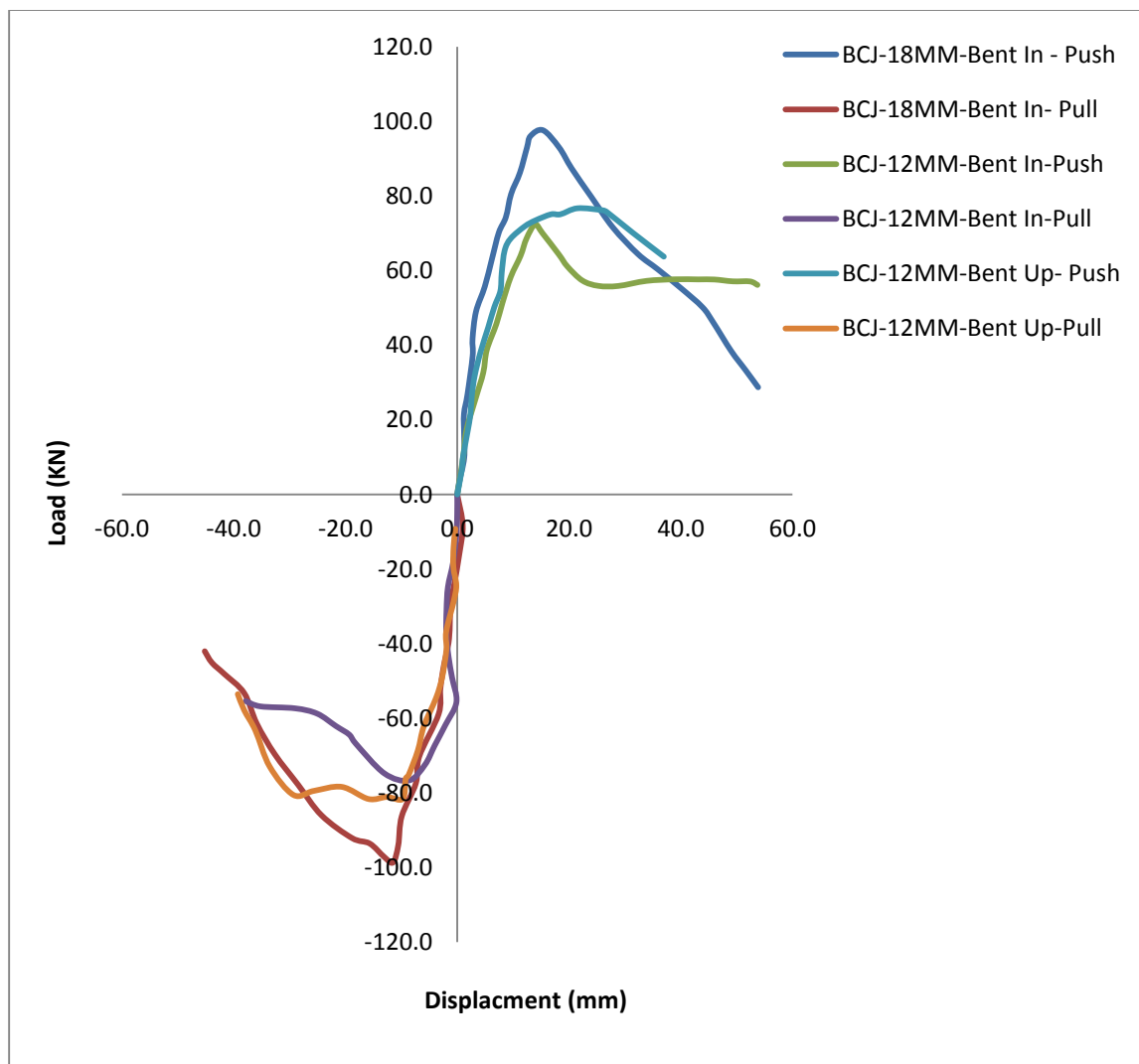
Figure 5.77: Comparison of hysteresis envelope of all control specimens
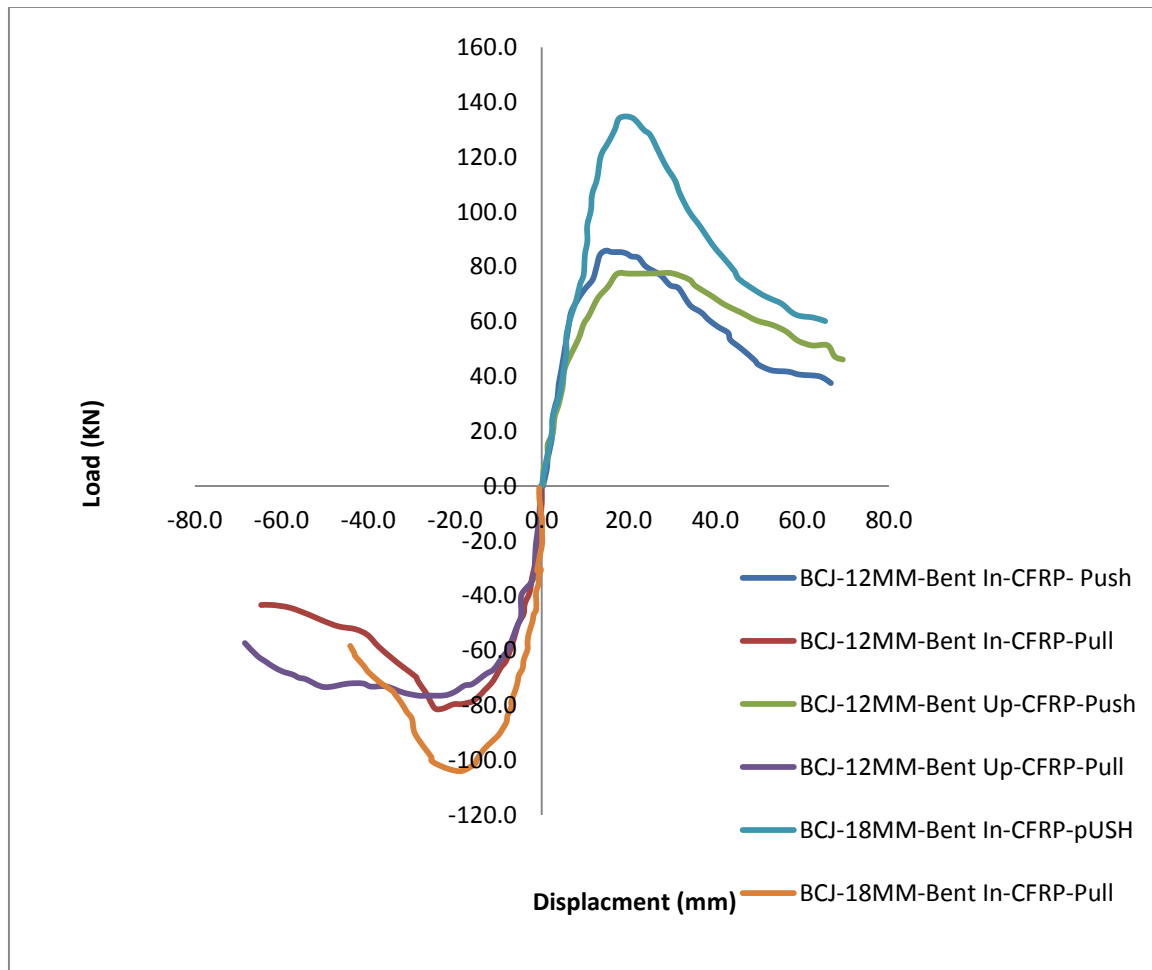
Figure 5.78: Comparison of hysteresis envelope of all retrofitted specimens

A comparison for all the specimens tested under monotonic and cyclic loadings were tabulated in **Tables 5.1 and 5.2.** The comparison takes the consideration that the ultimate load capacity, enhancement for the load capacity after retrofitting of the BCJs with CFRP sheets, crack opening at the joint, and the maximum strain in CFRP sheet in the strong direction of the fibers.

Table 5-1: Comparison between all Specimens in terms of Load

Specimens #	Ultimate load control- KN	Ultimate load with CFRP - KN	Enhancement %
BCJ-12MM-Bent Up- Monotonic	71.2	85.15	19.55
BCJ-12MM-Bent In- Monotonic	73.1	82.55	12.9
BCJ-18MM-Bent In- Monotonic	97.5	117.8	20.78
BCJ-12MM-Bent Up- Cyclic	67.1	74.83	10.62
BCJ-12MM-Bent In- Cyclic	68.42	74.68	9.14
BCJ-18MM-Bent In- Cyclic	98.98	126.2	27.5

Table 5-2: Comparison between all Specimens in terms of Load

Specimens #	Crack Width -Control - MM	Crack Width with CFRP- MM	CFRP Strain -μ_s
BCJ-12MM-Bent Up-Monotonic	0.83	1.83	3894
BCJ-12MM-Bent In-Monotonic	0.814	1.822	5397
BCJ-18MM-Bent In-Monotonic	9.928	10.22	5336
BCJ-12MM-Bent Up-Cyclic	13.038	6.492	5364
BCJ-12MM-Bent In-Cyclic	3.1	2.8	3182
BCJ-18MM-Bent In-Cyclic	0.49	13.9	5860

CHAPTER 6

FINITE ELEMENT MODELING OF CFRP

RETROFITTED BEAM-COLUMN JOINT

6.1 Introduction

Finite element studies and their comparison with the experimental test results for the verification are extremely important in order to idealize the real behavior of the actual tested specimens and predict behavior of other components that cannot be tested.

In recent years, more studies and tests have been conducted on the beam-column joints due to their important role in the stability of RC structures. Many research works and studies have been conducted in the last few years on the finite element modeling of beam-column joints to understand the behavior of their mode of failure using different finite element software, i.e. ANSYS, ABAQUS, Vector 2 and DIANA as mentioned in literature review in Chapter 2. ABAQUS will be used in this research to model the tested beam-column joints.

In this research, models were developed to study the behavior of beam-column joints under monotonic and cyclic load, which are:

- 3D model for BCJ-12 MM-Bent-In without CFRP
- 3D model for BCJ-18 MM-Bent-In without CFRP
- 3D model for BCJ-12 MM-Bent-Up without CFRP

- 3D model for BCJ-12 MM-Bent-In with CFRP
- 3D model for BCJ-18 MM-Bent-In with CFRP
- 3D model for BCJ-12 MM-Bent-Up with CFRP

The finite element simulation of the beam-column joint for various scenarios are carried out using the commercial F.E software ABAQUS13.0, utilizing the Damage Plasticity Model (DPM) for concrete, which is well-known for modeling concrete structures due to its wide range of concrete material models and advanced numerical tools. The non-linear mechanisms that are considered in modeling are cracking and crushing of concrete and yielding of reinforcement.

6.2   Review of Plastic Damage Model

This section essentially follows the development given in the ABAQUS6.13, (Hibbit, Karlsson et al. 1998) manual work. Some new comments and details have been provided to better understand the elasto-plastic damage model of (Lubliner, Oliver et al. 1989), (Lee and Fenves 1998), (Červenka and Papanikolaou 2008), and (Jankowiak and Lodygowski 2005). Concrete Damage Plasticity (CDP) is one of the possible constitutive models that can efficiently and accurately describe the behavior of granular type materials under different conditions of loading. The elastic-plastic response of the concrete damaged plasticity model is described in terms of the effective stress $\bar{\sigma}$ and the hardening variable $\tilde{\varepsilon}^{pl}$ with scalar isotropic damage.

$$\bar{\sigma} = D_0^{el} : (\varepsilon - \varepsilon^{pl}) \in \{\bar{\sigma} | F(\bar{\sigma}, \tilde{\varepsilon}^{pl}) \leq 0\} \qquad [6.1]$$

$$\dot{\tilde{\varepsilon}}^{pl} = h(\bar{\sigma}, \tilde{\varepsilon}^{pl}).\hat{\dot{\varepsilon}}^{pl} \qquad [6.2]$$

$$\dot{\varepsilon}^{pl} = \dot{\lambda}\frac{\partial G(\bar{\sigma})}{\partial \bar{\sigma}} \qquad [6.3]$$

Where:

$\dot{\lambda}$ and F obey the Kuhn-Tucker conditions: $\dot{\lambda}F = 0$; $\dot{\lambda} \geq 0$; $F \leq 0$. The Cauchy stress is

calculated in terms of the stiffness degradation variable, $d = d(\bar{\sigma}, \tilde{\varepsilon}^{pl})$, and the effective

stress as:

$$\sigma = (1 - d)\bar{\sigma} \qquad (6.4)$$

The constitute relations for the elastic-plastic response, Eq. 6.1-6.3 are decoupled from

the stiffness degradation response, Eq. 6.4, which makes the model attractive for an

effective numerical implementing.

In general, the CDP mode consists of following fundamental concepts: (i) strain rate

decomposition, (ii) stress-strain relation, (iii) stiffness degradation and hardening rule,

(iv) yield function, and (v) flow rule.

6.2.1 Strain Rate Decomposition

Additive strain rate decomposition is assumed for the rate-independent model:

$$\dot{\varepsilon} = \dot{\varepsilon}^{el} + \dot{\varepsilon}^{pl} \qquad [6.5]$$

Where:

$\dot{\varepsilon}$ is the total strain rate.

$\dot{\varepsilon}^{el}$ is the elastic part of the strain rate.

$\dot{\varepsilon}^{pl}$ is the plastic part of the strain rate.

6.2.2 Stress-Strain Relation

The stress-strain relations are governed by scalar damaged elasticity:

$$\sigma = (1-d)D_0^{el} : (\varepsilon - \varepsilon^{pl}) = D^{el} : (\varepsilon - \varepsilon^{pl}) \qquad [6.6]$$

$$D^{el} = D_0^{el}(1-d) \qquad [6.7]$$

Where:

σ is Cauchy stress tensor.

d is the scalar stiffness degradation variable, which can take values in the range from zero (undamaged material) to one (fully damaged material).

ε is the strain tensor.

ε^{pl} is the plastic strain tensor.

D_0^{el} the initial (undamaged) elastic stiffness of the material.

D^{el} is the degraded elastic stiffness tensor.

The effective stress tensor is defined as:

$$\bar{\sigma} = D_0^{el} : (\varepsilon - \varepsilon^{pl})$$

[6.8]

In the formulation, it is necessary to propose the evolution of the scalar degradation variable to be a function of effective stress and effective plastic strain.

$$d = d(\bar{\sigma}, \tilde{\varepsilon}^{pl})$$

[6.9]

In CDP model, the stiffness degradation is initially isotropic and defined by degradation variable d_c in a compression zone and variable d_t in tension zone.

Thus, finally the Cauchy stress tensor σ is related to the effective stress tensor $\bar{\sigma}$ through the scalar degradation parameter (1- d):

$$\sigma = (1 - d)\bar{\sigma}$$

[6.10]

6.2.3 Stiffness Degradation and Hardening Rule

Damage states in tension and compression are characterized independently by two hardening variables, $\tilde{\varepsilon}_c^{pl}$, and $\tilde{\varepsilon}_t^{pl}$, which are referred to equivalent plastic strains in tension and compression, respectively.

The evolution equations of the hardening variables $\tilde{\varepsilon}_t^{pl}$ and $\tilde{\varepsilon}_c^{pl}$ are conveniently formulated by considering uniaxial loading conditions first and then extended to multiracial conditions.

6.2.4 Uniaxial Conditions

It is assumed that the uniaxial stress-strain curves can be converted into stress versus plastic strain curves of the form:

$$\sigma_t = \sigma_t\left(\tilde{\varepsilon}_t^{pl}, \dot{\tilde{\varepsilon}}_t^{pl}, ..\right) \tag{6.11}$$

$$\sigma_c = \sigma_c\left(\tilde{\varepsilon}_c^{pl}, \dot{\tilde{\varepsilon}}_c^{pl}, ..\right) \tag{6.12}$$

Where the subscripts t and c refer to tension and compression, respectively; $\dot{\tilde{\varepsilon}}_t^{pl}$ and $\dot{\tilde{\varepsilon}}_c^{pl}$ are the equivalent plastic strain rates, $\tilde{\varepsilon}_t^{pl} = \int_0^t \dot{\tilde{\varepsilon}}_t^{pl} dt$ and $\tilde{\varepsilon}_c^{pl} = \int_0^t \dot{\tilde{\varepsilon}}_c^{pl} dt$ are the equivalent plastic strains. Under uniaxial loading conditions, the effective plastic strain rates are given as:

$$\dot{\tilde{\varepsilon}}_t^{pl} = \dot{\tilde{\varepsilon}}_{11}^{pl} \tag{6.13}$$

$$\dot{\tilde{\varepsilon}}_c^{pl} = -\dot{\tilde{\varepsilon}}_{11}^{pl} \tag{6.14}$$

When the concrete specimen is unloaded from any point on the strain softening branch of the stress-strain curves, the unloading response is observed to be weakened, the elastic stiffness of the material appears to be damaged or degraded. The degradation of the elastic stiffness is significantly different between tension and compression tests; in either case, the effect is more pronounced as the plastic strain increases. The degraded response of concrete is characterized by two independent uniaxial damage variables, d_t and, d_c which are assumed to be functions of the plastic strains.

$$d_t = d_t\left(\tilde{\varepsilon}_t^{pl}, ..\right) \qquad\qquad\qquad [6.15]$$

$$d_c = d_c\left(\tilde{\varepsilon}_c^{pl}, ..\right) \qquad\qquad\qquad [6.16]$$

The evaluations of the damage parameter have been studied extensively and it can take several forms. The most used model for describing the variation of the damaged parameter d is based on the plastic energy dissipated during loading in which d will be the ratio between plastic energy dissipated up to certain plastic strain and the total plastic energy. This can be descripted as shown in Eq. 6.17.

$$k_t = \frac{\int_0^{\tilde{\varepsilon}_t^{pl}} d_t\left(\tilde{\varepsilon}_t^{pl}\right)}{\int_0^{\tilde{\varepsilon}_{tf}^{pl}} d_t\left(\tilde{\varepsilon}_t^{pl}\right)} \qquad\qquad\qquad [6.17]$$

Eq. 3.31 can be interpreted as shown in **Fig. 6.1**.
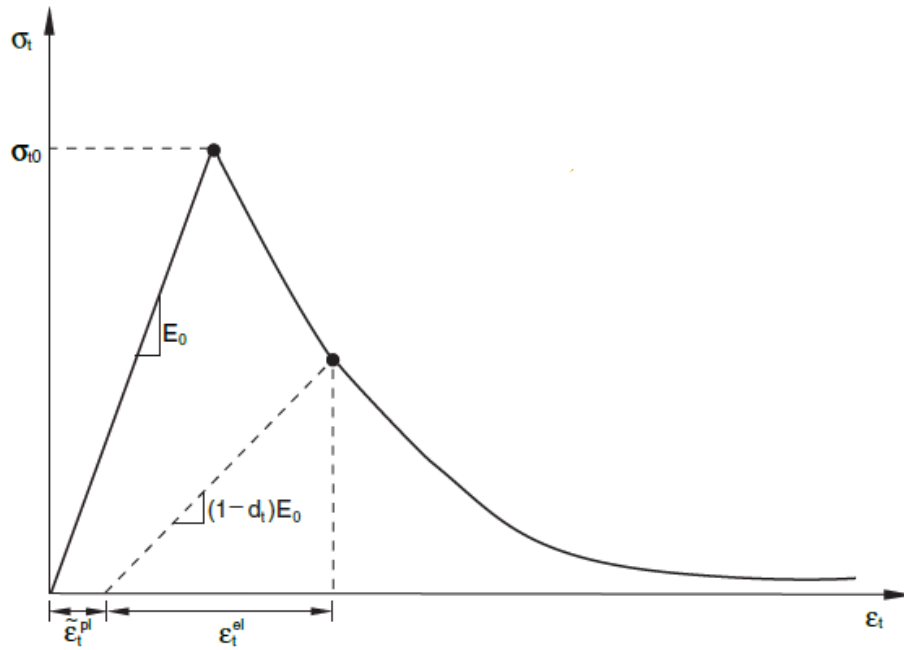
Figure 6.1: Variation of tension damage parameter k-t (ABAQUS Manual)

The shaded area in the right side of **Fig. 6.2** represents the level of damage in the stress-plastic strain space. The percentage of this area with respect to the total area is the amount of scalar damage at the continuum point.

Similarly, the compression damage can be calculated as shown in Eq 6.18.

$$k_c = \frac{\int_0^{\tilde{\varepsilon}_c^{pl}} d_c(\tilde{\varepsilon}_c^{pl})}{\int_0^{\tilde{\varepsilon}_{cf}^{pl}} d_c(\tilde{\varepsilon}_c^{pl})}$$ [6.18]

The graphical interpretation of Eq. 6.18 is shown in **Fig. 6.1**.
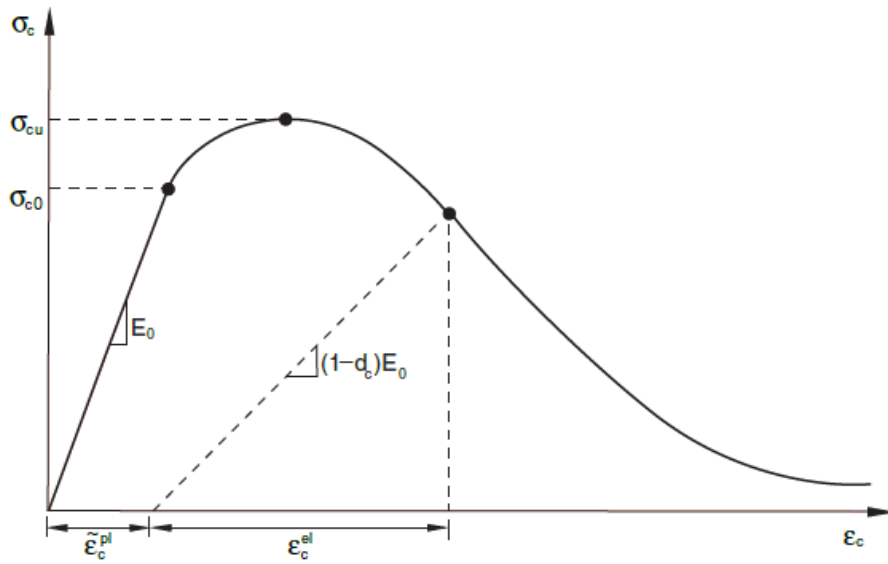
Figure 6.2: Variation of compression damage parameter d-c (ABAQUS Manual)

The uniaxial degradation variables are increasing functions of the equivalent plastic strains.

If E_0 is the initial (undamaged) elastic stiffness of the material, the stress-strain relations under uniaxial tension and compression loading are, respectively:

171

$$\sigma_t = (1 - d_t)E_0\left(\varepsilon_t - \tilde{\varepsilon}_t^{pl}\right) \qquad [6.19]$$

$$\sigma_c = (1 - d_c)E_0\left(\varepsilon_c - \tilde{\varepsilon}_c^{pl}\right) \qquad [6.20]$$

The effective uniaxial cohesion stresses, $\bar{\sigma}_t$ and, $\bar{\sigma}_c$ are given as:

$$\bar{\sigma}_t = \frac{\sigma_t}{(1-d_t)} = E_0\left(\varepsilon_t - \tilde{\varepsilon}_t^{pl}\right) \qquad [6.21]$$

$$\bar{\sigma}_c = \frac{\sigma_t}{(1-d_c)} = E_0\left(\varepsilon_c - \tilde{\varepsilon}_c^{pl}\right) \qquad [6.22]$$

The effective uniaxial cohesion stresses determine the size of the yield or failure surface.

6.2.5 Yield Function

The yield function $F(\bar{\sigma}, \tilde{\varepsilon}^{pl})$ represents a surface in effective stress space which determines the state of failure or damage. For the in viscid plastic-damage model the yield function can be expressed as:

$$F(\bar{\sigma}, \tilde{\varepsilon}^{pl}) \leq 0 \qquad [6.23]$$

The plastic-damage concrete model uses a yield condition based on the yield function originally proposed by (Lubliner, Oliver et al. 1989) and incorporates the modifications proposed subsequently (Lee and Fenves 1998) to account for different evolution of strength under tension and compression. In terms of effective stresses, the yield function takes the form (the classical two-parameter Drucker-Prager model) is a special case of Eq. 6.24.

$$F(\bar{\sigma}, \tilde{\varepsilon}^{pl}) = \frac{1}{1-\alpha}\left(\bar{q} - 3\alpha\bar{p} + \beta(\tilde{\varepsilon}^{pl})\langle\hat{\bar{\sigma}}_{max}\rangle - \gamma\langle-\hat{\bar{\sigma}}_{max}\rangle\right) - \bar{\sigma}_c\left(\tilde{\varepsilon}_c^{pl}\right) \leq 0 \quad [6.24]$$

Where:

α, γ are dimensionless material constants.

$\bar{p}$ is the effective hydrostatic pressure.

$$\bar{p} = -\frac{1}{3}\bar{\sigma}_{ii} = -\frac{1}{3}\bar{I}_1 \qquad [6.25]$$

$\bar{q}$ is the Mises equivalent effective stress.

$$\bar{q} = \sqrt{\frac{3}{2}\bar{s}_{ij}\bar{s}_{ij}} = \sqrt{3\bar{J}_2} \qquad [6.26]$$

$\bar{s}_{ij}$ is the deviatoric component of effective stress $\bar{\sigma}$.

$\hat{\bar{\sigma}}_{max}$ is the algebraically maximum eigenvalue of $\bar{\sigma}$.

The function $\beta(\tilde{\varepsilon}^{pl})$ is given as:

$$\beta(\tilde{\varepsilon}^{pl}) = \frac{\bar{\sigma}_c(\tilde{\varepsilon}_c^{pl})}{\bar{\sigma}_t(\tilde{\varepsilon}_c^{pl})}(1 - \alpha) - (1 + \alpha) \qquad [6.27]$$

$\bar{\sigma}_c, \bar{\sigma}_t$ are the effective tensile and compressive cohesion stress, respectively, and obtained from 1-D tests in uniaxial compression and uniaxial tension (stress-plastic strain data), and expressed as:

$$\bar{\sigma}_c(\tilde{\varepsilon}_c^{pl}) = \frac{\sigma_c}{(1 - d_c)} = E_0(\varepsilon_c - \tilde{\varepsilon}_c^{pl}) \qquad [6.28]$$

$$\bar{\sigma}_t(\tilde{\varepsilon}_t^{pl}) = \frac{\sigma_t}{(1 - d_t)} = E_0(\varepsilon_t - \tilde{\varepsilon}_t^{pl}) \qquad [6.29]$$

The $\beta(\tilde{\varepsilon}^{pl})$ parameter controls the size of the yield surface in regions where $\hat{\bar{\sigma}}_{max} \geq 0$ whereas γ controls the shape of the trace of yield surface in the deviatoric plane for stress states of biaxial and tri-axial compression $\hat{\bar{\sigma}}_{max} \leq 0$.

173

In biaxial compression, with $\hat{\bar{\sigma}}_{max} = 0$, Eq. 6.24 reduces to the well-known Drucker-Prager yield condition. The coefficient α can be determined by direct application of yield criteria as given by Eq. 6.24 for equal biaxial compression and for uniaxial compression (for both cases, $\hat{\bar{\sigma}}_{max} = 0$) and solving for α, one obtains:

$$\alpha = \frac{(\sigma_{b0}/\sigma_{c0}) - 1}{2(\sigma_{b0}/\sigma_{c0}) - 1} \qquad [6.30]$$

where:

σ_{c0} is the uniaxial compression strength of concrete.

σ_{b0} is the biaxial compression strength of concrete.

Typical experimental values of the ratio σ_{b0}/σ_{c0} for concrete are in the range from 1.10 to 1.16, yielding values of α between 0.08 and 0.12 (Lubliner, Oliver et al. 1989).

The coefficient γ enters the yield function only for stress states of tri-axial compression, when $\hat{\bar{\sigma}}_{max} \leq 0$. This coefficient can be determined by comparing the yield conditions along the tensile and compressive meridians. By definition, the Tensile Meridian (TM) is the locus of stress states satisfying the condition $\hat{\bar{\sigma}}_{max} = \hat{\bar{\sigma}}_1 \geq \hat{\bar{\sigma}}_2 = \hat{\bar{\sigma}}_3$, and the Compressive Meridian (CM) is the locus of stress states such that $\hat{\bar{\sigma}}_{max} = \hat{\bar{\sigma}}_1 = \hat{\bar{\sigma}}_2 \geq \hat{\bar{\sigma}}_3$, where , $\hat{\bar{\sigma}}_1, \hat{\bar{\sigma}}_2$, and $\hat{\bar{\sigma}}_3$ are the eigenvalues of the effective stress tensor.

One may show in general:

$$\bar{s}_1 = \frac{2}{\sqrt{3}} \sqrt{\bar{J}_2} \cos \theta \qquad [6.31]$$

$$\bar{s}_2 = \frac{2}{\sqrt{3}} \sqrt{\bar{J}_2} \cos \left(\frac{2\pi}{3} - \theta \right) \qquad [6.32]$$

$$\bar{s}_3 = \frac{2}{\sqrt{3}} \sqrt{\bar{J}_2} \cos \left(\frac{2\pi}{3} + \theta \right) \qquad [6.33]$$

Where $\bar{s}_i$ the principal values of the effective are deviatoric stress tensor $\overline{s}_{ij}$, and θ is the angle of similarity measured from the projection of $\bar{\sigma}_1$ in the deviatoric plane. For the tensile meridian $= 0$, whereas for the compression meridian, $\theta = 60^o$.

Substituting the appropriate values of θ in expressions for $\bar{s}_i$ and expressing $\bar{\sigma}_1$ in terms of $\bar{s}_1$.

$$(\hat{\bar{\sigma}}_{max})_{TM} = \bar{\sigma}_1 = \bar{s}_1 - \bar{p} = \frac{2}{\sqrt{3}}\sqrt{\bar{J}_2} - \bar{p} = \frac{2\bar{q}}{3} - \bar{p} \qquad [6.34]$$

$$(\hat{\bar{\sigma}}_{max})_{CM} = \bar{\sigma}_1 = \bar{s}_1 - \bar{p} = \frac{1}{\sqrt{3}}\sqrt{\bar{J}_2} - \bar{p} = \frac{\bar{q}}{3} - \bar{p} \qquad [6.35]$$

With $\hat{\bar{\sigma}}_{max} < 0$, the corresponding yield conditions are:

$$\left(\frac{2}{3}\gamma + 1\right)\bar{q} - (\gamma + 3\alpha)\bar{p} = (1 - \alpha)\bar{\sigma}_c \quad (TM) \qquad [6.36]$$

$$\left(\frac{1}{3}\gamma + 1\right)\bar{q} - (\gamma + 3\alpha)\bar{p} = (1 - \alpha)\bar{\sigma}_c \quad (CM) \qquad [6.37]$$

Let $K_c = \bar{q}_{(TM)}/\bar{q}_{(CM)}$ for any given value of the hydrostatic pressure $\bar{p}$ with $\hat{\bar{\sigma}}_{max} < 0$; then:

$$K_c = \frac{\gamma+3}{2\gamma+3} \qquad [6.38]$$

The fact that K_c is constant does not seem to be contradicted by experimental evidence (Lubliner et al [27]. The coefficient γ is, therefore, evaluated as:

$$\gamma = \frac{3(1-K_c)}{2K_c-1} \qquad [6.39]$$

It was suggested by (Lubliner, Oliver et al. 1989) that, the value of K_c ranging from 0.66 to 0.8.

If $\hat{\bar{\sigma}}_{max} > 0$, the yield conditions along the tensile and compressive meridians reduce to:

$$\left(\frac{2}{3}\beta + 1\right)\bar{q} - (\beta + 3\alpha)\bar{p} = (1 - \alpha)\bar{\sigma}_c \quad (TM) \qquad [6.40]$$

$$\left(\frac{1}{3}\beta + 1\right)\bar{q} - (\beta + 3\alpha)\bar{p} = (1 - \alpha)\bar{\sigma}_c \quad (CM) \qquad [6.41]$$

Let $K_t = \bar{q}_{(TM)}/\bar{q}_{(CM)}$ for any given value of the hydrostatic pressure $\bar{p}$ with $\hat{\bar{\sigma}}_{max} > 0$; then:

$$K_t = \frac{\beta + 3}{2\beta + 3} \qquad [6.42]$$

Typical yield surfaces are shown in **Fig. 6.3** in the deviatoric plane for $\hat{\bar{\sigma}}_{max} \leq 0$ and **Fig. 6.4** shows plane-stress conditions. Eq. 6.56, when plotted, would trace locus of yield surface in deviatoric plane for $\hat{\bar{\sigma}}_{max} > 0$.
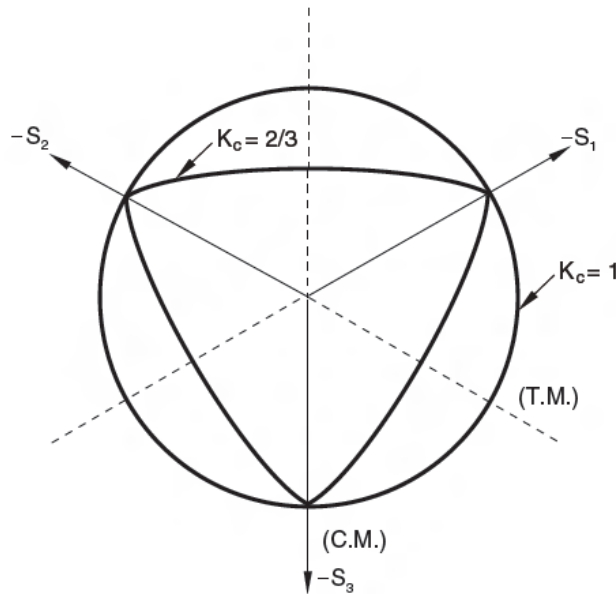
Figure 6.3: Yield surfaces in the deviatoric plane, corresponding to different values of K_c (ABAQUS Manual)
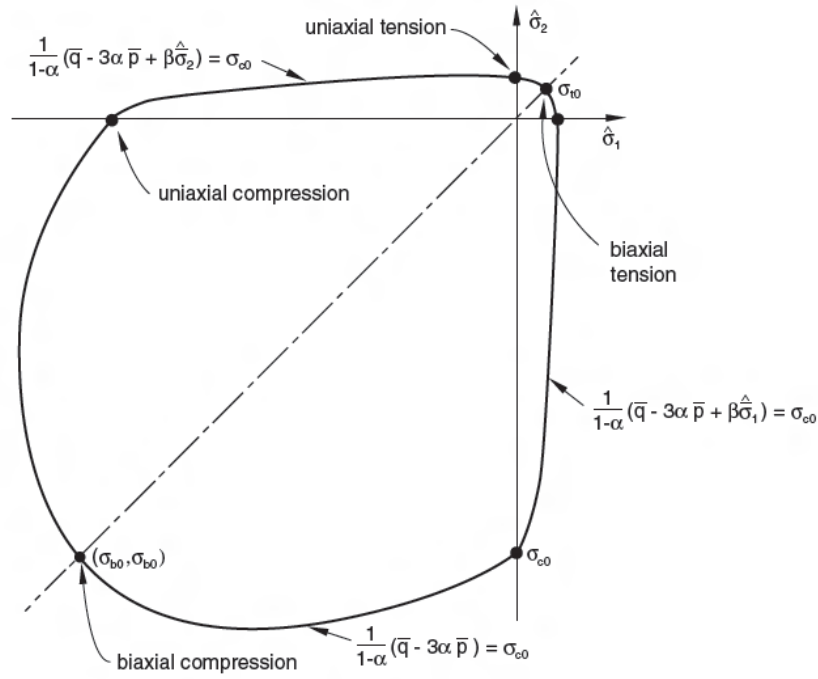
Figure 6.4: Yield surface in plane stress (ABAQUS Manual)

6.2.6 Flow Rule

Plastic flow is governed by a flow potential function $G(\bar{\sigma})$ according to non-associative flow rule:

$$\dot{\varepsilon}^{pl} = \dot{\lambda}\frac{\partial G(\bar{\sigma})}{\partial\bar{\sigma}}$$
(6.43)

Where $\dot{\lambda}$ is the non-negative plastic multiplier. The plastic potential is defined in the effective stress space. The model uses non-associated plasticity; therefore, requiring the solution of nonsymmetrical equations. The fundamental group of the constitutive parameters consists of four values, which identify the shape of the potential flow surface and the yield surface. In this model for the flow potential G, the Drucker-Prager hyperbolic function is accepted in the form:

$$G = \sqrt{(\epsilon\sigma_{t0}\tan\psi)^2 + \bar{q}^2} - \bar{p}\tan\psi \tag{6.44}$$

where ψ is the dilation angle measured in the *p–q* plane at high confining pressure; σ_{t0} is the uniaxial tensile stress at failure; and ϵ is a parameter, referred to as the eccentricity, that defines the rate at which the function approaches the asymptote (the flow potential tends to a straight line as the eccentricity tends to zero). This flow potential, which is continuous and smooth, ensures that the flow direction is defined uniquely.

6.3 Numerical Simulation Conducted for BCJ Tested in the Study

In this study, finite element simulation of the beam-column joint was carried out using the commercial F.E software ABAQUS13.0, which is well-known for modeling concrete structures due to its wide range of concrete material models and advanced numerical tools. The non-linear mechanisms that are considered in modeling are cracking and crushing of concrete and yielding of reinforcement.

In this research 3-D models will be used to study the behavior of beam-column joints under monotonic and cyclic load which are:

1. 3D model for BCJ-12MM-Bent Up without CFRP

2. 3D model for BCJ-12MM-Bent In without CFRP

3. 3D model for BCJ-18MM-Bent In without CFRP

4. 3D model for BCJ-12MM-Bent Up without CFRP

5. 3D model for BCJ-12MM-Bent In without CFRP

6. 3D model for BCJ-18MM-Bent In without CFRP

6.4   Material Models

6.4.1   Computational Simulation of Concrete

As shown in the review of the plastic damage model, several parameters are needed as input in ABAQUS to carry out the simulations. Some of these parameters were found experimentally while some others were assumed to be the default values. **Table 6.1** gives the plastic model parameters associated with concrete. As seen in the damage model explained before, the stress-plastic strain for concrete material is also needed in the finite element simulation. Uniaxial stress-plastic strain data for both concrete in compression and tension have been used in the plastic damage model incorporated in an ABAQUS environment. **Figs. 6.5 and 6.6** show the stress-plastic strain curve for both uniaxial compression and uniaxial tension.
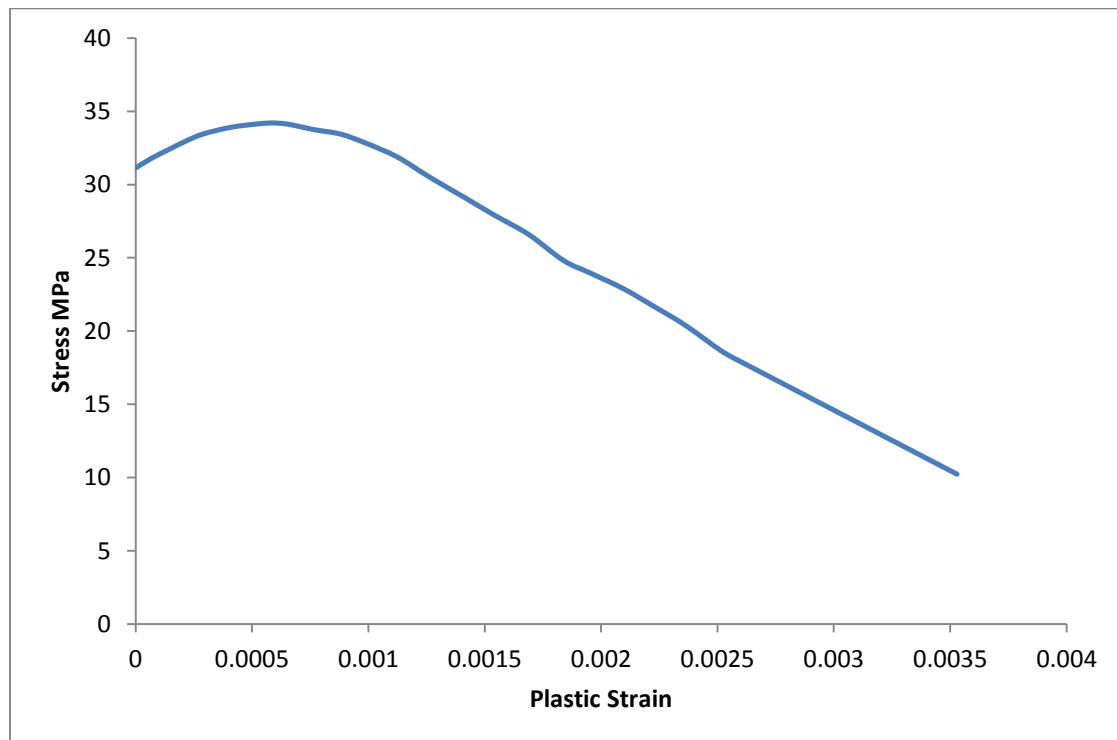
Figure 6.5: Plastic strain vs stress in compression for concrete
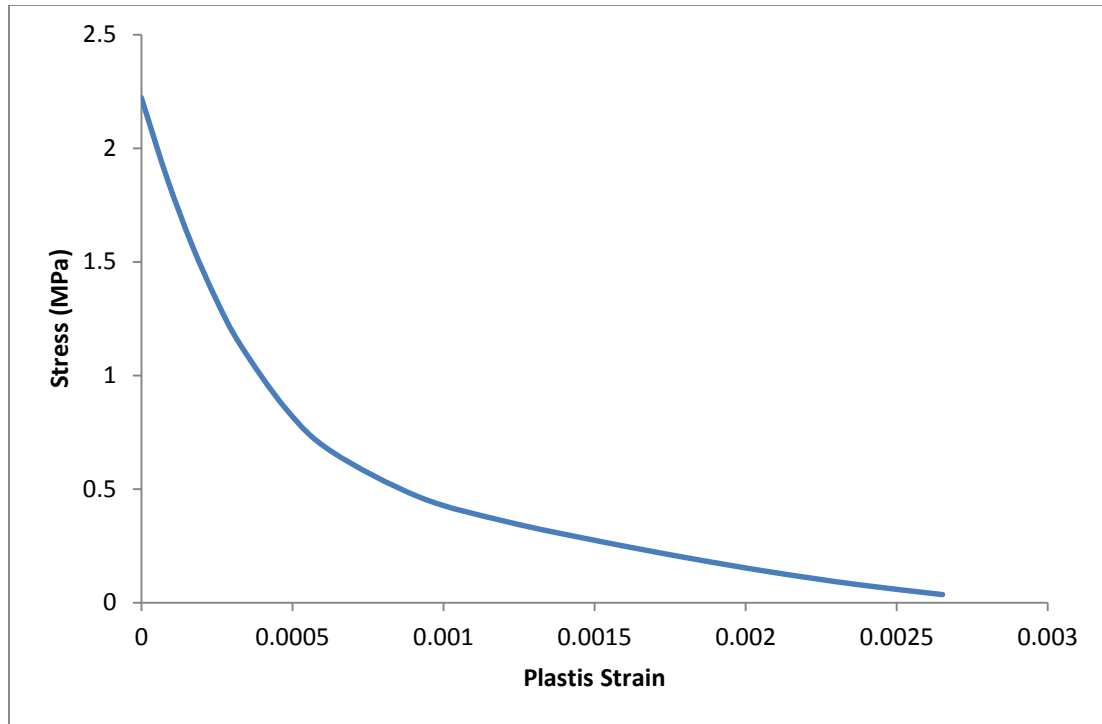
Figure 6.6: Plastic strain vs stress in tension for concrete

The hardening and softening rule and the evolution of the scalar damage variable for compression and tension are presented in **Table 6.1**. Both depend on the crushing or cracking strains.

Table 6-1: Concrete Parameters used in Plastic Damage Model

Mass Density (Tone/mm3)	Young's Modulus (MPa)	Poisson's Ratio	Dilation Angle Ψ (Degree)	Eccentricity ε	f_{bo}/f_{co}	K
2.4E-009	2900	0.2	36	0.1	1.16	0.67

Where:

Ψ: Dilation angle.

ε: Eccentricity which define the flow potential tends to a straight line as the eccentricity tend to zero.

f_{bo}/f_{co} : Ratio of initial biaxial compressive yield stress to initial uniaxial compressive yield stress (the default value is 1.16).

K: is the ratio of the second stress invariant on the tensile meridian (TM) to that on the compressive meridian (CM), the default value is 0.67.

6.4.2 Steel Reinforcement

In ABAQUS, reinforcement in concrete structures is typically provided by means of rebars, which are one-dimensional rods that can be defined singly or embedded in oriented surfaces. Rebars are typically used with metal plasticity models to describe the behavior of the rebar material and are superposed on a mesh of standard element types used to model the concrete for steel reinforcement Elastic-Plasticity with work hardening is used. **Fig. 6.7** shows the stress-plastic strain for the steel reinforcement.
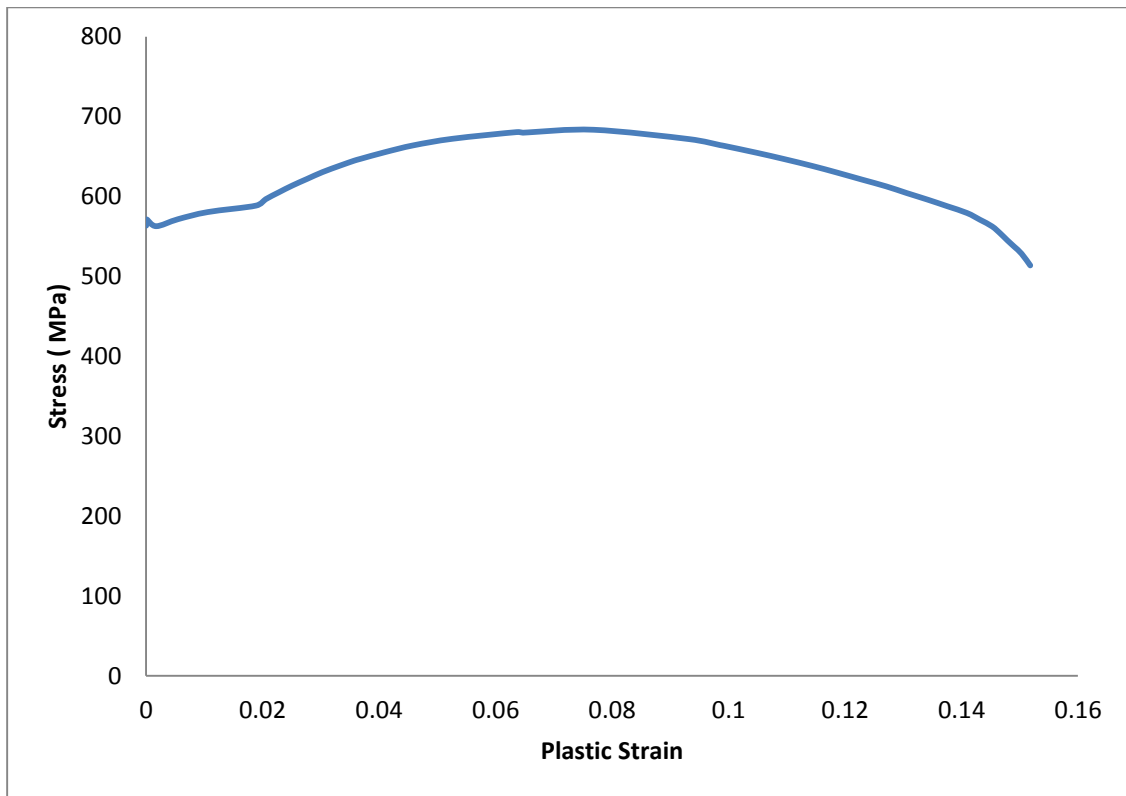
Figure 6.7: Stress-plastic strain for steel

6.4.3 CFRP Material Model

A linear elastic lamina model for CFRP, the subscripts in **Table 6.2** represent the principal material directions of the CFRP lamina. In order to consider the cohesive contact between CFRP sheet and concrete surface the stiffness coefficients, (Ziraba, Baluch et al. 1994) studied the non-linear finite elements analysis of reinforced concrete beam repaired by plate bending, the values for stiffness coefficient are shown in **Table 6.3**.

Table 6-2: Proprieties of CFRP Lamina

E_1 (MPa)	E_2 (MPa)	v_{12}	G_{12} (MPa)	G_{13} (MPa)	G_{23} (MPa)	σ_u (MPa)
70000	7000	0.25	5000	0	0	800

Table 6-3: Stiffness Coefficient for Cohesive Contact

K_{nn} MPa/mm	K_{ss} MPa/mm	K_{tt} MPa/mm
12	32	32

6.5 Element Type and Meshing and Boundary Condition

Dynamic explicit analysis in ABAQUS was used in this simulation. The element used for each part of the model and description of the element is shown in **Table 6.4**. The interaction between the wall and the CFRP was assumed to be a cohesive contact. **Fig. 6.8** shows the 3-D finite element model of the beam-column joint and the 3-D model of BCJ and mesh. The top end of the column surface is constrained in x and z-direction and the bottom end of the column is constrained in x, y, and z -direction. The tip of beam is constrained in y-direction for application of displacement which is 70 mm. The top of the column have a constant axial load of 150 kN is applied on the column as pressure load equal to 2 MPa. **Fig. 6.9** shows the load and boundary condition for the model. The steel reinforcement model as linear element as shown in **Fig. 6.10**.

Table 6-4: Element Properties

Part	Element	Element description
Concrete	C3D8R	8 node linear brick, reduced integration
Steel plate	C3D8R	8 node linear brick, reduced integration
Steel bar	T3D2	2 node truss element
CFRP	S4R	A 4-node doubly curved thin or thick shell, reduced integration,
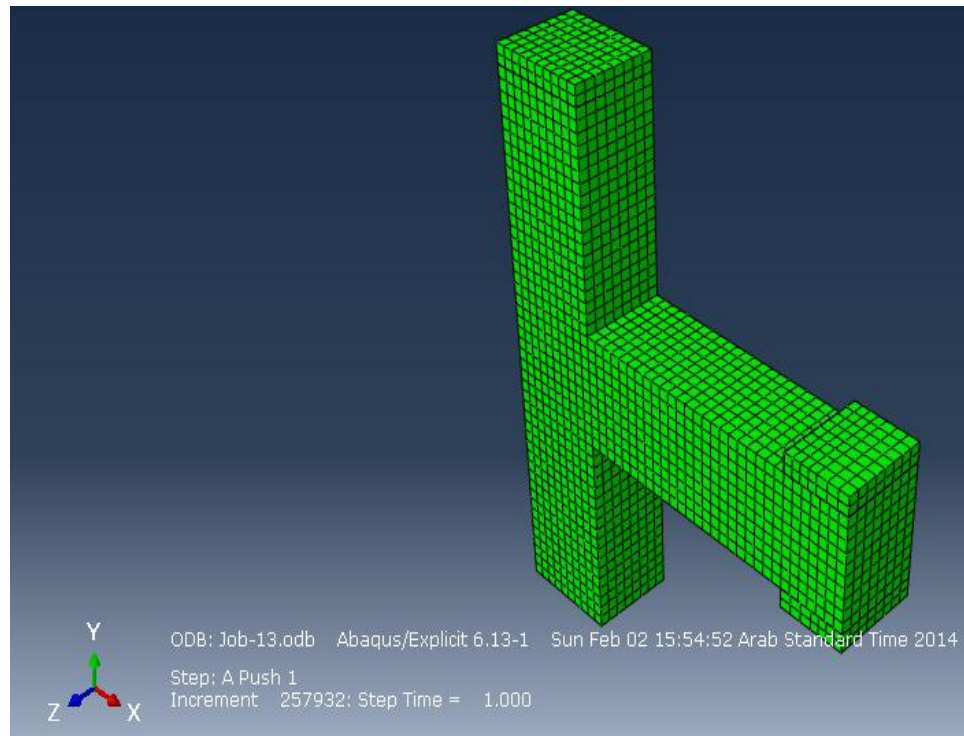
Figure 6.8: 3-D FE model of BCJ Specimen and Meshing
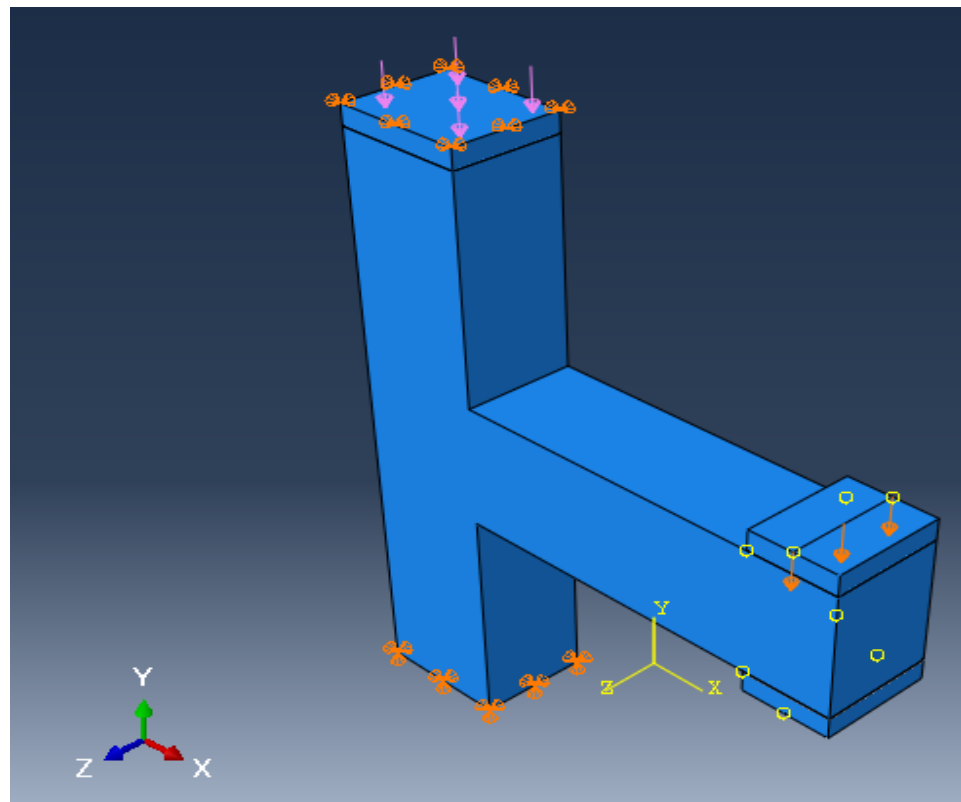
Figure 6.9: Applied loads and boundary condition

185
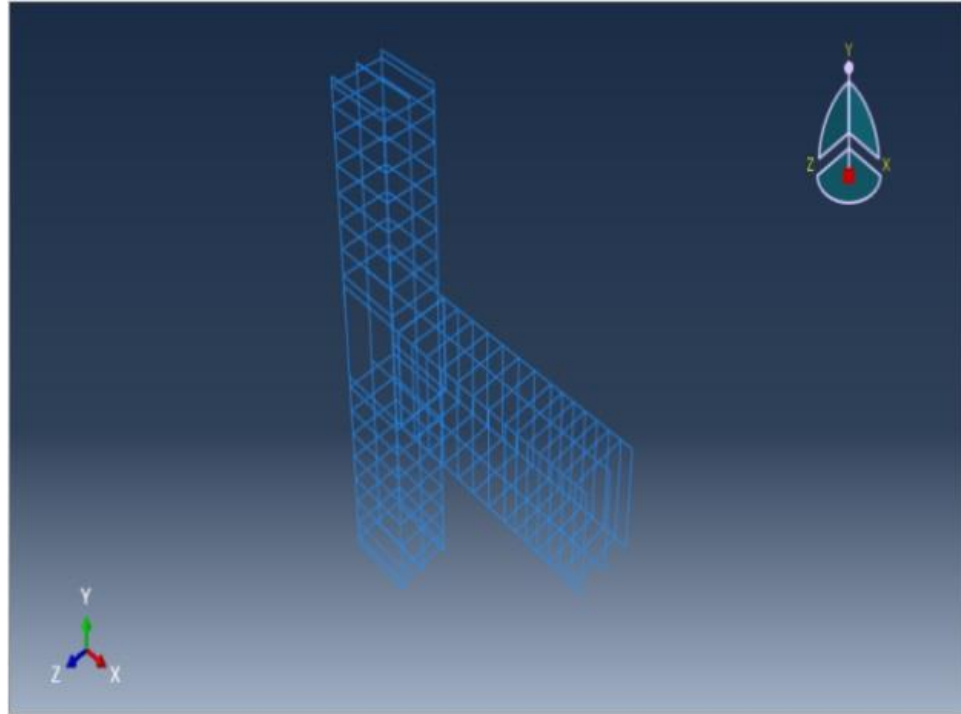
Figure 6.10: Reinforcement bar model

6.6   Numerical Simulation for BCJs

The goals targeted in this study, in terms of numerical simulation, are related to simulating the response of the BCJs subjected to loads that were applied in the experimental work for both the monotonic and cyclic load. To achieve this goal, several trials have been made for finding the best parameters so that perfect matching between excremental and numerical results is achieved. Several numerical simulations trails have been carried out to get these parameters. As shown in Chapter 3, the finite element simulation was quite difficult due to the complexity of the problem under consideration. The results of numerical simulation have shown that a good match was achieved between excremental and numerical results as have been discussed in the following section.

6.6.1   Numerical Simulation of BCJ-12MM-Bent in without CFRP

The experimental and finite element results of load-displacement response of the beam-column joint without CFRP retrofitting, under monotonic load up to failure are shown in **Fig. 6.11**. The result of finite element simulation matches closely with experimental results as shown in **Fig. 6.11**. In addition, **Fig. 6.12** shows that a good match was achieved between experimental and numerical results for the cyclic load test.
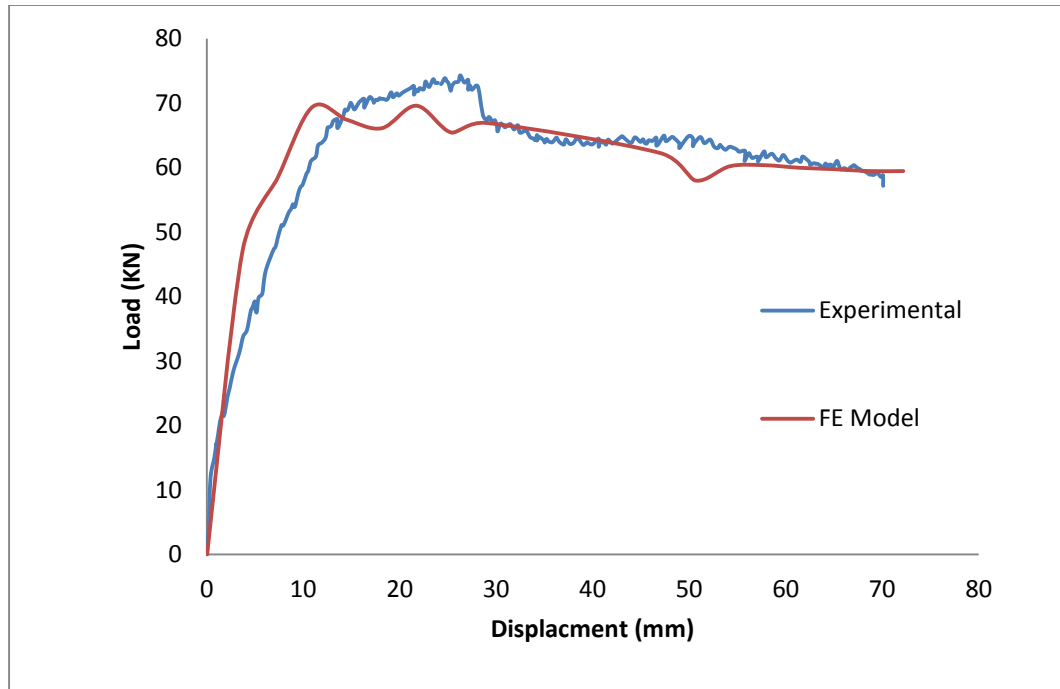
Figure 6.11: Load displacement response for BCJ-12MM-Bent in without CFRP
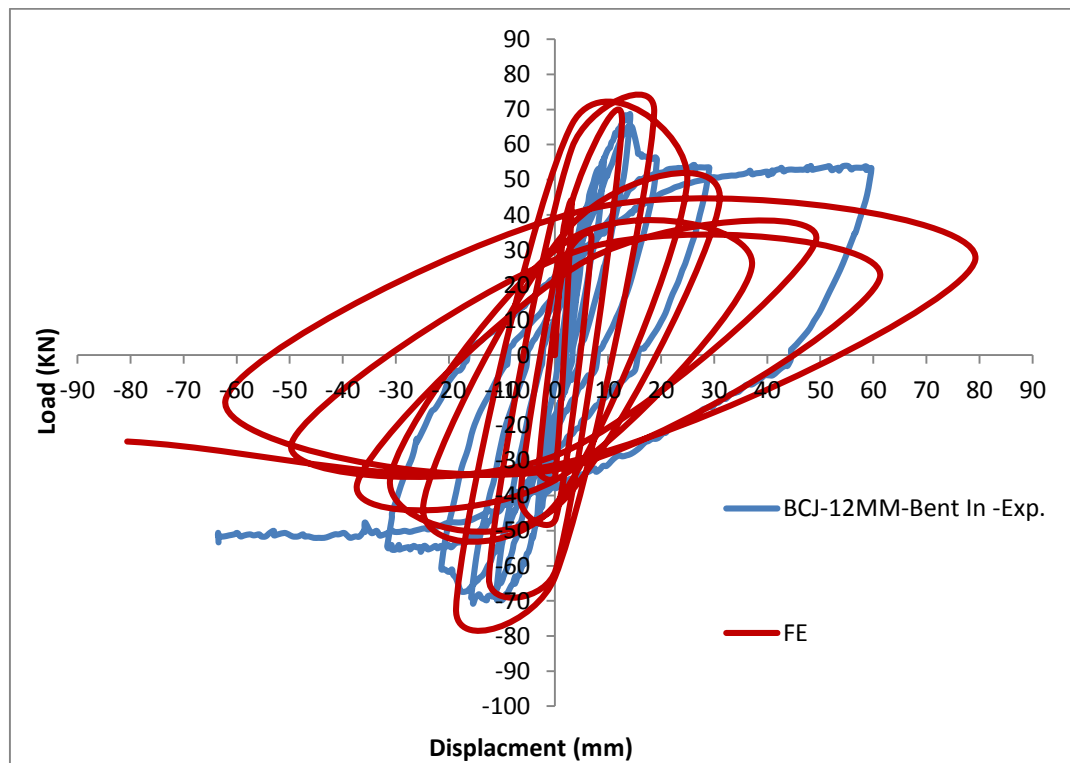
Figure 6.12: Load displacement response under cyclic load for BCJ-12MM-Bent in without CFRP

The maximum stress levels in steel at ultimate load which is corresponding to tip displacement of 21.7 mm are shown in **Fig. 6.13**. The stresses S11, S22 and S12 at yielding and ultimate load are shown in **Figs. 6.14, 6.15, 6.16, 6.17, 6.18 and 6.19**. The diagonal crack patterns at the joints as shown in **Figs. 6.20, 6.22 and 6.24**, closely resemble the crack patterns observed in the experimental program and shown in **Figs. 6.21, 6.23 and 6.25**.
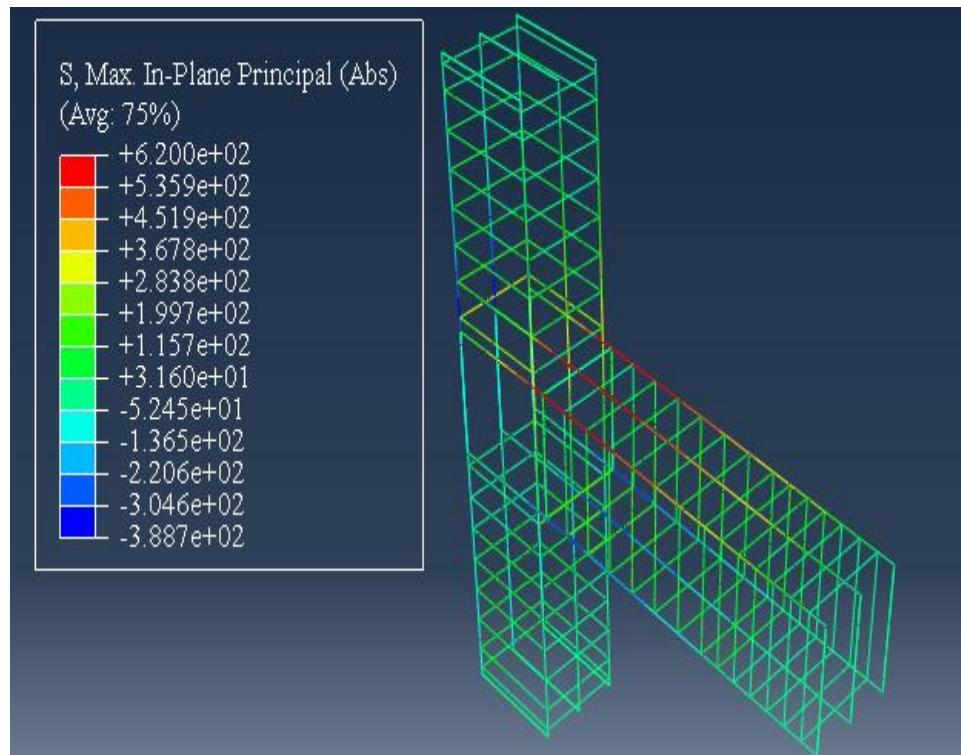
Figure 6.13: Steel stress at ultimate load (Δ = 21.7mm) for BCJ-12MM-Bent in without CFRP
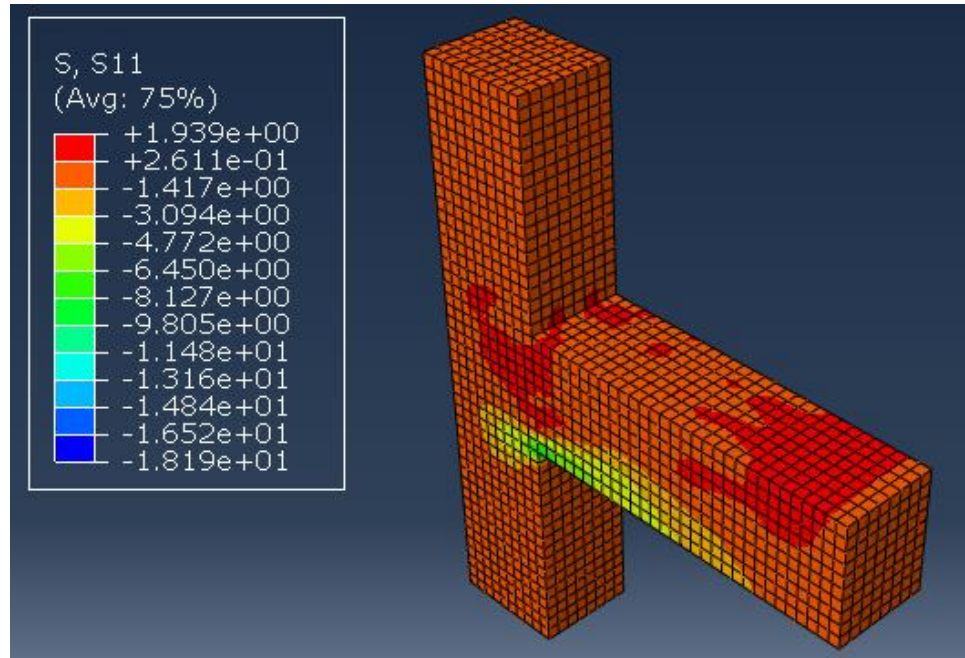
Figure 6.14: Stress S11 in concrete at yielding load (∆ = 5.95mm) for BCJ-12MM-Bent in without CFRP
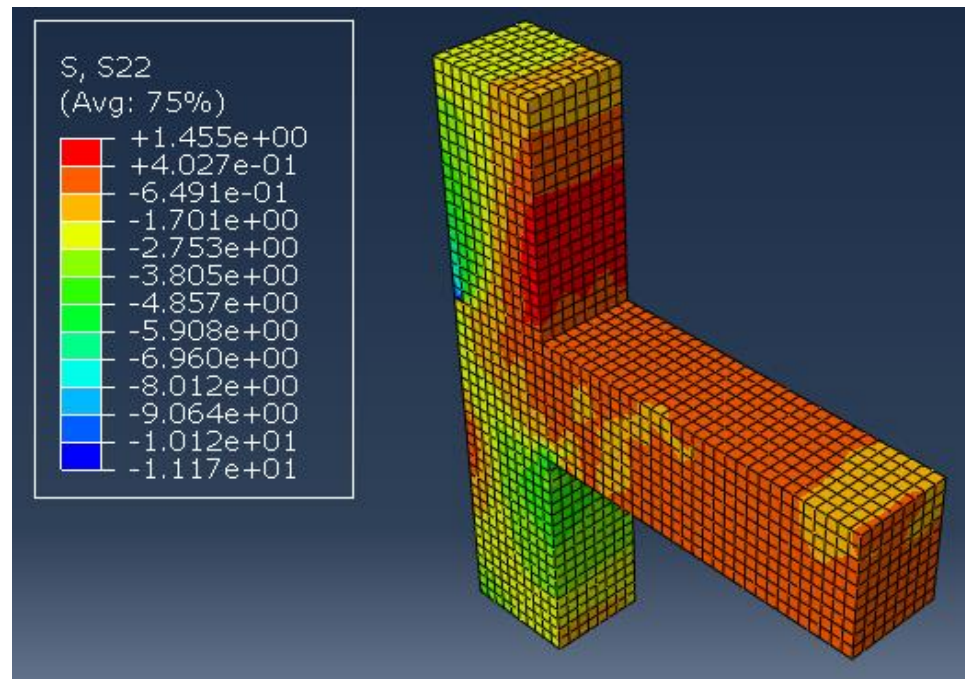
Figure 6.15: Stress S22 in concrete at yielding load (∆ = 5.95mm) for BCJ-12MM-Bent in without CFRP
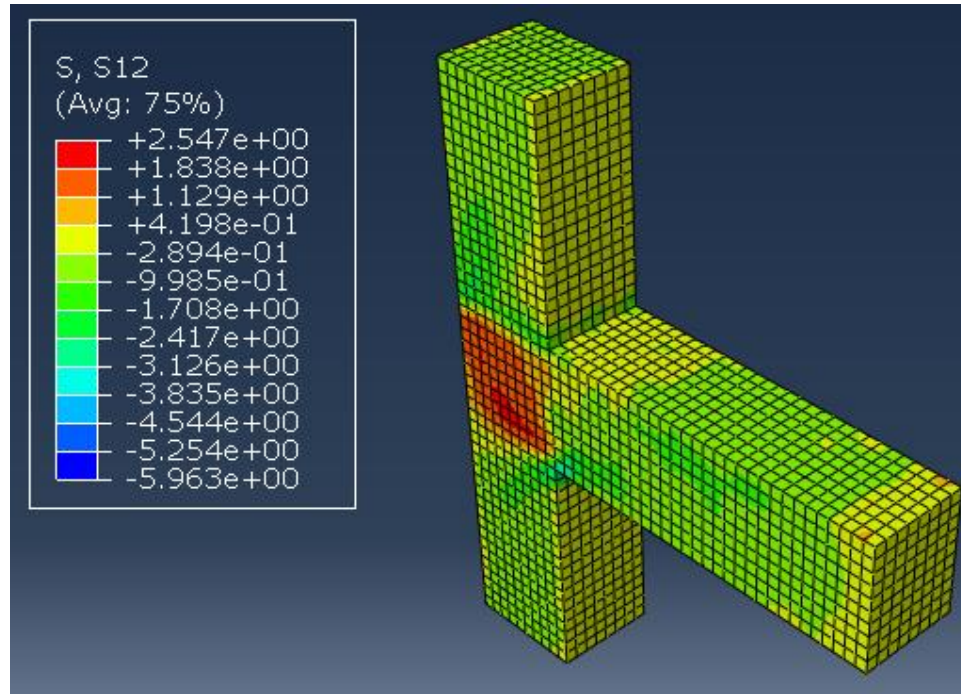
Figure 6.16: Stress S12 in concrete at yielding load (Δ = 5.95mm) for BCJ-12MM-Bent in without CFRP
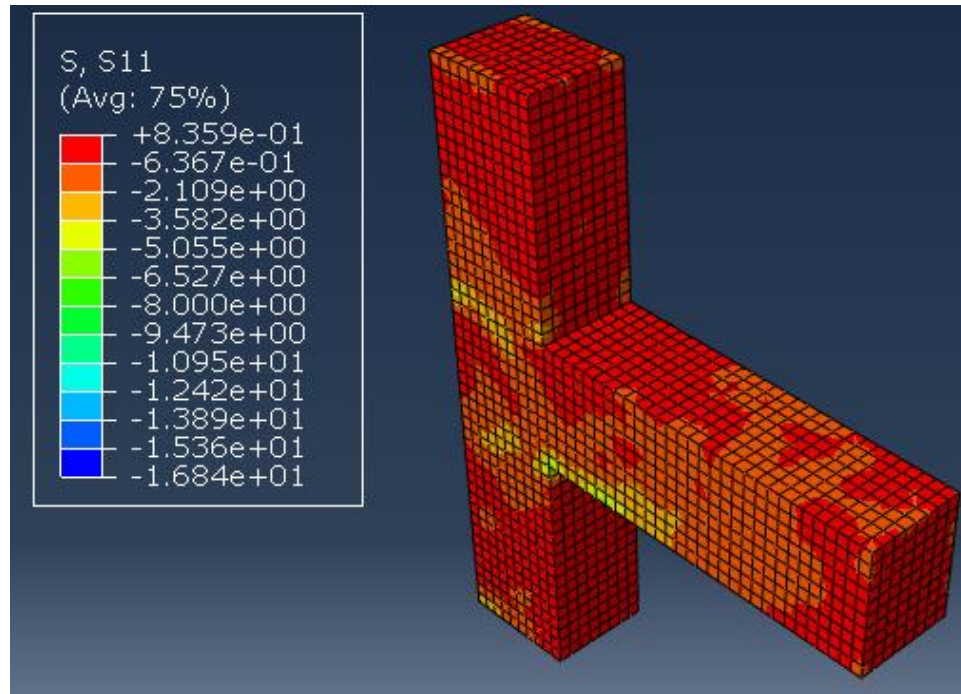
Figure 6.17: Stress S11 in concrete at ultimate load (Δ = 21.7mm) for BCJ-12MM-Bent in without CFRP
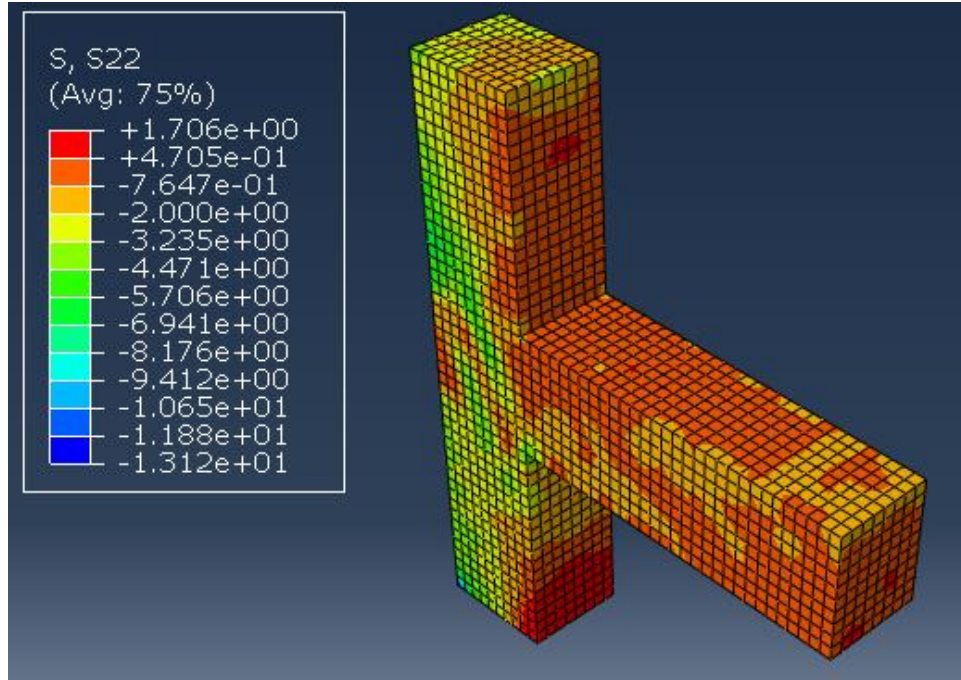
Figure 6.18: Stress S22 in concrete at ultimate load (Δ = 21.7mm) for BCJ-12MM-Bent in without CFRP
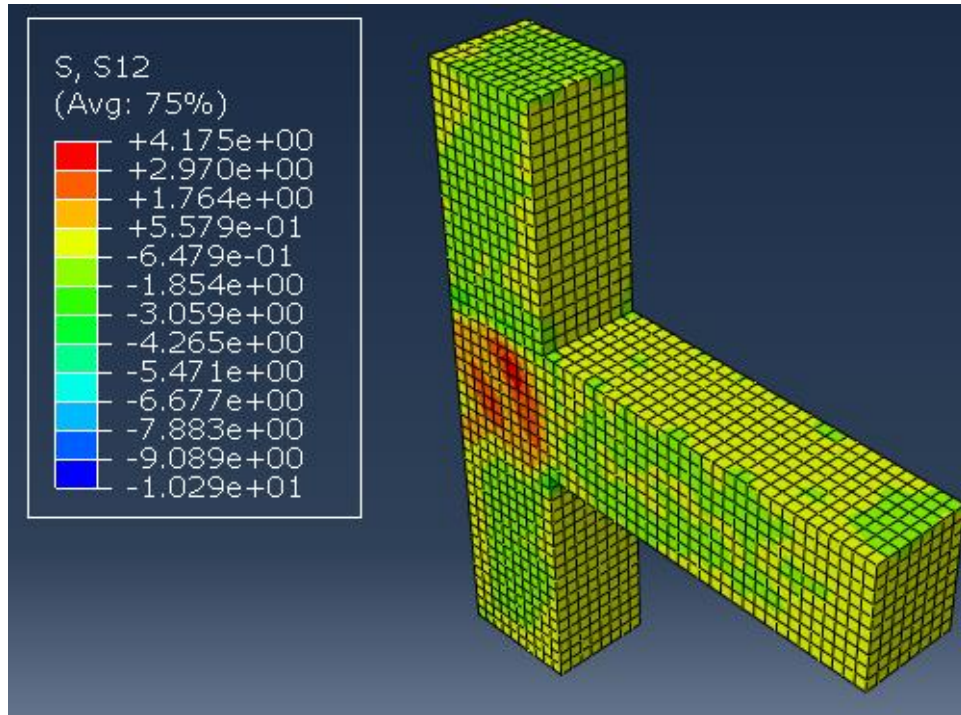
Figure 6.19: Stress S12 in concrete at ultimate load (Δ = 21.7mm) for BCJ-12MM-Bent in without CFRP
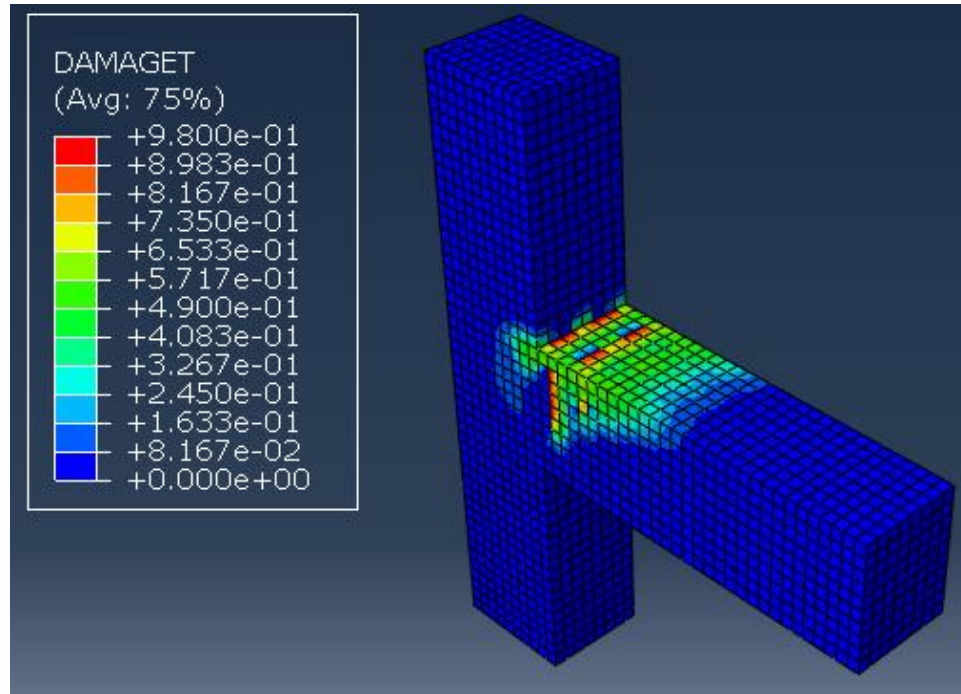
Figure 6.20: Damage propagation and crack pattern at displacement level (Δ = 2.2mm) for BCJ-12MM-Bent in without CFRP

Figure 6.21: Damage propagation and crack pattern from experimental test for BCJ-12MM-Bent in without CFRP
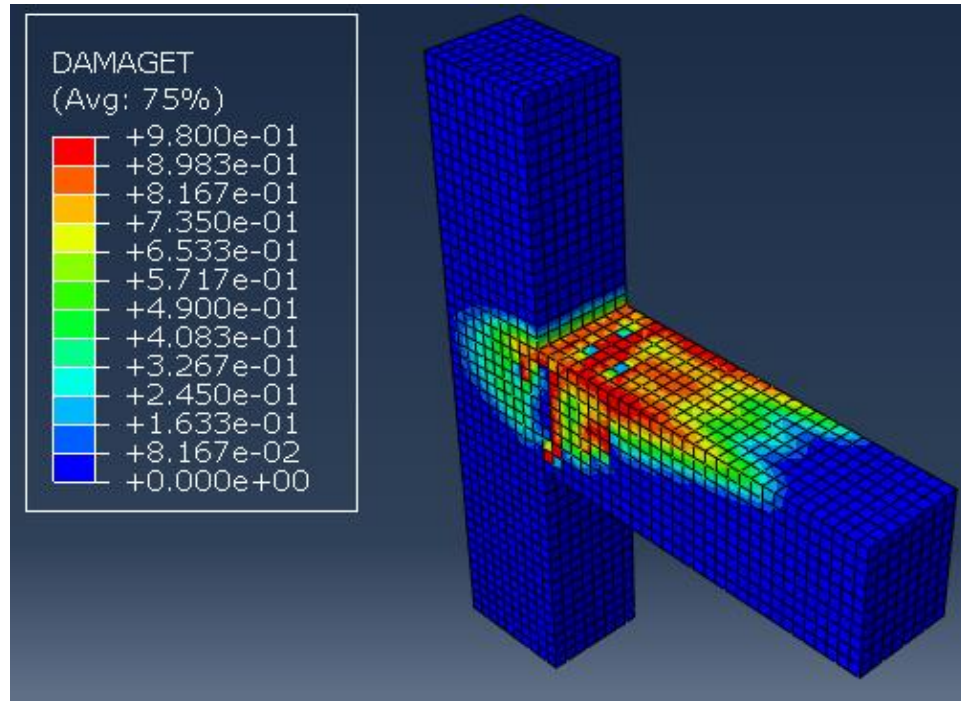
Figure 6.22: Damage propagation and crack pattern at displacement level (Δ = 5.3mm) for BCJ-12MM-Bent in without CFRP

Figure 6.23: Damage propagation and crack pattern from experimental test for BCJ-12MM-Bent in without CFRP
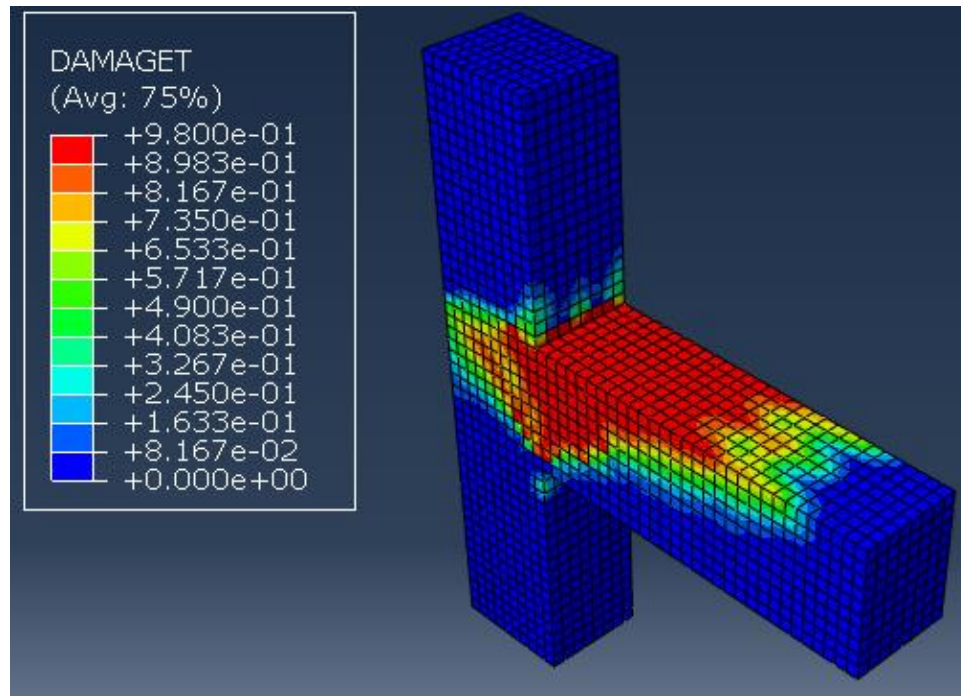
Figure 6.24: Damage propagation and crack pattern at displacement level (Δ = 11.2mm) for BCJ-12MM-Bent in without CFRP

Figure 6.25: Damage propagation and crack pattern from experimental test for BCJ-12MM-Bent in without CFRP

It is clear that almost exact failure mode and crack pattern was achieved from numerical simulation compared to the experimental result.

6.7   Numerical Simulation of BCJ-12MM-Bent in with CFRP

The experimental and finite element results of load-displacement response of the beam-column joint with CFRP retrofitting under monotonic load up to failure are shown in **Fig. 6.26**. The result of finite element simulation matches closely with experimental results as shown in **Fig. 6.26**.
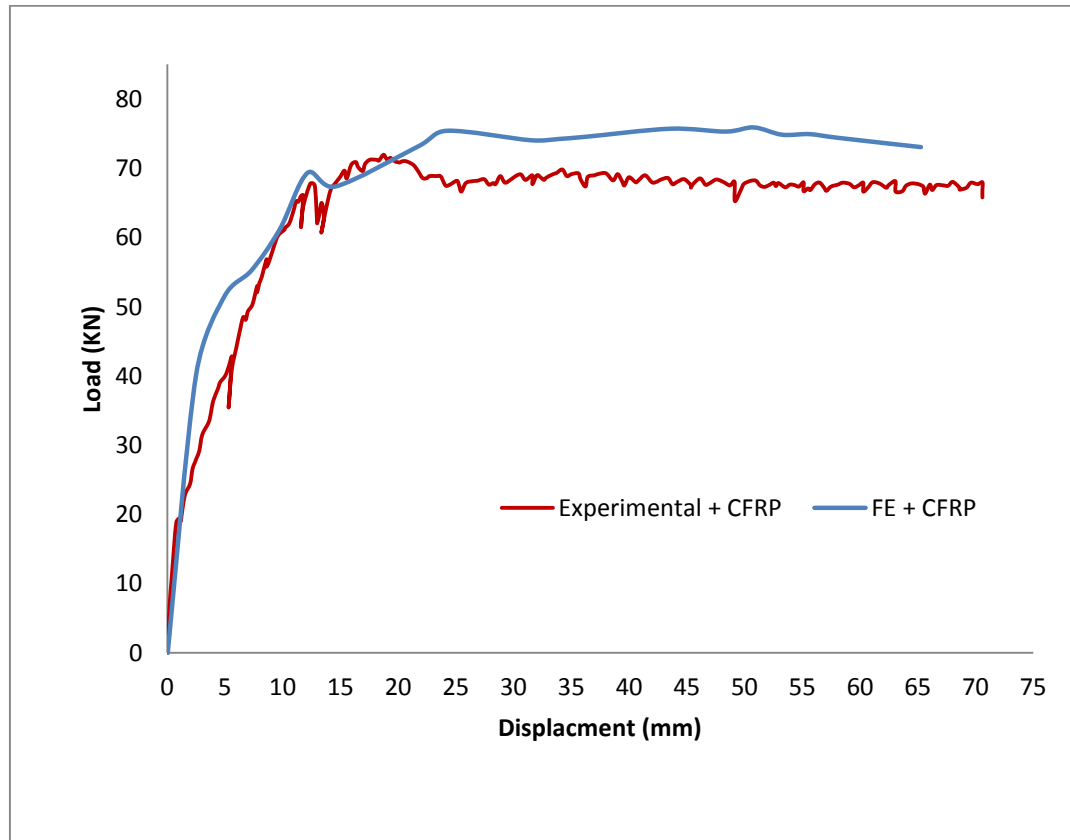
Figure 6.26: Load displacement response for BCJ-12MM-Bent in with CFRP

The maximum stresses in steel at ultimate load which is corresponding to displacement 24.2 mm respectively, are shown in **Fig. 6.27**. The stresses S11, S22 and S12 at yielding and ultimate load are shown in **Figs. 6.28, 6.29, 6.30, 6.31, 6.32 and 6.33**. The diagonal crack patterns at the joint are shown in **Figs. 6.34, 6.35 and 6.36**, closely resemble the crack patterns as observed in the experimental program and shown in **Fig. 6.37**. Stresses and strains in CFRP sheet in strong direction (direction of fiber) at yielding and ultimate load are shown in **Figs. 6.38, 6.39, 6.40 and 6.41**. The stress-strain diagram for CFRP is shown in **Figs. 6.42**.
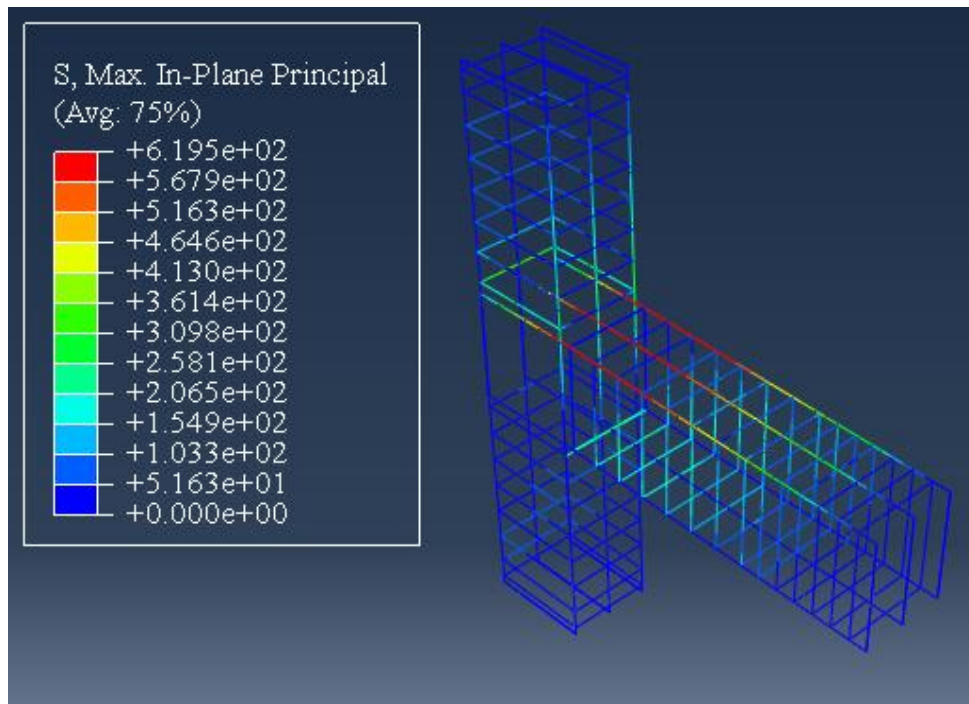
Figure 6.27: Steel stress at ultimate load (Δ = 24.2mm) for BCJ-12MM-Bent in with CFRP
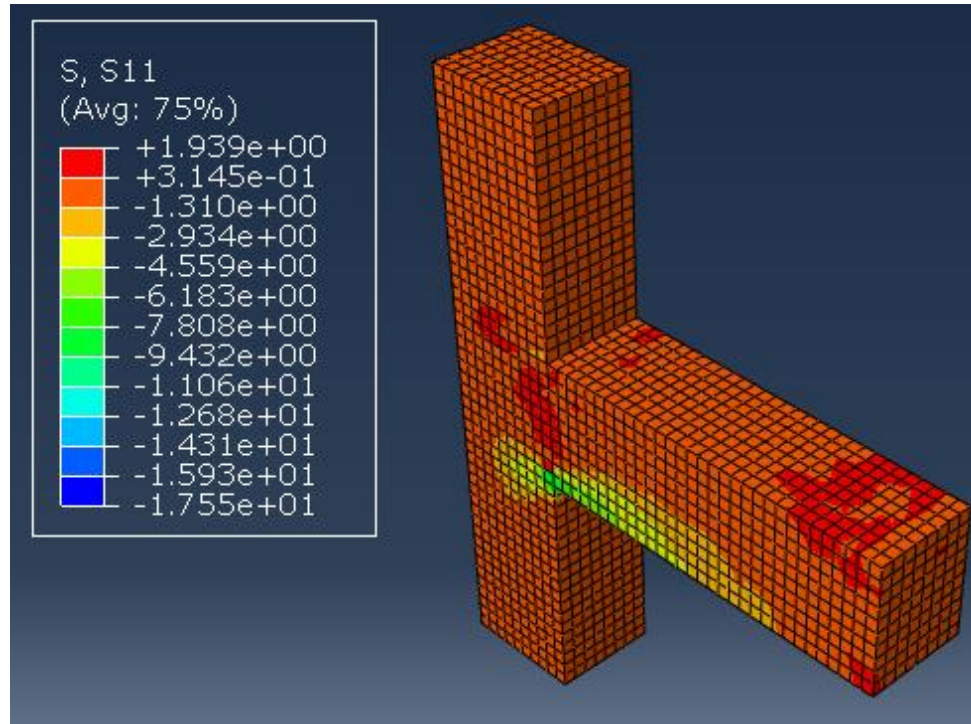
Figure 6.28: Stress S11 in concrete at yielding load (Δ = 7mm) for BCJ-12MM-Bent in with CFRP
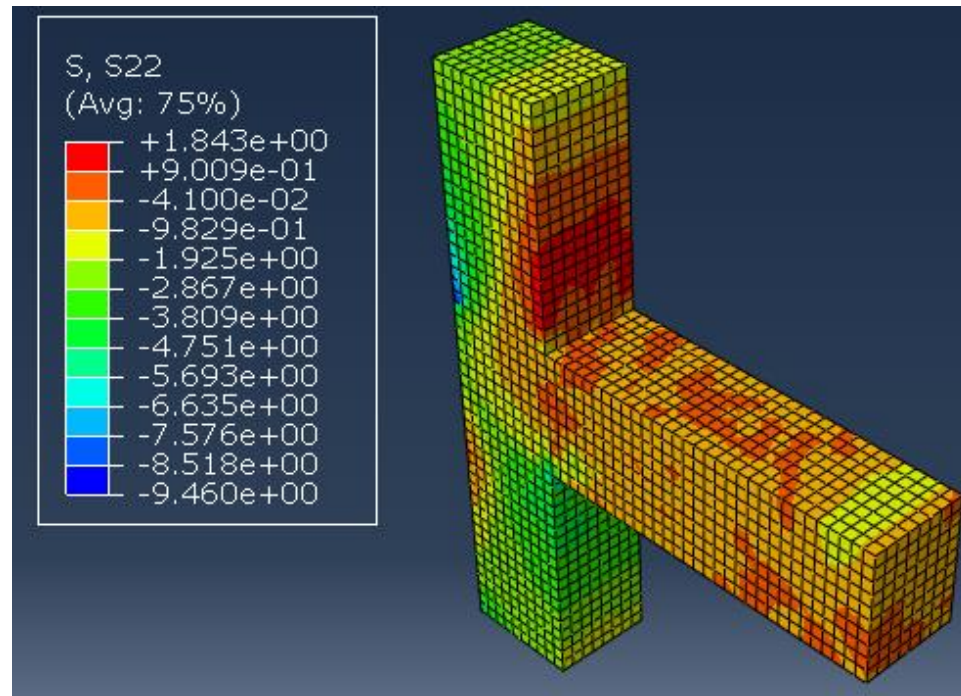
Figure 6.29: Stress S22 in concrete at yielding load (Δ = 7mm) for BCJ-12MM-Bent in with CFRP

200
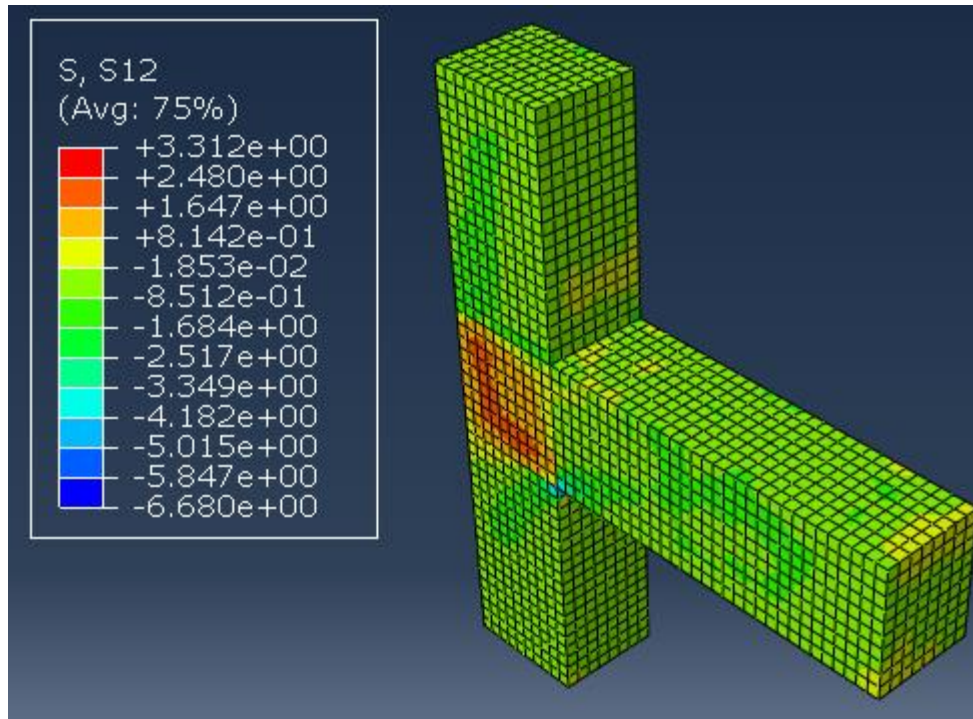
Figure 6.30: Stress S12 in concrete at yielding load (Δ = 7mm) for BCJ-12MM-Bent in with CFRP
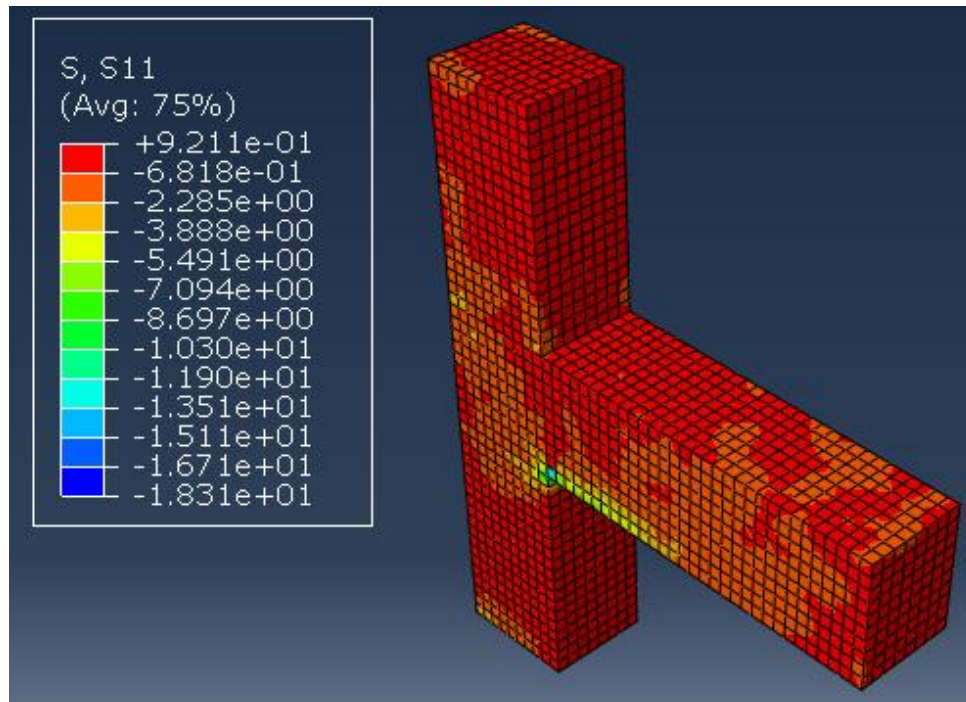
Figure 6.31: Stress S11 in concrete at ultimate load (Δ = 24.2mm) for BCJ-12MM-Bent in with CFRP
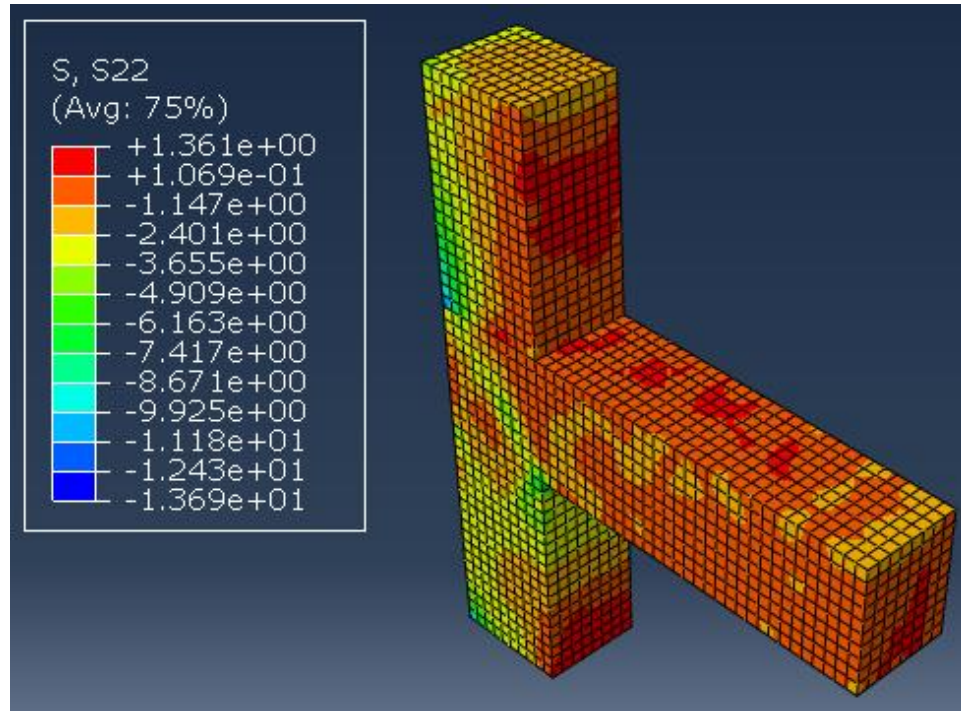
Figure 6.32: Stress S22 in concrete at ultimate load (Δ = 24.2mm) for BCJ-12MM-Bent in with CFRP
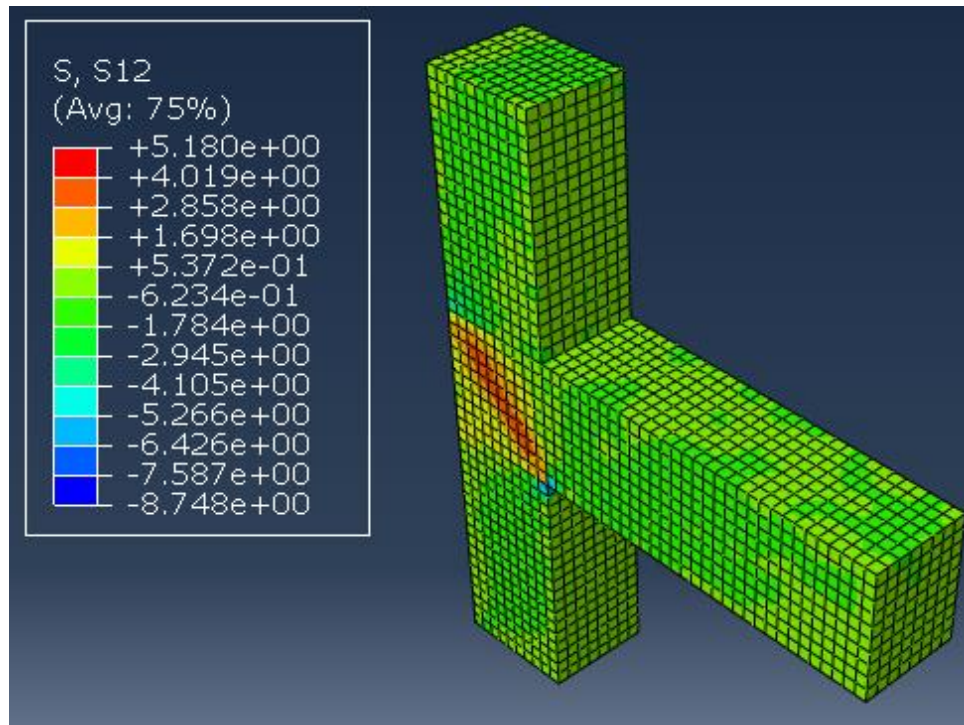
Figure 6.33: Stress S12 in concrete at ultimate load (Δ = 24.2mm) for BCJ-12MM-Bent in with CFRP
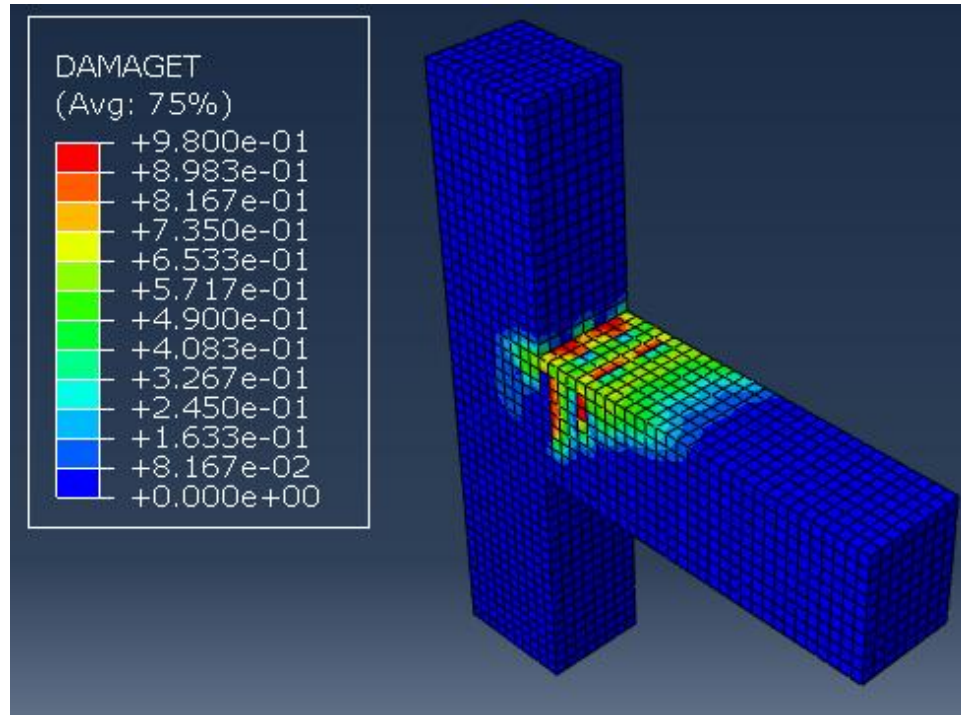
Figure 6.34: Damage propagation and crack pattern at displacement level (Δ = 2.8mm) for BCJ-12MM-Bent in with CFRP
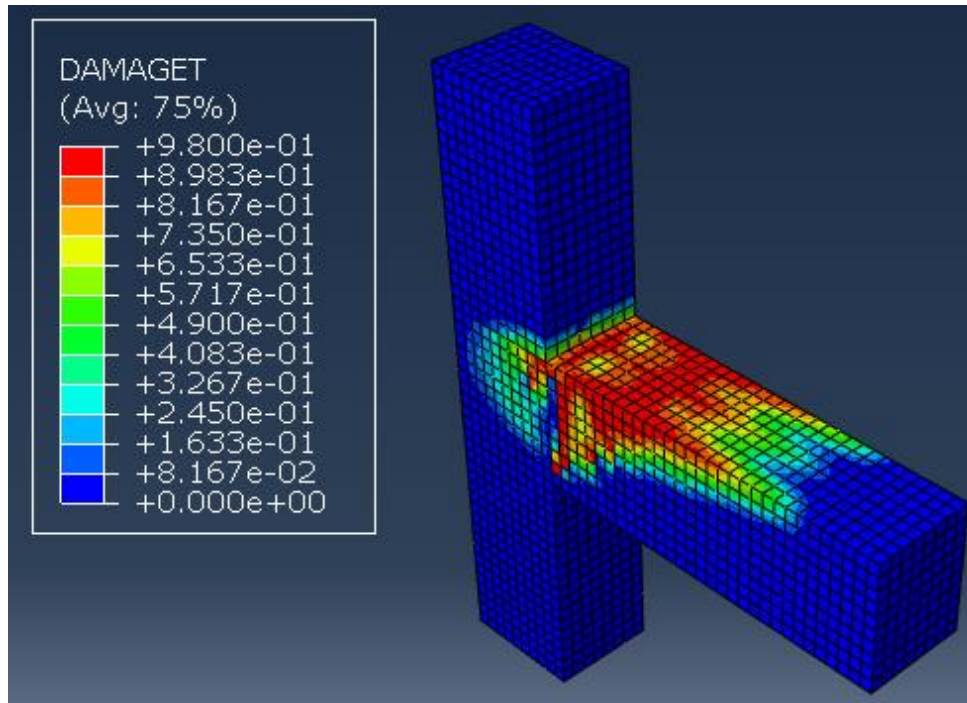
Figure 6.35: Damage propagation and crack pattern at displacement level (Δ = 4.9mm) for BCJ-12MM-Bent in with CFRP
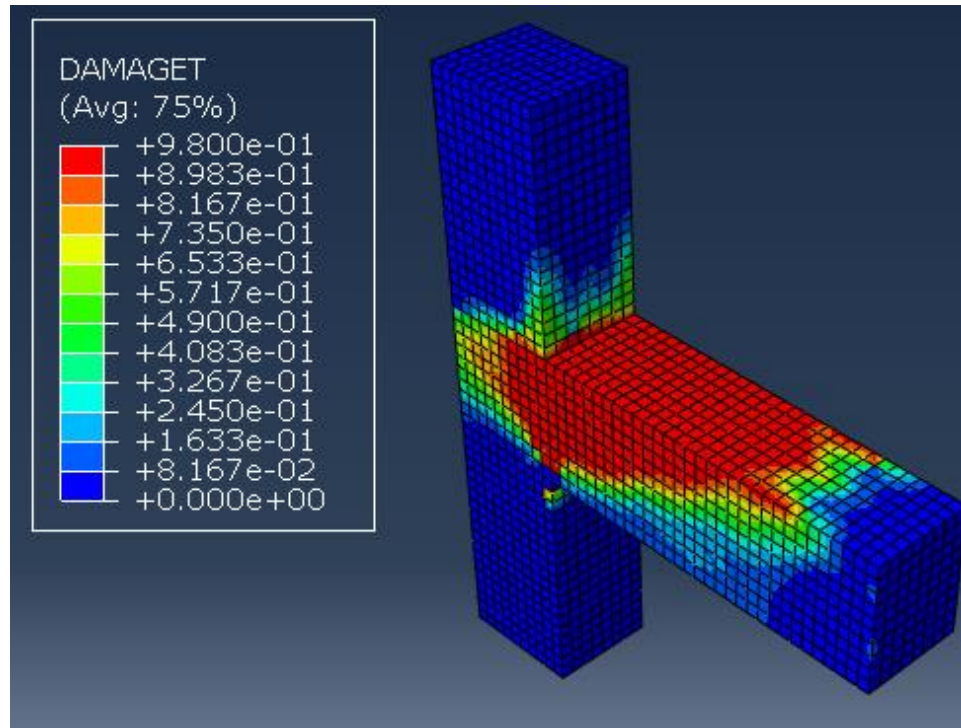
Figure 6.36: Damage propagation and crack pattern at displacement level (Δ = 16.1mm) for BCJ-12MM-Bent in with CFRP

Figure 6.37: Damage propagation and crack pattern from experimental test for BCJ-12MM-Bent in with CFRP
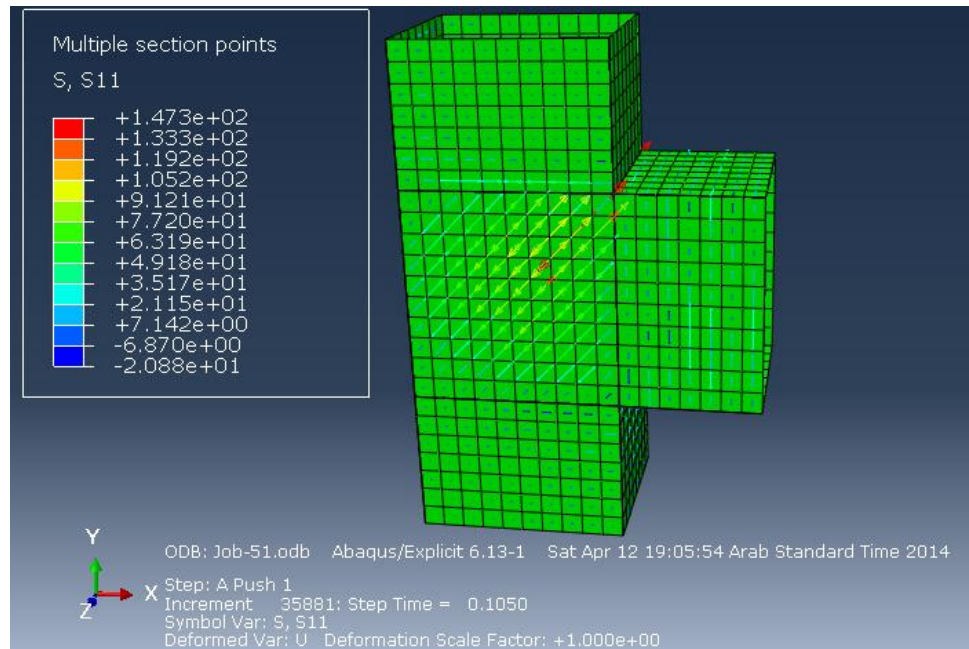
Figure 6.38: Stress S11 in CFRP at yielding load (Δ = 7mm) for BCJ-12MM-Bent in with CFRP

Figure 6.39: Strain L11 in CFRP at yielding load (Δ = 7mm) for BCJ-12MM-Bent in with CFRP

Figure 6.40: Stress S11 in CFRP at ultimate load (Δ = 24.2mm) for BCJ-12MM-Bent in with CFRP
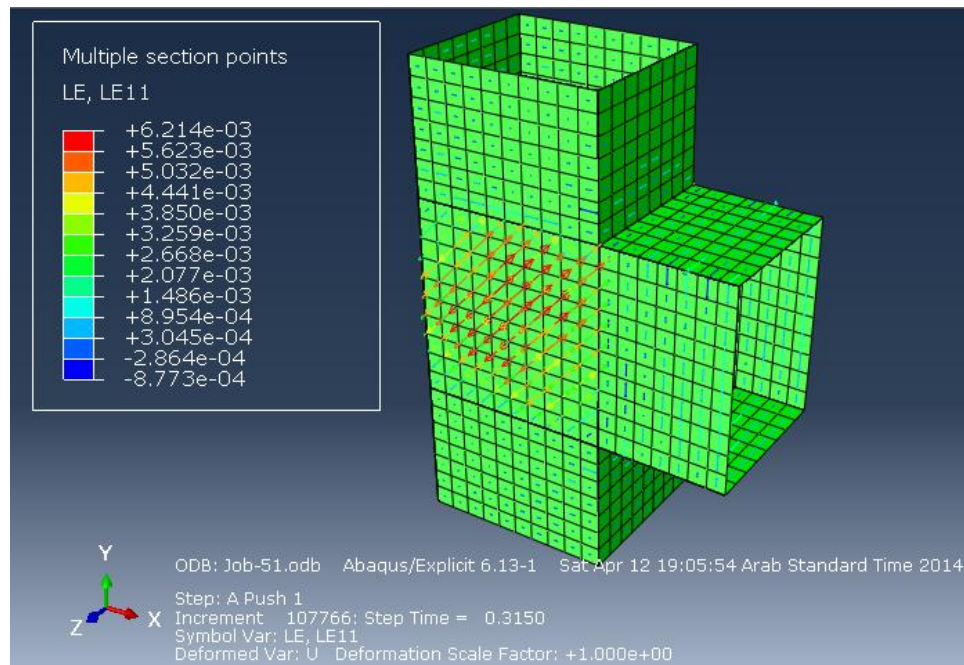
Figure 6.41: Strain L11 in CFRP at ultimate load (Δ = 24.2mm) for BCJ-12MM-Bent in with CFRP

It is clear that almost exact failure mode and crack pattern was achieved from numerical simulation compared to the experimental result.
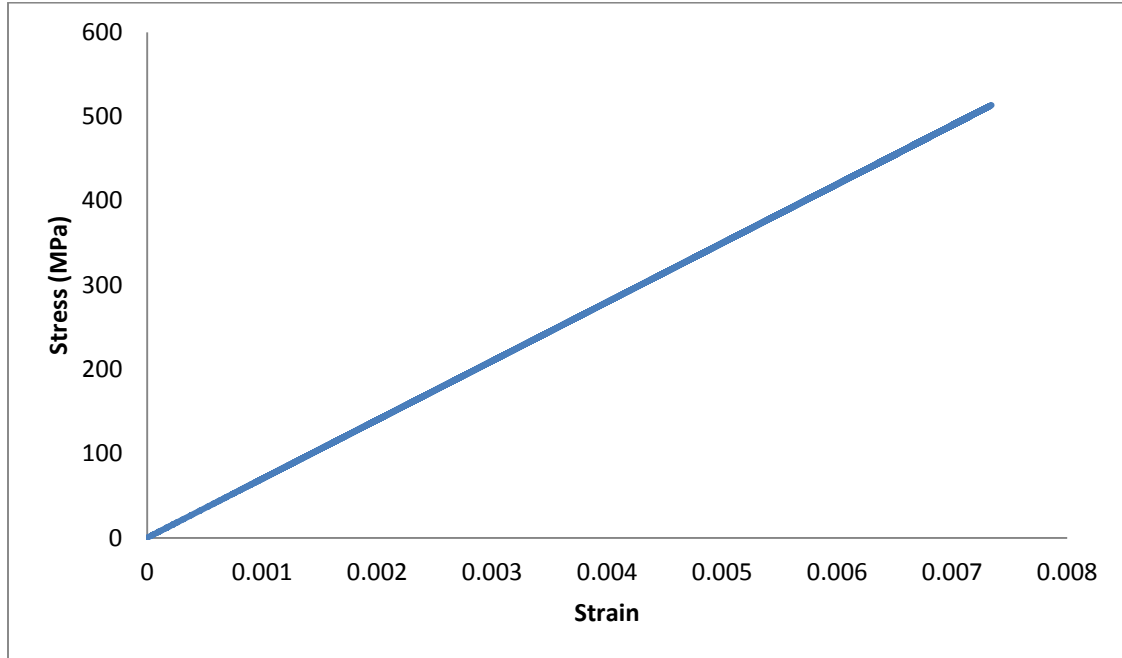
Figure 6.42: Stress strain response for CFRP for BCJ-12MM-Bent for BCJ-12MM-Bent in with CFRP

6.8   Numerical Simulation of BCJ-12MM-Bent Up without CFRP

The experimental and finite element results of load-displacement response of the beam-column joint without CFRP retrofitting, under monotonic load up to failure are shown in **Fig. 6.43**. The result of finite element simulation matches closely with experimental results as shown in **Fig. 6.43**. In addition, **Fig. 6.44** shows that a good match was achieved between experimental and numerical results for the cyclic load test.
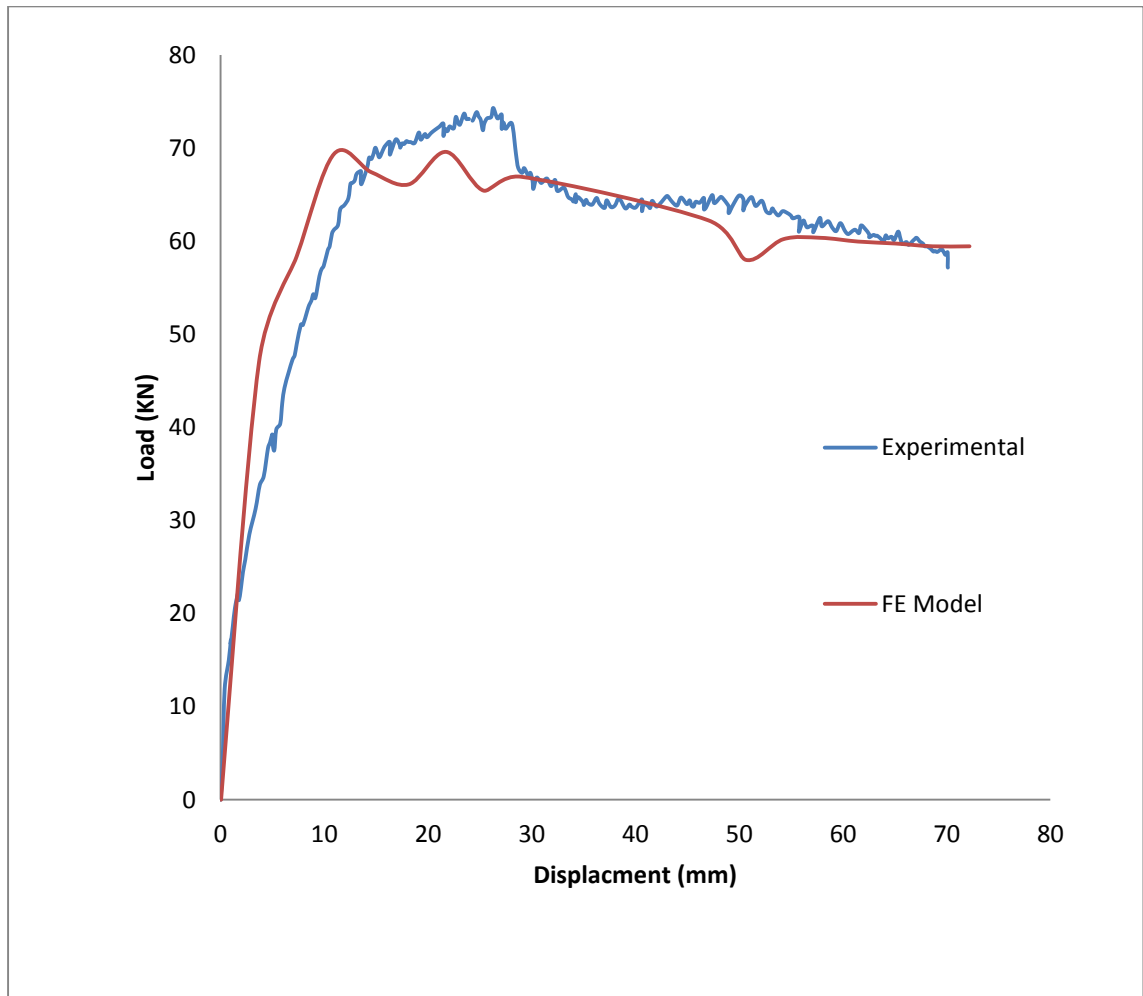
Figure 6.43: Load displacement response for BCJ-12MM-Bent Up without CFRP

Figure 6.44: Load displacement response for cyclic test for BCJ-12MM-Bent Up without CFRP

The maximum stresses in steel at ultimate load which is corresponding to tip displacement of 23 mm respectively, are shown in **Fig. 6.45**. The stresses S11, S22 and S12 at yielding and ultimate load are shown in **Figs. 6.46, 6.47, 6.48, 6.49, 6.50 and 6.51**. The diagonal crack patterns at the joint as shown in **Figs. 6.52, 6.54 and 6.56**, closely resemble the crack patterns as observed in the experimental program and shown in **Figs. 6.53, 6.55 and 6.57.**

S, Max. In-Plane Principal (Abs)
(Avg: 75%)
+6.048e+02
+5.288e+02
+4.529e+02
+3.769e+02
+3.010e+02
+2.250e+02
+1.490e+02
+7.306e+01
-2.901e+00
-7.886e+01
-1.548e+02
-2.308e+02
-3.068e+02

Figure 6.45: Steel stress at ultimate load ($\varDelta$ = 21mm) for BCJ-12MM-Bent Up without CFRP

Figure 6.46: Stress S11 in concrete at yielding load (Δ = 5.95mm) for BCJ-12MM-Bent Up without CFRP

Figure 6.47: Stress S22 in concrete at yielding load (Δ = 5.95mm) for BCJ-12MM-Bent Up without CFRP

211

Figure 6.48: Stress S12 in concrete at yielding load (Δ = 5.95mm) for BCJ-12MM-Bent Up without CFRP

Figure 6.49: Stress S11 in concrete at ultimate load (Δ = 21.7mm) for BCJ-12MM-Bent Up without CFRP

Figure 6.50: Stress S22 in concrete at ultimate load (Δ = 21.7mm) for BCJ-12MM-Bent Up without CFRP

Figure 6.51: Stress S12 in concrete at ultimate load (Δ = 21.7mm) for BCJ-12MM-Bent Up without CFRP

Figure 6.52: Damage propagation and crack pattern at displacement pattern (Δ = 2.8mm) for BCJ-12MM-Bent Up without CFRP

Figure 6.53: Damage propagation and crack pattern from experimental test for BCJ-12MM-Bent Up without CFRP

Figure 6.54: Damage propagation and crack pattern at displacement pattern (Δ= 5.6 mm) for BCJ-12MM-Bent Up without CFRP

Figure 6.55: Damage propagation and crack pattern from experimental test for BCJ-12MM-Bent Up without CFRP

Figure 6.56: Damage propagation and crack pattern at displacement pattern (Δ = 11.7 mm) for BCJ-12MM-Bent Up without CFRP

Figure 6.57: Damage propagation and crack pattern from experimental test for BCJ-12MM-Bent Up without CFRP

It is clear from the result of experimental test that almost exact failure mode and crack pattern was achieved from numerical simulation compared to the experimental result.

6.8.1   Numerical Simulation of BCJ-12MM-Bent up with CFRP

The experimental and finite element results of load-displacement response of the beam-column joint with CFRP retrofitting, under monotonic load up to failure are shown in **Fig. 6.58**. The result of finite element simulation matches closely with experimental results as shown in **Fig. 6.58**.

Figure 6.58: Load displacement response for BCJ-12MM-Bent up with CFRP

The maximum stresses in steel at load which is corresponding to displacement 21.8 mm respectively, are shown in **Fig. 6.59**. The stresses S11, S22 and S12 at yielding and ultimate load are shown in **Figs. 6.60, 6.61, 6.62, 6.63, 6.64 and 6.65**. The stresses and strains in CFRP sheet at yielding and ultimate load are shown in **Figs. 6.66, 6.67, 6.68 and 6.69**. Stress-strain response for CFRP is shown in **Fig. 6.70**. The diagonal crack patterns at the joint as shown in **Figs. 6.71, 6.72 and 6.73** closely resemble the crack pattern as observed in the experimental program as shown in **Fig. 6.74**.

Figure 6.59: Steel stress at ultimate load (Δ = 21.8mm) for BCJ-12MM-Bent up with CFRP

Figure 6.60: Stress S11 in concrete at yielding load (Δ = 7.35mm) for BCJ-12MM-Bent up with CFRP

Figure 6.61: Stress S22 in concrete at yielding load (Δ = 7.35mm) for BCJ-12MM-Bent up with CFRP

Figure 6.62: Stress S12 in concrete at yielding load (Δ = 7.35mm) for BCJ-12MM-Bent up with CFRP

Figure 6.63: Stress S11 in concrete at ultimate load (Δ = 21.8mm) for BCJ-12MM-Bent up with CFRP
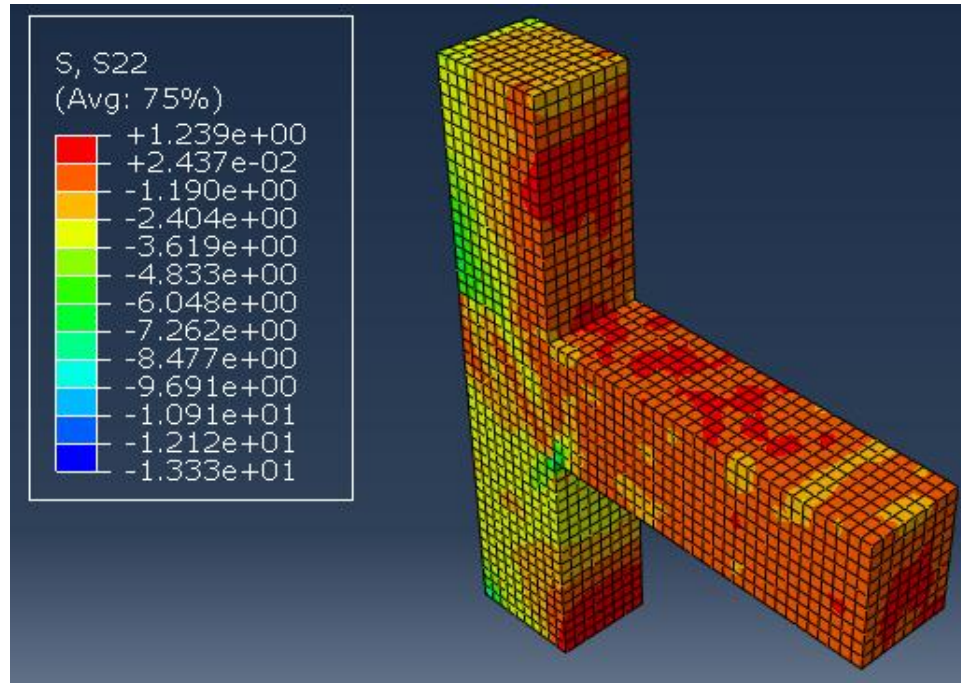
Figure 6.64: Stress S22 in concrete at ultimate load (Δ = 21.8mm) for BCJ-12MM-Bent up with CFRP
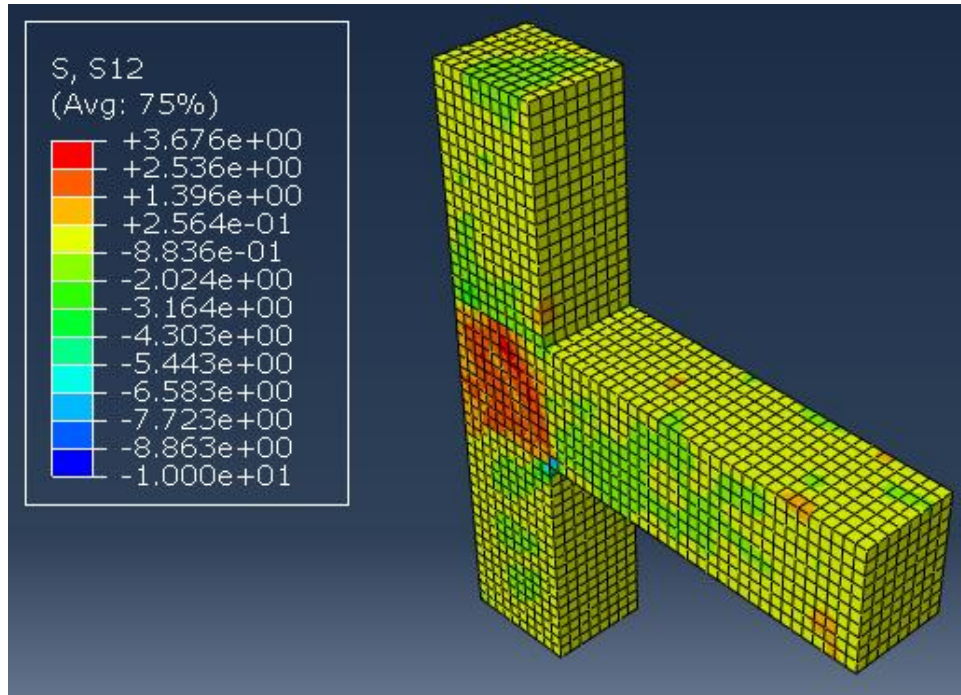
**Figure 6.65: Stress S12 in concrete at ultimate load (Δ = 21.8mm) for BCJ-12MM-Bent up with CFRP**
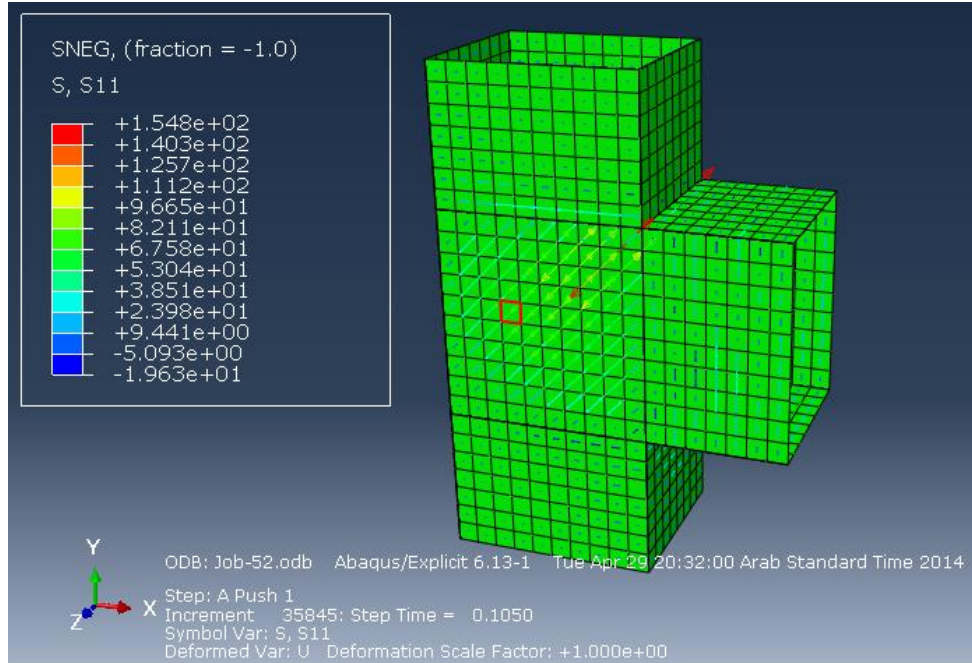
Figure 6.66: Stress S11 in CFRP at yielding load (Δ = 7.35mm) for BCJ-12MM-Bent up with CFRP
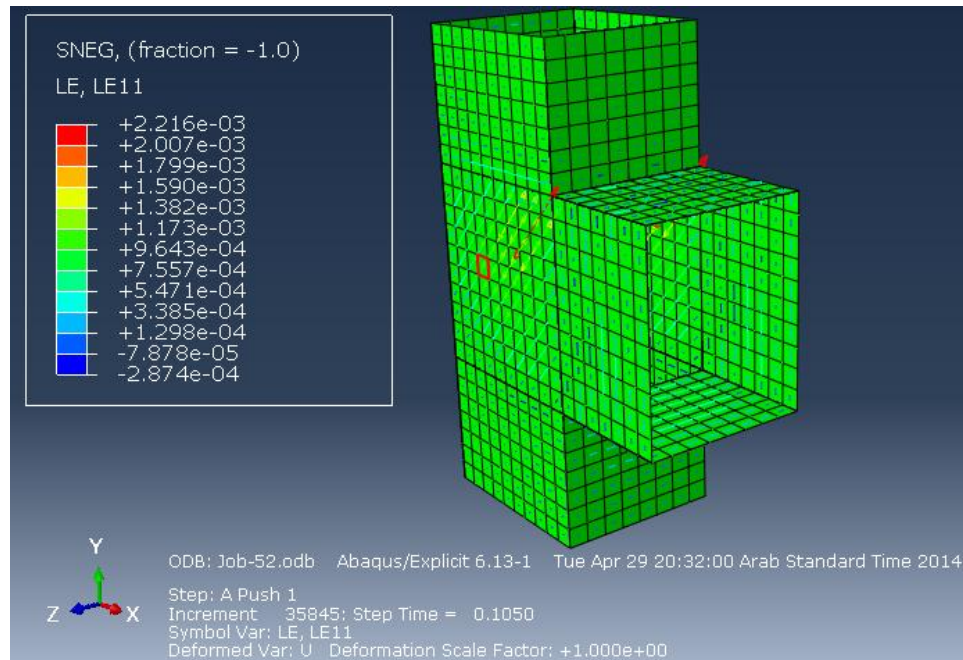
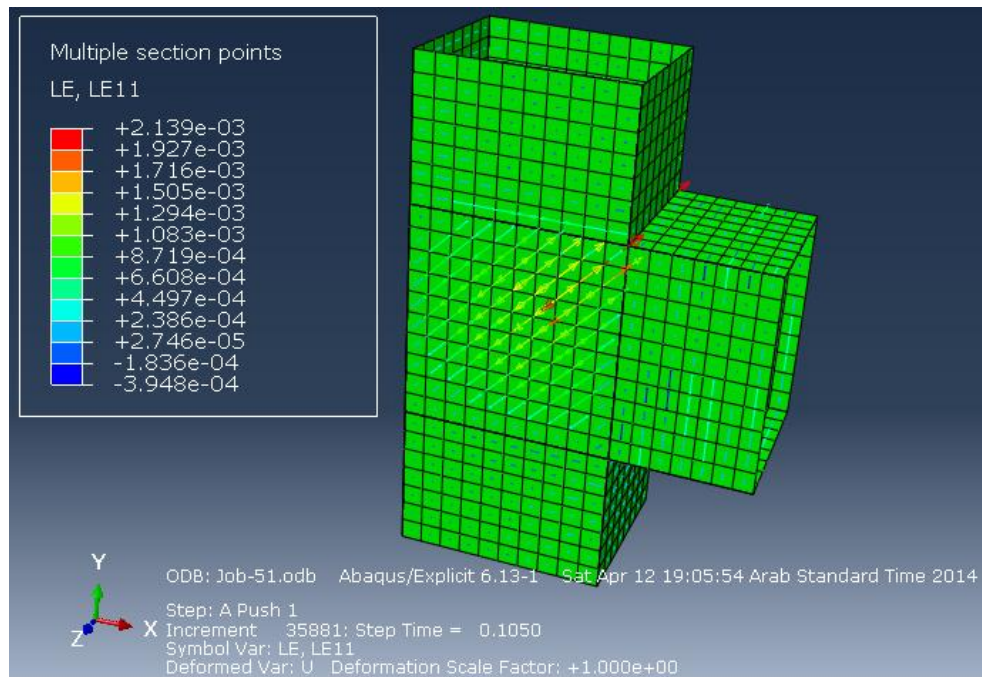**Figure 6.67: Strain L11 in CFRP at yielding load (Δ = 7.35mm) for BCJ-12MM-Bent up with CFRP**
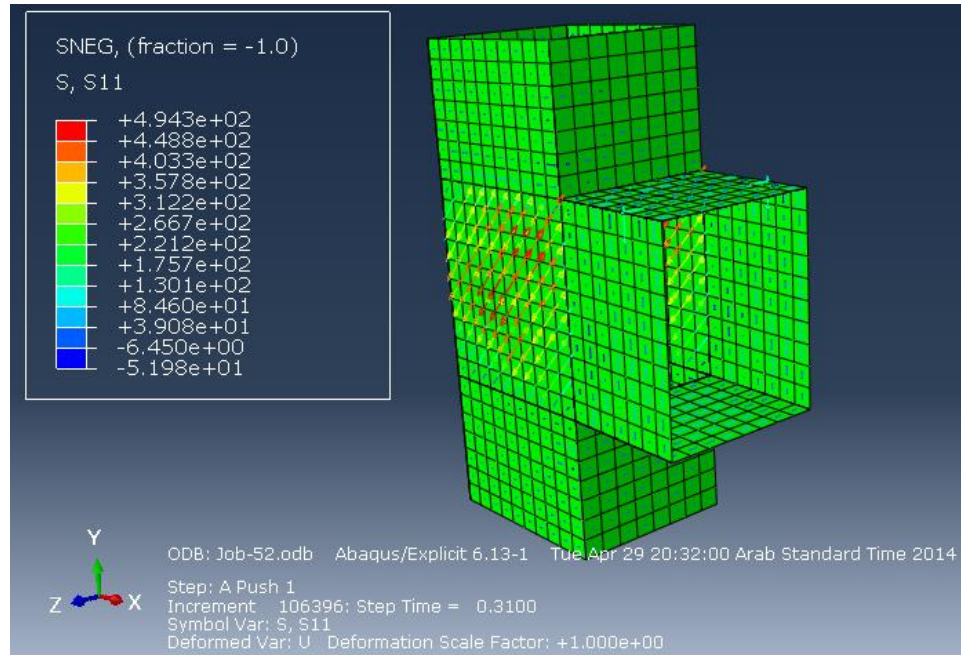
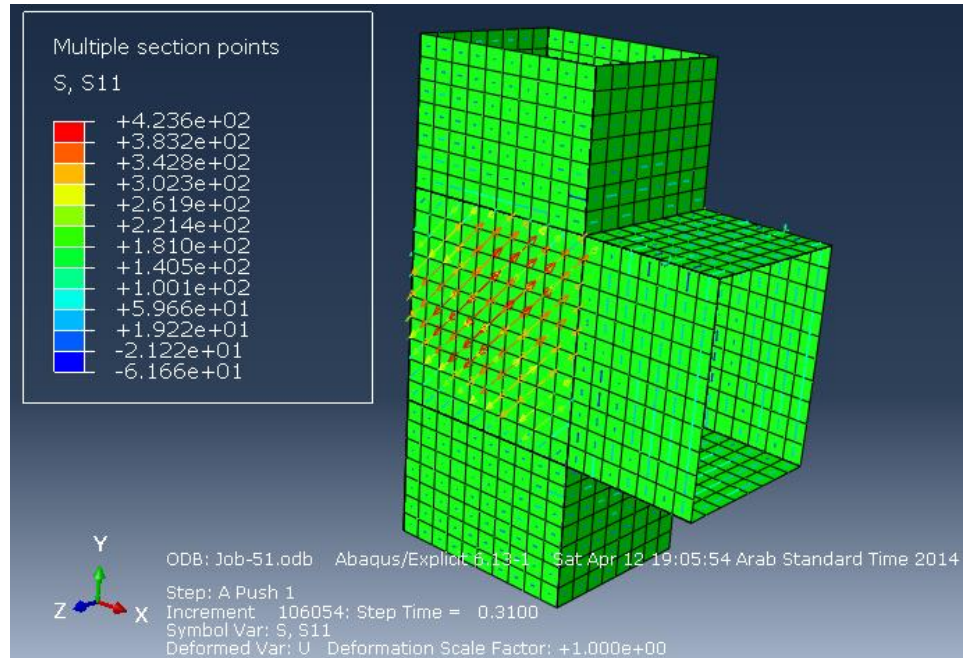**Figure 6.68: Stress S11 in CFRP at ultimate load (Δ = 21.8mm) for BCJ-12MM-Bent up with CFRP**
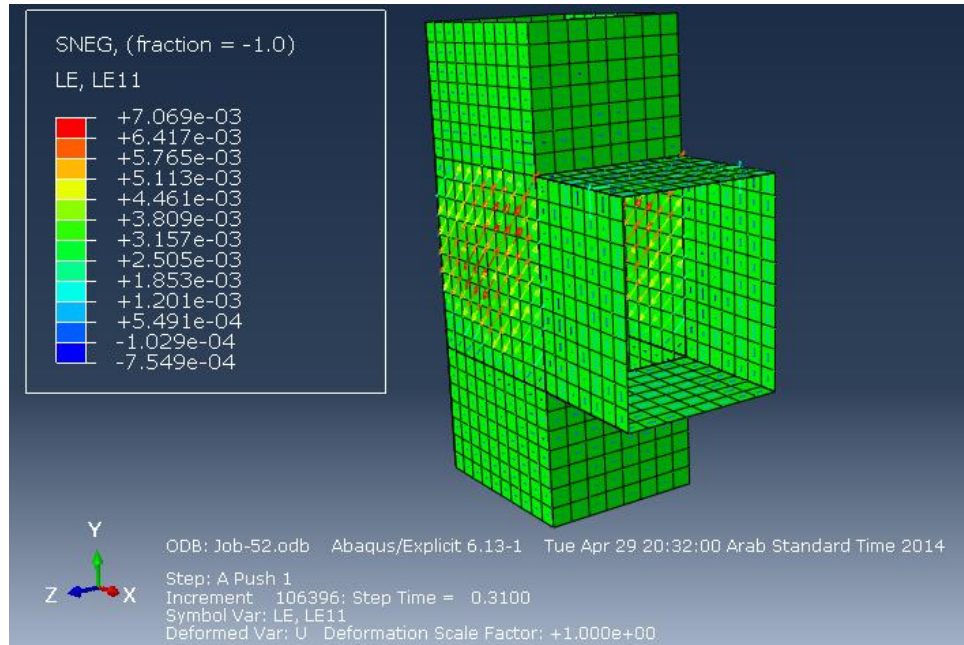
Figure 6.69: Strain L11 in CFRP at ultimate load (Δ = 21.8mm) for BCJ-12MM-Bent up with CFRP
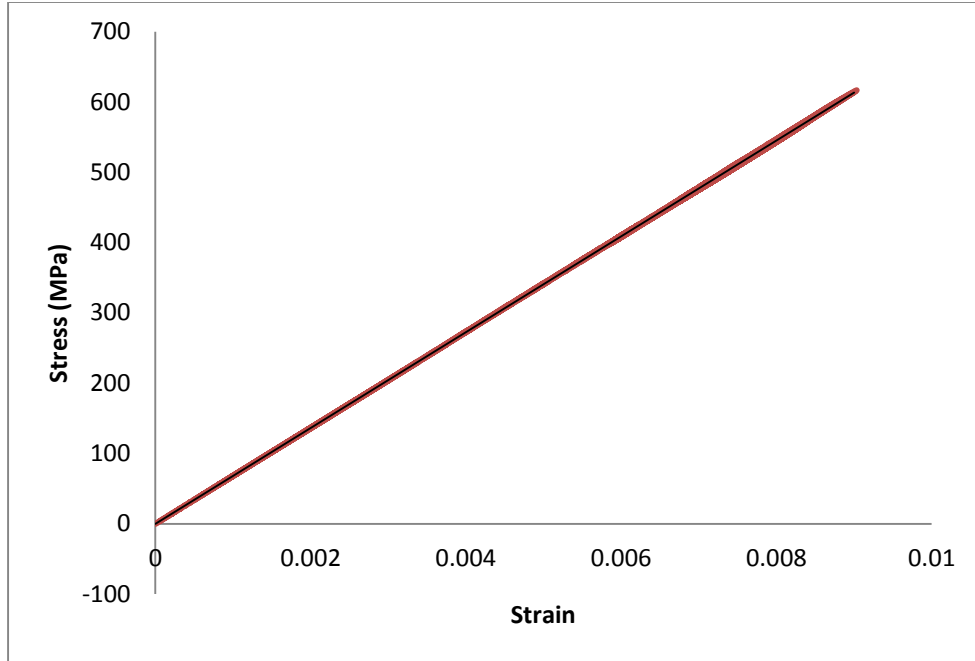
Figure 6.70: Stress-strain response for CFRP in BCJ-12-MM-Bent Up with CFRP
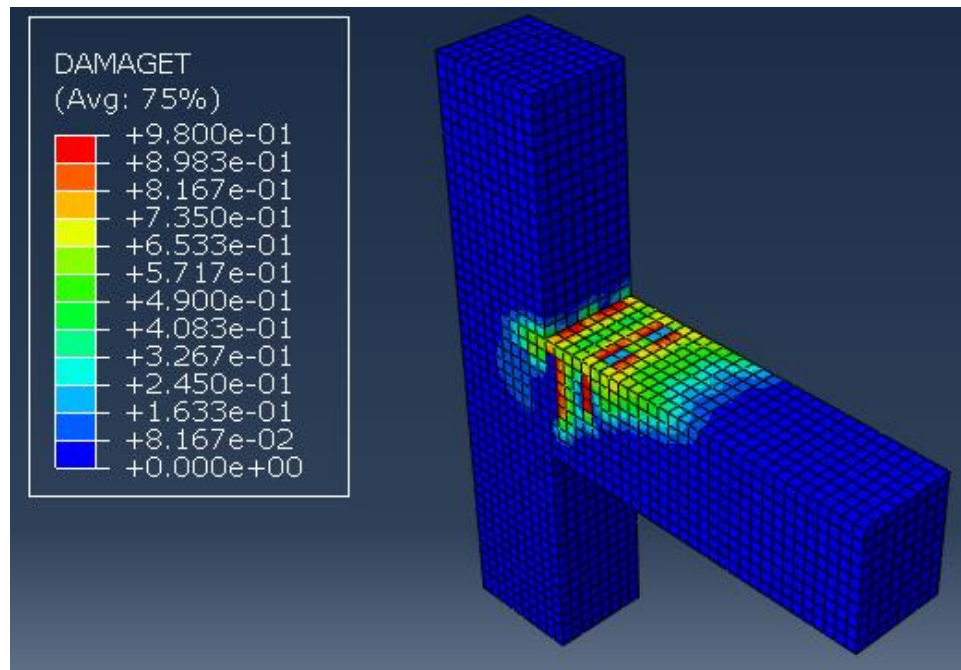
Figure 6.71: Damage propagation and crack pattern at displacement pattern (Δ = 2.8 mm) for BCJ-12MM-Bent up with CFRP
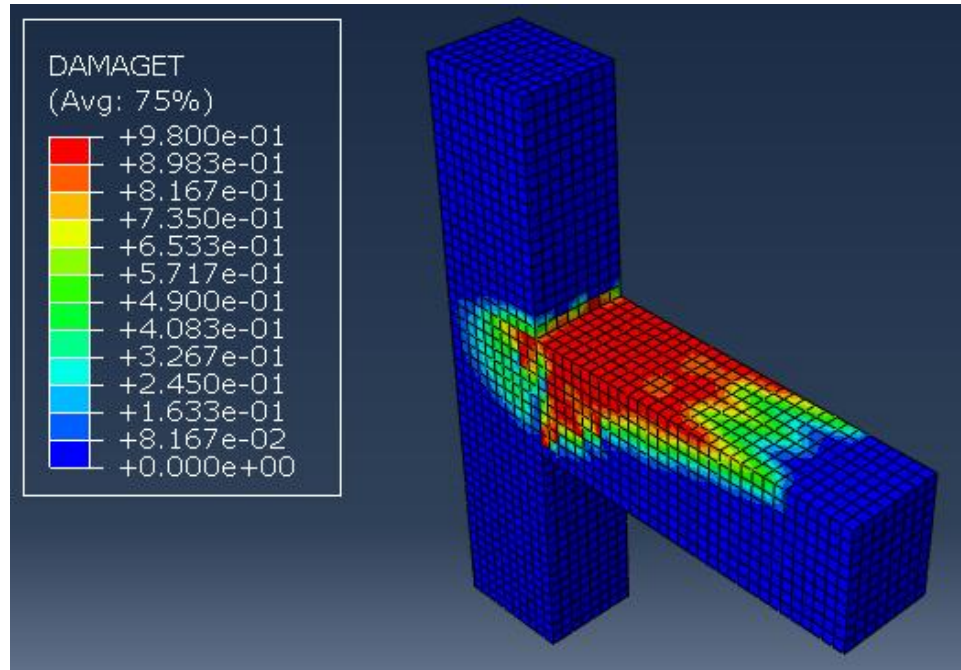
Figure 6.72: Damage propagation and crack pattern at displacement pattern (Δ = 7 mm) for BCJ-12MM-Bent up with CFRP
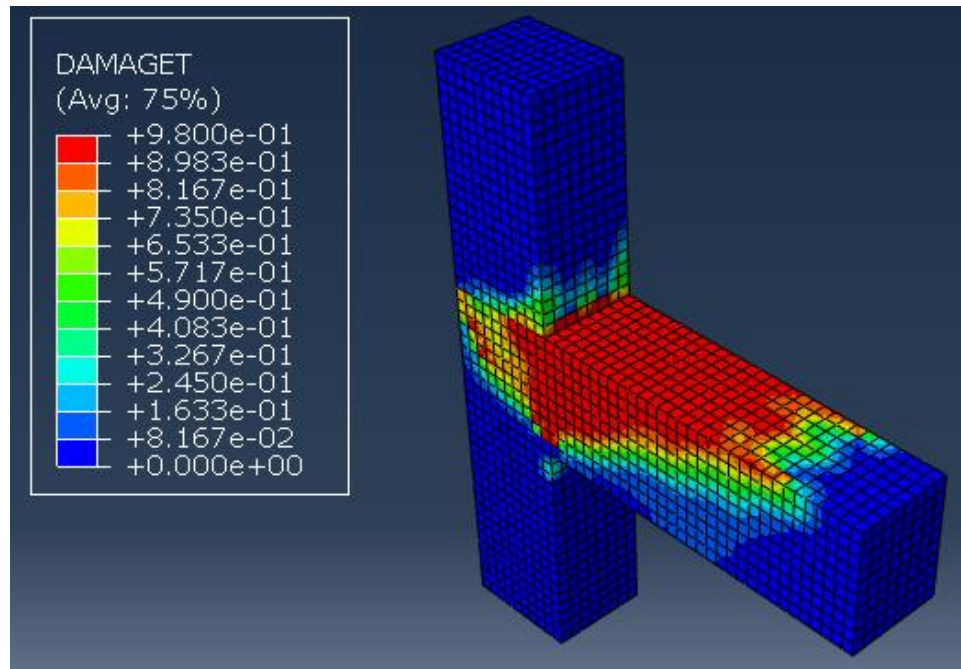
Figure 6.73: Damage propagation and crack pattern at displacement pattern (Δ =13.3 mm) for BCJ-12MM-Bent up with CFRP

Figure 6.74: Damage propagation and crack pattern from experimental test for BCJ-12MM-Bent up with CFRP

It is clear that almost exact failure mode and crack pattern was achieved from numerical

simulation compared to the experimental result.

6.9 Numerical Simulation of BCJ-18MM-Bent In without CFRP

The experimental and finite element results of load-displacement response of the beam-column joint without CFRP retrofitting, under monotonic load up to failure are shown **Fig. 6.75**. The result of finite element simulation matches closely with experimental results as shown in **Figs. 6.75 and 6.76**.
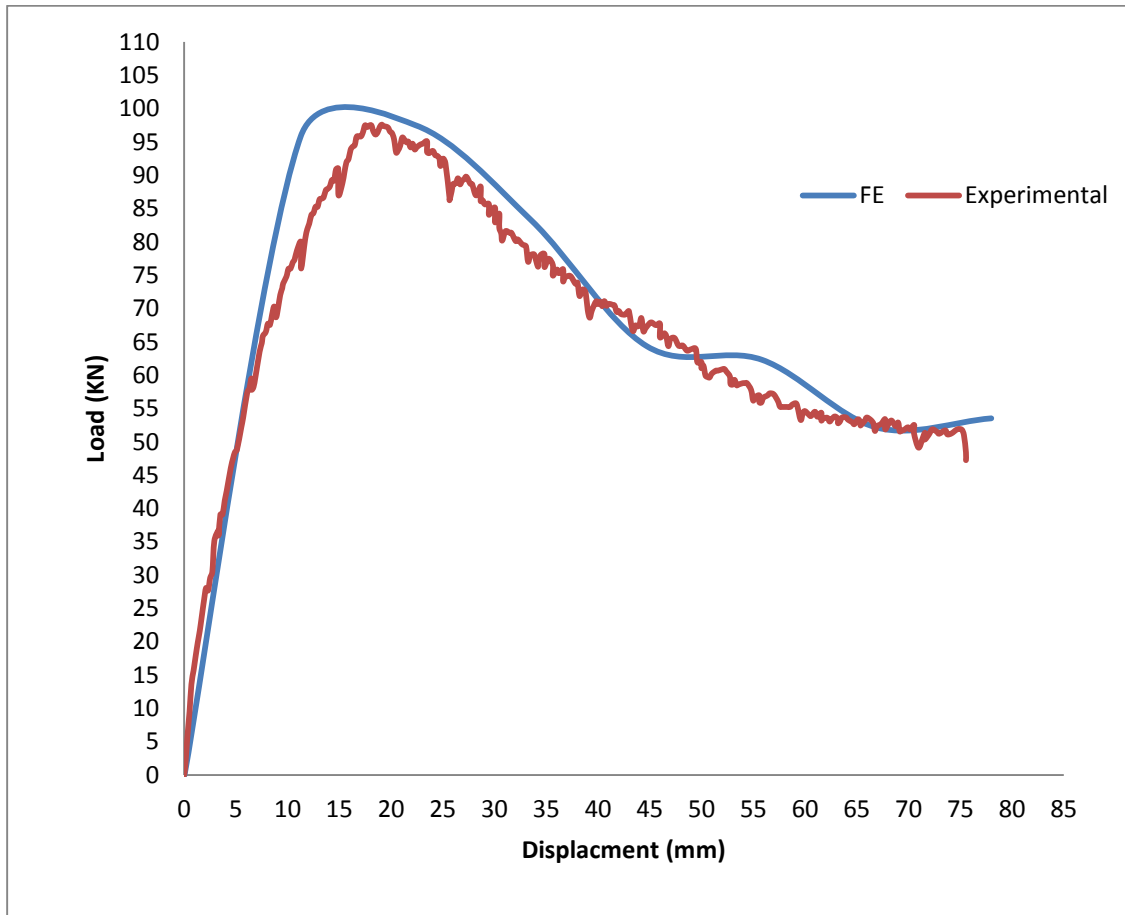
Figure 6.75: Load displacement response for BCJ-18MM-Bent In without CFRP
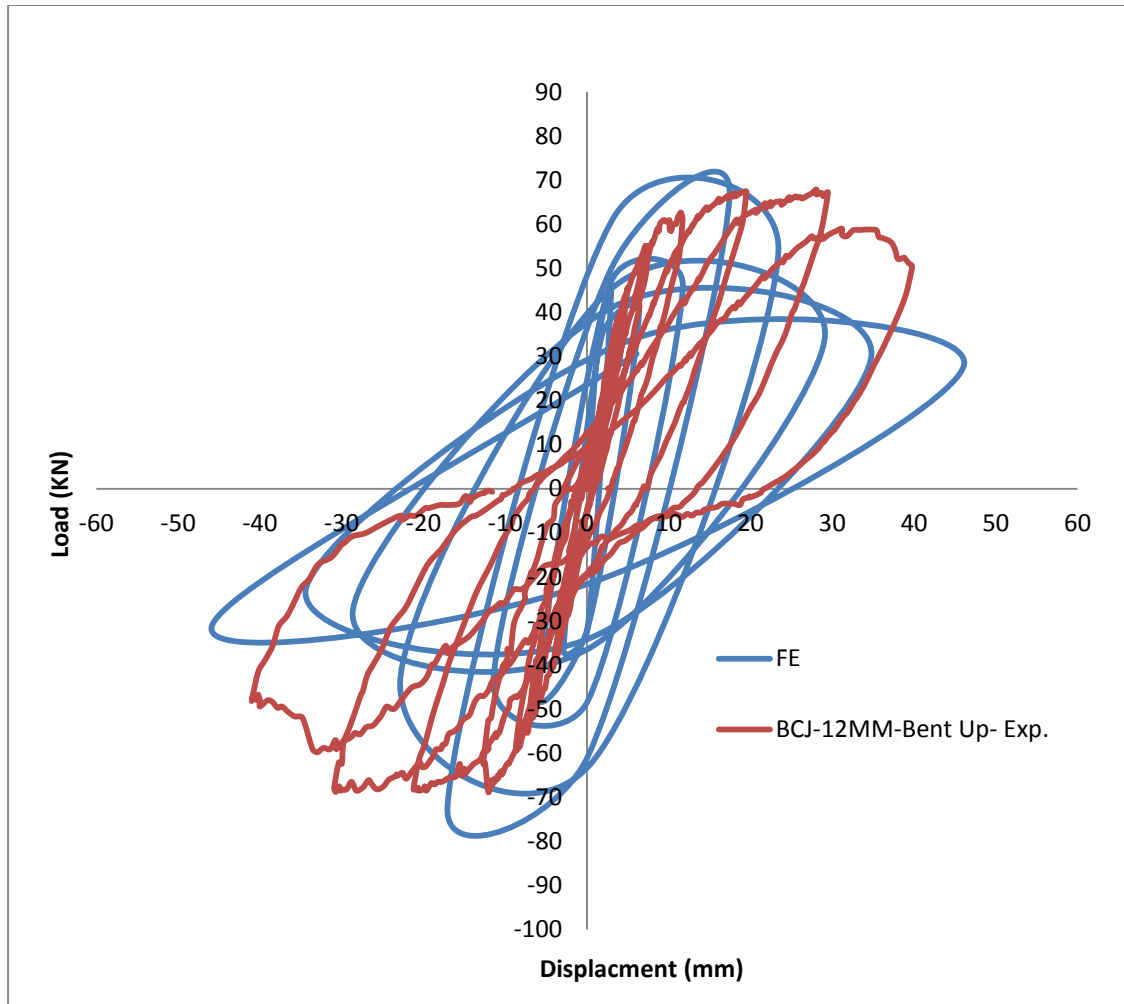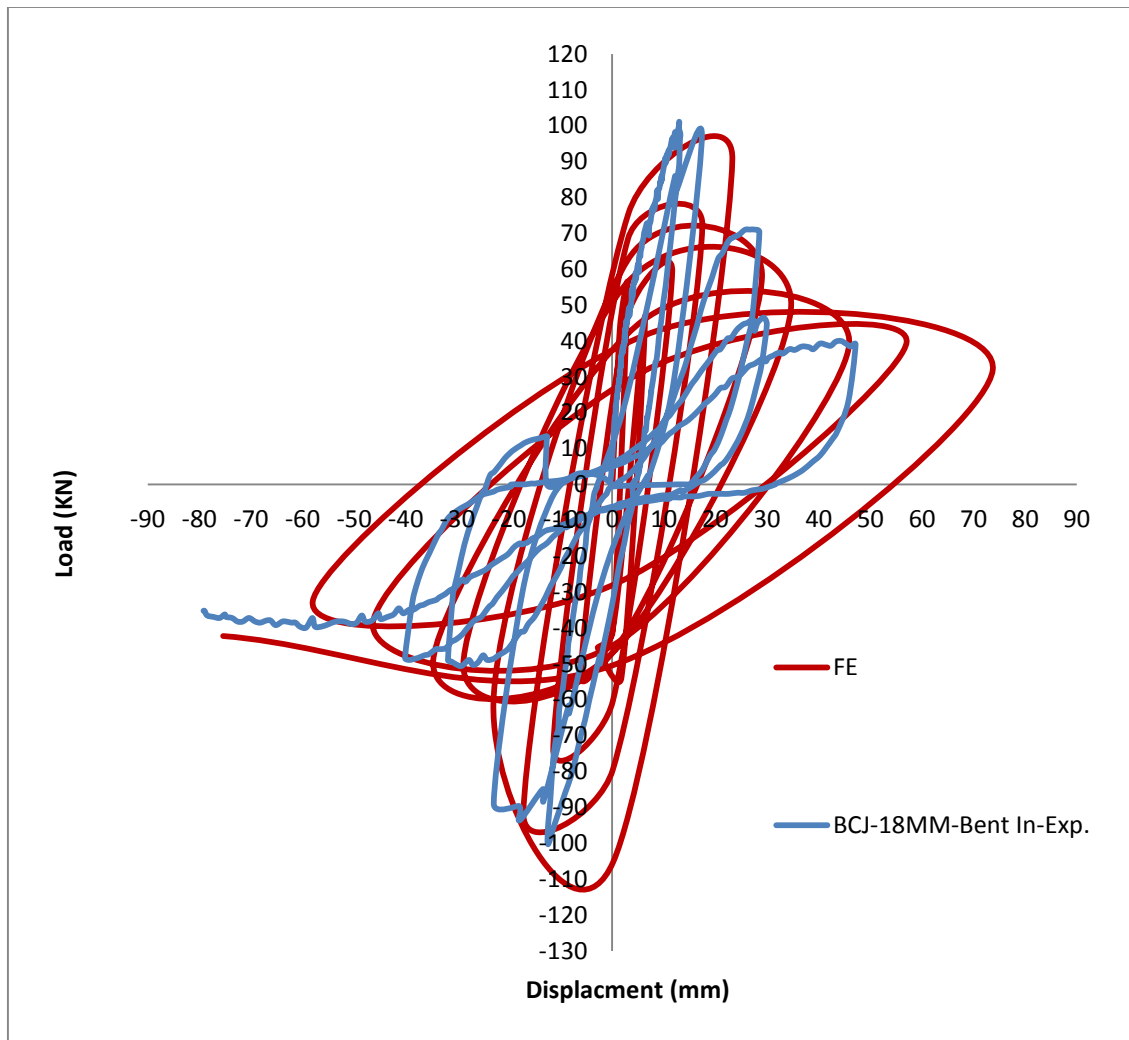
Figure 6.76: Load displacement response for cyclic test for BCJ-18MM-Bent In without CFRP

The maximum stresses in steel at ultimate load which is corresponding to tip 28.7 mm respectively, are shown in **Fig. 6.77**. The stresses S11, S22 and S12 at yielding and ultimate load are shown in **Fig. 6.78, 6.79, 6.80, 6.81, 6.82 and 6.83**. The diagonal crack patterns at the joint as shown in **Figs. 6.84, 6.86 and 6.88**, closely resemble the crack pattern as observed in the experimental program and shown in **Figs. 6.85, 6.87 and 6.89**.
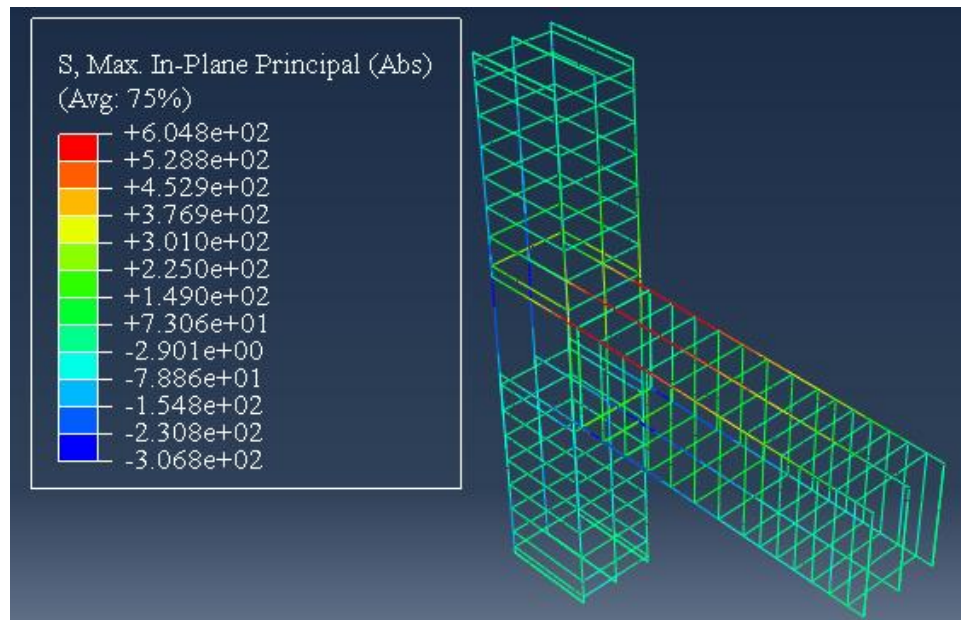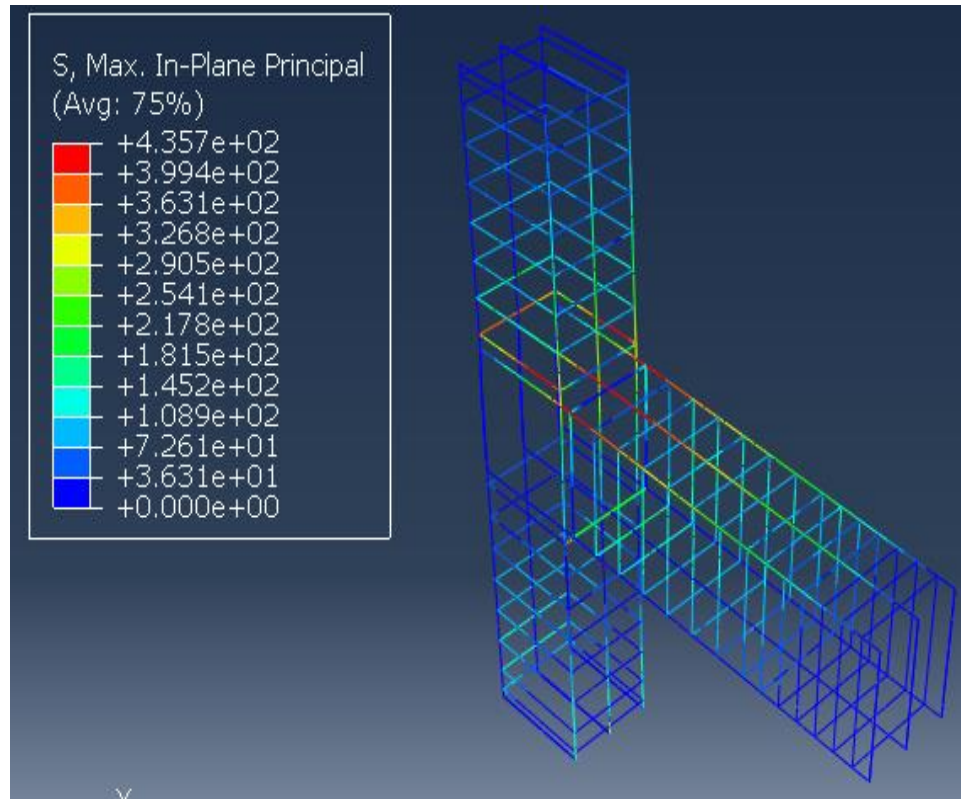

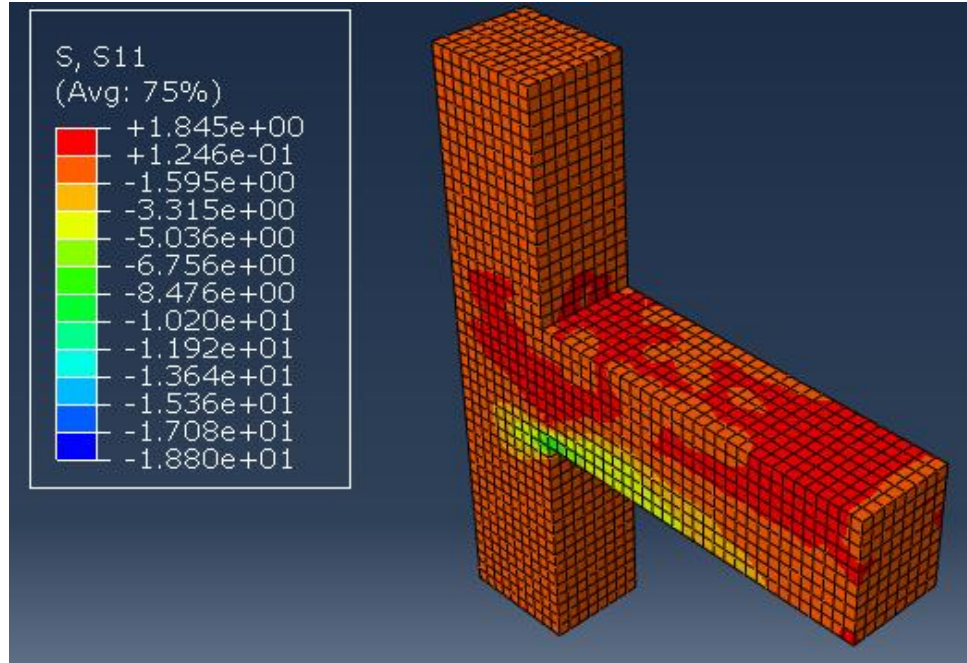**Figure 6.77: Steel stress at ultimate load (Δ = 28.7mm) for BCJ-18MM-Bent In without CFRP**
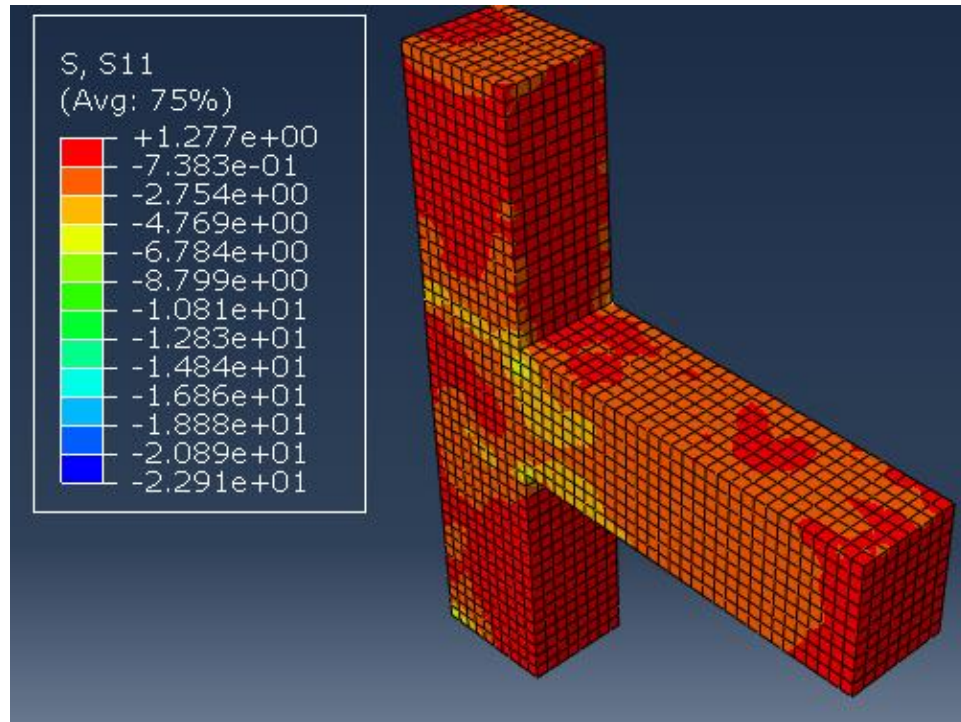
Figure 6.78: Stress S11 in concrete at yielding load (Δ = 21mm) for BCJ-18MM-Bent In without CFRP
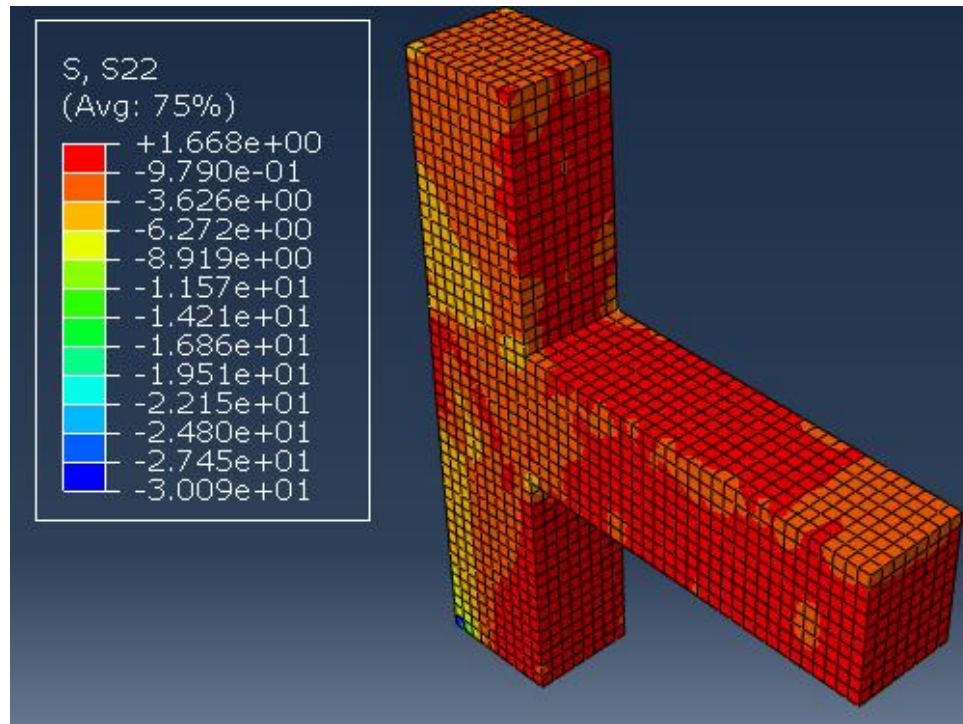
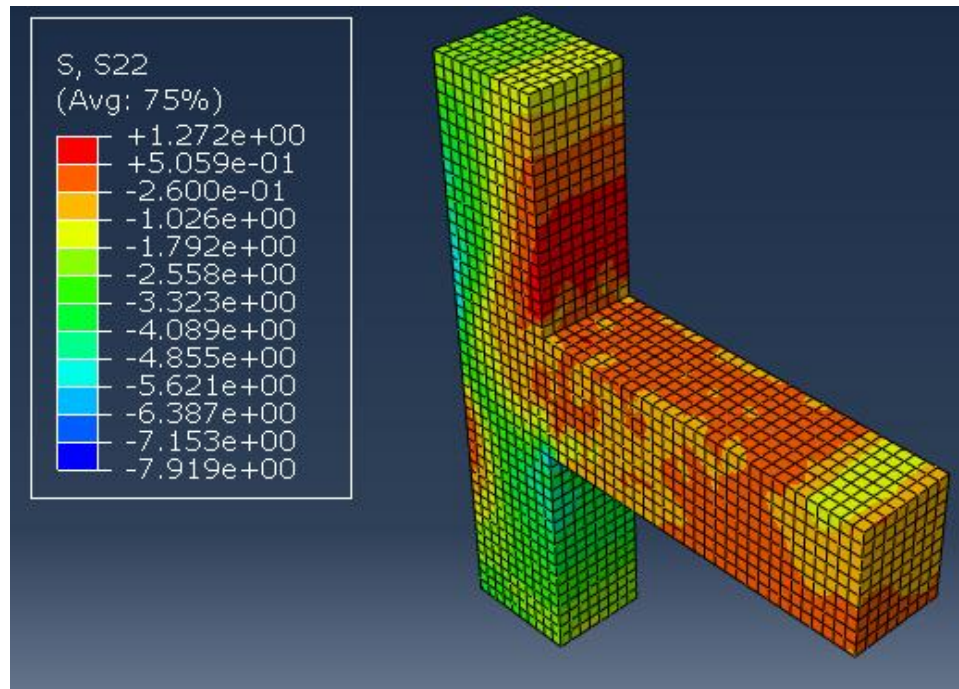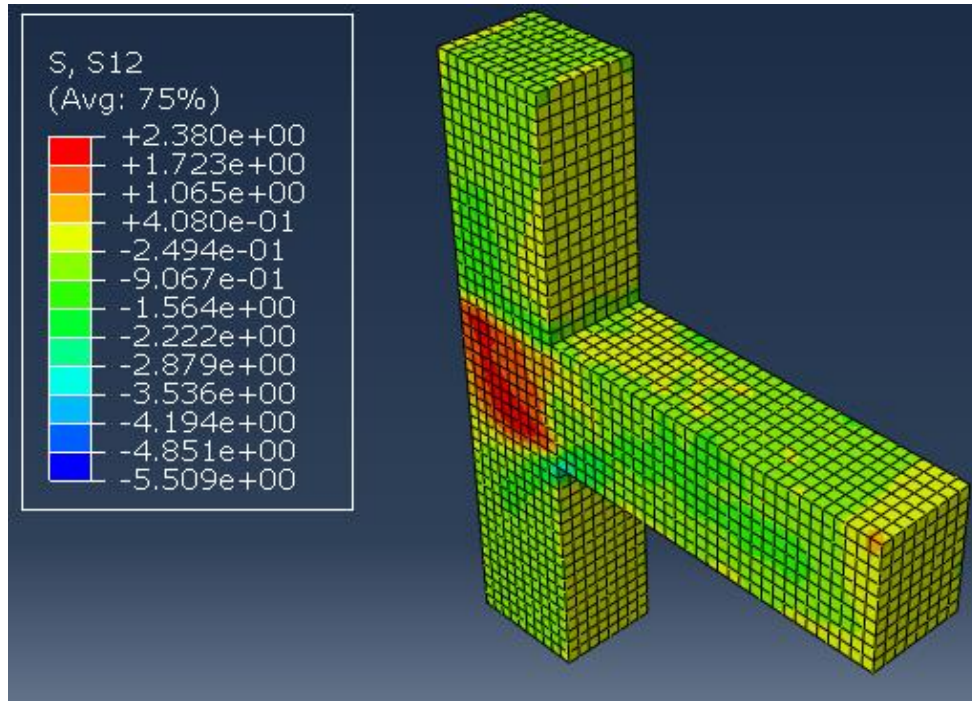**Figure 6.79: Stress S22 in concrete at yielding load (Δ = 21mm) for BCJ-18MM-Bent In without CFRP**
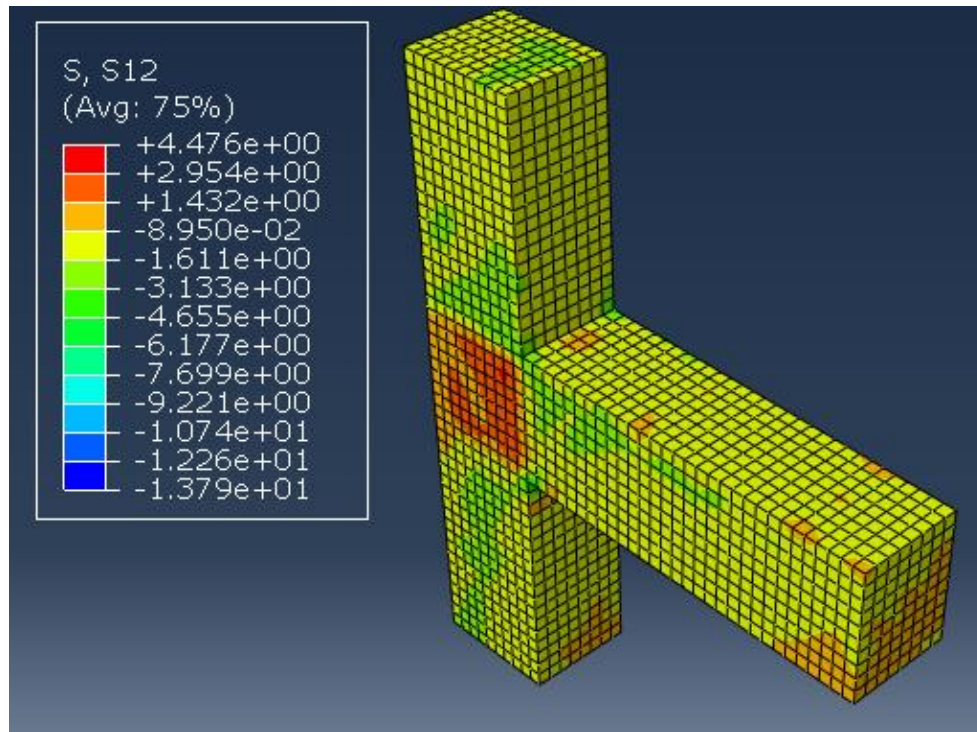
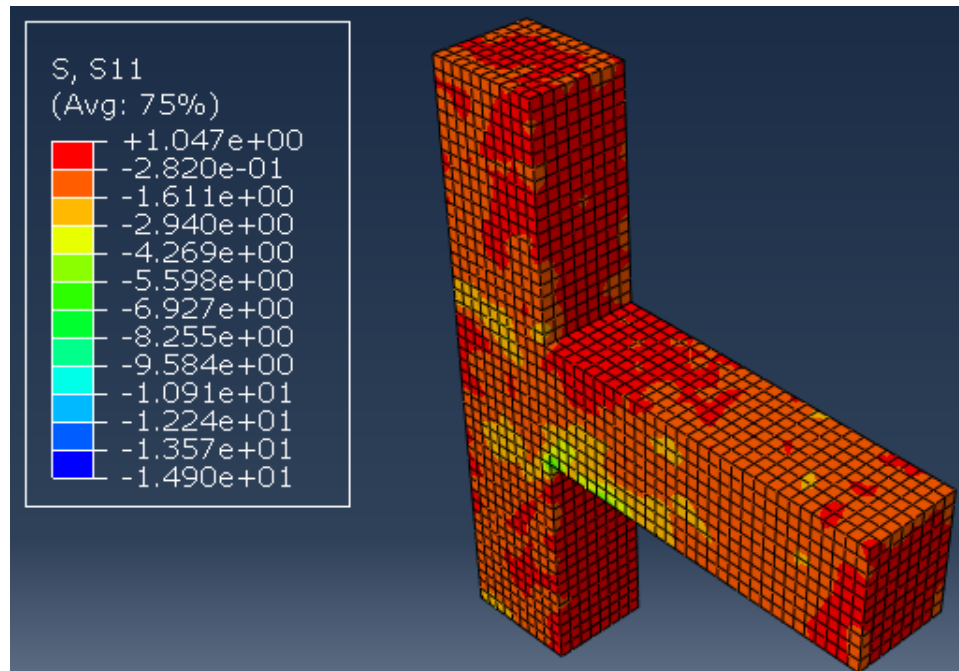**Figure 6.80: Stress S12 in concrete at yielding load (Δ = 21mm) for BCJ-18MM-Bent In without CFRP**
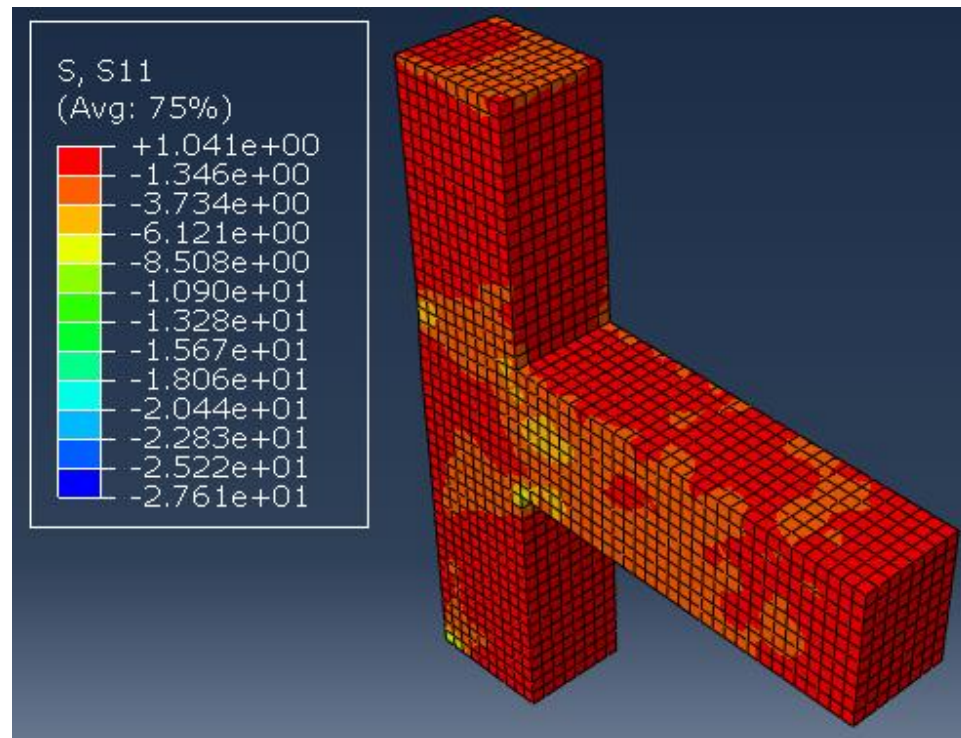
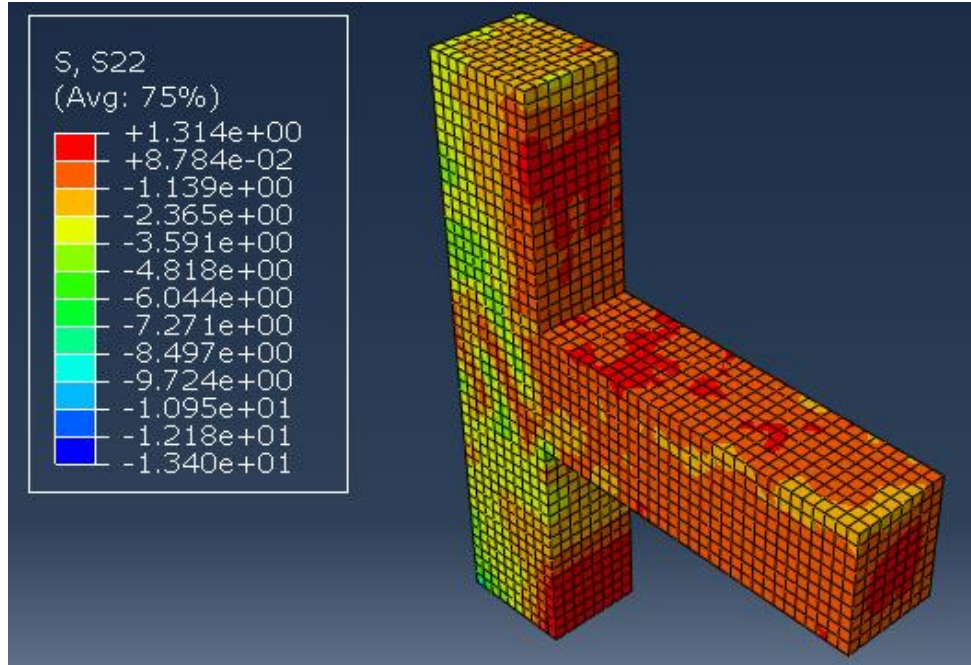**Figure 6.81: Stress S11 in concrete at ultimate load (Δ = 28.7mm) for BCJ-18MM-Bent In without CFRP**
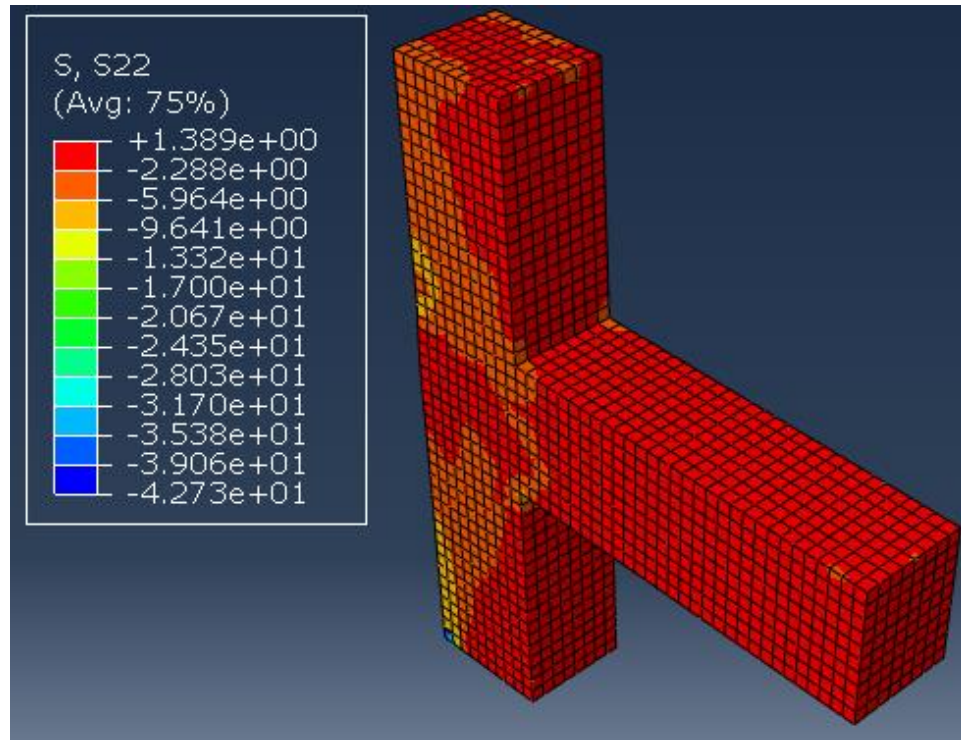
Figure 6.82: Stress S22 in concrete at ultimate load (Δ = 28.7mm) for BCJ-18MM-Bent In without CFRP
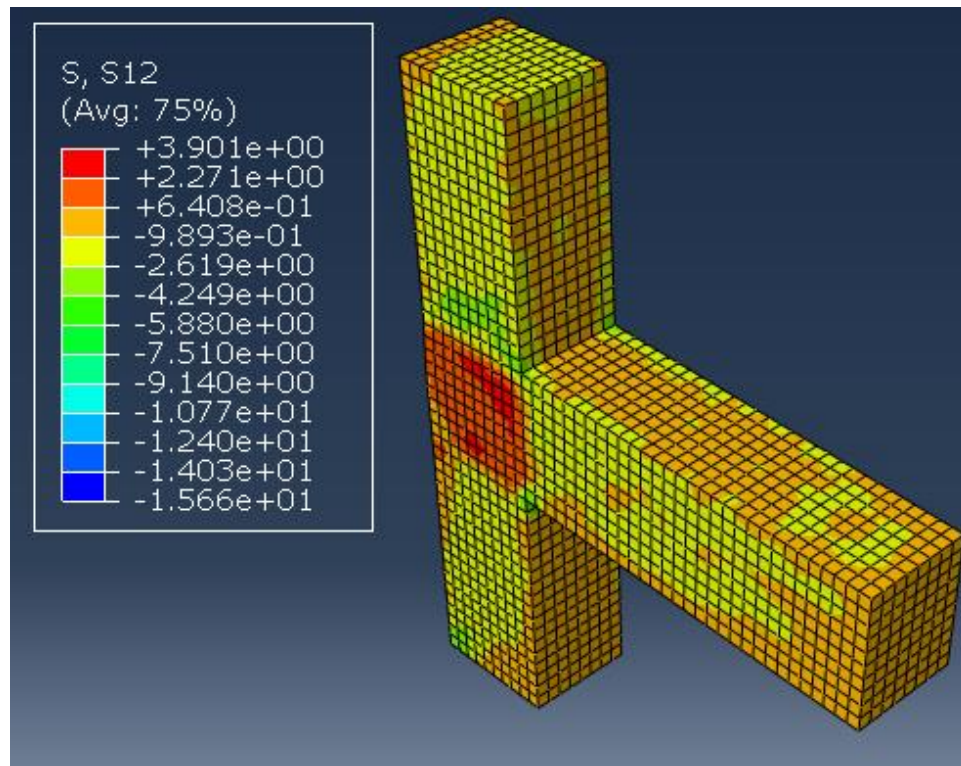
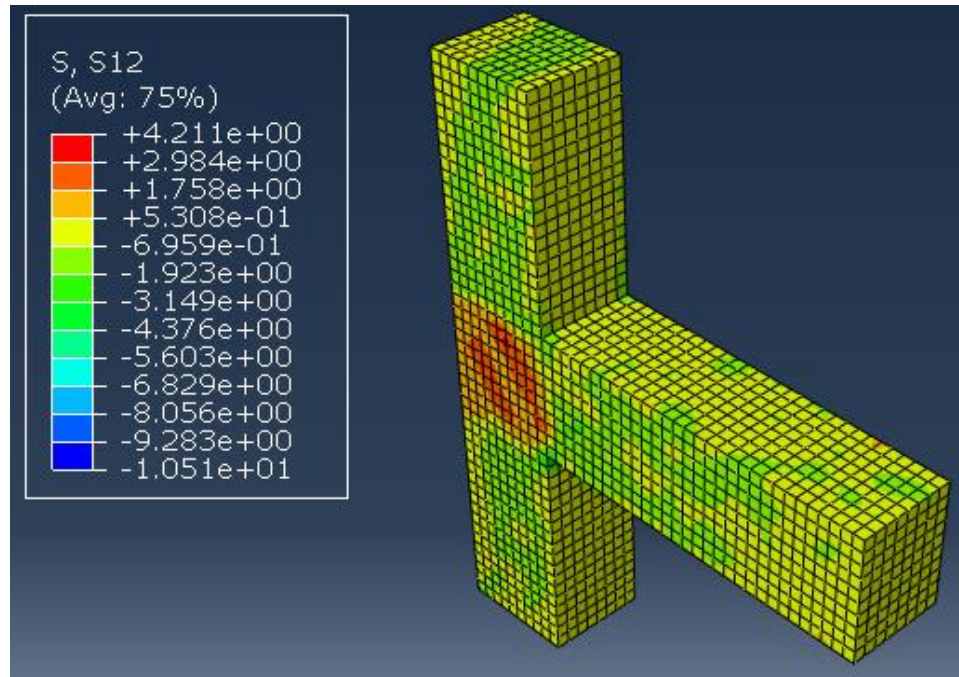**Figure 6.83: Stress S12 in concrete at ultimate load (Δ = 28.7mm) for BCJ-18MM-Bent In without CFRP**
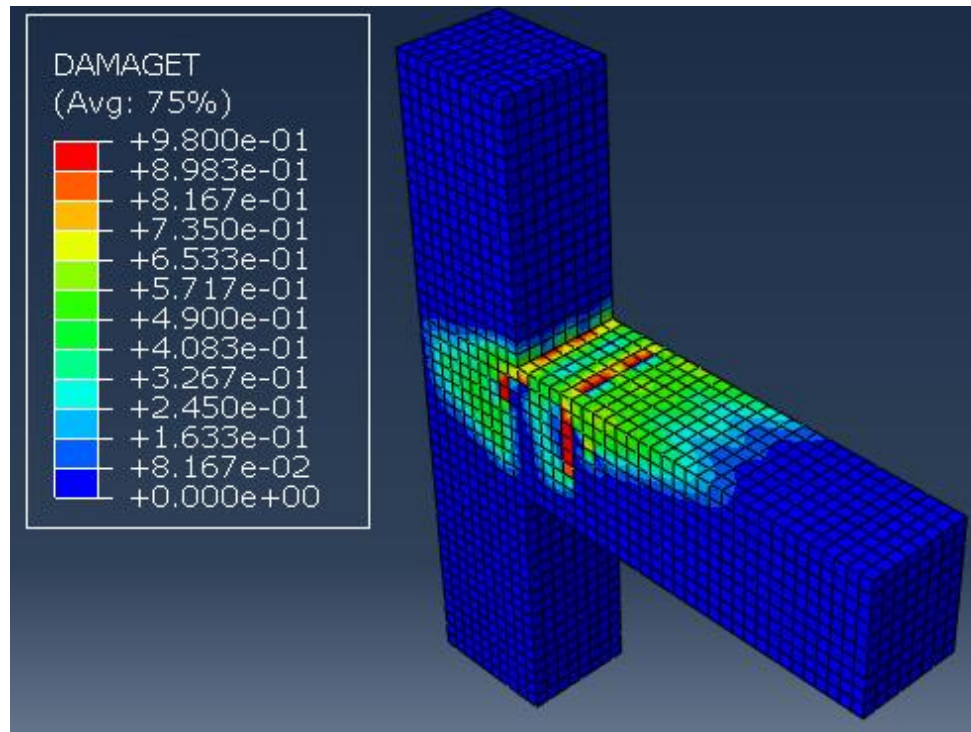
Figure 6.84: Damage propagation and crack pattern at displacement pattern (Δ = 3.7mm) for BCJ-18MM-Bent In without CFRP

Figure 6.85: Damage propagation and crack pattern from experimental test for BCJ-18MM-Bent In without CFRP
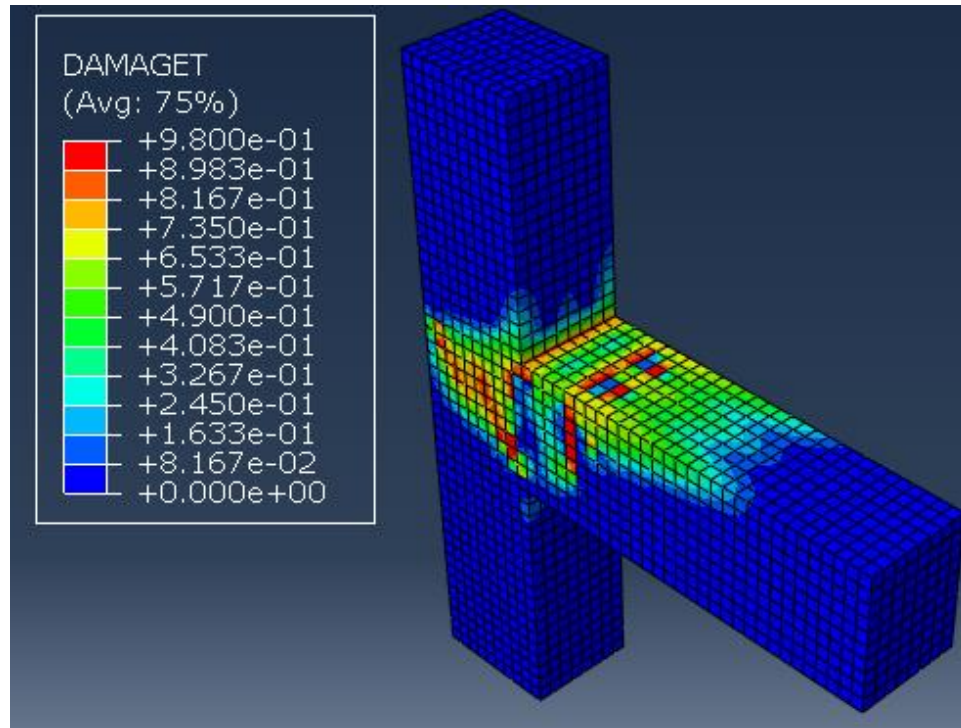
Figure 6.86: Damage propagation and crack pattern at displacement pattern (Δ = 5.5 mm) for BCJ-18MM-Bent In without CFRP
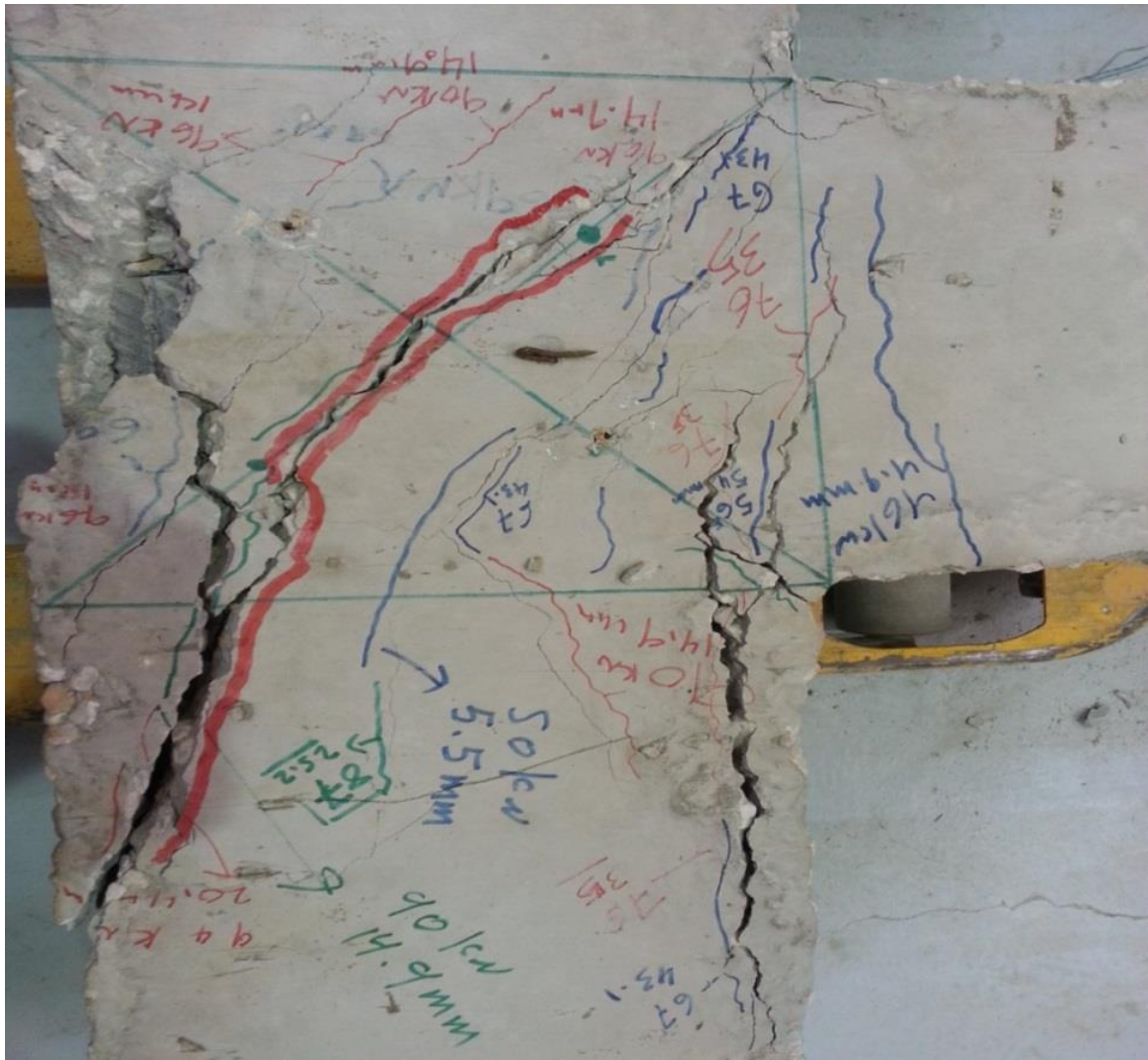
Figure 6.87: Damage propagation and crack pattern from experimental test for BCJ-18MM-Bent In without CFRP
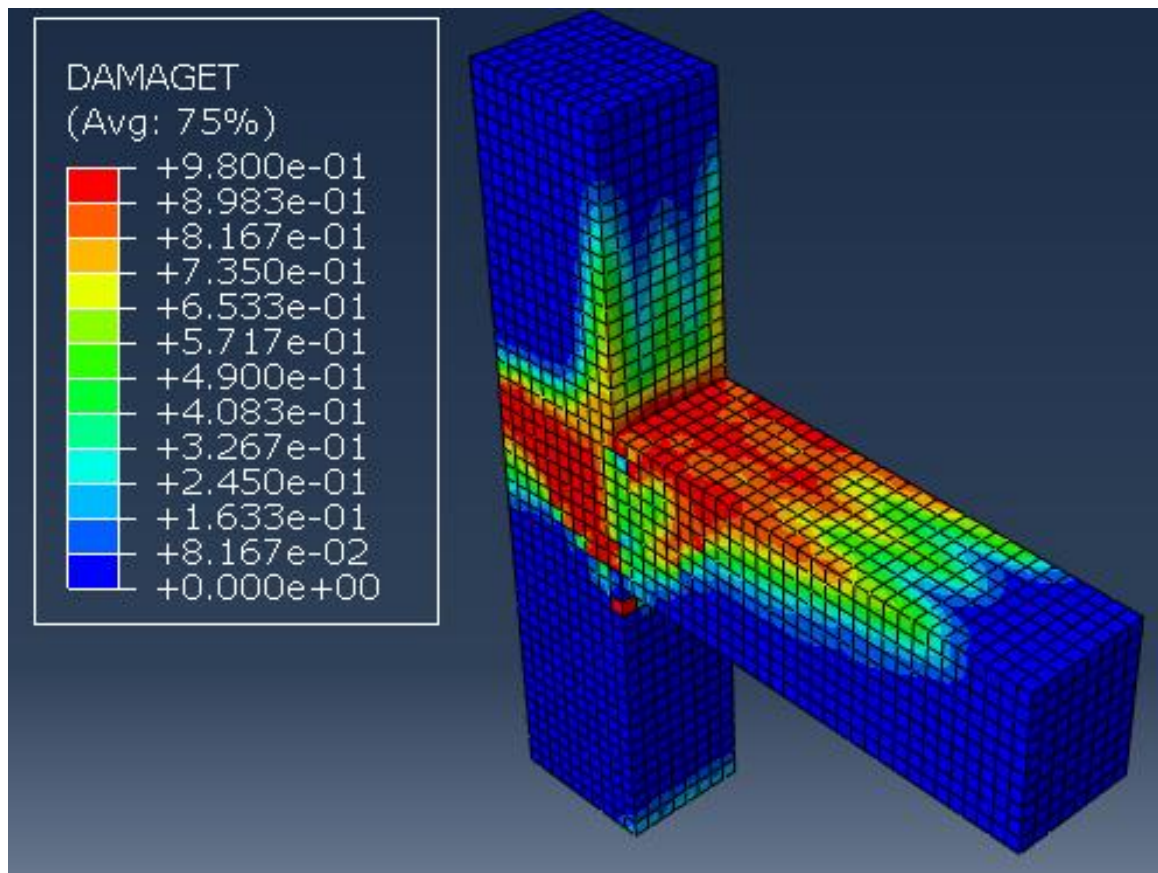
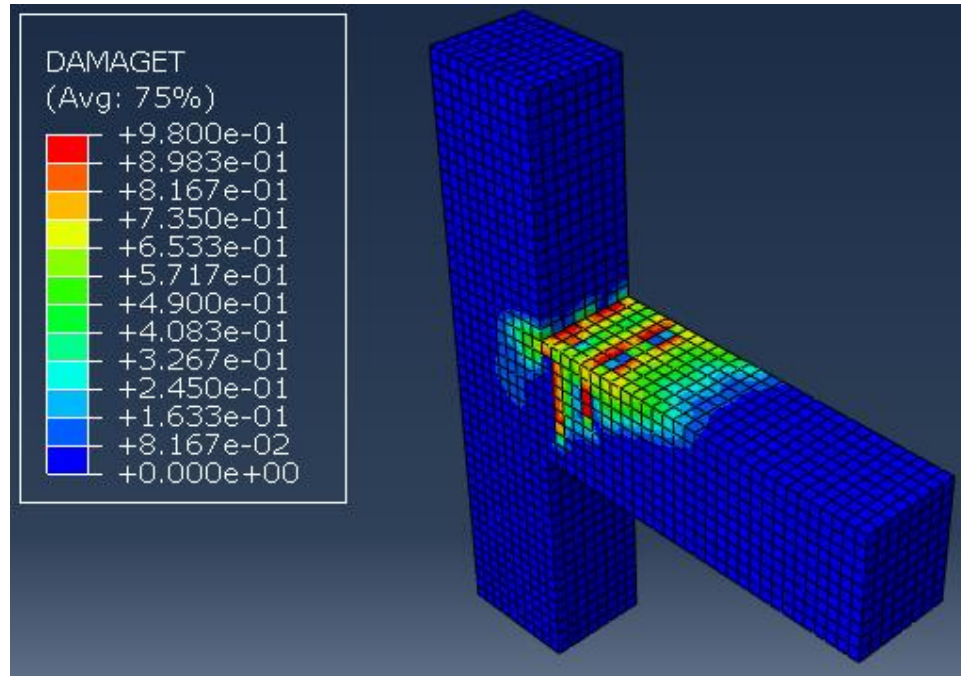**Figure 6.88: Damage propagation and crack pattern at displacement pattern (Δ = 14 mm) for BCJ-18MM-Bent In without CFRP**

Figure 6.89: Damage propagation and crack pattern from experimental test for BCJ-18MM-Bent In without CFRP
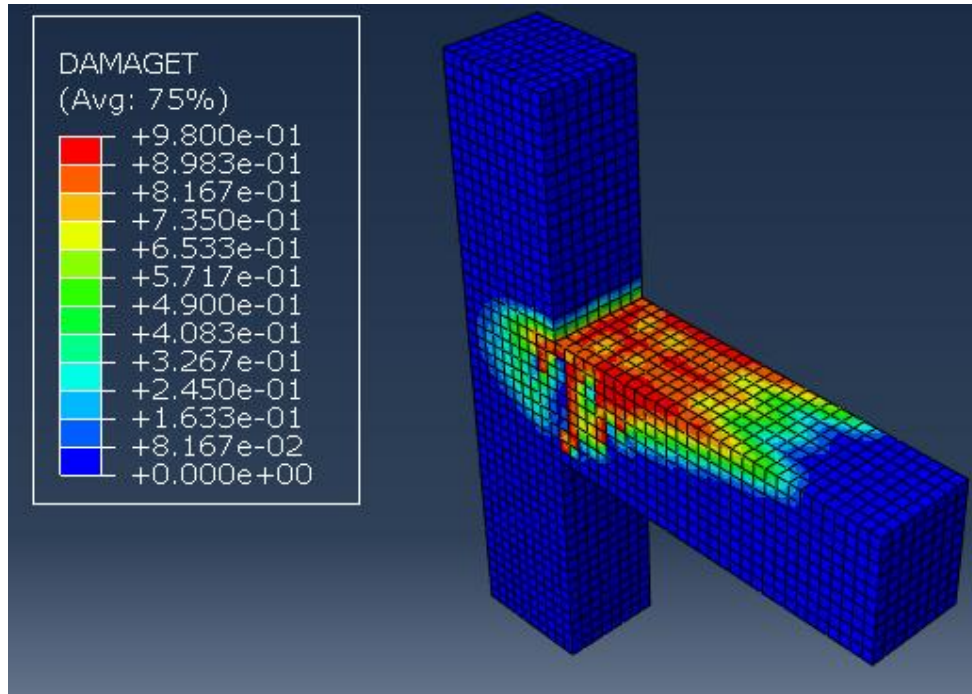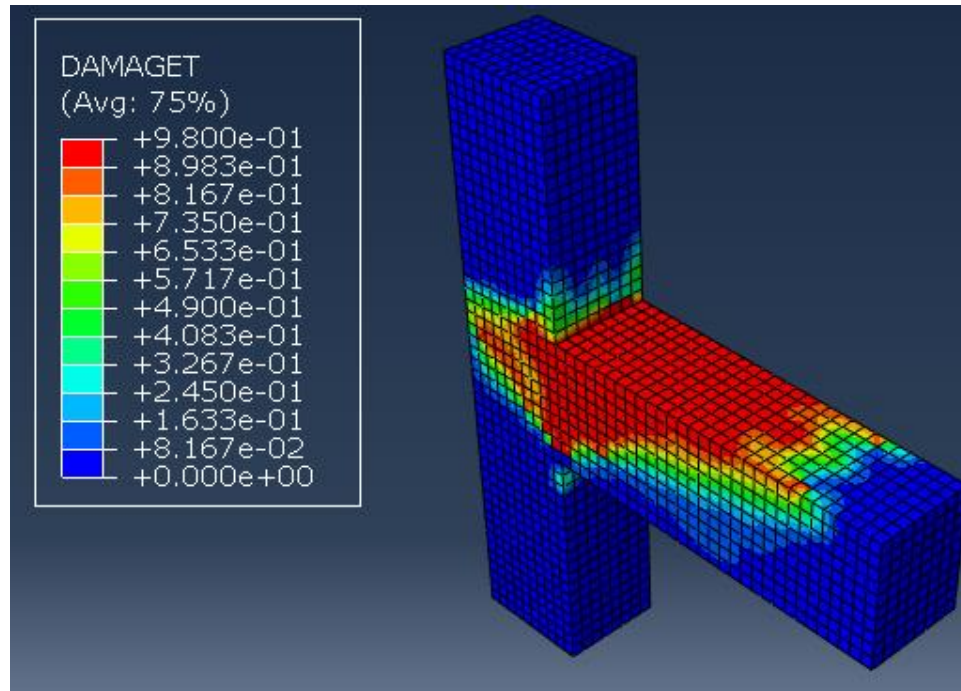
It is clear from the result of experimental test and simulation that almost exact failure mode and crack pattern was achieved from numerical simulation compared to the experimental result. The first flexural in experimental test was at displacement equals to 3.7 mm, and after diagonal crack occurs at displacement equals to 5.5 mm, flexural crack extended due to large displacement.

6.10   Numerical Simulation of BCJ-18MM-Bent in with CFRP

The experimental and finite element results of load-displacement response of the beam-column joint with CFRP retrofitting, under monotonic load up to failure are shown in **Fig. 6.90**. The result of finite element simulation matches closely with experimental results as shown in **Fig. 6.90**.
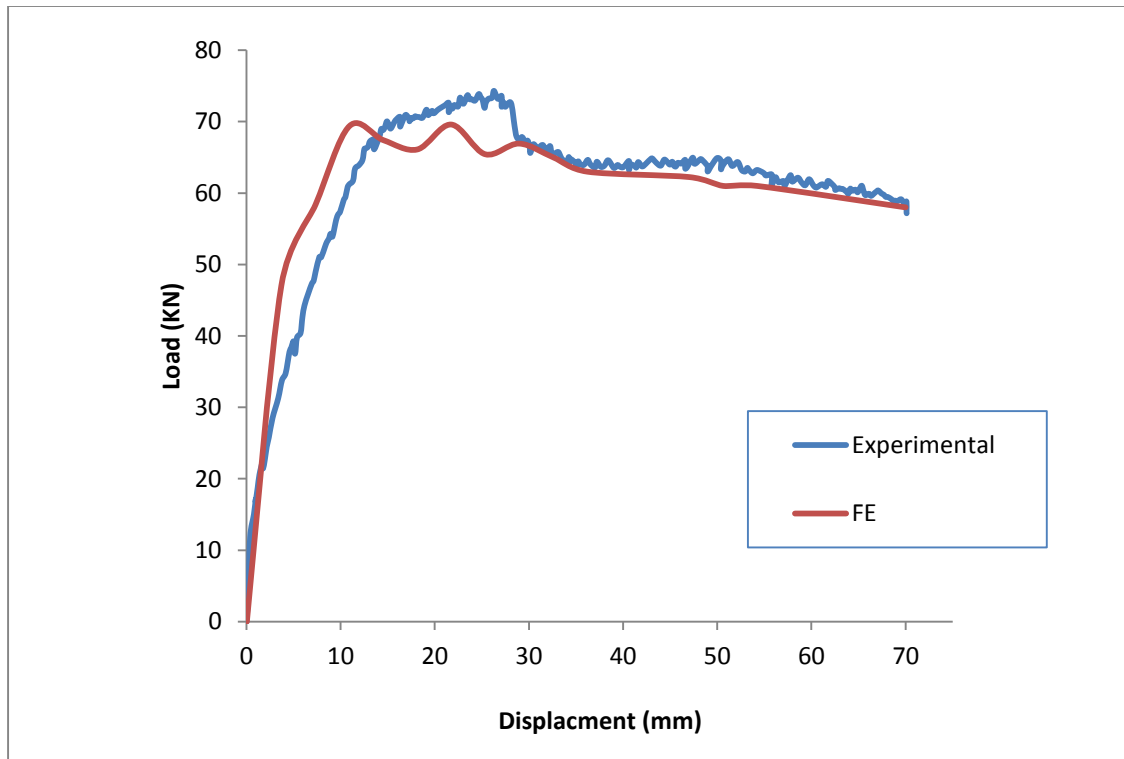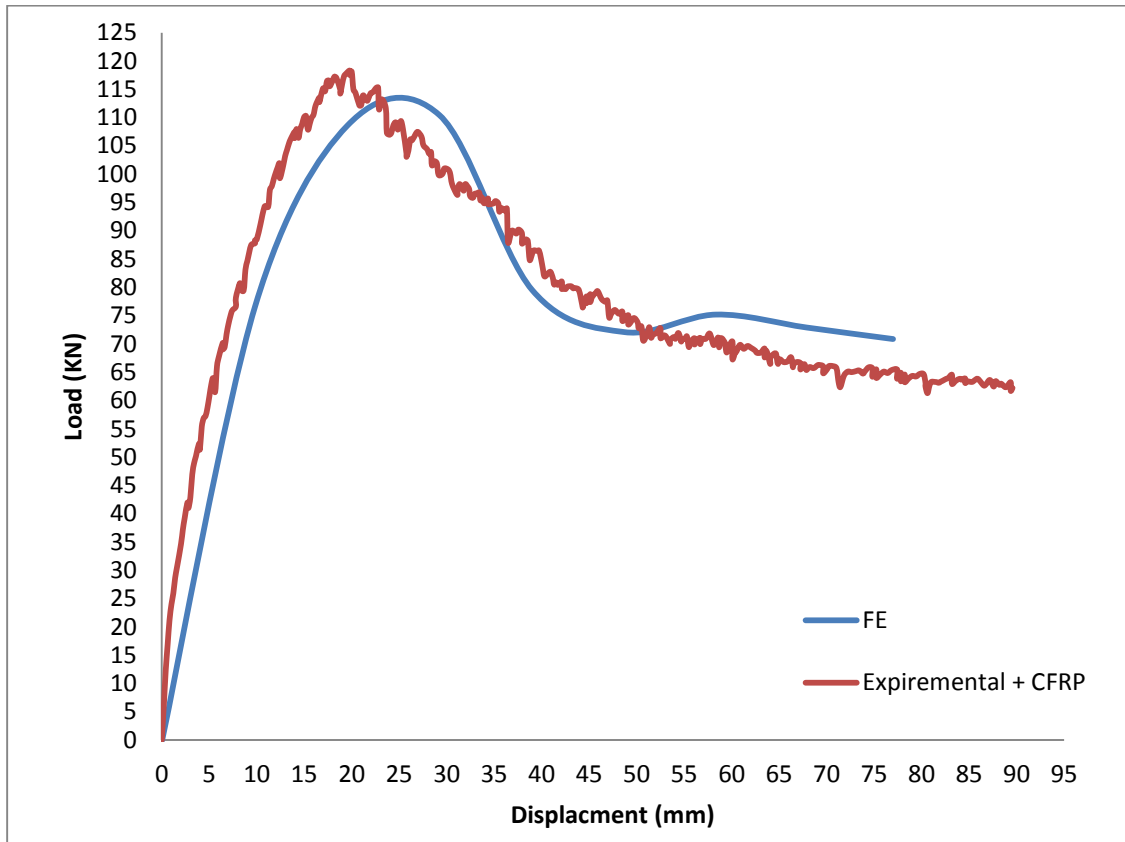

Figure 6.90: Load displacement response for BCJ-18MM-Bent in with CFRP

The maximum stresses in steel at yielding and ultimate load which is corresponding to displacement 13 mm and 23 mm respectively, are shown in **Fig. 6.91**. The stresses S11, S22 and S12 at yielding and ultimate load are shown in **Figs. 6.92, 6.93, 6.94, 6.95, 6.96 and 6.97**. The stresses and strains in CFRP sheet at yielding and ultimate load is shown in **Figs. 6.98, 6.99, 6.100 and 6.101**. The stress-strain response for CFRP is shown in **Fig. 255**. The diagonal crack patterns at the joint as shown in **Fig. 6.102, 6.103 and 6.104**, closely resemble the crack pattern as observed in the experimental program as shown in **Fig. 6.105**.
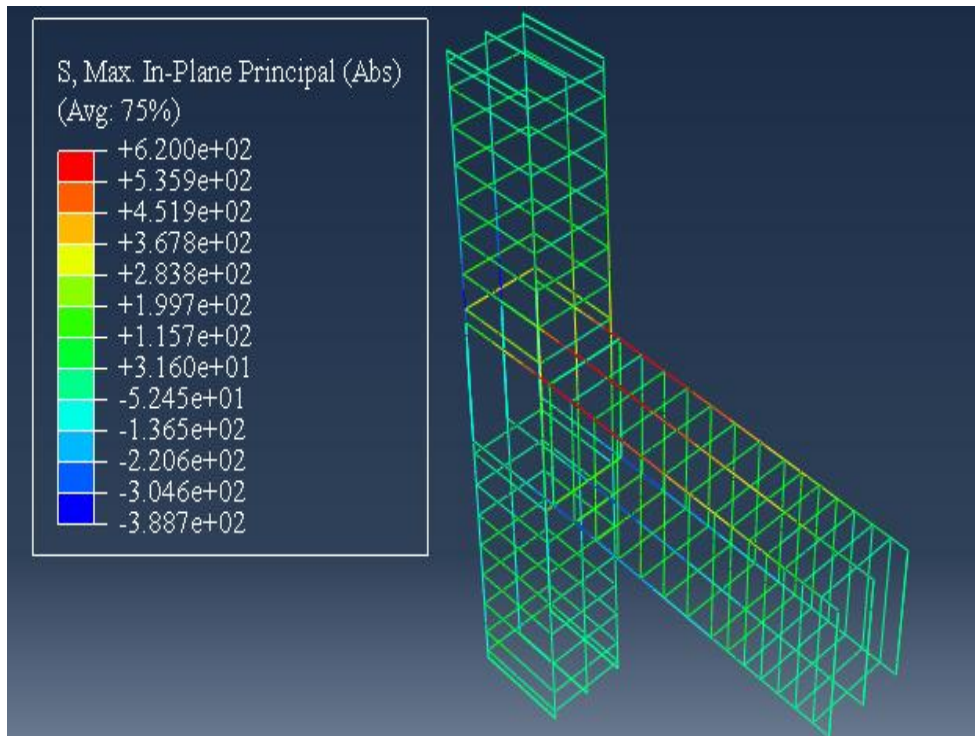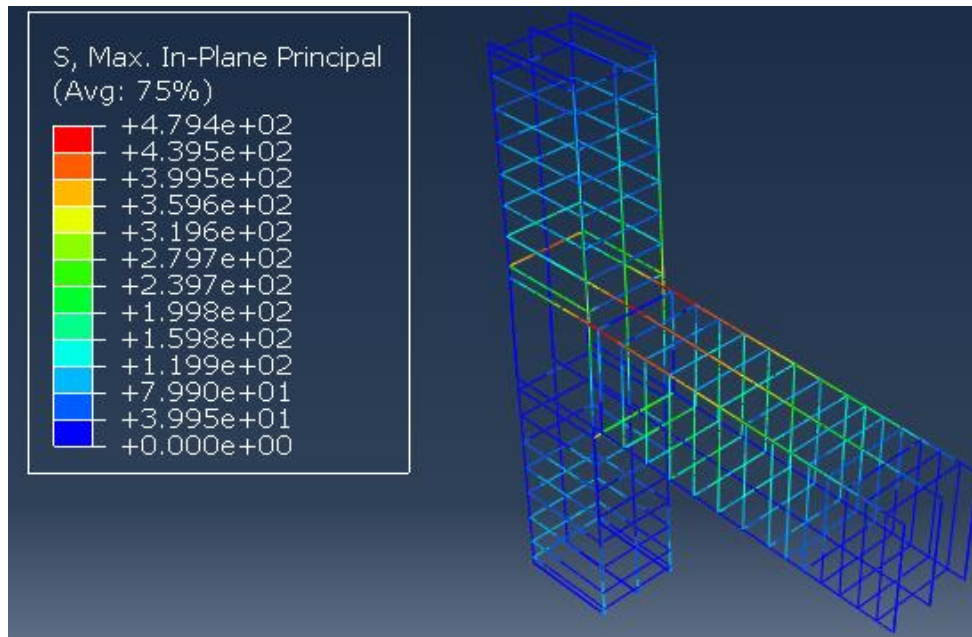

Figure 6.91: Steel stress at ultimate load (_Δ_ = 29mm) for BCJ-18MM-Bent in with CFRP
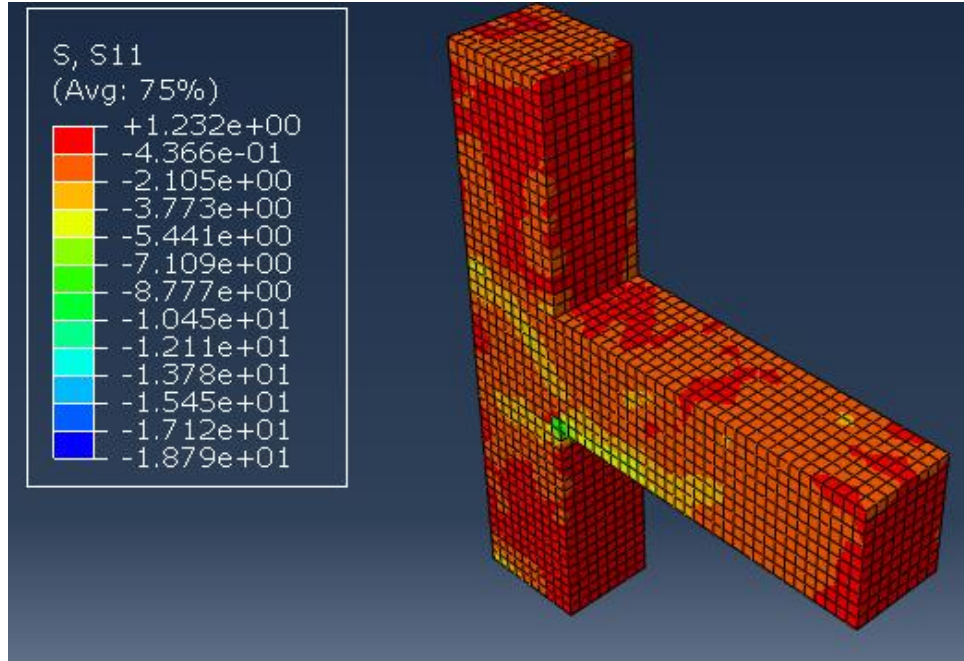
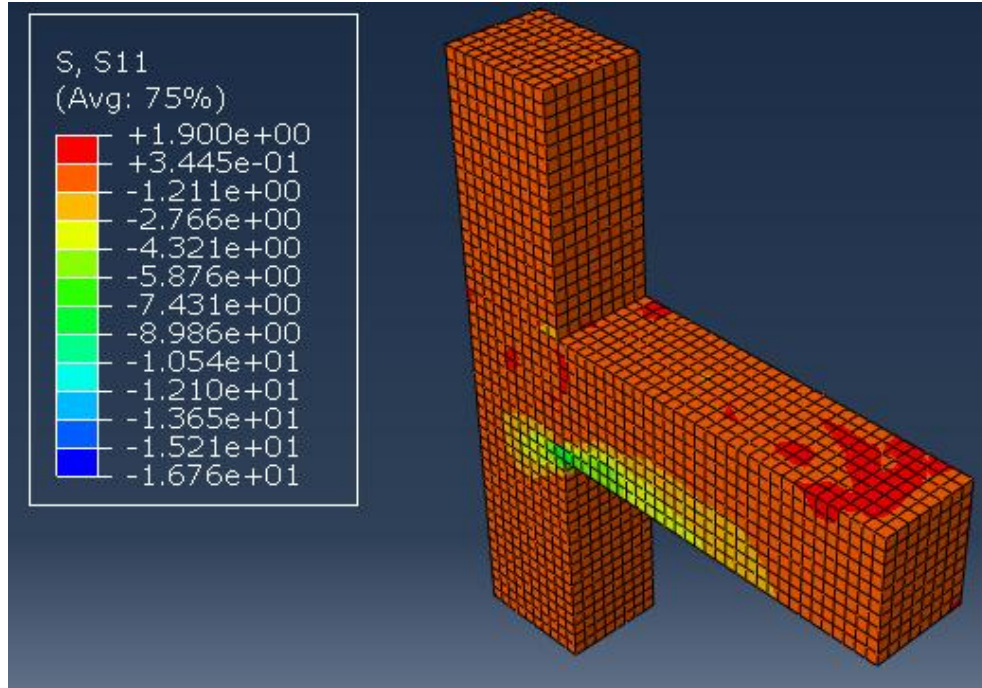**Figure 6.92: Stress S11 in concrete at yielding load (Δ = 14mm) for BCJ-18MM-Bent in with CFRP**
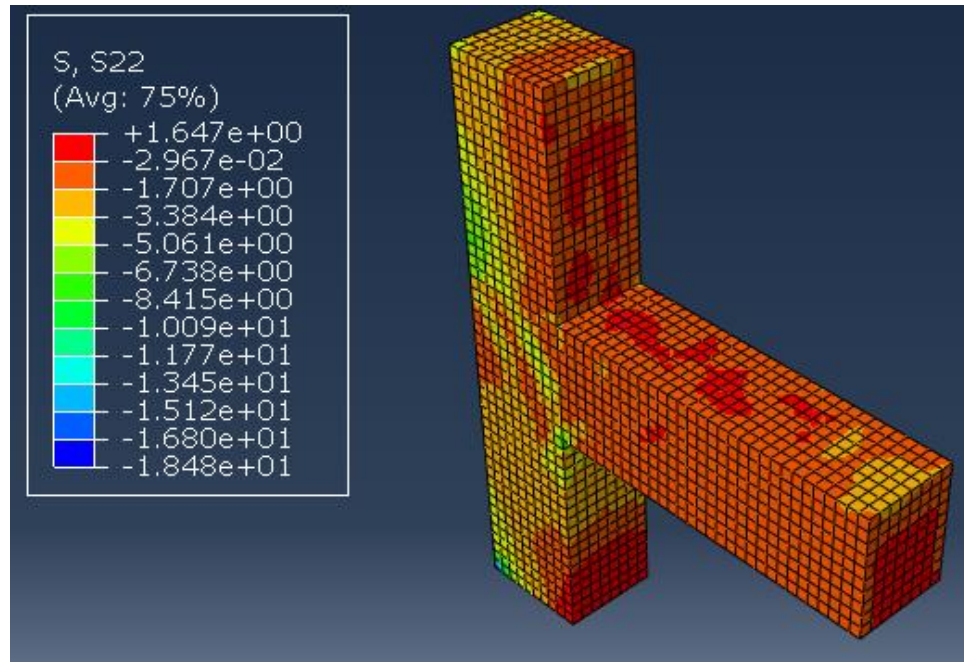
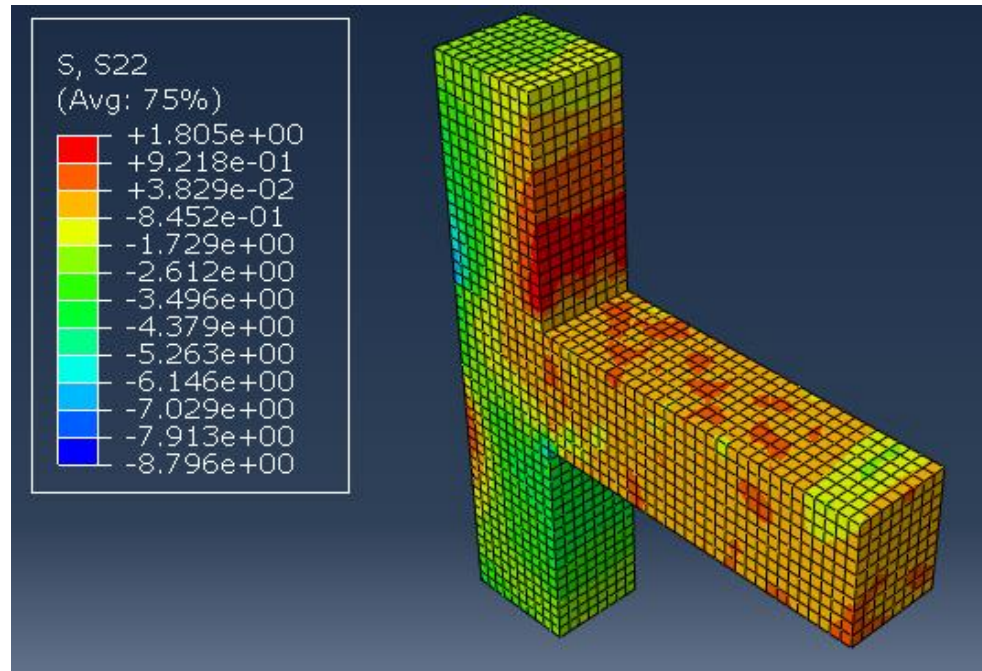**Figure 6.93: Stress S22 in concrete at yielding load (Δ = 14mm) for BCJ-18MM-Bent in with CFRP**
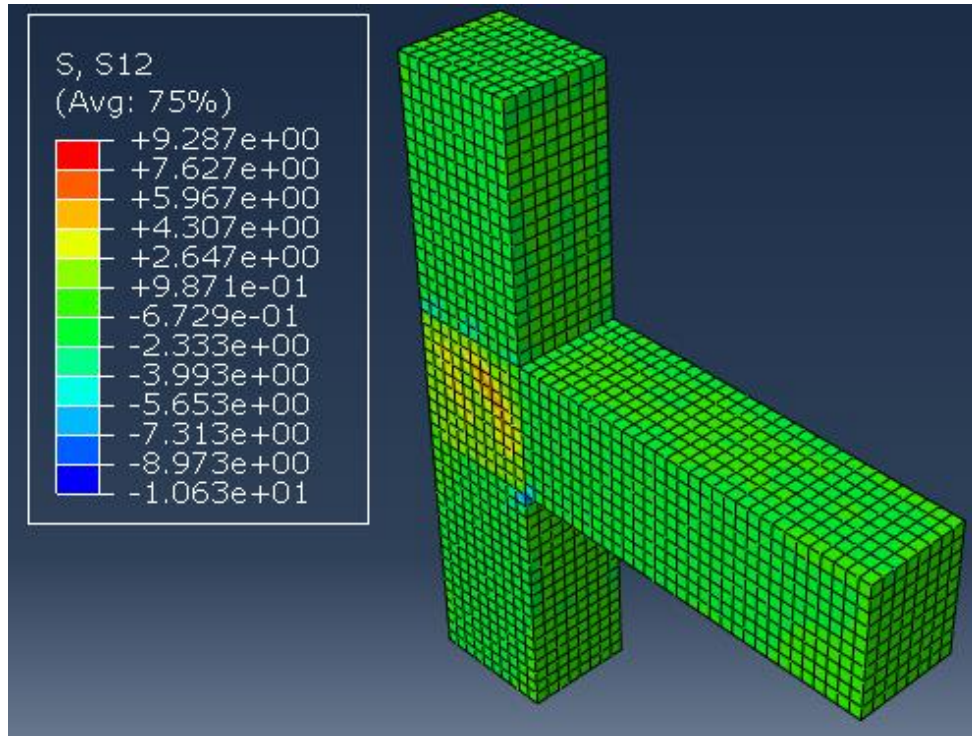
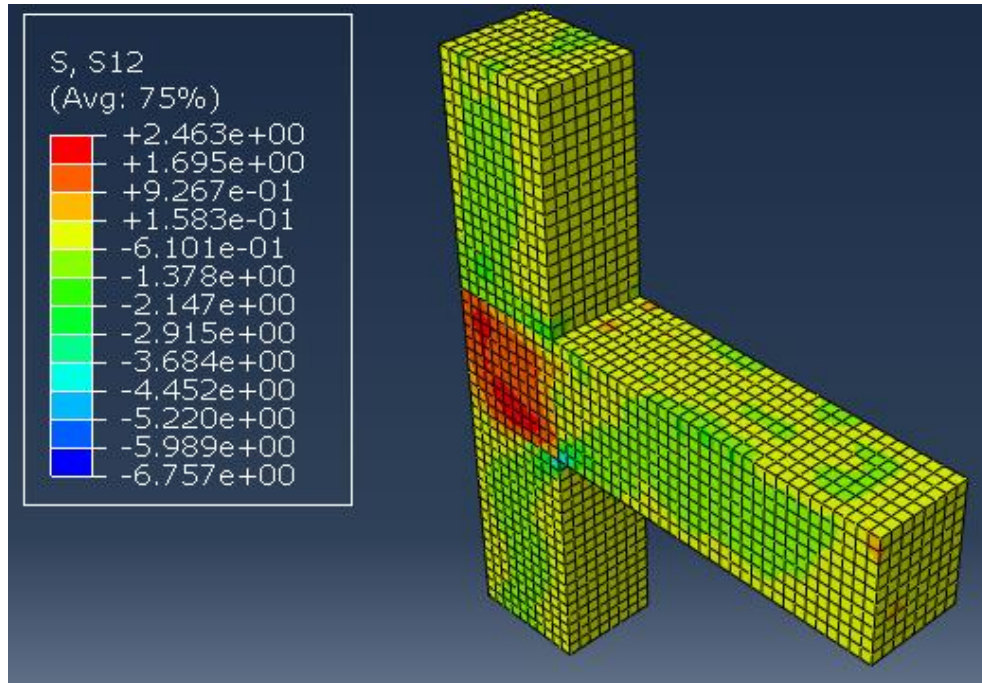**Figure 6.94: Stress S12 in concrete at yielding load (Δ = 14mm) for BCJ-18MM-Bent in with CFRP**
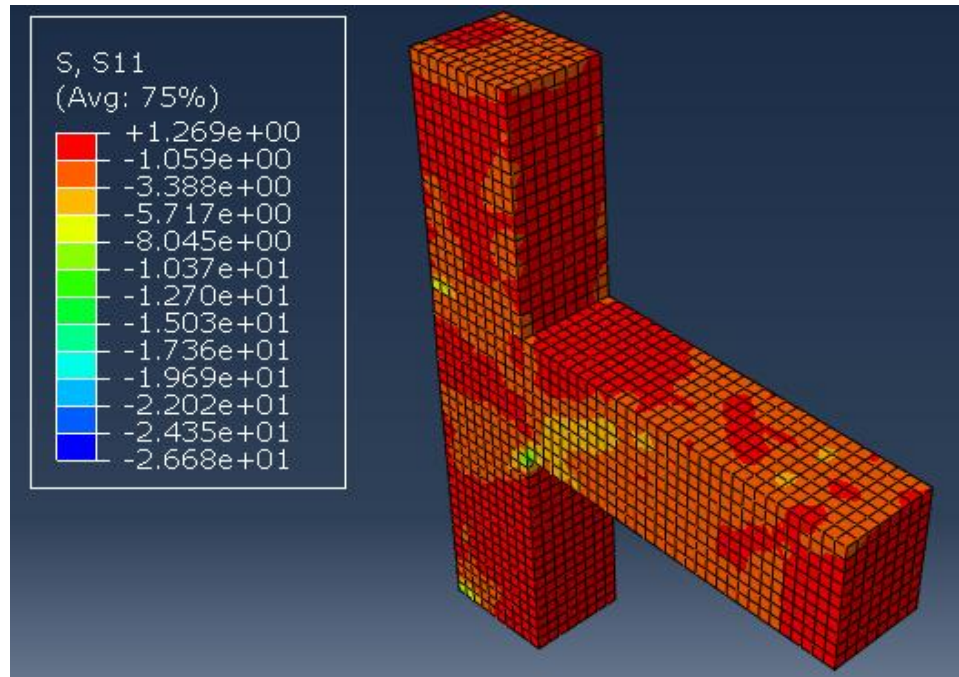
Figure 6.95: Stress S11 in concrete at ultimate load (Δ = 29mm) for BCJ-18MM-Bent in with CFRP
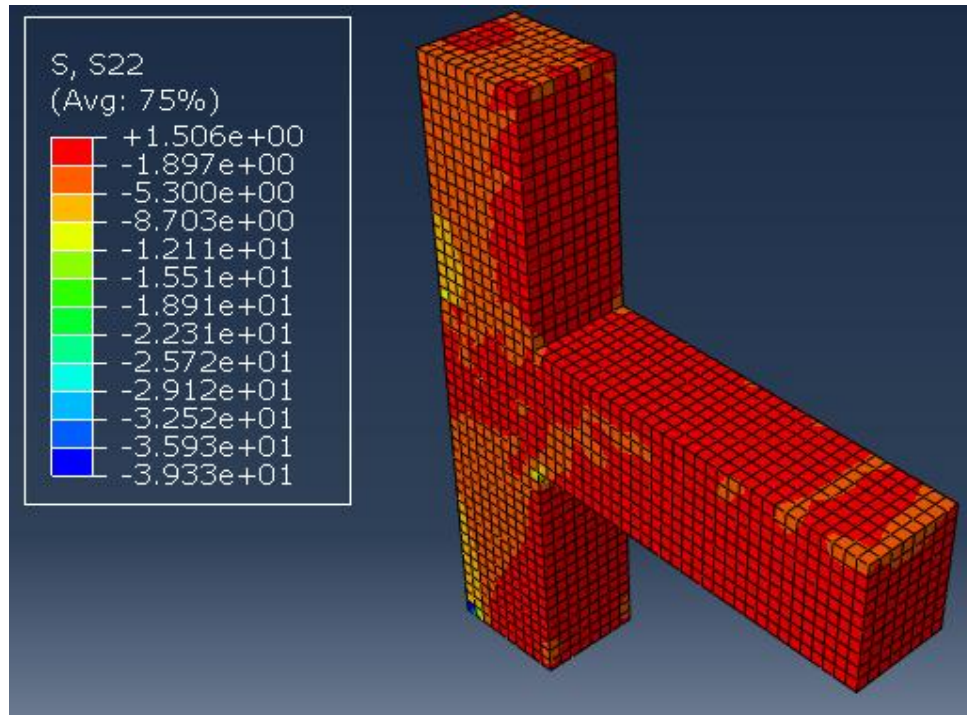
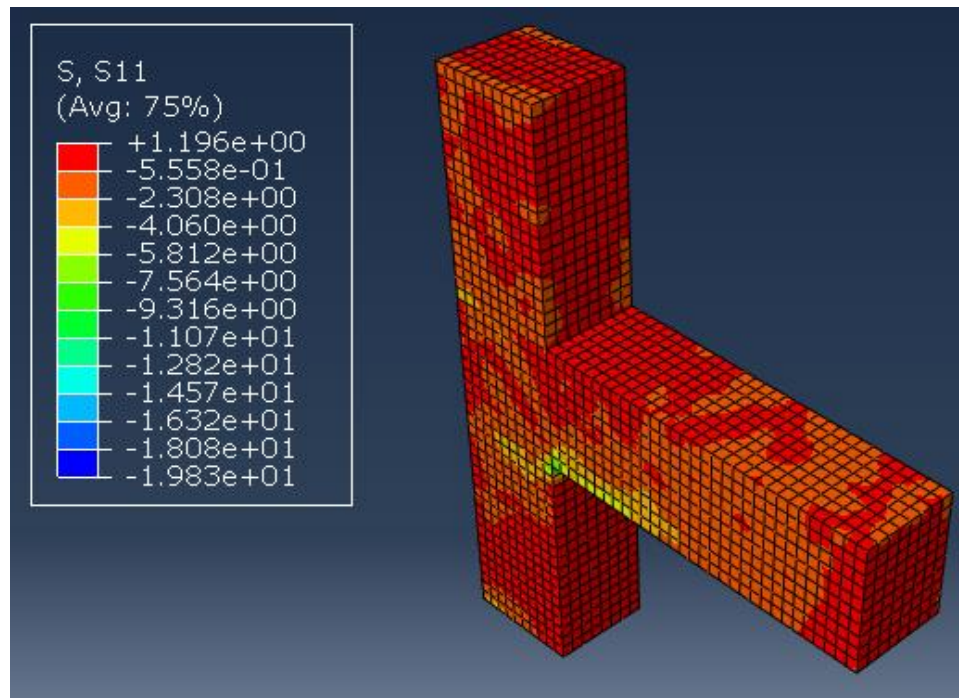**Figure 6.96: Stress S22 in concrete at ultimate load (Δ = 29mm) for BCJ-18MM-Bent in with CFRP**
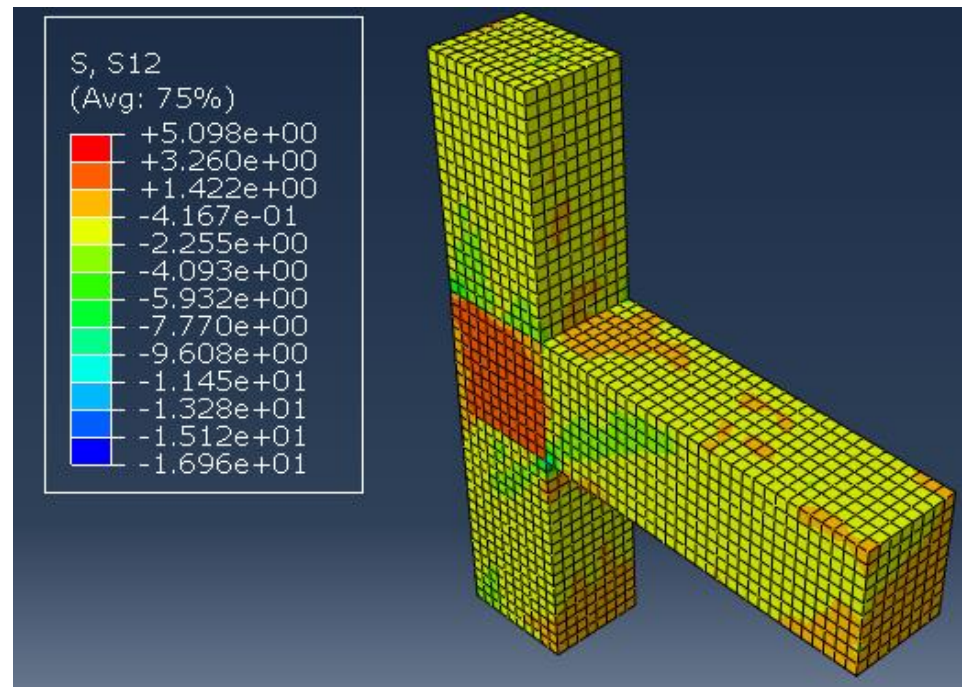
Figure 6.97: Stress S22 in concrete at ultimate load (Δ = 29mm) for BCJ-18MM-Bent in with CFRP
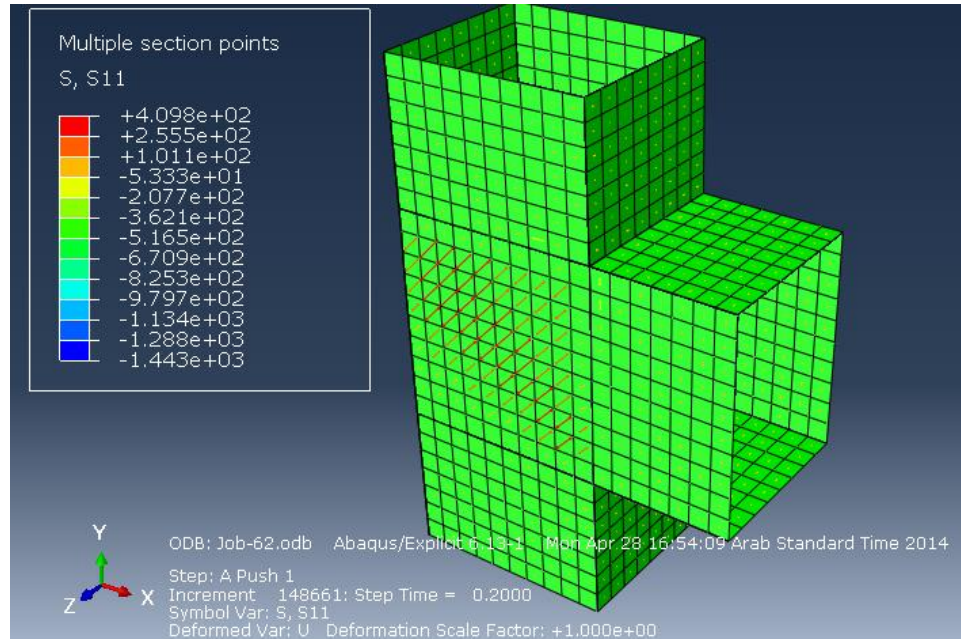
Figure 6.98: Stress S11 in CFRP at yielding load (Δ = 14mm) for BCJ-18MM-Bent in with CFRP
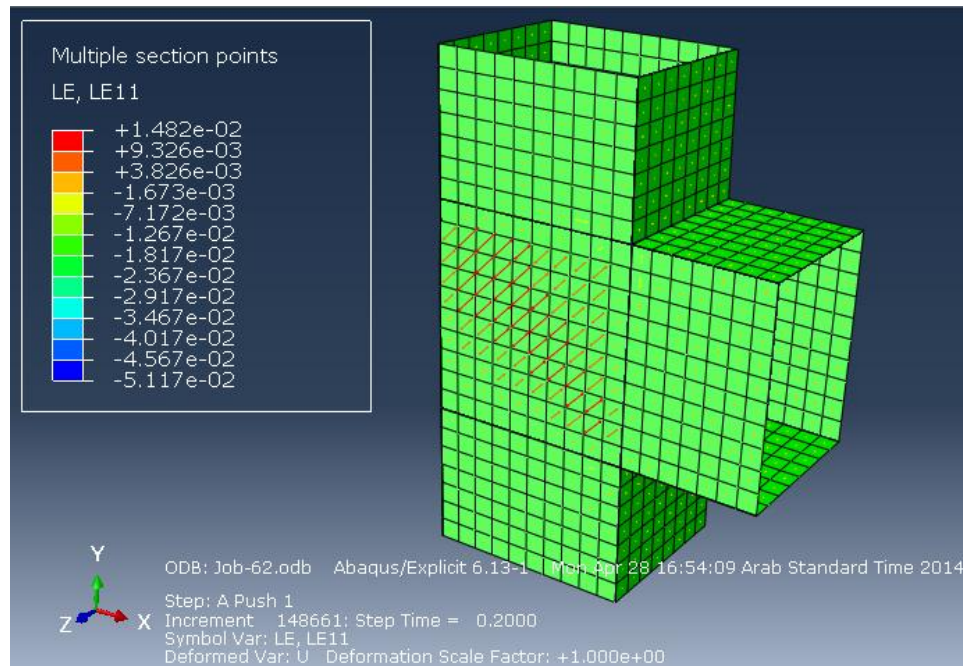
Figure 6.99: Strain L11 in CFRP at yielding load (Δ = 14mm) for BCJ-18MM-Bent in with CFRP
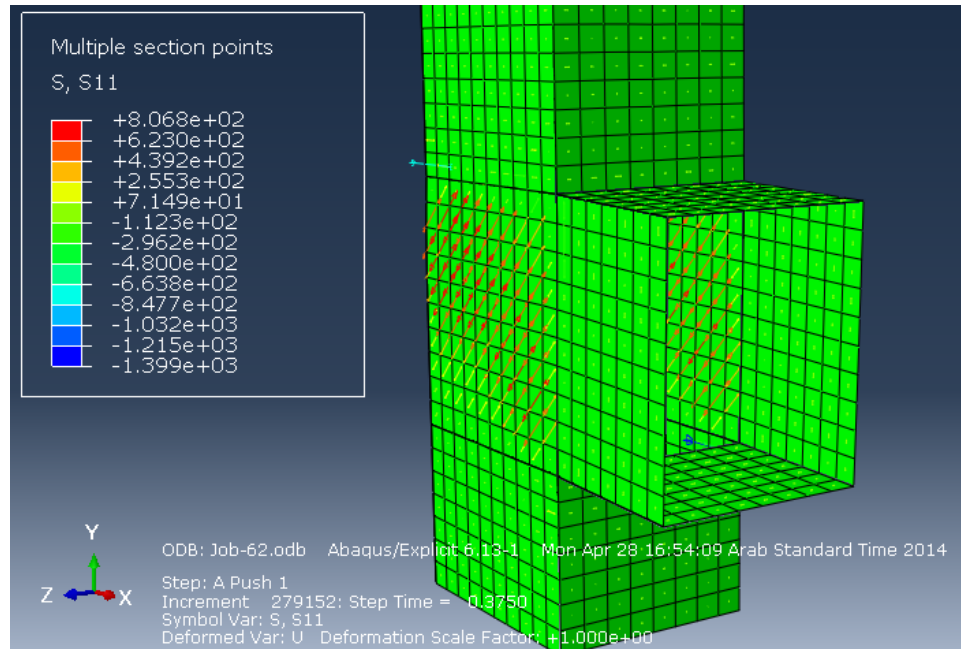
Figure 6.100: Stress S11 in CFRP at Ultimate load (Δ = 29mm) for BCJ-18MM-Bent in with CFRP
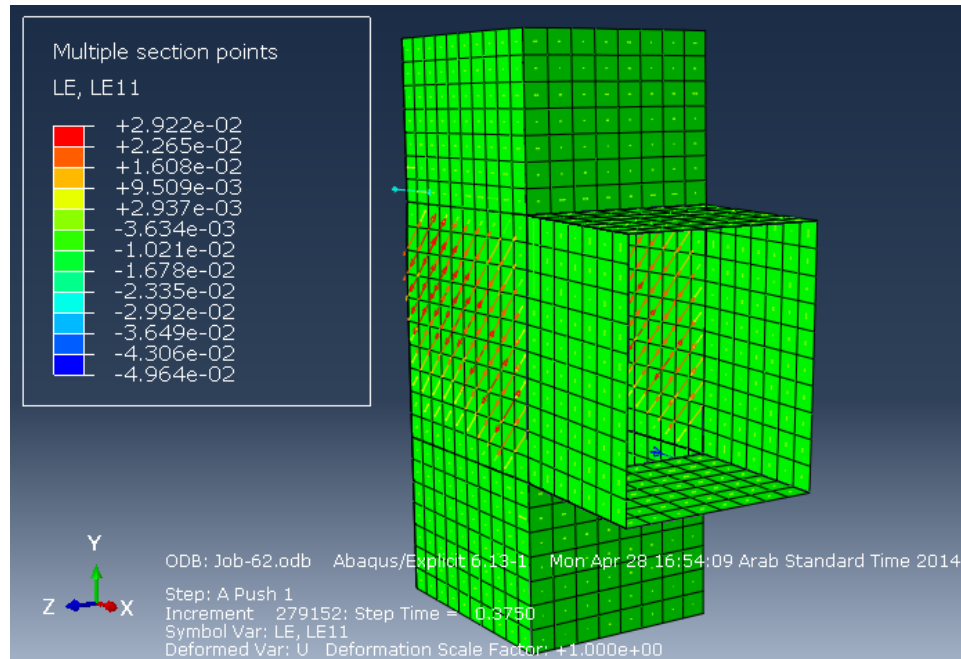
Figure 6.101: Strain L11 in CFRP at ultimate load (Δ = 29mm) for BCJ-18MM-Bent in with CFRP
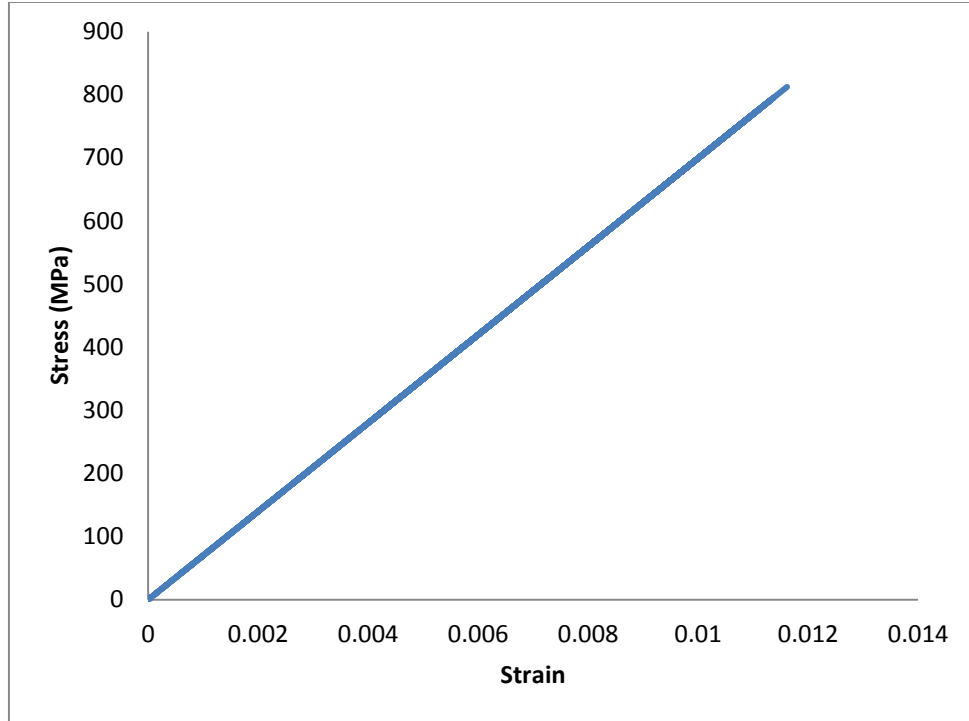
Figure 6.102: Stress-strain Response in CFRP for BCJ-18MM-Bent In for BCJ-18MM-Bent in with CFRP
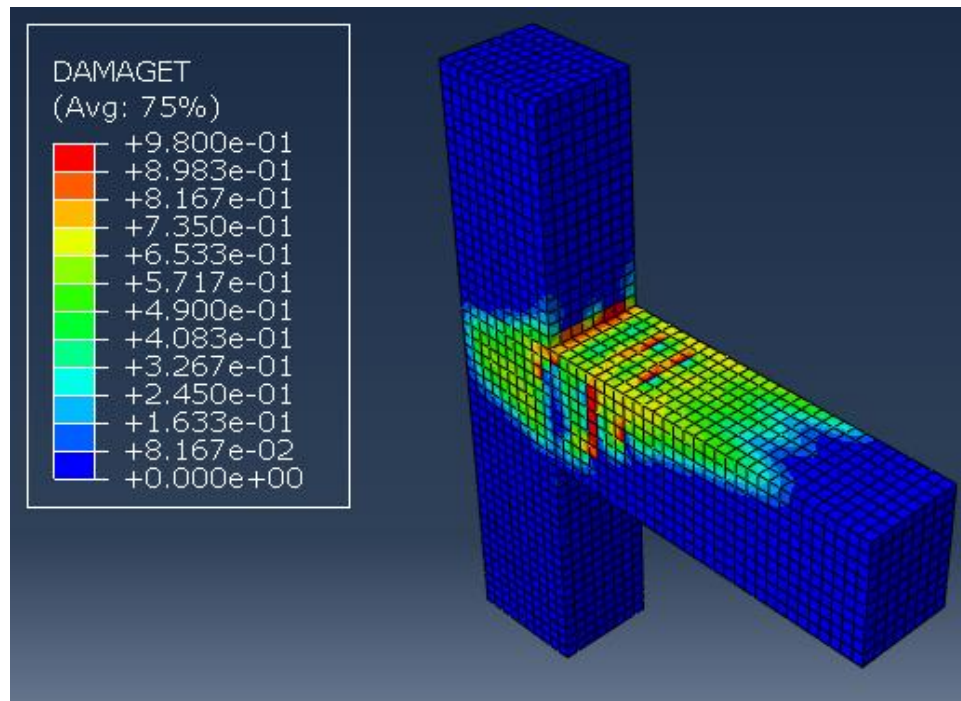
Figure 6.103: Damage propagation and crack pattern at displacement pattern ($\varDelta$ = 5.2 mm) for BCJ-18MM-Bent in with CFRP
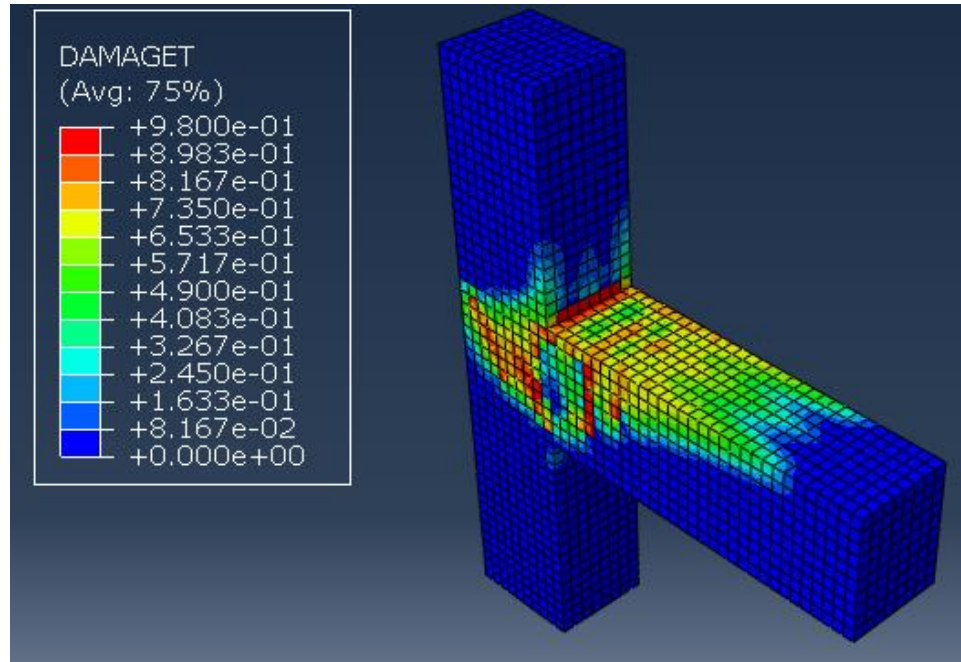
Figure 6.104: Damage propagation and crack pattern at displacement pattern (Δ = 6.5 mm) for BCJ-18MM-Bent in with CFRP
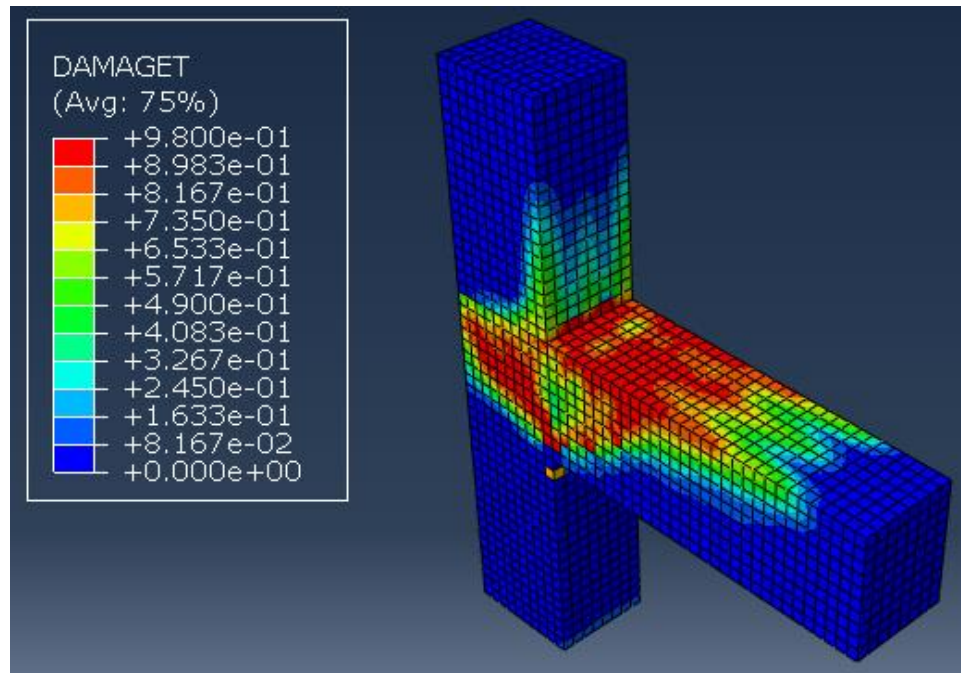
Figure 6.105: Damage propagation and crack pattern at displacement pattern (Δ =10.5 mm) for BCJ-18MM-Bent in with CFRP

Figure 6.106: Damage propagation and crack pattern at displacement from the experimental test for BCJ-18MM-Bent In with CFRP

It is clear that almost exact failure mode and crack pattern was achieved from numerical simulation compared to the experimental result.

CHAPTER 7

CONCLUSIONS AND RECOMMENDATION

As seen in this study, several experiments as well as several numerical simulations have been carried out. All of this work was aiming at better understanding the response of the behavior of beam-column joint under cyclic load. Several studies are just completed and others are started and all of those studies are representing great changes for adding new things and new ideas to the world of reinforced concrete beam-column joint mechanics.

7.1   Conclusions

Based on the experimental and computational modeling carried out for the thirteen exterior reinforced concrete beam-column joint specimens at KFUPM, following conclusions may be drawn:

1- The mode of failure of the BCJ is dictated by the geometry of the beam, column, and the joint, and the amount of reinforcement in the beam and the column, together with the reinforcement detailing of joint.

2- For the control specimens, one can notice that:

A- Two cracking loads have been identified. One is associated with flexural cracking of the beam and controlled by the modulus of rupture of the beam concrete, the other with a diagonal crack in the joint which results when the maximum principal stress exceeds the tensile strength of concrete and which

is controlled by direct tensile strength of joint concrete. For the specimen considered in this task, the P_{cr} due to flexure < P_{cr} due to joint shear.

B- For specimens designed with ρ=0.0045 (BCJ-12MM-Bent Up and BCJ-12MM-Bent In), the experimental results showed that the ultimate capacity of the specimen was reached when the load corresponded to the flexural capacity of the beam. This was further confirmed by results obtained from computational model under ABAQUS environment.

C- Stresses in the beam, column and joints are in good agreement and model predicts good result for stress which indicates that beam-column joint is well modeled by Damage Plasticity Model.

D- For specimen designed with higher ρ=0.01 (BCJ-18MM-Bent In) experimental results showed that the specimen collapsed due to failure of joint under shear, as the collapse load was lower than the flexural capacity of the beam (27.6% lower). That was confirmed from the combined experimental computations and also further corroborated from ABAQUS results.

3- For the retrofitted specimens with CFRP, we can notice that:

A- The behavior of beam-column joints retrofitted with CFRP sheets was investigated.

B- For BCJ-12MM-Bent-Up, joint shear capacity approximately equals the flexural beam capacity. Retrofitting the joint with CFRP wrap and extending 20 cm into the beam, enhanced the capacity by 19.55% in case of monotonic load, and 10.62 in case of cyclic load. The reason that in case of cyclic load,

there is less enhancement due to the fatigue of concrete because of the repeated cycles of high loads.

C- For BCJ-12MM-Bent-In, joint shear capacity approximately equals the flexural beam capacity. Retrofitting the joint with CFRP wrap and extending 20 cm into the beam enhanced capacity by 12.9% in case of monotonic load, and 9.2% in case of cyclic load. The reason being that in case of cyclic load, less enhancement was noted due to the fatigue of concrete because of repeated cycles at high load.

D- Once the CFRP ruptured, the residual strength was the same as the flexural capacity of control with ductile mode as the main beam steel was designed to yield at failure.

E- For BCJ-18MM-Bent In, the control specimens have shear joint capacity significantly less than flexural beam capacity. Retrofitting with CFRP increased joint shear capacity.

F- Mode of failure did not change, however, even though the joint capacity was increased by 20.8% in case of monotonic test, and 27.5% in case of cyclic test. The joint integrity was sustained for large beam tip displacement tip in contrast to the control specimen where failure of the joint was accompanied by considerable spalling of joint concrete.

G- If greater amount of CFRP for BCJ-18MM is provided such that the joint capacity becomes greater than the flexural beam capacity, this would provide the desired flexural mode of failure (weak beam/ strong column) under seismic loading.

H- We can conclude from the experimental test that even we reach the ultimate load and the concrete were cracked, the stress in CFRP increase, because all the load is carrying by CFRP sheet.

I- The design of the experiment to yield flexural failure of the beam in one set of specimens (12 mm bars) and joint shear failure in another set (18 mm bars) was confirmed during the actual testing of the 13 BCJ specimens.

J- The flexural failure was noted to be ductile with considerable yielding of the main beam steel, whereas the joint shear failure was more brittle and of the softening type, with no yielding of main reinforcement.

K- For the 12 mm bar specimens, the failure load due to flexural yielding was reasonably close to the shear capacity of the joint. Hence, CFRP retrofit of the joint, with extension of CFRP as a wrap around the beam at the beam-column interface, resulted in an increase of 10 to 19% in the ultimate capacity of the specimens. This probably was a result of confinement of the beam concrete, much like what is recommended in seismic detailing, to increase crushing strain of concrete.

L- For the 18 mm bar specimens, the failure mode was noted to be due to the shear failure of the joint. Hence, CFRP retrofit of the joint, with extension of CFRP as a wrap around the beam at the beam-column interface, resulted in a significant increase of 20 to 27% in the ultimate capacity. This can be attributed to enhancement of the shear capacity by virtue of the CFRP bridging diagonal cracking in the joint.

4- The FEM modeling using Damage Plasticity Model in ABAQUS environment was noted to yield reasonably accurate results for the beam-column joint specimens.

5- The Concrete Damage Plasticity (CPD) model was noted to predict not only beam flexural failure mode of the BCJ, but also the softening mode of failure resulting from shear failure of the joint. Such softening modes are usually very difficult to capture with other existing non-linear FE software which use traditional elasto-plastic constitutive models.

6- ABAQUS simulation for both monotonic and cyclic loading of the 18 mm bar specimens resulted in scalar damage predictions that showed diagonal profiling of maximum damage through the joint region at loads matching those as observed in the experiments.

7- For the 12 mm bar specimens, damage contours were observed to propagate initially along the beam, starting from the interface. The joint damage contours evolved at a much later stage of loading for this case.

8- Damage contours in the CDP model were noted to simulate realistically the observed modes of failure in the various BCJ specimens.

9- Cohesive contact model in ABAQUS for CFRP lamina resulted in close simulation of retrofitted specimens in terms of load enhancement. CFRP were modelled as orthotropic lamina, with linear elastic behavior to rupture.

10- Numerical strains in CFRP were noted to correspond reasonably to the experimentally measured values. Numerically obtained CFRP stresses were within the specified rupture values.

11- For cyclic loading of all specimens, the recommended stiffness recovery factors for tension and compression in the CPD model resulted in reasonable numerical simulation of the observed cyclic response of the BCJ specimens.

12- The load-displacement response of the BCJ under cyclic loading was noted closely to match the corresponding failure envelop for the monotonic loading cases at equal values of prescribed displacement.

13- This study also has demonstrated the simulation of BCJs using an elasto-plastic damage developed by Lubliner (1989) and further extended by Lee, and Fenves (1998) and made available in ABAQUS environment. The use of this model requires certain material parameters, including the stress-plastic strain data for hardening and softening in uniaxial compression and a corresponding one for uniaxial tension in addition to other parameters related to defining the yield surface and plastic potential function. Those parameters can be found using the appropriate tests including uniaxial and biaxial tension and compression tests.

14- It can also be concluded that concrete damage mechanics approach implemented in ABAQUS can be used efficiently to model reinforced concrete BCJs. The results give good agreement between experimental and numerical load-deflection response of the BCJs, although fine mesh is required so that the aspect ratio of the elements are within the acceptable range. The mode of

failure and development of cracks in the BCJs were also captured with significant accuracy using the plastic-damage model.

15- It is found that the interface approach is very efficient when the cohesive strength of layers that connects the components of the structure is high. This means that the fracture energy, needed to create the crack, is also high. This interface element would be very efficient in case of simulation for CFRP attached to the BCJs.

16- Using CFRP is one of the major methods of strengthening and retrofitting the BCJs. The only thing that has to be taking into account is the bond strength between CFRP and concrete surface. The use of CFRP enhanced the lateral strength of the BCJs.

17- From the FEM simulation, it can be concluded that the CFRP sheets have a pronounced effect in enhancing the strength and integrity of the BCJs. The numerical model for the CFRP retrofit BCJs shows that with proper configuration of the CFRP the failure mode of the control BCJs can be modified so as to enhance the strength and integrity of the joint.

7.2 Engineering Guidelines for Assessment and Retrofitted Beam – Column Joints

For typical Exterior reinforced beam-column joints, requiring strengthening or retrofitting, the following approach can be adopted.

1. Identification of material properties.

2. Evaluation of shear capacity of BCJs for the existing structure using existing ACI guidelines.

3. Development of 3-D finite element model of the BCJs and its simulation using plastic damage model to the existing level of desired load impacting the experimentally determined material properties.

4. Based on the mode of failure and cracking patterns observed in the finite element simulation, a strategy for strengthening or retrofitting the BCJs, the best configuration can be developed using CFRP or any other strengthening technique.

5. The procedure for strengthening the BCJs should be determined numerically and implemented in the real construction.

7.3　Recommendations for Future Work

It can be seen that there are several things that have to be investigated as future work. Some of these topics can be summarized as follows:

1- This study was conducted for exterior BCJ. This study can be extended to all types of the joints including exterior, interior, edge, and effect of confinement of slab. Perhaps, the testing of a full scale reinforced concrete frame would be one such option.

2- Regarding the strengthen techniques; investigation has to be done on different patterns of CFRP laminate sheets. Another possible study is using other type of material for strengthen purposes such as ultra-high performance fiber concrete and shape memory alloy.

3- Parametric study with different types of CFRP and configuration can be carried out using FE.

4- When looking at the plastic damage model developed by Lubliner (1989) and further extended by Lee, and Fenves (1998), the two damage parameters (compression damage and tension damage) are assumed to be a scalar quantities in which they are similar or isotropic. In reality, the compression damage can be accurately assumed as a scalar quantity because the crushing of the microstructure of concrete due to loading affects the compression capacity in the other directions. However, the tension damage cannot be accurately assumed to be a scalar quantity in which when loading is done in one direction, the damage evolved in the loading direction is not really affecting the other directions. Based on that, the

damage quantity in tension has to be assumed as a vector in which each one of the three principle directions has to have its own tension damage parameters.

References

Akguzel, U. (2011). "Seismic performance of FRP retrofitted exterior RC beam-column joints under varying axial and bidirectional loading." <u>PhD Thesis</u>, School of Civil and Environmental Engineering University of Canterbury, 2011.

Alhaddad, M. S., et al. (2011). "Numerical investigations on the seismic behavior of FRP and TRM upgraded RC exterior beam-column joints." <u>Journal of Composites for Construction</u> **16**(3): 308-321.

Alsayed, S. H., et al. (2010). "Seismic response of FRP-upgraded exterior RC beam-column joints." <u>Journal of Composites for Construction</u> **14**(2): 195-208.

Anderson, D. L., et al. (1996). "Performance of concrete bridges during the Hyogo-ken Nanbu (Kobe) earthquake on January 17, 1995." <u>Canadian Journal of Civil Engineering</u> **23**(3): 714-726.

Antonopoulos, C. P. and T. C. Triantafillou (2003). "Experimental investigation of FRP-strengthened RC beam-column joints." <u>Journal of Composites for Construction</u> **7**(1): 39-49.

Baluch, M., et al. (2012). "Finite Element Simulation of Low Concrete Strength Beam Beam-Column Joint Strengthened with CFRP." <u>15th World Conference in Earthquake Engineering</u>. Lisbon, Portugal

Bindhu, K. and K. Jaya (2010). "Strength and behaviour of exterior beam column joints with diagonal cross bracing bars." <u>Asian Journal of Civil Engineering (Building and Housing)</u> **11**(3): 397-410.

Birely, A. C., et al. (2012). "A model for the practical nonlinear analysis of reinforced-concrete frames including joint flexibility." <u>Engineering Structures</u> **34**: 455-465.

Braga, F., et al. (2009). "R/C Existing Structures with Smooth Reinforcing Bars: Experimental Behaviour of Beam-Column Joints Subject to Cyclic Lateral Loads." <u>Open Construction and Building Technology Journal</u> **3**: 52-67.

Červenka, J. and V. K. Papanikolaou (2008). "Three dimensional combined fracture–plastic material model for concrete." <u>International Journal of Plasticity</u> **24**(12): 2192-2220.

Deaton, James B, "Nonlinear finite element analysis of reinforced concrete exterior beam-column joints with no seismic detailing", <u>PhD Thesis</u>, School of Civil and Environmental Engineering Georgia Institute of Technology, 2013.

El-Amoury, T. and A. Ghobarah (2002). "Seismic rehabilitation of beam–column joint using GFRP sheets." <u>Engineering Structures</u> **24**(11): 1397-1407.

Gencoglu, M. and B. Mobasher (1993). "The strengthening of the deficient RC exterior beam-column joints using CFRP for seismic excitation." roceedings of the <u>3 rd international conference on structural engineering, mechanics and computation</u>. 2007.

Hakuto, S., et al. (2000). "Seismic load tests on interior and exterior beam-column joints with substandard reinforcing details." <u>ACI Structural Journal</u> **97**(1).

Hibbit, H., et al. (1998). "ABAQUS users and theory manuals, version 6.3." <u>RI: HKS Inc</u>.

Ibrahim, A. M. and M. S. Mahmood (2009). "Finite element modeling of reinforced concrete beams strengthened with FRP laminates." <u>European journal of scientific research</u> **30**(4): 526-541.

Ilki, A., et al. (2010). "Behavior of FRP-retrofitted joints built with plain bars and low-strength concrete." <u>Journal of Composites for Construction</u> **15**(3): 312-326.

Jankowiak, T. and T. Lodygowski (2005). "Identification of parameters of concrete damage plasticity constitutive model." <u>Foundations of civil and environmental engineering</u> **6**: 53-69.

Le-Trung, K., et al. (2010). "Experimental study of RC beam–column joints strengthened using CFRP composites." <u>Composites Part B: Engineering</u> **41**(1): 76-85.

Lee, J. and G. L. Fenves (1998). "Plastic-damage model for cyclic loading of concrete structures." <u>Journal of engineering mechanics</u> **124**(8): 892-900.

Lubliner, J., et al. (1989). "A plastic-damage model for concrete." <u>International Journal of Solids and Structures</u> **25**(3): 299-326.

Mostofinejad, D. and S. Talaeitaba (2006). "Finite element modeling of RC connections strengthened with FRP laminates." Iranian Journal of Science and Technology, Transaction B, Engineering **30**: 21-30.

Niroomandi, A., et al. (2010). "Seismic performance of ordinary RC frames retrofitted at joints by FRP sheets." Engineering Structures **32**(8): 2326-2336.

Olsen, E. and S. Billington (2011). "Cyclic response of precast high-performance fiber-reinforced concrete infill panels." ACI Structural Journal **108**(1): 51-60.

Pampanin, S., et al. (2002). "Seismic behavior of RC beam-column joints designed for gravity only."

Pantelides, C., et al. (2000). Rehabilitation of R/C building joints with FRP composites. 12th World Conference on Earthquake Engineering, Auckland, New Zealand.

Parra-Montesinos, G. and J. Wight (2001). "Prediction of strength and shear distortion in R/C beam-column joints." ACI SPECIAL PUBLICATIONS **197**: 191-214.

Parra-Montesinos, G. J., et al. (2005). "Highly damage-tolerant beam-column joints through use of high-performance fiber-reinforced cement composites." ACI Structural Journal-American Concrete Institute **102**(3): 487-495.

Parvin, A., et al. (2009). "CFRP rehabilitation of concrete frame joints with inadequate shear and anchorage details." Journal of Composites for Construction **14**(1): 72-82.

Patil, S. and S. Manekari (2013). "Analysis of Reinforced Beam-Column Joint Subjected to Monotonic Loading." International Journal of Engineering and Innovative Technology (IJEIT), Analysis **2**.

Priestley, M. (1996). "DISPLACEMENT-BASED SEISMIC ASSESSMENT CF EXISTING REINFORCED CONCRETE BUILDINGS."

Ravi, S. R. and G. P. Arulraj (2010). "Finite Element Modeling on behavior of Reinforced Concrete Beam-Column Joints Retrofitted with Carbon Fiber Reinforced Polymer Sheets." International Journal of Civil & Structural Engineering **1**(3): 576-582.

Ravi, S. R. and G. P. Arulraj (2012). "Experimental investigation on behavior of reinforced Concrete Beam Column Joints Retrofitted with GFRP-AFRP Hybrid wrapping." International Journal of Civil & Structural Engineering **1**(2): 245-253.

Saatcioglu, M., et al. (2001). "The August 17, 1999, Kocaeli (Turkey) earthquake damage to structures." Canadian Journal of Civil Engineering **28**(4): 715-737.

Sasmal, S., et al. (2011). "Seismic retrofitting of nonductile beam-column sub-assemblage using FRP wrapping and steel plate jacketing." Construction and Building Materials **25**(1): 175-182.

Ziraba, Y., et al. (1994). "Guidelines toward the design of reinforced concrete (RC) beams with external plates." ACI Structural Journal **91**(6).

APPENDIX

DESIGN OF SPECIMEN J-BI-18

DESIGN PARAMETERS:

CONCRETE COMPRESSIVE STRENGTH: f'c	4350	30	MPa	concrete cover: (in)	0.590551181	15	mm

STEEL LONGITUDINAL REBER YIELD STRENGTH: fy	95700	660	Mpa

STEEL TRANSVERSE REBAR YIELD STRENGTH: fy_h	69600	480	Mpa

STEEL MODULUS OF ELASTICITY: Es	29000000	200000	Mpa

SHEAR STRENGTH REDUCTION FACTOR: ϕv	0.75

MAX. CONCRETE COMPRESSIVE STRENGTH STRAIN: εc	0.003

Increase factor for yield stress in beam tensile rebar (ACI 21.5.1.1) : α	1.25

Joint shear strength factor based on confinement (ACI 21.5.3.1) : γ	15

COLUMN DESIGN :

    COLUMN DIMENSIONS:

	b in	h in	Ag in2	Lcol in
	9.84252	11.81102362	116.2502325	55.11811024
mm	250	300	75000	1400

LONGITUDINAL REINFORCEMENT:

	bar loc.(in)	bar size (#)	bar area (in2)	no. bars
levels of reinforcement:	1.06988189	5.669291339	0.394586503	3
	0	0	0	0
	10.74114173	5.669291339	0.394586503	3

TRANSVERSE REINFORCEMENT :

Diameter of transverse reinforcing bars:	dtr: (in)	0.375

Area of transverse reinforcing bars:	Atr: (in2)	0.110491071

Number of closed hoops:	nclosed	1

Total area of transverse reinforcing steel:	Asv: (in2)	0.220982143

Steel Reinforcement Layout:

Area of steel at each level: (in2)	As	1.18375951		763.7142857mm²
		0		0
		1.18375951		763.7142857mm²

Total area of steel: (in2)	Ast	2.367519021

Reinforcement ratio:	0.020365714

Nominal axial load capacity: (Kips)	647.6529034	2882.05KN

12.5% of P0: (Kips)	32.38264517	144.10KN

Flexure Design:

Equivalent stress block factor:	β1	0.8325	

Location of neutral axis: (in)	c	2.789	69.52872048	mm

Strain in each level of rebar: (+) tension, (-) compression:	εS = εc.(d-c)/c	-0.001758966	
		-0.003	
		0.008703257	

Stress in each level of reber: (+) tension, (-) compression:	fs=Es.εS (Ksi)	-51.01001654	-351.793218	Mpa
		-87	-600	Mpa
		95.7	660	Mpa

Forces in each level of reber: (+) tension, (-) compression:	Fs=As.fs (Kips)	-60.3835922	-268.706985	KN
		0	0	KN
		113.2857851	504.1217439	KN

Compressive axial force in effective concrete stress block:	Fc=0.85f'c.b.(β1.c) (kips)	82.93335553	369.0534321	KN

Sum of axial forces to show that the sum is appx zero:	Fc-∑Fs-Pn (lb)	0.0028

Moment capacity of column:	∑[Fs.(d-a/2)]+0.85.f'c.b.(β1.c).(h/2-β1c/2) (Kips.in)	1454.0832	164355	KN-mm

Beam Design

Beam		hb (in)	bb (in)	Agb (in2)	lb(in)

Dimensions:		11.81102362	9.842519685	116.2502325	35.43307087
	mm	300	250	75000	900

Beam Reinforcement:

level of reinforcement:	bar loc (in)	bar size (#)	bar area (in2)	no.bars
	1.13238189	5.669291339	0.394586503	3
	10.67864173	5.669291339	0.394586503	3

Transverse Reinforcement:

Diameter of transverse reinforcing bars :	dtrb (in)	0.375
Area of transverse reinforcing bars:	Atrb (in2)	0.110491071
number of closed hoops:	nclosedb	1
total area of transverse reinforcing steel:	Asvb (in2)	0.220982143

Steel Reinforcement Layout:

Area of steel at each level:	Asb (in2)	1.18375951	763.7142857mm²
		1.18375951	763.7142857mm²

Total area of steel:	Astb (in2)	2.367519021

Reinforcement ratio:	0.010182857

265

Flexure Design:

Location of neutral axis:	cb (in)	2.1392633	54.33728782	mm

| Strain in each level of rebar: (+) tension, (-) compression: | $\varepsilon Sb = \varepsilon c.(dbeam-cb)/cb$ | -0.001412002 | | |
| | | 0.011975214 | | |

| Stresses in each level of rebar: (+) tension, (-) compression: | fsb=Es.εSb (Ksi) | -40.94806034 | -282.4004161 | Mpa |
| | | 95.7 | 660 | Mpa |

| Forces in each level of rebar: (+) tension, (-) compression: | Fsb= (Asb.fsb) (Kips) | Fcs | -48.47265586 | -215.70KN |
| | | T | 113.2857851 | 504.12KN |

| compressive axial force in effective concrete stress block: | Fcb=0.85f'c.bb.(β1.cb) (Kips) | 64.81312439 | 288.4184035 | KN |
| Sum of axial forces to show that the sum is appx zero: | Fcb+Fcs-T=0 | 4.89405E-06 | | |

Moment capacity of beam:	Mnb (Kips-in)	(Fcb(d-(β1.cb)/2))+Fcs(d-d')	1097.13	124009.131	KN-mm	KN load
						137.7879238

Joint Shear Design:

Tensile force in beam rebar:	**Tn=α.fy.Astb (Kips)**	141.6072314

Joint area	**Aj=bb.h (in2)**	116.2502325

Length of column to inflection points, used to calculate shear in column:	**Ipc= Lcol (in)**	55.11811024

Shear in column:	**Vcol=Mnb/Ipc (Kips)**	0

Total shear force in joint:	**Vuj=Tn-Vcol (kips)**	141.6072314

Design shear strength of joint:	**ϕVnj=0.75.ɣ.√(f'c).Aj (kips)**	86.25633101

Beam shear design:

length of beam from load point to column face: (in)	beam-length	35.43307087	900mm
load required to reach design moment: Pmax (Kips)	Mnb/beam-length	30.96357838	137.78KN
Max. shear load in beam: (Kips)	Vu = Pmax	30.96357838	137.78KN
Design shear strength: (Kips)	Vn=Vu/ϕv	41.28477118	183.71KN
Shear strength of concrete: (kips)	Vc=2.√(f'c).bb.db	13.8642676	61.69KN
Required steel reinforcing shear strength: (Kips)	Vsreq=Vn-Vc	27.42050358	122.02KN
Min spacing factor: Ψ	2 if Vsreq≥2.√(f'c).bb.db or else 1	1	
Area of transverse reinforcing per hoop: (in2)	Av=2.Atrb	0.220982143	142.56mm^2
Required spacing of shear reinforcement: (in)	s=Av.Fyh.dbeam/Vsreq	5.989726746	152.13mm
Minimum spacing requirments (ACI 21.3.3.2): (in)	Sreqb=min{s,dbeamNb/2Ψ,24in}	5.339320866	135.61mm

column shear design:

max. shear load in column: (kips)	Vcu=Vcol	19.90515753	88.57KN

design shear strength: (kips)	Vnc=Vuc/φv	26.54021004	118.10KN

shear strength of concrete: (kips)	Vcc=2{1+Pn/2000.Ag}.√f'c .dN.b	15.79528163	70.28KN

required steel reinforcing shear strength: (kips)	Vsc=max((Vnc-Vcc,0.001kip)	10.74492842

Min spacing factor: Ψ	Ψ=2 if Vsc≥4.√(f'c).b.dcol or else 1	1

Required spacing of shear reinforcement: (in)	Sc=Av.fyh.dN/Vsc	15.28547397

Min stirrup spacing: (in)	Sreqc=min{Sc,dcol/2.Ψ,16dbb,48.dtrb,24in,bb}	5.339320866	135.61mm

DESIGN OF SPECIMENS J-BU-12 & J-BI-12

DESIGN PARAMETERS:

CONCRETE COMPRESSIVE STRENGTH: f'c	4350	30	MPa	concrete cover: (in)	0.590551181	15	mm

STEEL LONGITUDINAL REBER YIELD STRENGTH: fy	88450	610	Mpa

STEEL TRANSVERSE REBAR YIELD STRENGTH: fy_h	69600	480	Mpa

STEEL MODULUS OF ELASTICITY: Es	29000000	200000	Mpa

SHEAR STRENGTH REDUCTION FACTOR: ϕv	0.75

MAX. CONCRETE COMPRESSIVE STRENGTH STRAIN: εc	0.003

Increase factor for yield stress in beam tensile rebar (ACI 21.5.1.1) : α	1.25

Joint shear strength factor based on confinement (ACI 21.5.3.1) : γ	15

COLUMN DESIGN :

COLUMN DIMENSIONS:

b in	h in	Ag in2	Lcol in
9.84252	11.81102362	116.2502325	55.11811024

mm	250	300	75000	1400

LONGITUDINAL REINFORCEMENT:

	bar loc.(in)	bar size (#)	bar area (in2)	no. bars
	0.951771654	3.779527559	0.175371779	3
levels of reinforcement:	0	0	0	0
	10.85925197	3.779527559	0.175371779	3

TRANSVERSE REINFORCEMENT :

Diameter of transverse reinforcing bars:	dtr: (in)	0.375

Area of transverse reinforcing bars:	Atr: (in2)	0.110491071

Number of closed hoops:	nclosed	1

Total area of transverse reinforcing steel:	Asv: (in2)	0.220982143

Steel Reinforcement Layout:

Area of steel at each level: (in2)	As	0.526115338	339.4285714
		0	0
		0.526115338	339.4285714

Total area of steel: (in2)	Ast	1.052230676

Reinforcement ratio:	0.009051429

Nominal axial load capacity: (Kips)	519.014415	2309.614147	KN

12.5% of P0: (Kips)	33.03526752	147.0069404	KN

Flexure Design:

Equivalent stress block factor:	β1	0.8325

Location of neutral axis: (in)	c	1.880294	47.7594676	mm

Strain in each level	$\varepsilon S = \varepsilon c.(d-c)/c$	-0.001481453

of rebar: (+) tension, (-) compression:		-0.003
		0.014325884

Stress in each level of reber: (+) tension, (-) compression:	fs=Es.εS (Ksi)	-42.96213472	-296.290584	Mpa
		-87	-600	Mpa
		88.45	610	Mpa

Forces in each level of reber: (+) tension, (-) compression:	Fs=As.fs (Kips)	-22.60303803	-100.583519	KN
		0	0	KN
		46.53490164	207.0803123	KN

Compressive axial force in effective concrete stress block:	Fc=0.85f'c.b.(β1.c) (kips)	56.96714795	253.5038084	KN

Sum of axial forces to show that the sum is appx zero:	Fc-∑Fs-Pn (lb)	1.68183E-05

Moment capacity of column:	∑[Fs.(d-a/2)]+0.85.f'c.b.(β1.c).(h/2-β1c/2) (Kips.in)	748.6284532	84617.47	KN-mm

Beam Design

Beam Dimensions:	hb (in)	bb (in)	Agb (in2)	lb(in)
	11.81102362	9.842519685	116.2502325	35.43307087
	mm	300	250	

bar loc (in)	bar size (#)	bar area (in2)	no.bars
1.014271654	3.779527559	0.175371779	3
10.79675197	3.779527559	0.175371779	3

273

dtrb (in)	0.375
Atrb (in2)	0.110491071
nclosedb	1
Asvb (in2)	0.220982143

Asb (in2)	0.526115338	339.42mm^2
	0.526115338	339.42mm^2

Astb (in2)	1.052230676

0.004525714

Flexure Design:

Location of neutral axis:	cb (in)	1.250532	31.7635128	mm

Strain in each level of rebar: (+) tension, (-) compression:	εSb = εc.(dbeam-cb)/cb	-0.000566784		
		0.022901181		

Stresses in each level of rebar: (+) tension, (-) compression:	fsb=Es.εSb (Ksi)	-16.43672464	-113.35	Mpa
		88.45	610	Mpa

Forces in each level of rebar: (+) tension, (-) compression:	Fsb= (Asb.fsb) (Kips)	Fcs	-8.64761294	-38.48	KN
		T	46.53490164	207.08	KN

compressive axial force in effective concrete stress block:	Fcb=0.85f'c.b b.(β1.cb) (Kips)	37.88728861	168.59	KN

Sum of axial forces to show that the sum is appx zero:	Fcb+Fcs-T=0	8.58616E-08

Moment capacity of beam:	Mnb (Kips-in)	(Fcb(d-(β1.cb)/2))+Fcs(d-d')	473.93	53568.663	KN-mm	KN load
						59.52

Joint Shear Design:

Tensile force in beam rebar:	**Tn=α.fy.Astb (Kips)**	58.16862705

Joint area	**Aj=bb.h (in2)**	116.2502325

Length of column to inflection points, used to calculate shear in column:	**Ipc= Lcol (in)**	55.11811024

Shear in column:	**Vcol=Mnb/Ipc (Kips)**	0

Total shear force in joint:	**Vuj=Tn-Vcol (kips)**	58.16862705

Design shear strength of joint:	**φVnj=0.75.ɣ.√(f'c).Aj (kips)**	86.25633101

Beam shear design:

length of beam from load point to column face: (in)	beam-length	35.43307087	900	mm

load required to reach design moment: Pmax (Kips)	Mnb/beam-length	13.37544644	59.52	KN

Max. shear load in beam: (Kips)	Vu = Pmax	13.37544644	59.52	KN

Design shear strength: (Kips)	Vn=Vu/φv	17.83392858	79.36	KN

Shear strength of concrete: (kips)	Vc=2.√(f'c).bb.db	14.01761219	62.37	KN

Required steel reinforcing shear strength: (Kips)	Vsreq=Vn-Vc	3.816316391	16.98	KN

Min spacing factor: Ψ	2 if Vsreq≥2.√(f'c).bb.db or else 1	1	

Area of transverse reinforcing per hoop: (in2)	Av=2.Atrb	0.098214286	63.36	mm²

Required spacing of shear reinforcement: (in)	s=Av.Fyh.dbeam/Vsreq	19.33893946	491.20	mm

Minimum spacing requirments (ACI 21.3.3.2): (in)	Sreqb=min{s,dbeamNb/2Ψ,24in}	5.398375984	137.11	mm

column shear design:

max. shear load in column: (kips)	Vcu=Vcol	8.598501281	38.26KN

design shear strength: (kips)	Vnc=Vuc/ϕv	11.46466838	51.01KN

shear strength of concrete: (kips)	Vcc=2{1+Pn/2000.Ag}.√f'c .dN.b	16.10200555	71.65KN

required steel reinforcing shear strength: (kips)	Vsc=max((Vnc-Vcc,0.001kip)	0.001

Min spacing factor: Ψ	Ψ=2 if Vsc≥4.√(f'c).b.dcol or else 1	1

Required spacing of shear reinforcement: (in)	Sc=Av.fyh.dN/Vsc	74230.74

Min stirrup spacing: (in)	Sreqc=min{Sc,dcol/2.Ψ,16dbb,48.dtrb,24in,bb}	5.429625984	137.91mm

VITAE

Name	:AbdulSamee Mohammad Halahla
Nationality	:Palestinian
Date of Birth	:12/20/1982
Email	:eng.halahla@gmail.com
Address	:Department of Civil EngineeringP.O.Box 14, Birzeit, West Bank, Palestine
Academic Background	:B.Sc. Degree from the Civil Engineering Department, College of Engineering, An-Najah National University"- Nablus, Palestine, June 2007

M.Sc. degree in Civil Engineering from the Civil Engineering Department, College of Engineering, Politecnico di Milano" – Milan, Italy, October 2009

PhD degree in Civil Engineering from the Civil Engineering Department, College of Engineering, King Fahd University of Petroleum and Minerals, Dhahran, Saudi Arabia, May 2014.